Phenomenology of non-minimal supersymmetric models at linear colliders

Dissertation

zur Erlangung des Doktorgrades
an der Fakultät für Mathematik,
Informatik und Naturwissenschaften
Fachbereich Physik
der Universität Hamburg

vorgelegt von

Stefano Porto

aus

Venedig, Italien

Hamburg
2015

Gutachter/in der Dissertation:	Prof. Dr. Gudrid Moortgat-Pick Dr. Jürgen Reuter
Gutachter/in der Disputation:	Dr. Thomas Konstandin Prof. Dr. Gudrid Moortgat-Pick Dr. Jürgen Reuter Jun.-Prof. Dr. Christian Sanders
Datum der Disputation:	27. April 2015
Vorsitzender des Prüfungsausschusses:	Prof. Dr. Jan Louis
Vorsitzender des Promotionsausschusses:	Prof. Dr. Jan Louis
Dekan des Fachbereichs Physik:	Prof. Dr. Heinrich Graener

Abstract

The focus of this thesis is on the phenomenology of several non-minimal supersymmetric models in the context of future linear colliders (LCs). Extensions of the minimal supersymmetric Standard Model (MSSM) may accommodate the observed Higgs boson mass at about 125 GeV in a more natural way than the MSSM, with a richer phenomenology. We consider both F-term extensions of the MSSM, as for instance the non-minimal supersymmetric Standard Model (NMSSM), as well as D-terms extensions arising at low energies from gauge extended supersymmetric models. The NMSSM offers a solution to the μ-problem with an additional gauge singlet supermultiplet. The enlarged neutralino sector of the NMSSM can be accurately studied at a LC and used to distinguish the model from the MSSM. We show that exploiting the power of the polarised beams of a LC can be used to reconstruct the neutralino and chargino sector and eventually distinguish the NMSSM even considering challenging scenarios that resemble the MSSM. Non-decoupling D-terms extensions of the MSSM can raise the tree-level Higgs mass with respect to the MSSM. This is done through additional contributions to the Higgs quartic potential, effectively generated by an extended gauge group. We study how this can happen and we show how these additional non-decoupling D-terms affect the SM-like Higgs boson couplings to fermions and gauge bosons. We estimate how the deviations from the SM couplings can be spotted at the Large Hadron Collider (LHC) and at the International Linear Collider (ILC), showing how the ILC would be suitable for the model identification. Since our results prove that a linear collider is a fundamental machine for studying supersymmetry phenomenology at a high level of precision, we argue that also a thorough comprehension of the physics at the interaction point (IP) of a LC is needed. Therefore, we finally consider the possibility of observing intense electromagnetic field effects and nonlinear quantum electrodynamics (QED) processes at the IP, due to the strong electromagnetic fields generated by electron and positron bunches. We estimate the strength of the fields that would be generated at the planned LCs. We then argue that considering their effects on all physical processes may have strong impact on the ambitious precision physics program at the LC. We study how to test nonlinear QED colliding an intense laser on the beams of a LC, in an effort to improve and extend the success of SLAC experiment 144.

Zusammenfassung

Die vorliegende Arbeit befasst sich mit der Phänomenologie nicht-minimaler supersymmetrischer Modelle im Kontext zukünftiger Linearbeschleuniger. Erweiterungen des minimalen supersymmetrischen Standardmodells (MSSM) können die beobachtete Higgs-Boson Masse von ca. 125 GeV natürlicher beschreiben als das MSSM und haben eine reichere Phänomenologie. Wir betrachten sowohl F-Term-Erweiterungen des MSSM, wie beispielsweise das nichtminimale supersymmetrische Standardmodell (NMSSM), als auch D-Term-Erweiterungen, welche aus der Niederenergiebeschreibung von supersymmetrischen Modellen mit erweiterter Eichgruppe entstehen. Das NMSSM beinhaltet eine Lösung des μ-Problems mit einem zusätzlichen Eichsinglett-Supermultiplet. Der erweiterte Neutralinosektor des NMSSM kann an einem zukünftigen Linearbeschleuniger präzise studiert werden und dient NMSSM und MSSM zu unterscheiden. Wir zeigen, dass die polarisierten Strahlen eines Linearbeschleunigers wichtig werden können, um den Neutralino- und Charginosektor zu rekonstruieren und dadurch zwischen NMSSM und MSSM zu unterscheiden, selbst in Fällen, in denen die Teilchenspektra und eigenschaften in beiden Modelle sehr ähnlich sind. Nichtentkoppelnde D-Term-Erweiterungen des MSSM können die Higgs-Masse in niedrigster Ordnung durch zusätzliche Beiträge zum quartischen Potential des Higgsfeldes im Vergleich zum MSSM erhöhen. Diese Beiträge werden durch eine erweiterte Eichgruppe generiert. Wir beschreiben diesen Effekt und zeigen, wie diese zusätzlichen nichtentkoppelnden D-Terme die standardmodellartige Kopplung des Higgsbosons an die Fermionen und Eichbosonen verändert. Weiterhin beschreiben wir, wie diese Abweichungen von den Standardmodellkopplungen am Large Hadron Collider (LHC) und dem International Linear Collider (ILC) gefunden werden können und zeigen, dass der ILC essentiell für die Interpretation des Modells ist. Da unsere Ergebnisse zeigen, dass hochpräzise Messungen an einem Linearbeschleuniger von fundamentaler Bedeutung für die Phänomenologie supersymmetrischer Modelle ist, ist es ebenfalls wichtig, das physikalische Umfeld am Wechselwirkungspunkt eines Linearbeschleunigers genau zu verstehen. Daher beschreiben wir im letzten Teil der Arbeit nichtlineare Quantenelektrodynamik (QED) in Gegenwart starker elektromagnetischer Felder, welche durch die Elektronen- und Positronenbündel der Beschleunigerstrahlen erzeugt werden. Wir schätzen die Stärke dieser Felder bei zukünftigen Linearbeschleunigern ab und zeigen, dass der Effekt der Felder gegebenenfalls bei der Beschreibung aller physikalischer Prozesse berücksichtigt werden muss, um das ambitionierte Physikprogramm der geplanten Linearbeschleuniger umzusetzen. Unter Berücksichtigung dieser Effekte studieren wir mit Hilfe eines intensiven Laserstrahls –ähnlich dem SLAC Experiment 144– nichtlineare QED experimentell am LC getestet wereden kann.

List of publications

This thesis is based on the following publications:

- [1] G. Moortgat-Pick, S. Porto and K. Rolbiecki, *Neutralinos betray their singlino nature at the ILC*, JHEP **1409** (2014) 002, [arXiv:1406.7701 [hep-ph]].
- [2] S. Porto, G. A. Moortgat-Pick and K. Rolbiecki, *Towards discrimination of MSSM and NMSSM scenarios at colliders*, `arXiv:1404.1053` [hep-ph].
- [3] M. McGarrie, G. Moortgat-Pick, S. Porto, *Confronting Higgs couplings from D-term extensions and Natural SUSY at the LHC and ILC*, Eur.Phys.J. **C75** (2015) 150, [`arXiv:1411.2040` [hep-ph]].
- [4] A. Hartin, S. Porto and G. Moortgat-Pick, *Testing nonlinear-QED at the future linear collider with an intense laser*, `arXiv:1404.0810` [hep-ph].
- [5] S. Porto, A. Hartin and G. Moortgat-Pick, *Methods for evaluating physical processes in strong external fields at e^+e^- colliders: Furry picture and quasi-classical approach*, PoS Corfu **2012** (2013) 039. [`arXiv:1304.4241` [hep-ph]]
- [6] A. Hartin, G. Moortgat-Pick and S. Porto, *Strong field effects on physics processes at the Interaction Point of future linear colliders*, PoS ICHEP **2012** (2013) 480 [`arXiv:1304.2632` [hep-ph]].

Regarding the work in references [1] and [2], I contributed to:

- [7] G. Moortgat-Pick *et al.*, *Physics at the e^+e^- Linear Collider*, `arXiv:1504.01726` [hep-ph].

Eidesstattliche Erklärung

Hiermit erkläre ich an Eides statt, dass ich die vorliegende Dissertationsschrift selbst verfasst und keine anderen als die angegebenen Quellen und Hilfsmittel benutzt habe.

Hamburg, den 25. Februar 2015 Stefano Porto

Contents

Contents **xi**

1 Introduction **1**

2 Supersymmetry as completion of the Standard Model **5**
2.1 The Standard Model of Particle Physics 5
2.1.1 SM fields and Lagrangian 6
2.1.2 Electroweak symmetry breaking 8
2.1.3 Motivations for a Physics Beyond the Standard Model 10
2.2 Supersymmetry 12
2.2.1 Supersymmetry algebra 12
2.2.2 Cancellation of quadratic divergences 14
2.2.3 Supersymmetric lagrangian and soft SUSY-breaking terms 14
2.3 The minimal supersymmetric Standard Model 15
2.3.1 EWSB and the Higgs, chargino, and neutralino sectors 17
2.3.2 Supersymmetry breaking mechanisms 19
2.3.3 Goals and problems of the MSSM 20
2.4 Non-minimal supersymmetric Standard Models 21

3 SUSY searches: lessons from the LHC, prospects for the ILC **23**
3.1 Observation of a 125.5 GeV Higgs boson and the MSSM 23
3.2 Direct SUSY collider searches 25
3.3 Indirect searches and constraints 27

4 NMSSM: singlinos at the linear collider **31**
4.1 The next-to-minimal supersymmetric Standard Model 31
4.1.1 Concept and motivation 31
4.1.2 The generalised NMSSM 32
4.1.3 The $\mathbb{Z}_3$-NMSSM 32
4.1.4 NMSSM Higgs phenomenology and the MSSM 35
4.2 Distinguishing the NMSSM neutralino-chargino sector at the ILC 36
4.3 Classes of scenarios and model distinction 42

4.3.1 Light singlino scenario . . . 43
4.3.2 Light higgsino scenario, $\mu_{\text{eff}} < M_1 < M_2$ . . . 46
4.3.3 Light gaugino scenario, $\mu_{\text{eff}} > M_1 > M_2$ . . . 54
4.4 Summary and conclusions . . . 57

5 Non-decoupling D-terms and the Higgs boson 59
5.1 Introduction . . . 59
5.1.1 Concept . . . 59
5.1.2 Basic example: $SU(2) \otimes SU(2)$ . . . 60
5.1.3 EW-scale effects . . . 65
5.2 Non-decoupling D-terms and the tree-level Higgs mass . . . 66
5.2.1 Vector Higgs quiver model . . . 67
5.2.2 Chiral Higgs quiver model . . . 74
5.3 Higgs couplings and detection at the LHC and ILC . . . 80
5.3.1 Non-decoupling D-terms effects on the Higgs couplings . . . 80
5.3.2 Higgs couplings determination at the LHC and ILC . . . 82
5.3.3 Spotting non-decoupling D-terms at colliders . . . 83
5.4 Summary and conclusions . . . 89

6 Towards precision measurements in an intense field environment 91
6.1 The interaction point of a linear collider . . . 91
6.2 *Horror vacui*: Physics in intense fields . . . 94
6.2.1 Intense fields at the interaction point of a linear collider . . . 97
6.3 The Furry Picture . . . 100
6.4 Testing nonlinear QED at the LC: a proposal . . . 103
6.4.1 Possibility at the future LC . . . 108
6.5 Summary and conclusions . . . 110

7 Conclusions 113

A Superspace notation 117

B NMSSM: Higgs sector and conventions 119
B.1 $\mathbb{Z}_3$-NMSSM Higgs sector . . . 119
B.2 Standard Model constants . . . 120

C Non-decoupling D-terms 121
C.1 Perturbative unification and the size of the D-terms . . . 121
C.2 Derivation of κ_b . . . 122

D The QED Furry-Feynman rules 125

Bibliography 129

Acknowledgements **149**

Ringraziamenti **151**

Chapter 1

Introduction

Particle physics is at a turning point since July 2012, when the striking discovery of a 125.5 GeV particle at the Large Hadron Collider (LHC) was made [8,9]. The measurements from the ATLAS and CMS detectors suggest this new particle to be the Higgs boson, the last missing piece of the Standard Model of particle physics (SM) [10–12]. The measurements of the spin and of the couplings of the new particle, at the current accuracy, confirm this hypothesis [13–16]. The Higgs boson is the cornerstone of the SM formulation since it triggers spontaneous electroweak symmetry breaking (EWSB) through the Higgs mechanism [17–20]. The SM, so far, has described with impressively high accuracy almost all the strong and electroweak processes observed at colliders. The SM, however, cannot be the ultimate theory of Nature. First of all, it lacks a description of gravitational interactions. A second incompleteness comes from the fact that the SM cannot explain the matter-antimatter asymmetry. Furthermore, the SM does not provide any reliable dark matter (DM) candidate.

Another reason for exploring beyond the Standard Model (BSM) physics is to explain the effects of the radiative corrections on the Higgs mass. Since the Higgs is a scalar, there are no symmetries in the SM that could protect its mass from loop-diagrams contributions. These corrections are quadratic in the UV-scale Λ cutting off the theory. One may assume that the SM is valid up to the Planck scale $\Lambda_P \sim 10^{19}$ GeV. In this case, a cancellation with extremely high degree of fine tuning between the bare Higgs mass and its radiative corrections is needed in order to recover the observed Higgs mass $m_h = 125.5$ GeV. This implication seems in contrast with the idea of naturalness of the theory. It is a puzzle, called the *Hierarchy Problem* [21–23], which has lead to the formulation of many extensions of the SM.

There are two main solutions for the Hierarchy Problem. First, the introduction in the theory of a symmetry that could protect the Higgs mass. Second, the lowering of the cut-off of the theory by introducing new physics at a scale $\Lambda \ll \Lambda_P$. The first solution is adopted in supersymmetric theories [24–29], in which a symmetry between bosons and fermions cancels exactly the radiative corrections to the Higgs mass. In order to do this, supersymmetric models assign to each SM particle a *sparticle*, *i.e.* a partner particle with opposite-statistics.

The second solution to the Hierarchy problem can be implemented by considering the Higgs as a composite object, formed by novel strong interactions entering at a lower scale with respect to Λ_P [30,31]. The aforementioned BSM models are also interesting because they can explain the origin of Higgs scalar potential, responsible for EWSB.

Despite these premises, so far no experimental evidence for physics Beyond the SM has been detected. A first consequence on supersymmetry is that, if it is a symmetry of Nature, it must be broken at low energies. According to supersymmetry, indeed, a SM particle and its supersymmetric partner should have the same mass and charges. For this reason, a plethora of models have been introduced to explain supersymmetry breaking.

At the LHC, direct searches for supersymmetric particles or exotica, as well as indirect constraints from measurements of the Higgs coupling strengths have not yet given hints towards BSM [32,33]. For supersymmetric models, LHC constraints are particularly strong for coloured sparticles, with lower limits excluding the first two generations squarks and gluinos below $\sim$ 1 TeV, depending on the model assumptions [34, 35]. The limits are more relaxed for third generation squarks, and especially for sparticles of the electroweak sector, to which the LHC is less sensitive. Phenomenological studies have heavily constrained composite Higgs models too. For example, the lower bounds for some of the new particles' masses have been pushed up to several TeVs in partial compositeness models [36], while the scale of the new symmetry breaking in Little Higgs models is constrained to be higher than $\sim$ 700 GeV [37–39].

Focussing on supersymmetry (SUSY), however, it is very important to note that the most strict LHC limits are derived for simplified and/or highly constrained scenarios. The constrained supersymmetric models have much smaller parameter space to be explored, since they advocate a higher degree of symmetry between the parameters of the model. Therefore light supersymmetry is still a viable candidate for BSM physics [40], and future experimental results are awaited to give indications in this direction.

First, in 2015 the upgraded LHC will start running at a center-of-mass energy of 13 TeV, allowing the production and the direct detection of sparticles with higher masses than before. Second, in early 2016 Japan is expected to give its decision about hosting the International Linear Collider (ILC) [41–45]. The ILC would collide electron and positron beams at a center-of-mass energy up to 500 GeV, in a very clean environment. The ILC would be then particularly suitable for precision measurements of electroweak physics, especially in the Higgs sector, where a model independent measurement of Higgs coupling is possible, and top physics too. The supersymmetric electroweak sector could be precisely assessed, complementary to the LHC, despite the lower energies reached [7]. In fact, threshold scans allow to measure the masses of the resonances. Furthermore, the ILC polarised beams have a key role, since they enhance production cross sections, while lowering the background processes. Another precision tool is the measurement of spin correlation between initial and final states.

Therefore, in case of the discovery of supersymmetry, a future linear collider would be fundamental for revealing the structure and the determination of the underlying model, both looking at phenomenology of the new particles and of the Higgs. This is of particular interest,

since many supersymmetric extensions of the Standard Model have been proposed beyond the minimal option. One reason for this is to more easily accommodate the observed Higgs mass $m_h = 125.5$ GeV with respect to the minimal supersymmetric extension of the SM, where the tree-level Higgs mass below $m_Z = 91.2$ GeV requires large radiative corrections.

This thesis deals with a series of non-minimal supersymmetric extensions of the SM and it describes methods for distinguishing this models with respect to the SM or the MSSM, in particular in the context of linear colliders. The structure of the thesis is organised as follows.

In **Chapter** 2 supersymmetry is introduced as an extension of the Standard Model. First, the Standard Model is presented as the theory describing strong and electroweak interactions, explaining the origin of masses through the electroweak symmetry breaking mechanism. Then, the aforementioned shortcomings of the SM are pointed out, with a particular focus on the Hierarchy Problem. To meet these inconsistencies, the theoretical background of supersymmetry is then introduced. An explanation for the cancellation of quadratic divergent contributions to the Higgs mass then is illustrated. More concretely, a general supersymmetric Lagrangian is given, together with a general expression for the soft supersymmetry-breaking terms. The minimal supersymmetric SM (MSSM) is then introduced, with particular attention to the Higgs and EWSB, as well as the neutralino and chargino sectors. Since supersymmetry must be softly broken in order to explain the non-observation of sparticles, several viable supersymmetry breaking mechanisms are listed. Besides the achievements of the MSSM, a series of shortcomings, like the μ-problem and the naturalness of the stop sector, suggest to look beyond the MSSM. Therefore, an overview over possible extensions of the MSSM is offered.

A brief interlude on the experimental results and the perspectives concerning supersymmetry searches is given in **Chapter** 3. The consequences on the MSSM of the observation of the Higgs boson at LHC and of the direct SUSY searches are discussed, together with an overview on the possibilities offered by the ILC. Finally, a series of indirect constraints from dark matter and precision physics is mentioned.

Chapter 4 is dedicated to the research project on the model distinction between the next-to-minimal SM (NMSSM) and MSSM at a linear collider. The NMSSM solves the μ-problem by introducing an additional gauge singlet supermultiplet with respect to the MSSM. An effective μ-term, in fact, is generated at the SUSY breaking scale due to the vacuum expectation value (vev) of the singlet. A description of the enlarged Higgs and neutralino sectors of the NMSSM and a brief overview on the peculiarities of the NMSSM Higgs phenomenology are provided. The developed method of model distinction between the NMSSM and MSSM at a linear collider is illustrated. This method relies on the precise measurements of masses and cross sections of the neutralinos and charginos at the future linear collider. The admixtures of the lightest neutralino states allow for a definition of classes of NMSSM scenarios featuring different phenomenologies. The elaborated distinction method is then applied to a series of scenarios belonging to the previous classes that, at least at low region of the spectrum, behave very closely to the MSSM. The potential as well as the limits of the method for the different

classes are presented, together with possible integrations.

In **Chapter** 5 the attention is turned to another class of supersymmetric models, namely the non-decoupling D-terms extensions of the MSSM. These models are introduced in order to relax naturalness in the stop sector by raising the tree-level Higgs mass with additional quartic couplings. First, it is shown how these MSSM extensions may arise as low energy effective theories of quiver models, *i.e.* as models with an extended gauge symmetry. In particular the focus is on models with two copies of $SU(2) \otimes U(1)$ which spontaneously break to the electroweak gauge group $SU(2)_L \otimes U(1)_Y$, generating additional non-decoupling D-terms in the Higgs scalar potential. It is shown how these terms may raise the tree-level Higgs mass in two classes of these models, with different distribution of charges of the Higgs doublets. Non-decoupling D-terms also affect the couplings of the SM-like Higgs boson with SM fermions and gauge bosons. An analysis on the potential of the LHC and of the ILC energy stages to detect deviations from the SM couplings due to D-terms is performed for the two analysed classes. The results highlight the eminence that ILC may have in the study of these models.

Having shown the key role of a future linear collider in precision physics, and in particular in the study of supersymmetric models, it is of paramount importance to clearly understand the physics at the interaction point (IP) of the LC lepton beams. Therefore, **Chapter** 6 concerns itself with the effects on the physics processes at the IP due to the very intense electromagnetic fields associated to the lepton beams. In fact, the nominal luminosities of the planned linear colliders, the ILC and the Compact Linear Collider (CLIC), require very dense lepton bunches to collide. Therefore, the interacting particles see very intense external fields in their rest frames. As a consequence, background processes like beamstrahlung are generated. An overview of particle processes in very strong electromagnetic fields is given, together with the concept of critical field strength, corresponding to the strength at which an electron-positron pair is spontaneously created from the vacuum. The expected field strengths at the IPs of the planned LCs are estimated. It is concluded that operating a LC at several TeV, the effects of these fields on the processes that are of interest for the LC physics program should be taken into account. In order to do so, it is proposed to apply a method that includes the external fields into perturbation theory, called the Furry picture of quantum states. In this context, it is also proposed to exploit the future linear collider for testing nonlinear quantum electrodynamics (QED), *i.e.* QED processes with absorption of multiple photons from an external field. This is possible by colliding the LC beams with an intense laser, improving and extending the SLAC experiment 144 [46]. The potential of the proposed experiment is estimated, and a description of the processes that can be studied is given.

The thesis is resumed and its conclusions are given in **Chapter** 7. Additional contents on the topics discussed in Chapters 2, 4, 5, and 6 are provided in **Appendices** A, B, C, and D, respectively. Finally, the acknowledgements may be found after the Bibliography.

Following the guidelines for dissertations, at the beginning of chapters 2, 3, 4, 5, and 6 the contents of the chapter are outlined, pointing out the original contributions by the author in the collaborative work, together with the main literature resources.

Chapter 2

Supersymmetry as completion of the Standard Model

This chapter provides the basic introduction and motivation of supersymmetric models, that constitute the theoretical background of chapters 3 and 4. It briefly introduces the Standard Model and the Hierarchy problem in section 2.1, the supersymmetry basics in section 2.2, and the minimal supersymmetric Standard Model (MSSM) in sec. 2.3. In section 2.4 we list some extensions of the MSSM. The discussion will partially follow the description of known results from the references [47–51].

2.1 The Standard Model of Particle Physics

The Standard Model of Particle Physics (SM) describes the physics of all the observed fundamental particles and their interactions excluding gravity. The common denominator for such a model is the identification of a local gauge symmetry that could describe the interactions between the observed particles. The current formulation of the SM is the result of decades-long series of results starting from the formulation of a unified theory for electromagnetic and weak interactions by Glashow [10]. The latter is the electroweak theory to which Weinberg [11] and Salam [12] embedded the Higgs mechanism of symmetry breaking elaborated by Brout and Englert [17], Higgs [18, 19], and Guralnik, Hagen, and Kibble [20]. The electroweak interactions are described by the gauge symmetry $SU(2)_L \otimes U(1)_Y$. This symmetry is spontaneously broken at the electroweak scale to $U(1)_{\text{em}}$, the gauge symmetry describing electromagnetic interactions. Responsible for the breaking is the Higgs mechanism, which leaves the photons, *i.e.* the gauge bosons mediating electromagnetic interactions, massless. The gauge bosons W, Z that mediate the weak interactions, instead, correspond to the broken generators of the former gauge group and get masses. Furthermore, the description of the physics of strong interactions has been added through the symmetry $SU(3)_c$ as formulated in

Quantum Chromodynamics (QCD) [52]. We can resume the SM gauge structure as

$$\underbrace{SU(3)_C}_{\text{strong}} \otimes \underbrace{SU(2)_L \otimes U(1)_Y}_{\text{electroweak}} \xrightarrow{\text{EW breaking}} SU(3)_C \otimes \underbrace{U(1)_{\text{em}}}_{\text{electromagnetic}} . \tag{2.1}$$

For a thorough review on the model, we refer to [47].

2.1.1 SM fields and Lagrangian

The SM predicted the existence of several particles that were actually observed in the years following its formulation, with extremely high agreement to the experimental outcome. This culminated with the Higgs discovery at the LHC in July 2012 [8, 9], the last missing piece of such magnificent picture. The particle content of the SM before electroweak symmetry

Fields	**labels**	**spin**	$\mathbf{SU(3)_C \otimes SU(2)_L \otimes U(1)_Y}$
Gluons	g^i	1	$(\mathbf{8}, \mathbf{1}, 0)$
W bosons	W^a	1	$(\mathbf{1}, \mathbf{3}, 0)$
B boson	B	1	$(\mathbf{1}, \mathbf{1}, 0)$
Quarks	$Q_q = (u_L,\, d_L)_q$	$\frac{1}{2}$	$(\mathbf{3}, \mathbf{2}, \frac{1}{6})$
	$\bar{u}_q = u^\dagger_{Rq}$	$\frac{1}{2}$	$(\bar{\mathbf{3}}, \mathbf{1}, -\frac{2}{3})$
	$\bar{d}_q = d^\dagger_{Rq}$	$\frac{1}{2}$	$(\bar{\mathbf{3}}, \mathbf{1}, \frac{1}{3})$
Leptons	$\ell_l = (\nu\,, e_L)_l$	$\frac{1}{2}$	$(\mathbf{1}, \mathbf{2}, -\frac{1}{2})$
	$\bar{e}_l = e^\dagger_{Rl}$	$\frac{1}{2}$	$(\mathbf{1}, \mathbf{1}, 1)$
Higgs	$\phi = \left(H^+\,, H^0\right)$	0	$(\mathbf{1}, \mathbf{2}, -\frac{1}{2})$

Table 2.1: Standard Model particle content with the gauge transformation properties before electroweak symmetry breaking; $i = 1, \ldots, 3$, $a = 1, 2, 3$, $q = 1, 2, 3$, and $l = e,\, \mu,\, \tau$.

breaking (EWSB), *cf.* table 2.1, is given by:

- The gauge bosons of the theory, with spin 1: eight *gluons* g^a, three W^i bosons, and the B boson respectively corresponding to $SU(3)_c$, $SU(2)_L$, and $U(1)_Y$. In the Lagrangian density the kinetic terms for the gauge bosons are given by

$$\mathcal{L}_V = -\frac{1}{4} G_{i\mu\nu} G^{i\mu\nu} - \frac{1}{4} W_{a\mu\nu} W^{a\mu\nu} - \frac{1}{4} B_{\mu\nu} B^{\mu\nu}. \tag{2.2}$$

  Above $G^{i\mu\nu}$, $W^{a\mu\nu}$, $B^{\mu\nu}$ are respectively the gluon, the W and B bosons field strength tensors, defined as

$$F^i_{\mu\nu} = \partial_\mu A^i_\nu - \partial_\nu A^i_\mu - g f^{ijk} A^j_\mu A^k_\nu\,, \tag{2.3}$$

  for a generic gauge boson A^i, with g, f^{ijk} the corresponding gauge coupling and structure constants. We define the covariant derivative for the SM as

$$D_\mu = \partial_\mu + i g_3 \frac{\lambda^a}{2} g^a_\mu + i g_2 \frac{\sigma^i}{2} W^i_\mu + i g_1 \frac{Y}{2} B_\mu\,, \tag{2.4}$$

where g_1, g_2, g_3 respectively are the $U(1)_Y$, $SU(2)_L$, $SU(3)_C$ couplings; the Gell-Mann matrices λ^a are the generators of $SU(3)_C$, the Pauli matrices σ^i are the generators of $SU(2)_L$, and Y is the generator of $U(1)_Y$. The generator $I^3 \equiv \frac{\sigma^3}{2}$ defines the *weak isospin* of a field. A $SU(2)_L$-triplet has components with $I^3 = 0, \pm 1$; a $SU(2)_L$-doublet has $I^3 = \pm\frac{1}{2}$, and a singlet has $I^3 = 0$.

- The fermions of the SM, with spin $\frac{1}{2}$. They are *quarks*, that are charged under $SU(3)_c$ and then said to have *colour*, and *leptons*, that are colourless. They can be left-handed and charged under $SU(2)_L$, or right-handed $SU(2)_L$-singlets. There are three generations of fermions with the same quantum numbers. Each quark generation is made-up by left-handed up- and down-type quarks forming an $SU(2)_L$-doublet $Q_q = (u_L,\, d_L)_q$. Furthermore, there is the right-handed up-type quark $u_{q,\,R}$ and the down-type quark $d_{q,\,R}$, that are $SU(2)_L$-singlets. The three generations of leptons, instead, are formed by a left-handed $SU(2)_L$-doublet $\ell_l = (\nu_L,\, e_L)_l$ and by a right-handed down-type lepton $e_{l,\,R}$. The right-handed neutrinos, *i.e.* the right-handed up-type leptons, are not embedded in the SM. The kinetic terms for SM fermions are given by

$$\mathcal{L}_F = iQ_q^\dagger \not{D}\, Q_q + i\bar{u}_q \not{D}\, \bar{u}_q^\dagger + i\bar{d}_q \not{D}\, \bar{d}_q^\dagger + i\ell_l^\dagger \not{D}\, \ell_l + i\bar{e}_l \not{D}\, \bar{e}_l^\dagger \,, \tag{2.5}$$

  where $\bar{u}_q \equiv u_{Rq}^\dagger$, $\bar{d}_q \equiv d_{Rq}^\dagger$, $\bar{e}_l \equiv e_{Rl}^\dagger$, and $\not{D} = \gamma_D^\mu D_\mu$ denote the contraction of the covariant derivative with the Dirac matrices γ_D^μ.

- The spin-0 Higgs field ϕ. It is a complex scalar $SU(2)_L$-doublet $\phi = \left(H^+\,, H^0\right)$, whose kinetic terms and scalar potential read

$$\mathcal{L}_H = (D_\mu\phi)^\dagger(D^\mu\phi) - \mathcal{V}(\phi) = (D_\mu\phi)^\dagger(D^\mu\phi) - m^2(\phi^\dagger\phi) - \lambda(\phi^\dagger\phi)^2 \,. \tag{2.6}$$

  $\mathcal{V}(\phi)$ is a general scalar potential respecting gauge invariance and renormalisability. In order to grant spontaneous symmetry breaking with a potential bounded from below, λ is positive and $m^2 < 0$. In order to generate fermion masses through the Higgs mechanism, the Higgs interacts with the SM fermions through the Yukawa terms:

$$\mathcal{L}_Y = -\bar{e}\,\mathbf{y_e}(\phi^\dagger\ \ell) - \bar{d}\,\mathbf{y_d}(\phi^\dagger\ \ Q) - \bar{u}\,\mathbf{y_u}(\overline{\phi}^\dagger\ \ Q) + h.c.\,, \tag{2.7}$$

  where $\overline{\phi} = i\sigma_2\phi^*$. The Yukawa matrices $\mathbf{y_e}$, $\mathbf{y_u}$, $\mathbf{y_d}$ are complex 3×3 matrices in the lepton and quark generation spaces, and ℓ, e, Q, u, d, are 3-vectors.

The SM Lagrangian density, or simply Lagrangian, can be resumed as

$$\mathcal{L}_{\rm SM} = \mathcal{L}_V + \mathcal{L}_F + \mathcal{L}_H + \mathcal{L}_Y \,. \tag{2.8}$$

$\mathcal{L}_{\rm SM}$ is invariant under the SM gauge symmetry, under the special Poincaré group $\mathbf{R}^{(1,3)}$, under the special Lorentz group $SO(1,3)$, and also under the accidental global symmetries $\frac{B}{3} - \ell_l$, corresponding to a simultaneous phase-multiplication on the quarks and on the l-generation leptons.

In order to quantise the SM, one should follow the Faddeev-Popov procedure [53]. Gauge fixing terms shall be added to the Lagrangian density eq. (2.8), together with kinetic and gauge interaction terms for the *ghosts*, that are non-physical auxiliary fields, vanishing on-shell. In the physical quantities the dependence on the gauge fixing disappears, as well as contributions from ghosts. For more details we refer to the standard textbook [54].

2.1.2 Electroweak symmetry breaking

The Higgs scalar potential $\mathcal{V}(\phi)$ leads to the spontaneous symmetry-breaking $SU(2)_L \otimes U(1)_Y \to U(1)_{\text{em}}$. This happens through the Higgs mechanism, that is required to explain the experimentally observed masses of the W, Z gauge bosons and of the fermions. In fact, the SM Lagrangian density eq. (2.8) describes massless gauge bosons because their masses are protected by gauge symmetry. The mass of a fermion ψ, instead, is prevented by the chiral symmetry $\psi \to \exp[i\phi\gamma_5]\,\psi$. The scalar potential in eq. (2.6) is minimised by $\langle\phi\rangle = \left(0, \frac{v}{\sqrt{2}}\right) \neq 0$, where $v = \sqrt{-m^2/\lambda}$ is the Higgs vacuum expectation value (vev). Exploiting electroweak gauge invariance we can parametrise ϕ as:

$$\phi = \frac{1}{\sqrt{2}}\, e^{i\frac{\xi^a \sigma^a}{v}} \begin{pmatrix} 0 \\ v + H \end{pmatrix}. \tag{2.9}$$

The Higgs field ϕ has 4 real components: H and ξ^a ($a = 1, 2, 3$). The ξ^a components represent the Goldstone mode of the SM symmetry breaking. We adopt the *unitary gauge*, with $\xi^a = 0$, where the Goldstone modes are rotated away by a unitary transformation, such that they do not appear explicitly anymore.

Finally, we expand $\mathcal{L}_H + \mathcal{L}_Y$ around the minimum, substituting eq. (2.9) in eqs. (2.6) and (2.7), in order to derive the masses of all the SM particles. The scalar potential becomes:

$$\mathcal{V}(H) = cost + \lambda v^2 H^2 + \lambda v H^3 + \frac{1}{4}\lambda H^4\,, \tag{2.10}$$

so the Higgs H gets the mass $m_H^2 = 2\lambda v^2$.

At the minimum of the potential the gauge symmetry $SU(2)_L \otimes U(1)_Y$ is broken, and the following linear combinations of W_μ^a, B_μ are the mass eigenstates of the gauge boson sector:

$$W^\pm = \frac{1}{\sqrt{2}}\left(W^1 \mp iW^2\right), \tag{2.11}$$

$$Z = \cos\theta_W W^3 - \sin\theta_W B\,, \tag{2.12}$$

$$\gamma = \sin\theta_W W^3 + \cos\theta_W B\,. \tag{2.13}$$

At the tree-level, the weak mixing (*Weinberg*) angle is defined by $\sin\theta_W = \frac{g_1}{\sqrt{g_1^2+g_2^2}}$ and

Fields	labels	spin	$SU(3)_C \otimes U(1)_{\rm EM}$
Gluons	g^i	1	$(\mathbf{8}, 0)$
W bosons	$W^\pm$	1	$(\mathbf{1}, \pm 1)$
Photon, Z boson	γ, Z	1	$(\mathbf{1}, 0)$
Quarks	u_q	$\frac{1}{2}$	$(\mathbf{3}, \frac{2}{3})$
	d_q	$\frac{1}{2}$	$(\bar{\mathbf{3}}, -\frac{1}{3})$
Leptons	ν_l	$\frac{1}{2}$	$(\mathbf{1}, 0)$
	e_l	$\frac{1}{2}$	$(\mathbf{1}, -1)$
Higgs	H	0	$(\mathbf{1}, 0)$

Table 2.2: Standard Model particle content with the gauge transformation properties after electroweak symmetry breaking; $i = 1, \ldots, 3$, $a = 1, 2, 3$, $q = 1, 2, 3$, and $l = e$, μ, τ.

$\cos\theta_W = \frac{g_2}{\sqrt{g_1^2+g_2^2}}$.[1] The masses of the gauge bosons are:

$$m_W = \frac{g_2}{2} v\,, \quad m_Z = \frac{\sqrt{g_1^2 + g_2^2}}{2} v\,, \quad m_\gamma = 0\,. \tag{2.14}$$

Therefore we conclude that $v = \left(G_F\sqrt{2}\right)^{-\frac{1}{2}} \simeq 246.22$ GeV, where G_F is the Fermi constant. To the massless photon γ corresponds the remaining unbroken electromagnetic gauge symmetry $U(1)_{\rm EM}$, with charge $Q_{\rm EM} = I^3 + Y$ and coupling constant $g_{\rm em}$. The electromagnetic charges in the SM after electroweak breaking are reported in table 2.2. The $W^\pm$ and Z bosons mediate the weak interactions.

Expanding (2.7) around the vacuum, the fermions acquire masses. Excluding neutrinos, after EWSB the left- and right- handed components of a fermion can be wrapped together in a Dirac fermion. Lepton mass eigenstates are obtained diagonalising the Yukawa matrices, while the quark mass eigenstates can be derived by using a unitary transformation

$$\psi_L^f \to V_L^f\, \psi_L^f\,, \quad \psi_L^f \to V_R^f\, \psi_R^f\,, \tag{2.15}$$

where $V_L^f\,, V_R^f$ are 3×3 matrices in the generation space, with f labelling the type of quark: up or down. We can then write the fermion mass matrices as

$$\mathbf{m_u} = \frac{v}{\sqrt{2}} (V_L^u)^\dagger \mathbf{y_u} V_R^u\,, \quad \mathbf{m_d} = \frac{v}{\sqrt{2}} (V_L^d)^\dagger \mathbf{y_d} V_R^d\,, \quad \mathbf{m_e} = \frac{v}{\sqrt{2}} \mathbf{y_e}\,, \quad \mathbf{m}_\nu = 0\,. \tag{2.16}$$

We refer to the mixing matrix $V_{\rm CKM} = (V_L^u)^\dagger V_L^d$ as the *Cabibbo-Kobayashi-Maskawa* matrix. An analogue mixing matrix for leptons, the *Pontecorvo-Maki-Nakagawa-Saki* matrix $U_{\rm PMNS}$,

[1] Each of the new massive gauge bosons is said to have acquired mass because it has *eaten* a Goldstone boson, that has become its longitudinal component.

may also be considered, especially in the light of the observation of neutrino oscillations implying neutrino masses [55]. However, in this thesis we will stick to the established version of the SM, and we consider neutrinos as massless.

2.1.3 Motivations for a Physics Beyond the Standard Model

The SM has been widely tested at the LEP, the Tevatron, and the LHC showing no compelling discrepancies with the experiment up to the scale of electroweak interactions $\Lambda_{\text{ew}} \sim 10^2$ GeV. It is known, however, that the SM cannot be the ultimate theory for Particle Physics for a series of reasons, among which are the following.

Gravity, the Planck scale and the Hierarchy Problem

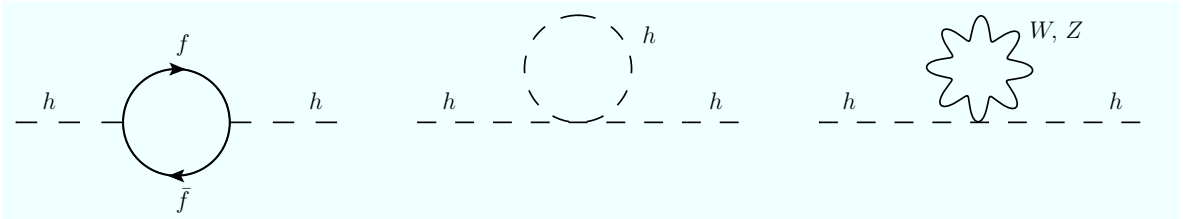

Figure 2.1: Feynman diagrams of the quadratically divergent 1-loop corrections to the Higgs boson mass in the SM.

The SM does not include any description of gravitational interactions. Therefore the SM can be seen as an effective field theory of quantum interactions valid up to the scale at which quantum gravitational effects are relevant for particle physics, *i.e.* the Planck scale $\Lambda_P \sim 10^{19}$ GeV. If new physics enters at a scale $\Lambda \leq \Lambda_P$, like the scale of unification of gauge couplings $\Lambda_{\text{GUT}} \sim 10^{15}$ GeV, this new scale sets the validity bound of the SM.
The observed SM-Higgs mass can be written as,

$$m_h^2 = m_{h,\,0}^2 + \delta m_{h,\,\text{loop}}^2 \,, \tag{2.17}$$

where $m_{h,\,0}^2$ is the bare squared mass, a free parameter, and $\delta m_{h,\,\text{loop}}^2$ represents the radiative corrections. The Higgs mass in the SM is not "protected" by any symmetry that can prevent large radiative corrections, contrarily to gauge bosons and fermions, whose masses are protected in the SM by gauge and chiral symmetries, respectively. In particular, the Higgs mass squared receives quadratically divergent contributions from the graphs in fig. 2.1, the most important of which is the one coming from the top loop. Taking into account the leading terms, the radiative corrections to the Higgs mass squared, cut off at the highest scale of the theory Λ, are [56]

$$\delta m_{h,\,\text{loop}}^2 = \frac{3\Lambda^2}{8\pi^2 v^2}\left[-4m_t^2 + m_h^2 + 2m_W^2 + m_Z^2\right] . \tag{2.18}$$

If we take $\Lambda = \Lambda_P$, then $\delta m_{h,\,\text{loop}}^2 \sim 10^{38}$ GeV^2. Therefore in order to recover the observed physical Higgs mass $m_h \simeq 125.5$ GeV, an enormous cancellation between the bare mass $m_{h,\,0}^2$

and $\delta m^2_{h,\,\text{loop}}$ is required. This results in a huge fine-tuning of 34 orders of magnitude to keep the Higgs mass at the electroweak scale.

This issue contrasts with the idea of naturalness of the model describing physical interactions, and it is dubbed as the *Hierarchy Problem*. The latter is not a real "problem" of the theory, but rather an aesthetic question, and it is arguably seen as the main motivation for introducing supersymmetry or composite-Higgs models. We will follow it as guiding principle in the rest of this thesis.

Baryogenesis

The origin of matter-antimatter asymmetry is unknown and it is believed to be a consequence of *baryogenesis*, the generation of an asymmetry between the number of baryons and antibaryons in the Universe. Baryogenesis can happen if the three Sakharov conditions [57] are fulfilled: (i) first that there must be a process that violates the baryon number B, (ii) second, that $\mathcal{C}$ and $\mathcal{CP}$ symmetries should be violated, (iii) third, that there has been a moment of non equilibrium in the universe. The SM satisfies these conditions in a quantitatively insufficient way by the CKM-matrix [58] and cannot explain the matter-antimatter asymmetry that has been observed experimentally.

Dark matter and Dark energy

From astrophysical and cosmological observations we know that the visible matter and light account only for a small amount of the energy in the universe. About the 68% of it is made up of the so called dark energy, and the 27% of dark matter (DM). DM is only weakly interacting to ordinary matter and it motivated because it can offer a correct description of galaxy-rotation, gravitational lensing etc. [59, 60]. The SM does not offer any reliable dark matter candidate, which currently is considered most likely to be a weakly interacting massive particle (WIMP) [61].

Neutrino masses

In the original formulation of the SM, neutrinos are considered to be massless. However, the observation of neutrino oscillations between neutrino states [55] implies that neutrinos should have masses. The nature of this masses, either Dirac-like or Majorana-like, is currently under probe at the GERDA experiment studying double β-decay [62]. Light neutrinos alone can only explain a small fraction of dark matter. Experimental limits from large-scale structure formation, in fact, suggest that light neutrino dark matter would be too hot [61].

Other questions, like the origin of flavour hierarchy, usually advocate for an explanation in a higher energy completion theory, as well.

2.2 Supersymmetry

Supersymmetry is a space-time symmetry that connects commuting, bosonic fields with anticommuting, fermionic fields. It has the very attracting property of protecting the scalar masses from quadratic divergences.

Similarly to the SM, the formulation of the theory of supersymmetry is the result of a series of independent studies that ultimately merged in a coherent picture. The idea of a symmetry between bosonic and fermionic degrees of freedom first appeared in the context of hadron physics by Miyazawa [24] and string theory by Ramond [25], Neveu and Schwarz [26], and Gervais and Sakita [27]. In the meanwhile, the Poincaré algebra, embedding the concept of spin, was extended to include four anticommuting spinor generators, *i.e.* the *supercharges*, in a first 4d-supersymmetry theory of massive spinors and scalars [28]. Shortly afterwards, nonlinear realisations of supersymmetry were proposed, giving birth to supergravity [63].

It has then been shown that supersymmetry generators have to mix with the transformations of the Poincaré group since supersymmetry is not an internal symmetry [29]. Supersymmetry, in fact, is the only possible additional symmetry of the S-matrix avoiding the Coleman-Mandula no-go theorem in a 4d-quantum field theory [64]. This was shown by the Haag-Łopuszański-Sohnius theorem [65], which extended the previous theorem to graded algebras, a class that includes the *Lie-superalgebra* of supersymmetry.

Only in a later phase, with the development of the minimal supersymmetric Standard Model (MSSM) [66], supersymmetry was considered as a concrete solution for the Hierarchy problem, the latter becoming its first theoretical and phenomenological motivation.

2.2.1 Supersymmetry algebra

Supersymmetry extends the Poincaré group by adding N anticommuting spin-$\frac{1}{2}$ operators, that can be written as Weyl spinors Q_α, $Q^{\dagger\,\dot{\alpha}}$, where $\alpha, \dot{\alpha} = 1, 2$ are spinor indices. These operators are fermionic, therefore a supersymmetry transformation acts sending a bosonic state into a fermionic state and vice versa, according to the spin-statistics theorem [50]. The Lie superalgebra for $N = 1$ supersymmetry reads:

$$\{Q_\alpha, Q^\dagger_{\dot{\alpha}}\} = -2\sigma^\mu_{\alpha\dot{\alpha}} P_\mu, \tag{2.19}$$

$$\{Q_\alpha, Q_\beta\} = \{Q^\dagger_{\dot{\alpha}}, Q^\dagger_{\dot{\beta}}\} = 0, \tag{2.20}$$

$$[P^\mu, Q_\alpha] = [P^\mu, Q^\dagger_{\dot{\alpha}}] = 0, \tag{2.21}$$

where P^μ is the four-momentum generator of space-time translations. A fermion and a boson related by $Q^{(\dagger)}$ are said to be *superpartners* and fall together in an irreducible representation of the supersymmetry algebra, called *supermultiplet*.

Any combination of Q and $Q^\dagger$ sends a state into another with the same momentum p^μ, *cf.* eq. (2.21), such that a subspace of states with equal momentum p^μ is closed under the action of supersymmetry generators. Therefore for every finite representation of the supersymmetry

algebra one can define a trace over the states of the subspace [48],

$$\sum_i \langle i|(-1)^{n_F}\{Q, Q^\dagger\}|i\rangle \equiv \mathrm{Tr}[(-1)^{n_F}\{Q, Q^\dagger\}]\,, \tag{2.22}$$

where on the right side the action on $|i\rangle$ is omitted. The fermion number operator $(-1)^{n_F}$, where $n_F = 2 \times$ spin, has eigenvalues $+1$ on bosonic states and -1 on fermionic states, and anticommutes with supersymmetry generators. Therefore we have

$$\mathrm{Tr}[(-1)^{n_F}\{Q, Q^\dagger\}] = 0\,. \tag{2.23}$$

Using eq. (2.19) in eq. (2.23) together with the fact that superpartners have the same momentum eigenvalues, we obtain

$$\mathrm{Tr}[(-1)^{n_F} P^\mu] = p^\mu \mathrm{Tr}[(-1)^{n_F}] = 0\,, \tag{2.24}$$

meaning that a supermultiplet contains the same number of fermionic and bosonic states, *i.e.* degrees of freedom (dofs). From eq.(2.21) we also see that, taking a state $|m\rangle$ with mass m:

$$P^2 Q|m\rangle \overset{(2.21)}{=} QP^2|m\rangle = m^2 Q|m\rangle\,, \tag{2.25}$$

meaning that superpartners have the same mass. Furthermore, since supersymmetric operators commute with all internal symmetries operators, like gauge generators, superpartners have the same gauge numbers.

We can list two types of supermultiplets in a renormalisable supersymmetric theory. *Chiral supermultiplets* are made-up by a complex scalar ϕ and by a Weyl fermion ψ as, for example, a quark. *Vector supermultiplets* are made-up by a (massless) Weyl fermion λ^a and by a (massless) vector boson A^a_μ, like gauge bosons are.[2] In order to preserve an equal number of bosonic and fermionic dofs also off-shell, an auxiliary non-dynamical scalar field F (D^a) is added to the chiral (vector) supermultiplet. F and D^a disappear on-shell, integrated out by the equations of motion from the Lagrangian.

If a supersymmetric extension of the SM describes Nature, supersymmetry at some scale should be broken. The superpartners, indeed, should have the same masses of the corresponding SM particles. Not having observed yet superpartners, a mass difference with the SM particles needs to be explained.

It is often useful to adopt the *superspace* formalism, according to which fermion and boson superpartners are components of a *superfield* in the *superspace*. We denote with $\hat{\Phi}$ a chiral superfield and with $\hat{V}$ a vector superfield, see appendix A for more details.

[2] Other combinations of single-particle states could be lead back to combinations of chiral and gauge supermultiplets. Furthermore, including in a supersymmetric theory a description of gravity, one obtains a supergravity theory that is non-renormalisable. Here, one should consider also the *supergravity multiplet* made by a spin-2 graviton together with its spin-$\frac{3}{2}$ partner gravitino, both carrying 2 helicity states when supersymmetry is unbroken.

2.2.2 Cancellation of quadratic divergences

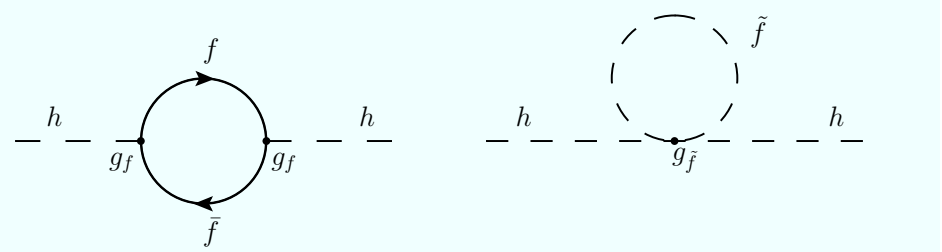

Figure 2.2: Quadratically divergent 1-loop diagrams of the Higgs propagator from a fermion f and its superpartner $\tilde{f}$.

Fermion and boson loops give quadratically divergent contributions to scalar propagators with opposite sign. Since supersymmetry relates bosons and fermions with the same masses and gauge numbers, the corresponding radiative corrections cancel exactly. This offers a concrete solution to the Hierarchy problem within a supersymmetric extension of the SM. In particular, the contribution to the Higgs mass by a fermion f and its scalar superpartner $\tilde{f}$, *cf.* fig. 2.2, reads:

$$\delta m_h^2 = -\frac{g_f^2}{8\pi}\Lambda^2 + \frac{g_{\tilde{f}}}{8\pi}\Lambda^2 + \text{logarithmic contributions}\ . \tag{2.26}$$

Ensuring that $g_f^2 = g_{\tilde{f}}$, as supersymmetry dictates, grants the exact cancellation of quadratic divergences. The subleading logarithmic contributions cancel if supersymmetry is not broken, as it happens, instead, when supersymmetry breaking masses are introduced such that $m_f \neq m_{\tilde{f}}$. Since SUSY must be broken in order to explain the non observation of superpartners, this must be done softly, i.e. preserving the cancellation of quadratic divergences.

2.2.3 Supersymmetric lagrangian and soft SUSY-breaking terms

We give here the general supersymmetric Lagrangian for a supersymmetric theory of i chiral superfields $\hat{\Phi}_i$, with scalar and fermionic components ϕ_i and ψ_i, and of a vector superfield $\hat{V}$, with fermionic and bosonic components λ^a and A_μ^a, where a is the gauge adjoint index. We can write, following [48, 49],[3]

$$\mathcal{L}_{\text{general SUSY}} = \mathcal{L}_{\text{chiral}} + \mathcal{L}_{\text{vector}} + \mathcal{L}_{\text{chiral-vector interactions}} \tag{2.27}$$

$$= D^\mu \phi^{*i} D_\mu \phi_i + i\psi^{\dagger i}\bar{\sigma}^\mu D_\mu \psi_i + F^{*\,i} F_i + \left(-\frac{1}{2}\mathcal{W}^{ij}\psi_i\psi_j + \mathcal{W}^i F_i + \text{c.c.}\right) \tag{2.28}$$

$$- \frac{1}{4}F^a_{\mu\nu}F^{\mu\nu a} + i\lambda^{\dagger a}\bar{\sigma}^\mu D_\mu \lambda^a + \frac{1}{2}D^a D^a \tag{2.29}$$

$$- \sqrt{2}g[(\phi_i^* T^a \psi_i)\lambda^a + \lambda^{\dagger a}(\psi_i^\dagger T^a \phi_i)] + g(\phi_i^* T^a \phi_i)D^a\ , \tag{2.30}$$

[3] We define the covariant derivative for ϕ_i, ψ_i as $D_\mu = \partial_\mu + igA_\mu^a T^a$, where T^a is the generator of gauge transformations. The covariant derivative for λ^a takes the form $D_\mu \lambda^a = \partial_\mu \lambda^a - g f^{abc} A_\mu^b \lambda^c$, where f^{abc} are the structure constants.

where the i, j, $k = 1, \ldots, n$ indices label the chiral supermultiplets. $\mathcal{W}^i$, $\mathcal{W}^{ij}$ are respectively defined as:

$$\mathcal{W}^i = \left(\frac{\partial \mathcal{W}}{\partial \hat{\Phi}_i}\right)_{\hat{\Phi}_i \to \phi_i}, \qquad \mathcal{W}^{ij} = \left(\frac{\partial^2 \mathcal{W}}{\partial \hat{\Phi}_i \partial \hat{\Phi}_j}\right)_{\hat{\Phi}_{i,j} \to \phi_{i,j}}. \tag{2.31}$$

$\mathcal{W}$, called the *superpotential*, is an holomorphic function of the chiral superfields $\hat{\Phi}_i$, which in $\mathcal{W}^i$ and $\mathcal{W}^{ij}$ should be substituted by their scalar components ϕ_i. The most general expression for $\mathcal{W}$ is given by

$$\mathcal{W} = L^i \hat{\Phi}_i + \frac{1}{2} M^{ij} \hat{\Phi}_i \hat{\Phi}_j + \frac{1}{6} y^{ijk} \hat{\Phi}_i \hat{\Phi}_j \hat{\Phi}_k \,, \tag{2.32}$$

where $L_i \neq 0$ only if $\hat{\Phi}_i$ is a gauge singlet; M^{ij} is a symmetric mass matrix; y^{ijk} is a Yukawa coupling totally symmetric in i, j, k.

The auxiliary fields are integrated out through their equation of motions, that read

$$F_i = -\mathcal{W}_i^* \,, \qquad D^a = -g(\phi_i^* T^a \phi_i) \,. \tag{2.33}$$

We can then write down the scalar potential as a sum of F- and D-terms:

$$\mathcal{V}(\phi, \phi^*) = F^{*\,i} F_i + \frac{1}{2} D^a D^a = \underbrace{\mathcal{W}_i^* \mathcal{W}^i}_{F-\text{terms}} + \underbrace{\frac{1}{2} g^2 (\phi_i^* T^a \phi_i)^2}_{D-\text{terms}}, \tag{2.34}$$

where we denote as F-terms the terms generated from the superpotential and D-terms the ones originated by the gauge interactions of chiral scalars. In order to parametrise our ignorance about supersymmetry breaking, we need a general and explicit parametrisation of soft supersymmetry breaking (SSB). The following terms should then be added to the Lagrangian [48, 67]:

$$\mathcal{L}_{\text{soft}} = -\left(\frac{1}{6} a^{ijk} \phi_i \phi_j \phi_k + \frac{1}{2} b^{ij} \phi_i \phi_j + t^i \phi_i + \frac{1}{2} M_a (\lambda^a)^2 + \text{c.c.}\right) - (m^2)^i_j \phi^{*j} \phi_i \tag{2.35}$$

$$- \frac{1}{2} c_i^{jk} \phi^{*i} \phi_j \phi_k + \text{c.c.} \,. \tag{2.36}$$

M_a and $(m^2)^i_j$ are, respectively, the gaugino and the scalar soft squared masses; a^{ijk}, b^{ij}, t^i are allowed by gauge invariance if the corresponding supersymmetric parameters y^{ijk}, M^{ij}, L^i are allowed as well. The c_i^{jk}-term can be written in the presence of gauge singlets.

2.3 The minimal supersymmetric Standard Model

The minimal supersymmetric extension of the SM (MSSM) associates a superpartner to each SM particle: spin-0 squarks and sleptons respectively to quark and leptons, spin-$\frac{1}{2}$ gauginos to gauge bosons, spin-$\frac{1}{2}$ higgsinos to Higgs doublets. The gauge group is the same, $SU(3)_C \otimes SU(2)_L \otimes U(1)_Y$. A substantial difference with the SM is that there are two Higgs doublets H_u and H_d instead of just one. The reason is to avoid an electroweak anomaly and therefore to provide masses to up- and down-type fields, respectively. The particle content before electroweak symmetry breaking is resumed in table 2.3.

Quarks-squarks	**Spin 0**	**Spin 1/2**	$\boldsymbol{SU(3)_C \otimes SU(2)_L \otimes U(1)_Y}$
$\hat{Q}_q$	$\tilde{Q} = \left(\tilde{u}_L\,, \tilde{d}_L\right)$	$(u_L\,, d_L)$	$(\mathbf{3}, \mathbf{2}, \frac{1}{6})$
$\hat{\bar{u}}_q$	$\tilde{u}^*_R$	$u^\dagger_R$	$(\bar{\mathbf{3}}, \mathbf{1}, -\frac{2}{3})$
$\hat{\bar{d}}_q$	$\tilde{d}^*_R$	$d^\dagger_R$	$(\bar{\mathbf{3}}, \mathbf{1}, \frac{1}{3})$
Leptons-sleptons	**Spin 0**	**Spin 1/2**	$\boldsymbol{SU(3)_C \otimes SU(2)_L \otimes U(1)_Y}$
$\hat{\ell}_l$	$\tilde{\ell} = (\tilde{\nu}\,, \tilde{e}_L)$	$(\nu\,, e_L)$	$(\mathbf{1}, \mathbf{2}, -\frac{1}{2})$
$\hat{\bar{e}}_l$	$\tilde{e}^*_R$	$e^\dagger_R$	$(\mathbf{1}, \mathbf{1}, 1)$
Higgs-higgsinos	**Spin 0**	**Spin 1/2**	$\boldsymbol{SU(3)_C \otimes SU(2)_L \otimes U(1)_Y}$
$\hat{H}_u$	$\left(H^+_u\,, H^0_u\right)$	$\tilde{H}_u = \left(\tilde{H}^+_u\,, \tilde{H}^0_u\right)$	$(\mathbf{1}, \mathbf{2}, +\frac{1}{2})$
$\hat{H}_d$	$\left(H^0_d\,, H^-_d\right)$	$\tilde{H}_d = \left(\tilde{H}^0_d\,, \tilde{H}^-_d\right)$	$(\mathbf{1}, \mathbf{2}, -\frac{1}{2})$
Gauge supermultiplets	**Spin $\frac{1}{2}$**	**Spin 1**	$\boldsymbol{SU(3)_C \otimes SU(2)_L \otimes U(1)_Y}$
Gluinos-gluons	$\tilde{g}$	g	$(\mathbf{8}, \mathbf{1}, 0)$
Winos-Ws	$\tilde{W}^\pm,\ \tilde{W}^3$	$W^\pm,\ W^3$	$(\mathbf{1}, \mathbf{3}, 0)$
Bino-B	$\tilde{B}^0$	B^0	$(\mathbf{1}, \mathbf{1}, 0)$

Table 2.3: MSSM superfield content with the gauge transformation properties before electroweak symmetry breaking; $i = 1, \ldots, 3$, $a = 1, 2, 3$, $q = u, c, t$, and $l = e,\ \mu,\ \tau$.

The superpotential describing the chiral superfield interactions is given by

$$\mathcal{W}_{\text{MSSM}} = \hat{\bar{u}}\mathbf{y_u}\hat{Q} \cdot \hat{H}_u - \hat{\bar{d}}\mathbf{y_d}\hat{Q} \cdot \hat{H}_d - \hat{\bar{e}}\mathbf{y_e}\hat{\ell} \cdot \hat{H}_d + \mu\hat{H}_u \cdot \hat{H}_d\,, \tag{2.37}$$

where we denote with $A \cdot B = A^\alpha \epsilon_{\alpha\beta} B^\beta$ the contraction with the Levi-Civita tensor ϵ with $SU(2)_L$-indices α and β. Gauge invariance would in principle allow to add in $\mathcal{W}_{\text{MSSM}}$ terms with an odd number either of quark or leptonic superfields. These terms would lead to lepton or baryon number violation, so far never observed, and in particular proton decay would be possible, in contrast with data from Super-Kamiokande [68].

In order to avoid this inconvenience, it is requested to the MSSM Lagrangian to respect *R-parity*, a discrete symmetry that does not permit these additional terms. According to this symmetry, to each ordinary SM particle an R-charge equal to $+1$ is assigned while to sparticles it is assigned -1. The R-charge of each term in the Lagrangian is defined as the product of the R-charges of the interacting fields: R-parity is preserved if the total R is equal to 1. Processes that lead to proton decay are not allowed by R-parity.

The introduction of R-parity symmetry has several phenomenologically interesting consequences since, if conserved, any interaction vertex must have an even number of sparticles. First, sparticles may only be produced in pairs. For the same reason, a sparticle must decay into another sparticle, such that the decay chain must end in the lightest-sparticle (LSP) that provides a valid dark matter candidate. The LSP experimentally results in missing energy, a

characteristic signature of SUSY at colliders.

In the light of gauge invariance and R-parity, the most general MSSM soft Lagrangian is

$$\begin{aligned}
\mathcal{L}_{\text{soft}}^{\text{MSSM}} = \; & -\tfrac{1}{2}M_1\,\tilde{B}\tilde{B} - \tfrac{1}{2}M_2\,\tilde{W}\tilde{W} - \tfrac{1}{2}M_3\,\tilde{g}\tilde{g} + \text{c.c.} && \text{gaugino mass terms} \\
& -\tilde{\bar{u}}\mathbf{A_u}\tilde{Q}H_u + \tilde{\bar{d}}\mathbf{A_d}\tilde{Q}H_d + \tilde{\bar{e}}\mathbf{A_e}\tilde{L}H_d + \text{c.c.} && A\text{-terms} \\
& -\mathbf{M_Q^2}|\tilde{Q}^2| - \mathbf{M_u^2}|\tilde{\bar{u}}^2| - \mathbf{M_d^2}|\tilde{\bar{d}}_R^2| && \text{squark mass terms} \\
& -\mathbf{M_\ell^2}|\tilde{\ell}^2| - \mathbf{M_e^2}|\tilde{\bar{e}}^2| && \text{slepton mass terms} \\
& -m_{H_u}^2 H_u^* H_u - m_{H_d}^2 H_d^* H_d && \text{Higgs mass terms} \\
& -B_\mu H_u H_d + \text{c.c.} && b\text{-terms}
\end{aligned} \tag{2.38}$$

where $\mathbf{A_u}$, $\mathbf{A_d}$, $\mathbf{M_Q^2}$, $\mathbf{M_u^2}$, $\mathbf{M_d^2}$ are 3×3 matrices in quark generation space and $\mathbf{A_e}$, $\mathbf{M_\ell^2}$, $\mathbf{M_e^2}$ in the lepton generation space. In the general MSSM lagrangian, taking into account generation mixing and complex phases, there are 105 soft parameters to be added to the 19 SM parameters, resulting in dimensionally huge parameter space that cannot be trivially studied. It is then of common use to restrict phenomenological studies on particular low-dimensional manifolds of the general MSSM parameter space, often advocating plausible symmetries and simplifying assumptions. Example models are minimal supergravity (mSUGRA) [69] and the constrained MSSM (CMSSM) [70]. Universal boundary conditions are assumed in these latter models, that are parametrised only by:

$$m_0,\; m_{1/2},\; A_0,\; \tan\beta,\; \text{sign}(\mu)\,, \tag{2.39}$$

where m_0, $m_{1/2}$, A_0 respectively are the universal scalar mass, gaugino mass, and trilinear coupling at the GUT scale.

2.3.1 EWSB and the Higgs, chargino, and neutralino sectors

As previously explained, a minimal supersymmetric extension of the SM needs two Higgs $SU(2)_L$-doublets H_u, H_d to avoid gauge anomalies. The extended Higgs sector is described by the scalar potential

$$\begin{aligned}
\mathcal{V}_{\text{MSSM}} = & + (|\mu|^2 + m_{H_u}^2)|H_u|^2 + (|\mu|^2 + m_{H_d}^2)|H_d|^2 + [B_\mu H_u \epsilon H_d + \text{c.c.}] \\
& + \frac{1}{8}(g_1^2 + g_2^2)(|H_u|^2 - |H_d|^2)^2 + \frac{1}{2}g_2^2|H_u^\dagger H_d|^2 .
\end{aligned} \tag{2.40}$$

The up- and down-Higgs doublets are written in terms of their electromagnetic components $H_u = (H_u^+, H_u^0)\,, \quad H_d = (H_d^0, H_d^-)$, such that $H_u\epsilon H_d = H_u^+ H_d^- - H_u^0 H_d^0$ and $H_{u/d}^+ = H_{u/d}^{-\,*}$. The minimum of $\mathcal{V}_{\text{MSSM}}$ triggers electroweak symmetry breaking $SU(2)_L \otimes U(1)_Y \to U(1)_{\text{em}}$. We define the neutral Higgs components, expanded around their vevs v_u, v_d as

$$H_u^0 = \frac{v_u}{\sqrt{2}} + \frac{1}{\sqrt{2}}\left(\text{Re}H_u^0 + i\text{Im}H_u^0\right)\,, \quad H_d^0 = \frac{v_d}{\sqrt{2}} + \frac{1}{\sqrt{2}}\left(\text{Re}H_d^0 + i\text{Im}H_d^0\right)\,, \tag{2.41}$$

such that we may write [71]

$$v^2 \equiv v_u^2 + v_d^2 \simeq (246\text{ GeV})^2\,, \quad \tan\beta \equiv \frac{v_u}{v_d}\,. \tag{2.42}$$

B_μ can be chosen to be real. The minimisation conditions (at tree level) can be written as

$$\sin(2\beta) = \frac{2B_\mu}{m_{H_u}^2 + m_{H_d}^2 + 2|\mu|^2}\,, \tag{2.43}$$

$$m_Z^2 = \frac{|m_{H_d}^2 - m_{H_u}^2|}{\sqrt{1-\sin^2(2\beta)}} - m_{H_u}^2 - m_{H_d}^2 - 2|\mu|^2\,. \tag{2.44}$$

From eq. (2.44) we can see that $m_{H_d}^2$, $m_{H_u}^2$ cannot be equal and in particular not both null, meaning that soft SUSY is needed for explaining electroweak symmetry breaking in the MSSM. This should be true at the weak scale: the difference between $m_{H_d}^2$, $m_{H_u}^2$ can be also due only to the running from a higher scale. In order to avoid large and unnatural cancellations, soft parameters are expected to be at the weak scale, see eqs. (2.43) and (2.44).

In the SM one physical Higgs h remains after EWSB, and three Goldstone bosons $G^0\,, G^\pm$ are eaten by $W^\pm\,, Z$ that get masses, *cf.* eq. (2.14). In the MSSM, instead, the eight Higgs degrees of freedom mix to give five physical scalar states $h\,, H\,, A^0\,, H^\pm$ and three unphysical Goldstone bosons $G^0\,, G^\pm$, respectively eaten by Z and $W^\pm$. The mass eigenstates are given by the rotations

$$\mathrm{Re}H_u^0\,, \mathrm{Re}H_d^0 \xrightarrow{\alpha} h\,, H \qquad \mathrm{Im}H_u^0\,, \mathrm{Im}H_d^0 \xrightarrow{\beta} A^0\,, G \qquad H_u^\pm\,, H_d^\pm \xrightarrow{\beta} H^\pm\,, G^\pm\,. \tag{2.45}$$

where the angle $-\frac{\pi}{2} < \alpha < 0$ is defined through $\tan 2\alpha = \frac{m_{A^0}^2 + m_Z^2}{m_{A^0}^2 - m_Z^2}\tan 2\beta$. The mass eigenstates h and H are $\mathcal{CP}$-even neutral scalars, A^0 is a $\mathcal{CP}$-odd neutral scalar and H^+, H^- are electrically charged. At the tree level the Higgs masses read

$$m_{h,H}^{2,\,\mathrm{MSSM}} = \frac{1}{2}\left(m_{A^0}^2 + m_Z^2 \mp \sqrt{(m_{A^0}^2 - m_Z^2)^2 + 4m_Z^2 m_{A^0}^2 \sin^2(2\beta)}\right)\,, \tag{2.46}$$

$$m_{A^0}^{2,\,\mathrm{MSSM}} \equiv \frac{2B_\mu}{\sin 2\beta} = 2|\mu|^2 + m_{H_u}^2 + m_{H_d}^2\,, \tag{2.47}$$

$$m_{H^\pm}^{2,\,\mathrm{MSSM}} = m_{A^0}^2 + m_W^2\,. \tag{2.48}$$

The tree level Higgs mass is bounded by

$$m_{h,\,\mathrm{tree}}^2 \leq m_Z^2 \cos^2 2\beta\,, \tag{2.49}$$

requiring large loop corrections to reproduce the measured SM-like Higgs mass at ~ 125.5 GeV. The MSSM Higgs mass squared can be approximated, taking into account one-loop and two-loop leading-log effects, by [51, 72–76],

$$\begin{aligned} m_h^{2\ \mathrm{MSSM}} \simeq\ & m_z^2 \cos^2 2\beta \\ & + \frac{3}{2\pi^2 v^2}\left[m_{t,r}^4\left(\sqrt{m_t M_{\tilde{t}}}\right)\ln\frac{M_{\tilde{t}}^2}{m_t^2} + m_{t,r}^4(M_{\tilde{t}})\frac{X_t^2}{M_{\tilde{t}}^2}\left(1 - \frac{X_t^2}{12M_{\tilde{t}}^2}\right)\right]\,, \end{aligned} \tag{2.50}$$

where $m_{t,r}(\Lambda)$ is the running top mass at the scale Λ and $M_{\tilde{t}}^2 = m_{\tilde{t}_1} m_{\tilde{t}_2}$. Then, $X_t = A_t - \mu^* \cot\beta$, with A_t the stop soft SUSY-breaking trilinear coupling, which quantifies stop

mixing.[4] The formula (2.50) assumes that the left and right soft parameters of the stops, *i.e.* M_{Q_3} and M_{U_3}, are equal.

After EWSB, the electrically charged higgsinos $\tilde{H}^\pm$ mix with the gauginos $\tilde{W}^\pm$ into *charginos*, labelled as $\tilde{\chi}^\pm_{1,2}$. The neutral higgsinos $\tilde{H}^0_u, \tilde{H}^0_d$ mix with $\tilde{W}^3$, $\tilde{B}$ into four *neutralinos*, labelled as $\tilde{\chi}^0_{1,\dots,4}$, where $\tilde{W}^3$, $\tilde{W}^\pm$, $\tilde{H}^\pm$ are defined similarly to W^3, $W^\pm$, $H^\pm$. We write here the mass matrices of MSSM electroweakinos, *i.e.* charginos and neutralinos, that will be useful later in chapter 4.

The tree level chargino mass matrix in the $(\tilde{W}^\pm, \tilde{H}^\pm)$ basis is given by

$$\mathcal{M}_C = \begin{pmatrix} M_2 & \sqrt{2}\, m_Z \cos\theta_W \cos\beta \\ \sqrt{2}\, m_Z \cos\theta_W \sin\beta & \mu \end{pmatrix}, \tag{2.51}$$

straightforward to diagonalise. For later convenience we define the mixing angles $\Phi_{L,R}$:

$$\begin{pmatrix} \tilde{\chi}^-_1 \\ \tilde{\chi}^-_2 \end{pmatrix}_{L,R} = \begin{pmatrix} \cos\Phi_{L,R} & \sin\Phi_{L,R} \\ -\sin\Phi_{L,R} & \cos\Phi_{L,R} \end{pmatrix} \begin{pmatrix} \tilde{W}^- \\ \tilde{H}^- \end{pmatrix}_{L,R}. \tag{2.52}$$

The tree-level MSSM neutralino mass matrix in the basis $(\tilde{B}, \tilde{W}^0, \tilde{H}_d, \tilde{H}_u)$ is:

$$\mathcal{M}_N^{\text{MSSM}} = \begin{pmatrix} M_1 & 0 & -\cos\beta\, s_W m_Z & \sin\beta\, s_W m_Z \\ 0 & M_2 & \cos\beta\, c_W m_Z & -\sin\beta\, c_W m_Z \\ -\cos\beta\, s_W m_Z & \cos\beta\, c_W m_Z & 0 & -\mu \\ \sin\beta\, s_W m_Z & -\sin\beta\, c_W m_Z & -\mu & 0 \end{pmatrix}, \tag{2.53}$$

where we denote $s_W = \sin\theta_W$ and $c_W = \cos\theta_W$. $\mathcal{M}_N^{\text{MSSM}}$ can be diagonalised by a unitary matrix N,

$$N^* \mathcal{M}_N^{\text{MSSM}} N^\dagger = \text{diag}\{m_{\tilde{\chi}^0_1}, \dots, m_{\tilde{\chi}^0_4}\}, \tag{2.54}$$

obtaining the neutralino eigenvectors and their masses

2.3.2 Supersymmetry breaking mechanisms

Planck-scale-mediated supersymmetry breaking

In Planck-scale-mediated supersymmetry breaking models, supersymmetry breaking (SSB) is communicated from a hidden sector to the visible sector through interactions suppressed by the Planck scale Λ_P. This kind of mediation can be done by gravity as in local supersymmetry, *i.e.* *supergravity* (SUGRA). In SUGRA the supergravity multiplet, made by the spin-2 graviton and spin-$\frac{3}{2}$ gravitino, connects the observable particles to a hidden sector. In the hidden sector, SSB takes place through the super Higgs mechanism [77]. SSB is then communicated to the gravitino, which acquires mass $m_{3/2} \sim \langle F \rangle / \Lambda_P$, where F is the SUSY-breaking vev acquired by the fields in the hidden sector, while the graviton remains massless.

[4] In the following we assume μ to be real.

Gauge-mediated supersymmetry breaking

In gauge mediated SUSY breaking (GMSB) models [78], SSB is communicated from a hidden sector via messengers charged under the SM group. Via loop effects the messengers trigger soft SSB in the visible sector. Here, sparticles get soft masses of order $\frac{g_{\mathrm{SM}}^2}{16\pi^2}\frac{F}{M_{\mathrm{mess}}}$, where M_{mess} is the messenger mass. Since the gravitino gets mass $m_{3/2} \sim \langle F\rangle/\Lambda_P$, it can be the LSP if $\Lambda_P \gg M_{\mathrm{mess}}$.

Anomaly-mediated supersymmetry breaking

In anomaly-mediated supersymmetry breaking (AMSB) models, soft masses generated by gravity- or gauge-mediation are suppressed, therefore the soft masses arising from the super-conformal anomaly become important [79, 80]. That is the case when the hidden sector is spacially separated by the visible sector due to extra dimensions. These models, however, present a series of phenomenological problems as, for instance, the presence of tachyonic sleptons.

2.3.3 Goals and problems of the MSSM

We have seen that the MSSM supersymmetrically extends the SM with a minimal particle content. Some important successes of the MSSM are

- **Radiative electroweak symmetry breaking.** Several supersymmetric models with SSB coming from a hidden sector, such as the CMSSM, expect a degenerate scalar spectrum at the scale of the mediators. The scalar spectrum becomes non-degenerate at lower scales due to radiative corrections, *i.e.* through RGE running. These radiative corrections can lead to negative mass squared of a scalar. Therefore they can naturally induce spontaneous symmetry breaking in the visible sector at a scale close to the SSB's one. This mechanism is called radiative electroweak symmetry breaking (REWSB). Its direction strictly depends on the couplings of the model, since contributions to scalar masses from the superpotential terms and those from the gauge interactions have different sign. For a review, see [81].

- **Gauge unification.** The rich fauna of particles introduced by the MSSM substantially modifies the RGE equations of the SM couplings. In particular, a unification of the gauge couplings g_1, g_2, g_3 may be achieved at high scale $\Lambda_{\mathrm{GUT}} \sim 10^{16}$ GeV, with a small imperfection possibly due to threshold corrections for new particles around Λ_{GUT} [82–84].

- **LSP and dark matter.** In the MSSM with R-parity, all sparticle decay chains end into the LSP, that is a stable particle. A neutralino LSP $\tilde{\chi}_1^0$ offers in many MSSM realisations a valid weakly interacting massive particle (WIMP) candidate for Dark Matter [85, 86].

However, the MSSM has some shortcomings too. We are interested in the following:

- **The μ-problem.** To have EWSB, such that the neutral components of both Higgs doublets get non zero vev, a negative soft SUSY-breaking b-term $-B_\mu H_u^0 H_d^0$ in the Higgs scalar potential is needed. Being a dimensionful superpotential parameter, μ could in principle be expected to be at a high scale, as Λ_P or $\Lambda_{\rm GUT}$ with no relation to the aforementioned soft terms. However, rewriting the minimisation conditions (2.43) and (2.44), one can see that μ should be within two orders of magnitude with the soft supersymmetry breaking terms at $M_{\rm SUSY} \sim 10^2$-10^3 GeV in order to have $v \simeq 246$ GeV without large tuning. This issue results in a puzzle, called the *μ-problem* [87], about why a supersymmetric parameter should approximately be within one or two orders of the soft parameters.

  Solutions to this problem introduce a mechanism that would relate SUSY breaking to an effective μ-term, as for example in the NMSSM [88], or with Giudice-Masiero mechanism [89].

- **The Little Hierarchy Problem.** The observed Higgs mass $m_h \simeq 125.5$ GeV is within the theoretical MSSM range ≤ 135 GeV. Nevertheless, the MSSM upper bound on the tree-level Higgs mass, $m^2_{h,\,\rm tree} \leq m_Z^2 \cos^2 2\beta$, suggests that such a Higgs mass in the MSSM requires large radiative corrections with a considerable large amount of tuning. These can be explained through heavy sparticle and/or large sparticle mixing, especially in the stop sector, see eq. (2.50). This issue is known as the *Little Hierarchy Problem*. To have a better understanding, we may define the fine tuning (FT) measure Δ_{FT}, as in [90], by

$$\Delta_{FT} = |m_h^2/(2\delta m^2_{H_u})|\,, \tag{2.55}$$

  where $\delta m^2_{H_u}$ are the loop corrections to $m^2_{H_u}$. We plot Δ_{FT} in the (X_t, m_{Q_3})-plane in figure 2.3, where also the contour line for $m_h = 125.5$ GeV is shown. We have only considered the main contribution to $\delta m^2_{H_u}$, coming from the stop sector, taking

$$\delta m^2_{H_u} = -\frac{3m_t^2}{4v^2}\left(m^2_{Q_3} + m^2_{u_3} + A_t^2\right) \ln\left(\frac{\Lambda_{SSBM}}{\rm TeV}\right)\,. \tag{2.56}$$

  The supersymmetry breaking mediation scale Λ_{SSBM} is taken to be conservatively at 20 TeV, as in [91]. While a standard request for naturalness is that FT has to be better than 10%, *i.e.* $\Delta_{FT} > 0.1$, we can see that this is more difficult to realise in the MSSM scenario displayed.

2.4 Non-minimal supersymmetric Standard Models

Several extensions of the MSSM have been proposed, featuring richer phenomenologies, while renouncing to a minimal particle content. We are especially interested in mechanisms that raise the tree-level Higgs mass in order to more easily accommodate the observed Higgs mass, relaxing naturalness in the stop sector. Here we give an incomplete list of examples.

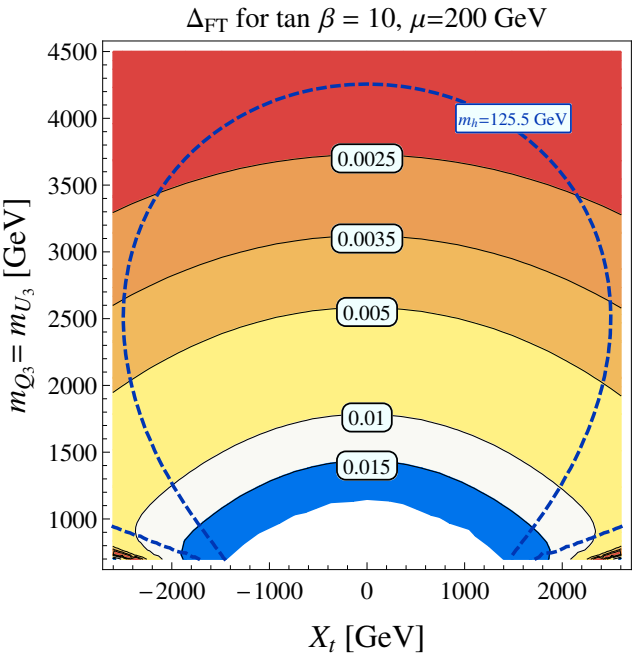

Figure 2.3: MSSM: contourlines of Δ_{FT} in the (X_t, m_{Q_3})-plane, for $m_{Q_3} = m_{U_3}$, $\tan\beta = 10$ and $\mu = 200$ GeV. The blue dashed contour corresponds to the Higgs mass $m_h = 125.5$ GeV.

F-term extensions of the MSSM

A positive F-term contribution to the Lagrangian enhances the tree-level squared mass of the Higgs, which mixes with additional scalars with coupling λ. The typical contribution is $\Delta m_h^2 \propto \lambda v^2$. Gauge symmetry constraints these additional scalars to be of the following types:

- Gauge singlets coupling to $H_u H_d$, as in the next-to-minimal supersymmetric Standard Model (NMSSM) [88], *cf.* chapter 4. In this model the μ-problem is also addressed.
- $SU(2)$-doublets coupling to $H_u H_u$ or $H_d H_d$, possibly emerging as composite objects from new strongly coupled dynamics [92, 93].
- $SU(2)$-triplets coupling either to H_u or to H_d [94, 95].

D-term extensions of the MSSM

Extending the gauge symmetry under which the Higgs superfields are charged leads to additional quartic couplings from the new D-terms. Examples are

- Extensions of the MSSM with non-decoupling D-terms [96–98], *cf.* chapter 5. These additional D-terms can arise in a series of different UV completion contexts.

Gauge extensions of the MSSM may introduce additional Higgs states, combining the effect of F- and D-terms: in order to break the gauge group to the SM group, as in the Left-Right models [99, 100], or seeking GUT multiplet completion as in the E_6-SSM [101].

Chapter 3

SUSY searches: lessons from the LHC, prospects for the ILC

In this chapter we briefly resume results of experimental searches that test supersymmetry, focusing in particular on the MSSM: Higgs discovery and searches for heavier Higgs resonances in section 3.1, direct collider supersymmetry searches at the LHC and at the planned ILC in section 3.2, and indirect searches and constraints from electroweak precision physics and dark matter experiments in section 3.3. The main resources for this chapter are [7, 102, 103].

3.1 Observation of a 125.5 GeV Higgs boson and the MSSM

Supersymmetric extensions of the SM are under probe in the light of the current and incoming experimental results from the LHC, and will carefully be studied by the linear collider program, particularly sensitive to the electroweak sector. SUSY models have been primarily proposed for solving the Hierarchy Problem and are therefore intimately related to Higgs physics.

With no sparticles observed so far, we start from the concrete discovery at the LHC of a scalar particle with mass $m_h \simeq 125.5$ GeV [8, 9], that behaves extremely close to the SM-like Higgs boson [13–16], while being consistent with several BSM models.

Interpreting the observed 125.5 GeV Higgs as the light $\mathcal{CP}$-even Higgs h of the MSSM implies that the heavy Higgs states H, A^0, and $H^\pm$ are decoupled. With $m_{A^0} \gg m_Z$ ($\gtrsim 200$ GeV), indeed, h has couplings that are SM-like [104]. This is consistent with current results within theory and experimental accuracies. In this regime the SM analyses can be applied to the MSSM too. Therefore, a high degree of accuracy in detecting deviations from the SM expectations for the Higgs production modes and decay channels is required. The main differences from the SM are expected by the contribution of light sparticles in loop processes.

At the LHC, ATLAS and CMS measure $\sigma(pp \to h) \cdot \mathrm{Br}(h \to i)$, *i.e.* the total Higgs production cross section times the branching ratios. The cross sections $\sigma(pp \to h)$ and the branching ratios $\mathrm{Br}(h \to i)$, instead, are not directly accessed. The LHC produces a SM Higgs boson with mass $m_h \sim 125.5$ GeV mainly via gluon-fusion, then also via vector boson fusion,

Higgsstrahlung, $t\bar{t}h$ production, *cf.* figures 3.1(a) and 3.1(b).

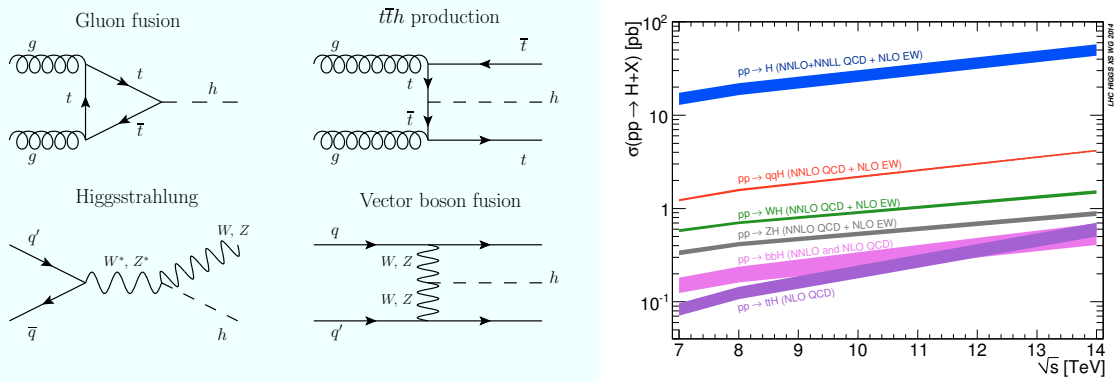

(a) (b)

Figure 3.1: Leading Higgs-production modes at the LHC. (a) The corresponding first-order Feynman diagrams; (b) the production cross sections of a SM-Higgs at $\sim$ 125.5 GeV in function of the LHC-beams $\sqrt{s}$, from [105].

The branching ratios for such a SM-Higgs are [106]:

$$\mathrm{Br}(h \to \gamma\gamma) \simeq 2.3 \times 10^{-3}\,, \quad \mathrm{Br}(h \to b\bar{b}) \simeq 5.6 \times 10^{-1}\,, \quad \mathrm{Br}(h \to c\bar{c}) \simeq 2.8 \times 10^{-2}\,,$$
$$\mathrm{Br}(h \to gg) \simeq 8.5 \times 10^{-2}\,, \quad \mathrm{Br}(h \to \tau^+\tau^-) \simeq 6.2 \times 10^{-2}\,, \quad \mathrm{Br}(h \to WW^*) \simeq 2.3 \times 10^{-1}\,,$$
$$\mathrm{Br}(h \to ZZ^*) \simeq 2.9 \times 10^{-2}\,, \quad \mathrm{Br}(h \to Z\gamma) \simeq 1.6 \times 10^{-3}\,, \quad \mathrm{Br}(h \to \mu^+\mu^-) \simeq 2.1 \times 10^{-4}\,.$$

Even though the $h \to b\bar{b}$ channel is dominant, it is affected by a large background from hadronic processes. The most sensitive channel, instead, is $h \to \gamma\gamma$, despite the small branching ratio, due to the very clear experimental signature of two high-energy photons. It was with this channel, together with the ZZ^* channel, that the Higgs excess was reported by ATLAS and CMS. Moreover, due to its loop structure, the di-photon channel is more sensitive to the contribution of supersymmetric particles and, in fact, a slight excess with respect to the SM is reported by ATLAS [107]. However, with the current experimental accuracy in both experiments, the signal strengths, defined as $\mu_i = (\sigma \cdot \mathrm{Br})/(\sigma \cdot \mathrm{Br})_{\mathrm{SM}}$, do not show very significant deviations from 1, corresponding to the SM [108, 109].

The determination of the Higgs couplings at the LHC is not model independent since the cross sections and decays cannot be independently derived, therefore some model assumption on the Higgs width is required at least. With the High Luminosity upgrade of the LHC (HL-LHC), a precision level on the couplings of order $\sim \mathcal{O}(5\text{–}10\%)$ could be reached [106]. As we will discuss in subsection 5.3.2, model-independent Higgs coupling determinations can be achieved at the ILC with (sub-)percent accuracy [110]. This is possible since from the production process $e^+e^- \to Zh \to l^+l^-h$, dominant at the ILC for $\sqrt{s} \in [200, 400]$ GeV, the coupling hZZ can be disentangled via recoil mass measurement. Another important SM-Higgs production mode in the range of energies $\sqrt{s} = 250\text{–}500$ GeV is W-boson fusion, $e^+e^- \to \nu_e\bar{\nu}_e h$, see fig. 3.2. A clear study of the $\mathcal{CP}$ properties of h, necessary to establish

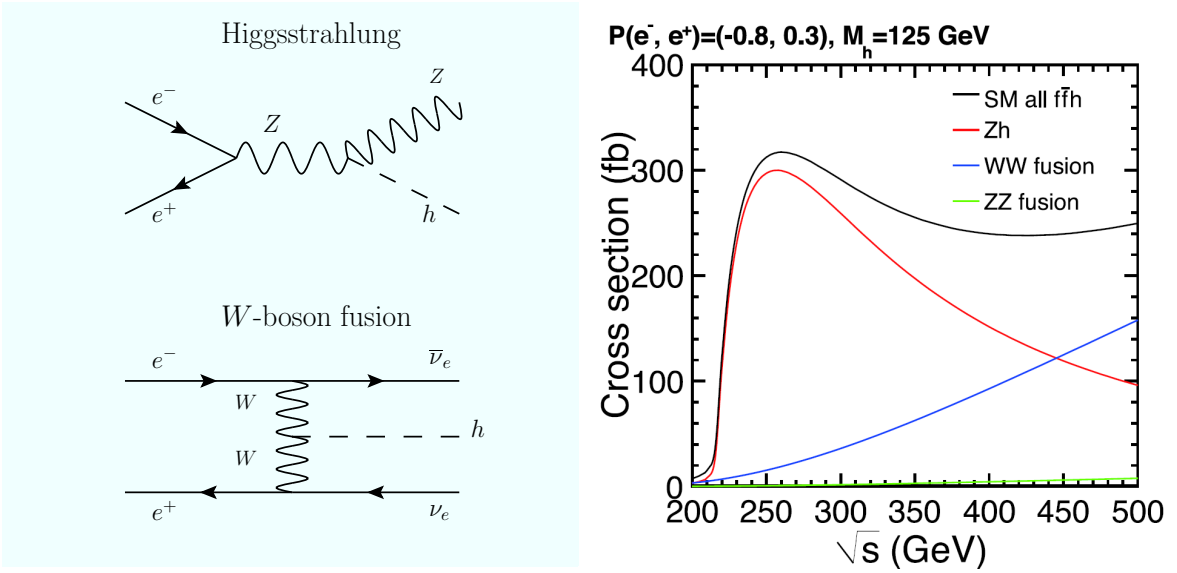

(a) (b)

Figure 3.2: Leading Higgs-production modes at the ILC. (a) The first-order Feynman diagrams of the two leading channels; (b) the production cross sections in function of the ILC-beams $\sqrt{s}$ for $(\mathcal{P}_{e^-}, \mathcal{P}_{e^+}) = (-0.8, 0.3)$, taken from [7].

the nature of the observed Higgs boson, is possible at the ILC exploiting the $t\bar{t}h$ associated production, that has a threshold at $\sqrt{s} = 500$ GeV.

Furthermore, at the linear collider the production modes $e^+e^- \to A^0H$, H^+H^- may allow the detection of H, A^0 and $H^\pm$ of the MSSM with decoupling limit, since the corresponding Higgs couplings are of the order of the gauge couplings. Searches for decoupled heavy Higgs bosons at the LHC are more complicated. In figure 3.3 we display the ATLAS limit on $\tan\beta$ values in the MSSM Higgs bosons searches in the $\tau\tau$ final state for the m_h^{max} scenario [111], which maximises m_h keeping fixed m_t, $\tan\beta$, and m_{soft}. So far, the searches for additional MSSM Higgs bosons have been so far unsuccessful. This is both true for the searches of heavier Higgs resonances and for a light $\mathcal{CP}$-even state if considering the observed Higgs as the heavier $\mathcal{CP}$-even state H. The latter interpretation is now under pressure [112, 113].

3.2 Direct SUSY collider searches

A vast program of direct sparticle searches is being carried out at the LHC, with ATLAS and CMS especially studying direct production modes and decay channels of sparticles resulting in final states with jets, leptons, and large missing transverse energy (MET). The analyses on the 7 and 8 TeV LHC data revealed no relevant excess over SM expectations [34, 35]. The typical expected signature is the presence of a large MET due to the LSP at the end of the sparticle decay chain. LHC searches are particularly sensitive to coloured sparticles, allowing to set limits that push gluinos and the first two generations squarks 1 TeV, however, the

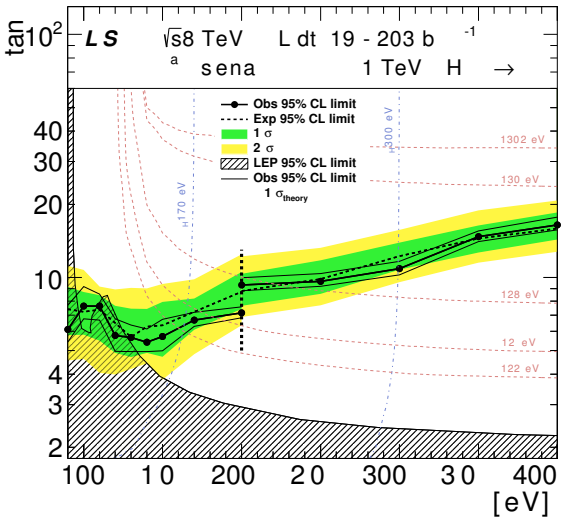

Figure 3.3: Expected and observed 95% confidence level (CL) upper limits on $\tan\beta$ as a function of m_A, for the MSSM benchmark scenario $m_h^{\max}$. Values of $\tan\beta$ above the lines are excluded. MSSM Higgs bosons are searched in the $\tau\tau$ final state. Plot taken from [111].

squark limits can be relaxed depending on the model assumptions, see for example [114, 115]. The highest sensitivity to electroweak sparticles like neutralinos and charginos comes from multi-lepton final states, that allow to distinguish the signal from the hadronic background, and limits on the masses are set to be at several hundred GeV, depending on the analysis.[1]

Constrained SUSY models as the CMSSM and mSUGRA are highly under pressure, as can be seen in the CMS limits in figure 3.4, and in the resume of ATLAS SUSY searches in figure 3.5. In fact, the constraints on strong interacting particles in these scenarios have effects also on the electroweak sector, pushing charginos, neutralinos, and sleptons at the TeV range, and in general the observed Higgs mass is hardly accommodated. For this reason, the attention has lately turned to less constrained models as the pMSSM [118] that, without implicit correlations between sparticle masses, have limits on squarks and gluinos with minor impact on electroweak interacting sparticles.

Limits from MET searches can be avoided, for example, in the case of compressed sparticle spectra with low transverse energies [119], or in scenarios with long-lived charged NLSP as in GMSB models [78], requiring more specific analyses. In the case of MSSM with R-parity violation (RPV) [120], the LSP decays hadronically completely covered by the QCD background.

Concluding, the LHC has mainly constrained gluinos and first two generations squarks, while third generation squarks and not-coloured sparticles are mildly constrained.

[1] The limits from SUSY searches have been recasted and applied also to other models as the Little Higgs, posing some severe constraints to the related additional states [38, 39, 116, 117].

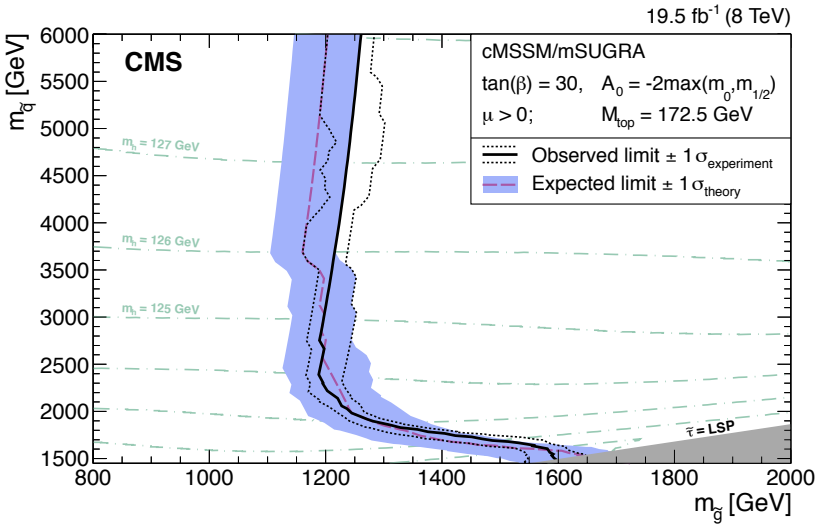

Figure 3.4: CMS-exclusion limits at 95% CL in the $(m_{\tilde{g}}, m_{\tilde{q}_{1,2}})$-plane for the constrained model cMSSM/mSUGRA, with $\tan\beta = 30$, $A_0 = -2\max(m_0, m_{1/2})$, and $\mu > 0$. Plot taken from [114].

Despite a lower energy reach with respect to the LHC, an e^+e^- linear collider can become a SUSY discovery machine, in the light of the low QCD-background and the high sensitivity to electroweak physics that may avoid the LHC searches. It has indeed been proven that many MSSM scenarios escaping the LHC can be seen at the ILC [121]. Direct sparticle searches would be particularly favoured by a machine that could precisely tune its center-of-mass energy over a wide range. This would allow to operate at the threshold of several production channels, that is particularly useful considering the rich supersymmetric spectrum that can be spread over a wide mass spectrum [7]. A powerful improvement to precision physics analyses is given by the possibility to polarise particle beams with different polarisation configuration.

Precise determination of sparticle masses would be possible through analyses in the continuum reconstructing end-points and through threshold scans.

3.3 Indirect searches and constraints

SUSY parameter space constraints from direct sparticles searches at colliders are complemented by a series of indirect constraints that need to be taken into account. These come from b-physics, from Dark Mark matter search experiments and cosmology, and from the $(g-2)_\mu$ measurements. For a review see also [122].

b-physics Flavour physics, in particular b-physics, opens a window on the SUSY parameter space, being sensitive to higher energy scales through loop effects or intermediate exchange of heavy particles. Decays of b-hadrons receive important no-SM contributions from sparticles or additional Higgs states that are not suppressed by loop factors as in $\bar{B} \to X_s\gamma$, or by helicity

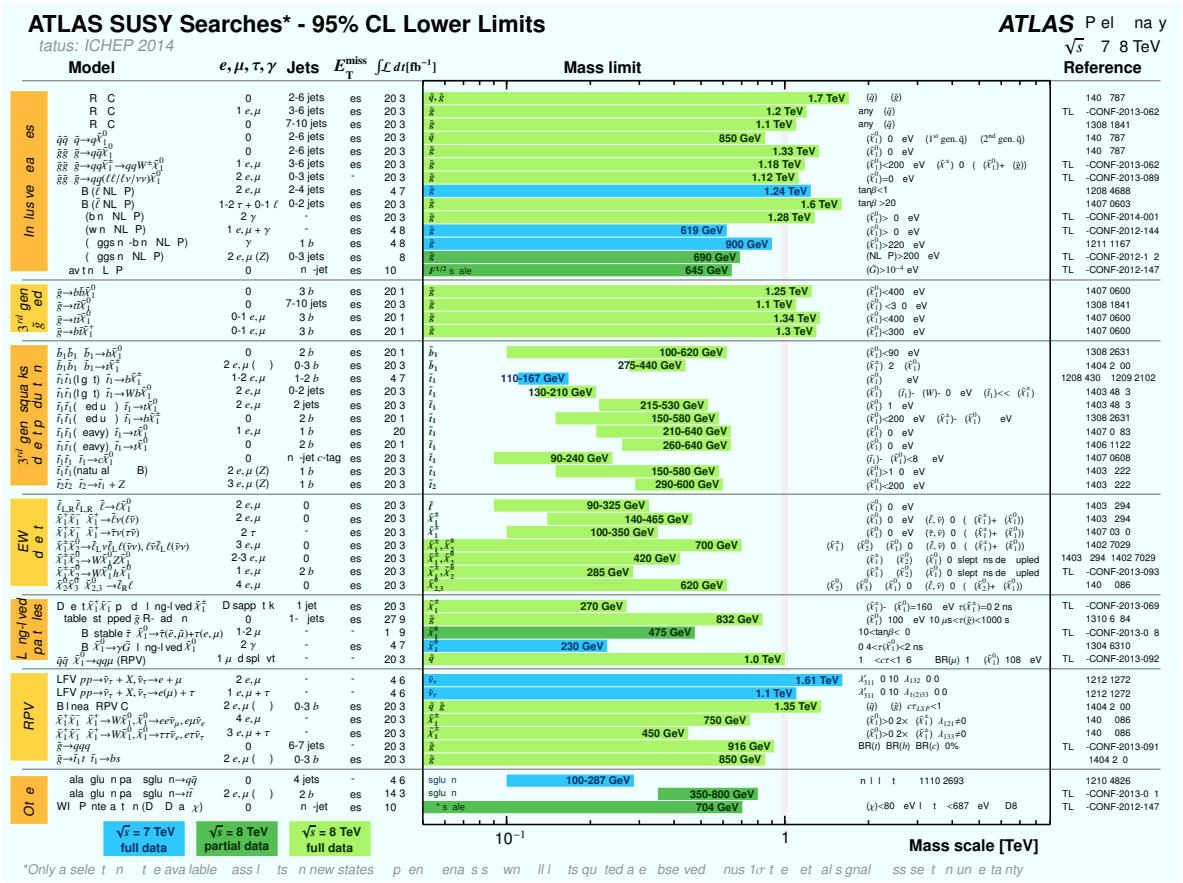

Figure 3.5: Summary of exclusion limits of ATLAS SUSY searches, from [34].

factors as in $B_s \to \mu^+\mu^-$, $B_u \to \tau\nu_\tau$. These kind of processes are particularly sensitive to parameter regions with high $\tan\beta$ and/or light stops, charginos, A or $H^\pm$.

Dark Matter and Cosmology Formulating a supersymmetric scenario with $\tilde{\chi}_1^0$ as LSP, one should compare the lightest neutralino relic abundance, $\Omega_{\text{LSP}}h^2$, with the measured dark matter relic density measured at WMAP [59] and Planck [60], Ωh^2. Here h is the Hubble constant in units of 100 km/(s·Mpc). Large uncertainties are coming on the limits from cosmology, therefore one needs to care only that the constraints are not violated too largely. Further constraints are given by the upper bound for the WIMP-nucleon scattering cross section, particularly sensitive to $\tan\beta$ and m_A, and studied at the LUX experiment [123].

Anomalous muon magnetic moment The value of the anomalous muon magnetic moment $a_\mu = \frac{(g-2)_\mu}{2}$ observed at Brookhaven Experiment E821 [124] shows a 3σ deviation from the SM estimate [125, 126]. The supersymmetric contribution to a_μ is proportional to

$$\sim \frac{m_\mu^2\, \mu M_i \tan\beta}{m^2_{\text{sparticle}}}\,, \tag{3.1}$$

possibly coming from $\tilde{\chi}_i^0$-$\tilde{\ell}$ and $\tilde{\chi}_i^{\pm}$-$\tilde{\nu}$ loops [51]. Therefore, if the observed deviation from the SM is assumed to stem from constrained supersymmetry as the CMSSM, it would imply a relatively small SUSY scale $m_{\text{sparticle}}$, in apparent contrast with the indications from collider experiments.

Chapter 4

NMSSM: singlinos at the linear collider

This chapter is based on the publications [1, 2], written in collaboration with Gudrid Moortgat-Pick and Krzysztof Rolbiecki. In section 4.1 the relevant features of the NMSSM are introduced. In section 4.2 the motivation and the strategy adopted in our work on the distinction between two supersymmetric models, the MSSM and the NMSSM, are outlined. In section 4.3 the strategy is applied to the case of some ambiguous scenarios, and the results of analysis are discussed. In section 4.4 I summarise and conclude. I have produced all the plots shown. Tree-level calculations were done by me extending and updating a previous code from my collaborators. Part of the text is derived from what I have written in [2]. The main resources for this chapter are refs. [51, 127–129].

4.1 The next-to-minimal supersymmetric Standard Model

4.1.1 Concept and motivation

The next-to-minimal supersymmetric SM (NMSSM) is the most simple extension of the MSSM. It adds to the MSSM spectrum a gauge singlet chiral superfield $\hat{S}$ coupling with the Higgs doublets $\hat{H}_u$, $\hat{H}_d$ in the superpotential. The main motivation for such a model is the elegant solution of the μ-problem, described in section 2.3.3. From the superpotential trilinear term $\lambda\hat{S}\hat{H}_u\hat{H}_d$, an effective μ-term $\mu_{\text{eff}}\hat{H}_u\hat{H}_d$ may be generated dynamically with the acquisition of the vev $\langle\hat{S}\rangle = s$ by $\hat{S}$:

$$\lambda\hat{S}\hat{H}_u\hat{H}_d \xrightarrow{\lambda\langle\hat{S}\rangle = \mu_{\text{eff}}} \mu_{\text{eff}}\hat{H}_u\hat{H}_d\,. \tag{4.1}$$

The vev s must be of the order of the SUSY breaking scale M_{SUSY} to solve the μ-problem. This can be done by introducing order $\mathcal{O}(M^2_{\text{SUSY}})$ negative soft mass squareds or soft trilinear couplings, such that the only scale of the theory is the supersymmetry breaking scale.

Furthermore, within the NMSSM it is easier to accommodate a Higgs mass at 125.5 GeV without large radiative corrections like in the MSSM. The additional singlet scalar S, indeed,

mixes with the Higgs doublets H_u, H_d. This results in a NMSSM contribution to the tree level mass of the lightest Higgs state. With such a positive contribution, smaller radiative corrections from the stop sector are required, *i.e.* naturalness is relaxed.

4.1.2 The generalised NMSSM

The most general, R-parity- and $\mathcal{CP}$-conserving version of the NMSSM, the generalised NMSSM (GNMSSM), features the Higgs sector superpotential [127]:

$$\mathcal{W}_{H,\,\mathrm{GNMSSM}} = \left(\mu + \lambda\,\hat{S}\right)\hat{H}_u \cdot \hat{H}_d + \xi_F \hat{S} + \frac{1}{2}\mu'\,\hat{S}^2 + \frac{\kappa}{3}\,\hat{S}^3 \tag{4.2}$$

$$+ \mathbf{y_u}\,\hat{Q}\cdot\hat{H}_u\,\hat{U}^c_R + \mathbf{y_d}\hat{H}_d\cdot\hat{Q}\,\hat{D}^c_R + \mathbf{y_e}\hat{H}_d\cdot\hat{\ell}\,\hat{E}^c_R\,. \tag{4.3}$$

$\hat{S}$ consists of a scalar Higgs singlet S and the singlino $\tilde{S}$. The GNMSSM soft Lagrangian may be written as:

$$\mathcal{L}_{\mathrm{GNMSSM}} = -\,m^2_{H_u}|H_u|^2 - m^2_{H_d}|H_d|^2 - m^2_S|S|^2 \tag{4.4}$$

$$-\,\mathbf{M^2_Q}|\tilde{Q}^2| - \mathbf{M^2_u}|\tilde{\bar{u}}^2| - \mathbf{M^2_d}|\tilde{\bar{d}}^2_R| - \mathbf{M^2_\ell}|\tilde{\ell}^2| - \mathbf{M^2_e}|\tilde{\bar{e}}^2| \tag{4.5}$$

$$-\,\tilde{\bar{u}}\,\mathbf{A_u}\,\tilde{Q}\cdot H_u + \tilde{\bar{d}}\,\mathbf{A_d}\,\tilde{Q}\cdot H_d + \tilde{\bar{e}}\,\mathbf{A_e}\,\tilde{\ell}\cdot H_d + \mathrm{h.c.} \tag{4.6}$$

$$-\,\lambda A_\lambda H_u\cdot H_d S - \frac{\kappa}{3}A_\kappa S^3 - B_\mu\,H_u\cdot H_d - B'_{\mu'}S^2 - \xi_S S + \mathrm{h.c.} \tag{4.7}$$

$$+\,\frac{1}{2}M_1\lambda_1\lambda_1 + \frac{1}{2}M_2\lambda^i_2\lambda^i_2 + \frac{1}{2}M_3\lambda^a_3\lambda^a_3\,. \tag{4.8}$$

Finally, the gauge group is the same as in the MSSM and in the SM.
The signs of some Lagrangian parameters that have no physical meaning, due to the possibility of field redefinition $\phi \to -\phi$. One finds [127] that keeping λ, v_u, v_d and the Yukawa couplings positive, then κ, s and the dimensionful parameters may have both signs.

4.1.3 The $\mathbb{Z}_3$-NMSSM

In order to solve the μ-problem, an overall $\mathbb{Z}_3$-symmetry is most commonly imposed, corresponding to the transformation:

$$\hat{\Phi} \to e^{2\pi i/3}\hat{\Phi}\,, \quad \hat{V} \to \hat{V}\,, \tag{4.9}$$

that is a phase multiplication for all chiral superfields $\hat{\Phi}$, while the vector superfields $\hat{V}$ are unchanged.[1] The $\mathbb{Z}_3$-symmetry requires

$$\mu = \mu' = \xi_F = B_\mu = B'_{\mu'} = \xi_S = 0\,. \tag{4.10}$$

This results in the so called the $\mathbb{Z}_3$-*invariant* NMSSM, with the scale invariant superpotential:

$$\mathcal{W}_{\mathbb{Z}_3\text{-NMSSM}} \supset \lambda\,\hat{S}\hat{H}_u\cdot\hat{H}_d + \frac{\kappa}{3}\,\hat{S}^3\,. \tag{4.11}$$

[1] Nevertheless, in the GNMSSM the μ-term may be removed by the redefinition $s \to s - \mu/\lambda$.

As mentioned above, an effective μ-term in the scalar potential may dynamically be generated by the vev of $\hat{S}$, triggered by the means of supersymmetry breaking:

$$\mu_{\text{eff}} = \lambda \langle \hat{S} \rangle = \lambda s \,. \tag{4.12}$$

The dimensional parameters A_λ and A_κ appear in the Higgs sector soft terms:

$$\mathcal{L}_{\text{soft, } \mathbb{Z}_3\text{-NMSSM}} \supset -\lambda A_\lambda H_u \cdot H_d S - \frac{\kappa}{3} A_\kappa S^3 . \tag{4.13}$$

From now on we will refer to the $\mathbb{Z}_3$-*invariant* NMSSM simply as the NMSSM. From equations (4.11) and (4.13) we can write the Higgs scalar potential

$$\begin{aligned} \mathcal{V}_{H,\text{ NMSSM}} = & \left|\lambda(H_u^+ H_d^- - H_u^0 H_d^0) + \kappa S\right|^2 \\ & + (m_{H_u}^2 + |\mu + \lambda S|^2)\left(|H_u^0|^2 + |H_u^+|^2\right) + (m_{H_d}^2 + |\mu + \lambda S|^2)\left(|H_d^0|^2 + |H_d^-|^2\right) \\ & + \frac{g_1^2 + g_2^2}{8}\left(|H_u^0|^2 + |H_u^+|^2 - |H_d^0|^2 - |H_d^-|^2\right) + \frac{g_2^2}{2}\left|H_u^+ H_d^{0\,*} + H_u^0 H_d^{-\,*}\right|^2 \\ & + m_S^2 |S|^2 + \left(\lambda A_\lambda (H_u^+ H_d^- - H_u^0 H_d^0) S + \frac{k}{3} A_\kappa S^3 + h.c.\right) . \end{aligned} \tag{4.14}$$

We define the scalar component of the singlet as

$$S = s + \frac{1}{\sqrt{2}}\left(\text{Re}S + i\text{Im}S\right) . \tag{4.15}$$

In the potential (4.14), the singlet S appears in bilinear terms together with the MSSM Higgs doublets H_u, H_d and therefore mixes with them due to the electroweak symmetry breaking. ReS mixes with ReH_u^0 and ReH_d^0, resulting in the three $\mathcal{CP}$-even neutral scalars h_1, h_2, and h_3, while ImS mixes with $A^0 = \cos\beta\,\text{Im}_u^0 + \sin\beta\,\text{Im}H_d^0$, resulting in the two $\mathcal{CP}$-odd neutral scalars a_1, a_2. For more details on the Higgs mass matrices see appendix B.

At the tree-level one obtains the upper bound for the lightest $\mathcal{CP}$-even Higgs:

$$m_Z^2 \cos^2 2\beta + \frac{\lambda^2 v^2}{2} \sin^2 2\beta \,. \tag{4.16}$$

With respect to the MSSM upper bound on the tree level Higgs mass, eq. (2.49), the distinctive NMSSM contribution, $\frac{1}{2} v^2 \lambda^2 \sin^2 2\beta$, is relevant particularly for small $\tan\beta$ values. Note that to grant perturbativity up to the GUT scale one needs $\lambda \lesssim 0.7$-0.8 [130]. It is possible, in the limit of a heavy singlet-like scalar, given by $\kappa s \gg |A_\kappa|, |A_\lambda|$, to write an approximate expression for the SM-like Higgs mass that takes into account of the leading radiative corrections from the top/stop sector [127],

$$\begin{aligned} m_h^{2,\,\text{NMSSM}} \simeq & \; m_Z^2 \cos^2 2\beta + \frac{\lambda^2 v^2}{2} \sin^2 2\beta - \frac{\lambda^2}{2\kappa^2} v^2 (\lambda - \kappa \sin 2\beta)^2 \\ & + \frac{3 m_t^4}{2\pi^2 v^2}\left(\ln\left(\frac{M_{\tilde{t}}^2}{m_t^2}\right) + \frac{A_t^2}{M_{\tilde{t}}^2}\left(1 - \frac{A_t^2}{12 M_{\tilde{t}}^2}\right)\right) . \end{aligned} \tag{4.17}$$

Passing to the fermionic component of the singlet superfield, the singlino $\tilde{S}$, we see that it mixes with the higgsinos $\tilde{H}_u^0$, $\tilde{H}_d^0$ and the gauginos $\lambda_1 = \tilde{B}$, $\lambda_2^i = \tilde{W}^i$, resulting in five neutralino mass eigenstates $\tilde{\chi}_1^0, \ldots, \tilde{\chi}_5^0$. The NMSSM neutralino mass matrix, $\mathcal{M}_{\text{NMSSM}}$, can be written in the basis $(\tilde{B}, \tilde{W}^0, \tilde{H}_d, \tilde{H}_u, \tilde{S})$:

$$\mathcal{M}_{\text{NMSSM}} = \left(\begin{array}{cccc|c} & & & & 0 \\ & & & & 0 \\ & \mathcal{M}_{\text{MSSM}}(\mu_{\text{eff}},\, \tan\beta, M_1, M_2) & & & -\frac{1}{\sqrt{2}}\lambda v \sin\beta \\ & & & & -\frac{1}{\sqrt{2}}\lambda v \cos\beta \\ \hline 0 & 0 & -\frac{1}{\sqrt{2}}\lambda v \sin\beta & -\frac{1}{\sqrt{2}}\lambda v \cos\beta & -2\kappa\, \mu_{\text{eff}} / \lambda \end{array}\right) . \tag{4.18}$$

The upper left block is equivalent to the MSSM neutralino mass matrix, equation (2.53), with the μ dependence substituted by the dependence on the singlet vev s, through μ_{eff}. The NMSSM neutralino sector depends on two additional singlet parameters with respect to the MSSM: λ, κ. Clearly the two charginos do not mix with the neutral $\tilde{S}$.

The additional neutralino state offers a richer phenomenology, in particular for its dark matter implications in case the LSP is singlino-like neutralino, *i.e.* $\tilde{\chi}_{\tilde{S}}^0$. This would result in particularly long lived NLSP (potentially also charged, as $\tilde{\tau}$), with typical collider signatures for sparticle decay chains and NLSP displaced vertices [127].

MSSM-limit

An MSSM-limit for the NMSSM is obtainable by setting null couplings of the singlet to the Higgs doublets and the other MSSM fields, $\lambda \to 0$, together with the conditions $\kappa \to 0$ and $\lambda/\kappa = \text{const}$. The other dimensionful parameters are kept fixed. The condition on κ is needed to keep $\mu_{\text{eff}} \gtrsim 100$ GeV, as requested by the LEP limits on chargino mass $m_{\tilde{\chi}_1^\pm} > 94$ GeV [103], since[2]

$$s \propto \frac{1}{\kappa} . \tag{4.19}$$

As a result of this limit, a singlet-like $\mathcal{CP}$-even Higgs, a singlet-like $\mathcal{CP}$-odd Higgs, and a singlino-like neutralino will be decoupled without necessarily being heavy.

$\mathbb{Z}_3$-symmetry and domain walls

Discrete symmetries, like the $\mathbb{Z}_3$-symmetry that has been introduced in the NMSSM Lagrangian, can trigger phenomenological problems [132]. Within the NMSSM, several regions or bubbles with the same vacuum energy may form during the electroweak symmetry phase transition in the early universe. These bubbles would have different ground states connected by $\mathbb{Z}_3$-transformations and would be separated by domain walls. Such domain walls have

[2] This follows from the condition $A_\kappa^2 \gtrsim 9 m_S^2$ [131], that grants an absolute minimum at $s \simeq \frac{1}{4\kappa}\left(-A_\kappa - \sqrt{A_\kappa^2 - 8 m_S^2}\right)$.

never been observed, so we refer to this issue as the *domain wall problem*. Solutions to this problem have been proposed for example by adding symmetries such as a continuous $U(1)'$ (in the USSM) [133]. Then, with a suitable set of charges, (suppressed) $\mathbb{Z}_3$-violating terms in the superpotential, that would allow for energy difference between bubbles and consequent collapse of the higher energetic ones, may be controlled.

4.1.4 NMSSM Higgs phenomenology and the MSSM

The enlarged NMSSM Higgs and neutralino sectors give the best signatures to distinguish the model from the MSSM. In particular, in the light of the expected high accuracy in the Higgs physics measurements both at the LHC and the ILC [106, 110], the Higgs sector is the first place where to look in order to distinguish MSSM and NMSSM scenarios. The discovery of a SM-like Higgs at 125.5 GeV poses a concrete test for both the MSSM and the NMSSM. A series of scenarios and analyses have been then proposed in order to interpret signal strength deviations from the SM. We give here an overview of typical NMSSM features that permit to distinguish the model from the MSSM looking at the Higgs decays.

First of all, the additional $\mathcal{CP}$-even and and $\mathcal{CP}$-odd states in the extended Higgs sector of the NMSSM make possible additional Higgs-to-Higgs decays of the type $h_i \to a_1 a_1$, $h_i \to h_1 h_1$ etc.. For example, in the MSSM the only possibility for a SM-like Higgs to decay to $a_1 a_1$ if it is identified with h_2, due to particular mass relations between Higgs mass eigenstates. In the NMSSM these relations are weakened and a SM-like h_1 decaying to $a_1 a_1$ is possible as well [134].

A light $\mathcal{CP}$-even and/or a light $\mathcal{CP}$-odd scalars may have high singlet component. This possibility potentially allows for new decay channels of the SM-like Higgs scalar, with impact on its decay width and branching ratios, like the ones relative to $h \to b\bar{b}$ and $h \to \tau^+\tau^-$ [134]. This, in turn, translates to the need of careful recasting of the experimental constraints from the Higgs sector for MSSM searches.

A possible $\gamma\gamma$-channel enhancement with respect to the SM has attracted lots of attention in the recent literature due to a would-be observed excess by ATLAS [107]. Within the MSSM such an enhancement would be possible only through light $\tilde{\tau}$ (and with a large amount of tuning), while the NMSSM offers a series of distinctive additional mechanisms. First of all, the mixing of the singlet with the Higgs doublets can result in a NMSSM suppression of the $b\bar{b}$-decay mode with a consequent enhancement of the $\gamma\gamma$ rate with respect to the MSSM [135–137]. Also light charginos or light $H^\pm$ can significantly contribute to the partial decay width related to the di-photon rate [138]. Furthermore, in the NMSSM a pseudoscalar with a mass very close to the SM-like Higgs mass may result, in an "effectively" enhanced $b\bar{b}$ and $\tau^+\tau^-$ rates with respect to the SM, if the two particles are not distinguished [139].

As already mentioned, both within the MSSM and the NMSSM it is possible to interpret the observed SM-like scalar as the heaviest $\mathcal{CP}$-even Higgs. In this case, a rather unique signature of the NMSSM is the decay into such a light scalar pair if h_1 is lighter than $\frac{125.5}{2}$ GeV. If this decay channel is open, the di-photon rate may also be suppressed as well as

$h \to b\bar{b}$. This possibility is more difficult to explain in the MSSM [140, 141]. In [142, 143] it has been studied how, within the NMSSM, a heavy SM-like Higgs could have the invisible decay channel $H \to \tilde{\chi}_1^0 \tilde{\chi}_1^0$, reducing the branching ratios of the other channels.

Furthermore, the singlet component in the SM-like Higgs can also enhance the signal rate of $pp \to h \to VV^*$, while this never happens with the MSSM [135].

It has also been shown that even if Higgs-to-Higgs decays are kinematically not allowed or are suppressed, in some regions of the NMSSM parameter space the Higgs boson di-photon decay mode could be observed at the LHC involving three different $\mathcal{CP}$-even Higgs bosons [144]. This is not a viable effect for the MSSM.

In general, while studying the NMSSM one has to reconsider the experimental results and recast the constraints obtained for the MSSM. An example is given by scenarios with light singlinos that translate in lower missing transverse energy (MET) from squarks and gluinos with an increased Higgs pair production [145].

Having listed this series of possible NMSSM-like decay patterns for the Higgs bosons, we conclude that for model distinction at the LHC it is well-motivated to look at the Higgs sector, where the LHC is expected to give the most precise indications on the NMSSM [146]. Since the ILC will be a Higgs-factory, the predicted accuracy will be even higher [110]. Even more, at the linear collider we will be able to complement the information from the Higgs sector by studying the extended neutralino sector of the NMSSM to look for deviations with respect to the MSSM, as we shall see below.

4.2 Distinguishing the NMSSM neutralino-chargino sector at the ILC

Looking at the extended NMSSM neutralino sector in order to distinguish the NMSSM phenomenology from that of the MSSM is well motivated due to the additional neutralino state. For example, the scenario of a higgsino-like $\tilde{\chi}_2^0$ decaying in a singlino-like $\tilde{\chi}_1^0$ leads to a rich decay pattern [147]. This may happen with soft decay products escaping the LHC detection, requiring a special treatment [148].

When a singlino-like neutralino is the LSP, the supersymmetric decay chains will behave just as in the MSSM till the NLSP. The NLSP may be particularly long lived, if R-parity is not violated, since the final decay width to the LSP plus SM particles is proportional to λ. The NLSP can be a charged slepton, and in this case it decays into $\tilde{\chi}_S^0$ with extra leptons in the final state. The NMSSM with a singlino-like LSP is easily distinguishable from the MSSM even in the MSSM limit, in which the singlino $\tilde{\chi}_S^0$ does not mix with higgsinos and gauginos and it is decoupled.

Some recent works, as [149], propose specific analysis of the neutralino sector at the LHC. However, the high precision achievable in the electroweak physics at a linear collider allows for an unprecedented focus lens on the neutralino sector. Charginos and neutralinos both in the MSSM and in the NMSSM are directly produced in pairs at the LC, *cf.* figures 4.1 and 4.2:

- $e^-e^+ \to \tilde{\chi}_i^0\tilde{\chi}_j^0$, occurring via s-channel with Z-exchange and t-/u-channel with $\tilde{e}_L$ and $\tilde{e}_R$ exchanges.
- $e^-e^+ \to \tilde{\chi}_i^-\tilde{\chi}_j^+$, occurring via s-channel with γ and Z exchanges and via the t-channel with $\tilde{\nu}_e$ exchange.

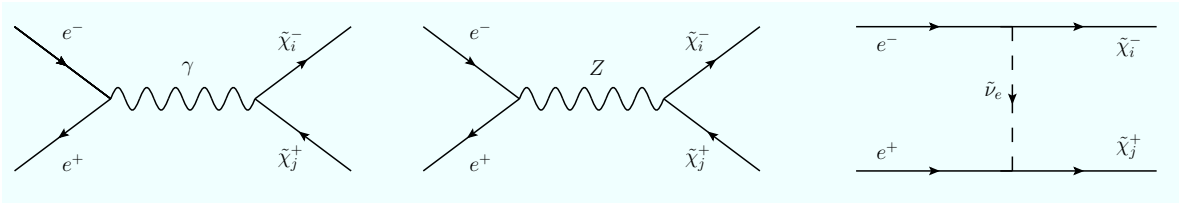

Figure 4.1: Chargino tree-level production channels at e^+e^- colliders.

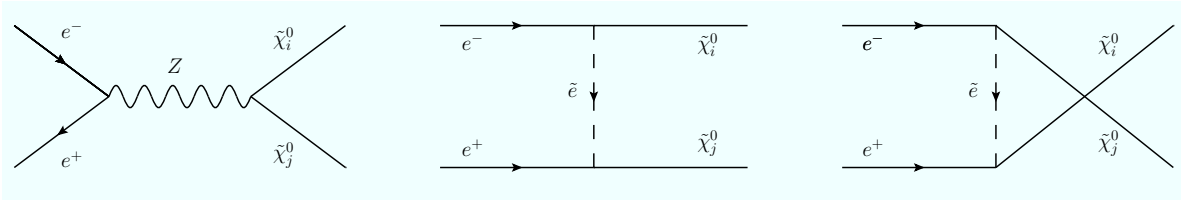

Figure 4.2: Neutralino tree-level production channels at e^+e^- colliders.

Once produced, $\tilde{\chi}_i^0$ and $\tilde{\chi}_j^\pm$ can be rather easily detected through their decays into lighter charginos and neutralinos, Higgses, gauge bosons, or into sfermion-fermion pairs [150].

Studying the higgsino/gaugino sector with high accuracy can be crucial for model distinction, for example in the case of relatively heavy scalar singlet states in comparison with the SM-like Higgs. In such a case, the observed Higgs sector can be interpreted within both the MSSM and the NMSSM, since the corresponding signatures at the LHC would indeed be very similar in the two models [110].

It makes therefore sense to develop strategies for model distinction not or not only looking at the Higgs sector, but rather also at the neutralino sector, and estimate how much information can be obtained from this sector.

The MSSM chargino and neutralino sector is completely described at the tree level by the parameters M_1, M_2, μ, $\tan\beta$, that are notably fundamental parameters without any assumption on the SUSY breaking scheme. It has been shown that for the MSSM a full reconstruction of the chargino and neutralino sectors is possible [128, 151, 152]. This can be done provided that $\tilde{\chi}_1^0$, $\tilde{\chi}_2^0$ and $\tilde{\chi}_1^\pm$ can be produced at the LC and their masses as well as the polarized cross sections $\sigma(e^+e^- \to \tilde{\chi}_1^0\tilde{\chi}_2^0)$, $\sigma(e^+e^- \to \tilde{\chi}_1^+\tilde{\chi}_1^-)$ are measurable. A χ^2-minimisation fit to the measured neutralino and chargino masses and production cross sections selects in an accurate and rather model-independent way M_1, M_2, μ, $\tan\beta$ [129, 153, 154]. Inferring the mass of the heavier neutralino states from combined analyses of LHC and LC data can strengthen such analysis [129]. Given the experimental observation of $\tilde{\chi}_1^0$, $\tilde{\chi}_2^0$ and

$\tilde{\chi}_1^\pm$, a result of the χ^2-fit that excludes the MSSM at 95% confidence level (C.L.) may suggest to look at supersymmetric models that minimally modify the neutralino/chargino sector. The first candidate is the NMSSM [1,2], as originally suggested in [155].

We adopt this idea and we estimate, with plausible assumptions, the potential of a LC to distinguish the MSSM and the NMSSM. In particular, we focus on the trickier case of NMSSM scenarios that may lead to chargino/neutralino masses and cross-sections similar to the MSSM. It has indeed been shown that relatively different mixings in the light neutralino and chargino states between MSSM and NMSSM scenarios can lead to very similar neutralino and chargino mass spectra in both models [155]. This is even more valid in the case of an MSSM and an NMSSM scenarios with similar soft parameters and with a decoupled singlet superfield [1,2]. We do an extensive analysis covering several classes of NMSSM scenarios with MSSM-like collider behaviour in the low spectrum, involving the following steps: we select suitable NMSSM scenarios, that are checked with experimental constraints from colliders and DM searches; we assume the expected experimental outcome with plausible uncertainties at a linear collider at different values of $\sqrt{s}$ and polarisations; we perform a fit based on these results to the MSSM parameters and check the consistency; we integrate the analysis with possible additional information coming from the Higgs sector.

NMSSM scenario selection.

The singlino, the higgsino, and the gaugino admixtures of lightest neutralino states allow to identify several classes of NMSSM scenarios. In particular we look at classes defined by the neutralino LSP that can be either singlino-, higgsino-, or gaugino-like, as described later in section 4.3. We identify NMSSM scenarios belonging to these classes, selecting a set of parameters suitable to get a mass spectrum for $\tilde{\chi}_1^\pm$, $\tilde{\chi}_1^0$, $\tilde{\chi}_2^0$ that can be attributed also to an MSSM scenario. We take care that this is valid also for the low Higgs spectrum.

With a dedicated FORTRAN code we calculate, from the input parameters at the electroweak scale $\tan\beta$, μ_{eff}, M_1, M_2, and the slepton masses, the corresponding NMSSM neutralino and chargino tree-level masses and polarized cross-sections for the processes $e^+e^- \to \tilde{\chi}_1^+\tilde{\chi}_1^-$ and $e^+e^- \to \tilde{\chi}_1^0\tilde{\chi}_2^0$. The slepton masses are needed to calculate the t- and u-channel contributions of neutralino pair production and the t-channel in the chargino pair production.

Experimental constraints from colliders and DM searches.

Each NMSSM scenario is defined in a SUSY Les Houches Accord (`SLHA`) file [156, 157] by the input parameters $\tan\beta$, μ_{eff}, λ, κ, A_λ, A_κ, and the soft parameters present both in the NMSSM and in the MSSM. The scenario has to fulfil a series of phenomenological and experimental constraints implemented in:

- `NMSSMTools-4.2.1`, that includes `NMHDECAY` [158–160] and `NMSDECAY` [161, 162]. These tools calculate the Higgs sector parameters, SUSY particle masses at the loop level and

their decays. These are confronted with limits from LEP, LHC and electroweak precision constraints.

- An interface between `NMSSMTools-4.2.1` to `MicrOMEGAS` [163], that provides Dark Matter constraints, including the LUX [123] and Planck [60] results. The LSP relic density is required to be $\Omega_{\rm LSP}h^2 < 0.131$, where h is the Hubble constant in units of 100 km/(s·Mpc).[3]

- A second interface to `HiggsBounds-4.0.0` [164] and `HiggsSignals-1.0.0` [165], that further controls Higgs sector constraints, and checks a compatibility with current data at the 95% (C.L.).[4]

Experimental assumption at a linear collider.

For each NMSSM scenario we assume to observe at least $\tilde{\chi}_1^\pm$, $\tilde{\chi}_1^0$ and $\tilde{\chi}_2^0$ at the ILC. We suppose to operate at two of the possible early ILC energy stages: $\sqrt{s} = 350$ GeV, corresponding to the $t\bar{t}$-threshold, and $\sqrt{s} = 500$ GeV. Therefore, we do not consider the option of operating at $\sqrt{s} = 1$ TeV. We assume to measure the masses, together with the total cross sections $\sigma(e^+e^- \to \tilde{\chi}_1^+\tilde{\chi}_1^-)$, $\sigma(e^+e^- \to \tilde{\chi}_1^0\tilde{\chi}_2^0)$. The electron-positron beam polarizations $(\mathcal{P}_{e^-}, \mathcal{P}_{e^+}) = (\pm 0.9, \mp 0.55)$ are considered. A precision of 0.5% on the masses and 1% on the cross sections is a reasonable and relatively conservative assumption for the scenarios considered, and are consistent with many detailed simulation studies [42, 150]. If kinematically accessible, also $m_{\tilde{\chi}_3^0}$, and the processes $e^+e^- \to \tilde{\chi}_1^0\tilde{\chi}_3^0$, $e^+e^- \to \tilde{\chi}_2^0\tilde{\chi}_3^0$ are taken into account.

We make a comment about the choice of the relatively high polarisation configurations $(\mathcal{P}_{e^-}, \mathcal{P}_{e^+}) = (\pm 0.9, \mp 0.55)$, rather than using the more traditional $(\mathcal{P}_{e^-}, \mathcal{P}_{e^+}) = (\pm 0.8, \mp 0.3)$. The neutralino and chargino pair production processes at the LC are mainly connected to vector-axial interactions [166]. Cross sections relative to processes of this type may be factorised as

$$\sigma_{\mathcal{P}_{e^-},\mathcal{P}_{e^+}} = (1 - \mathcal{P}_{e^-}\mathcal{P}_{e^+})\,\sigma_0\,[1 - \mathcal{P}_{\rm eff}\,A_{\rm LR}]\ . \tag{4.20}$$

Defining $\sigma_{\rm RL,\ LR}$ as the cross sections for the polarisation configurations $(\mathcal{P}_{e^-}, \mathcal{P}_{e^+}) = (\pm 1, \mp 1)$, we have introduced in eq. (4.20) the unpolarised cross section

$$\sigma_0 = \frac{\sigma_{\rm LR} + \sigma_{\rm RL}}{4}\,, \tag{4.21}$$

the left-right asymmetry

$$A_{\rm LR} = \frac{\sigma_{\rm LR} - \sigma_{\rm RL}}{\sigma_{\rm LR} + \sigma_{\rm RL}}\,, \tag{4.22}$$

[3] Requiring only for an upper limit implies that also other particles apart of the LSP can account for the observed relic density, such as, for example, light right-handed sneutrinos.

[4] When selecting a suitable NMSSM scenario, also the corresponding mimicking MSSM scenario is checked with `HiggsBounds-4.0.0` to ensure a sensible comparison.

and the effective polarisation

$$\mathcal{P}_{\text{eff}} = \frac{\mathcal{P}_{e^-} - \mathcal{P}_{e^+}}{1 - \mathcal{P}_{e^-}\mathcal{P}_{e^+}} \,. \tag{4.23}$$

We can see that the first factor in eq. (4.20) is enhanced by opposite-sign polarisations with increasing magnitude. Therefore with our choice $(\mathcal{P}_{e^-}, \mathcal{P}_{e^+}) = (\pm 0.9, \mp 0.55)$ we have a factor 1.21 times large than with $(\mathcal{P}_{e^-}, \mathcal{P}_{e^+}) = (\pm 0.8, \mp 0.3)$. In the meanwhile, $\mathcal{P}_{\text{eff}}$ is respectively ± 0.97 and ± 0.89 for the two pairs of configurations. Therefore we can conclude that in most of the cases with our configurations the polarised cross sections are larger. Furthermore, the effective luminosity

$$\mathscr{L}_{\text{eff}} = \frac{1}{2}\left(1 - \mathcal{P}_{e^-}\mathcal{P}_{e^+}\right)\mathscr{L} \,, \tag{4.24}$$

is also increased, with consequent improvement of statistics, that allows us to consider our assumption on the uncertainties safer. A more accurate analysis on the background would be required but it is beyond the scopes of this thesis.

χ^2-fit to the MSSM of the assumed measures.

The measured quantities and errors are used to perform a MSSM parameter determination through the χ^2-fit following the recipe in [129] and described in the following.

The chargino masses and mixing angles $\Phi_{L,R}$ can be expressed in terms of M_2, μ, $\tan\beta$ as, *cf.* eq. (2.52),

$$m^2_{\tilde{\chi}^\pm_{1,2}} = \frac{1}{2}(M_2^2 + \mu^2 + 2m_W^2 \mp \Delta_{\tilde{\chi}}) \,, \tag{4.25}$$

$$\cos 2\Phi_{L,R} = -(M_2^2 - \mu^2 \mp 2m_W^2 \cos 2\beta)/\Delta_{\tilde{\chi}} \,, \tag{4.26}$$

where $\Delta_{\tilde{\chi}} = [(M_2^2 - \mu^2)^2 + 4m_W^4 \cos^2 2\beta + 4m_W^2(M_2^2 + \mu^2) + 8m_W^2 M_2 \mu \sin 2\beta]^{1/2}$. These equations are reversed and allow to fit the parameters in terms of masses and cross-sections.

This is possible since the chargino pair production cross sections depend only on the chargino masses and mixing angles $\cos 2\Phi_{L,R}$. The latter enter the vertices $\tilde{\chi}^+\tilde{\chi}^- Z$ for the s-channel and $e^\pm\tilde{\chi}^\pm\tilde{\nu}_e$ for the t-channel of chargino pair production. Therefore the chargino (polarised) production cross-sections $\sigma^\pm\{ij\} = \sigma(e^+e^- \to \tilde{\chi}_i^\pm \tilde{\chi}_j^\mp)$ are bilinear functions in $\cos 2\Phi_{L,R}$ [167]:

$$\sigma^\pm\{ij\} = c_1 \cos^2 2\Phi_L + c_2 \cos 2\Phi_L + c_3 \cos^2 2\Phi_R + c_4 \cos 2\Phi_L + c_5 \cos 2\Phi_L \cos 2\Phi_R + c_6 \,, \tag{4.27}$$

where the coefficients $c_1, \ldots, c_6$, defined in [129], depend on the chargino masses. The angles $\cos 2\Phi_{L,R}$ can then be uniquely determined knowing $\sigma_L^\pm\{11\}$ and $\sigma_R^\pm\{11\}$, for instance, at two LC energies [128, 168], that we take to be $\sqrt{s} = 350$ GeV and $\sqrt{s} = 500$ GeV.

Finally M_2, μ, $\tan\beta$ may be obtained, using the notation in [128], as:

$$M_2 = \frac{m_W}{\sqrt{2}}[(p+q)\sin\beta - (p-q)\cos\beta]\,, \tag{4.28}$$

$$\mu = \frac{m_W}{\sqrt{2}}[(p-q)\sin\beta - (p+q)\cos\beta]\,, \tag{4.29}$$

$$\tan\beta = \left[\frac{p^2 - q^2 \pm \sqrt{r^2(p^2+q^2+2-r^2)}}{(\sqrt{1+p^2} - \sqrt{1+q^2})^2 - 2r^2}\right]^{\eta}\,, \tag{4.30}$$

where

$$p = \pm\left|\frac{\sin 2\Phi_L + \sin 2\Phi_R}{\cos 2\Phi_L - \cos 2\Phi_R}\right|, \qquad q = \frac{1}{p}\frac{\cos 2\Phi_L + \cos 2\Phi_R}{\cos 2\Phi_L - \cos 2\Phi_R}, \tag{4.31}$$

$r^2 = m^2_{\tilde{\chi}^\pm_1}/m^2_W$ and $\eta = \pm 1$ for $\cos 2\Phi_R \gtrless \cos 2\Phi_L$. In the CP-conserving MSSM, M_2, μ are uniquely fixed if $\tan\beta$ is chosen properly.

The last parameter missing is M_1, that can be uniquely extracted from neutralino sector as the solution of the characteristic equation of $\mathcal{M}_N\mathcal{M}_N^\dagger$ [129]:

$$x_i M_1^2 + y_i M_1 - z_i = 0 \text{ for } i = 1,2,3,4 \tag{4.32}$$

where x_i, y_i, z_i depend on $m_{\tilde{\chi}^0_i}$, M_2, μ and $\tan\beta$.

As previously mentioned, we assume the experimental outcome to be the tree-level masses and cross sections that we have calculated for our NMSSM scenario, with the assigned errors.

Then, we apply the MSSM parameter reconstruction method described above to deduce $M_1, M_2, \mu, \tan\beta$, as if we were supposing to have actually observed the MSSM. To understand whether we can distinguish our NMSSM scenario from the MSSM, we perform a χ^2-fit using `Minuit` [169]. This code minimizes the χ^2 function defined as

$$\chi^2 = \sum_i \left|\frac{\mathcal{O}_i - \bar{\mathcal{O}}_i}{\delta\mathcal{O}_i}\right|^2. \tag{4.33}$$

$\mathcal{O}_i$ are the input observables, δO_i are the associated experimental uncertainties and $\bar{O}_i$ are the theoretical values of the observables calculated using the fitted MSSM parameters.

The unknowns of the fit are M_1, M_2, μ, $\tan\beta$ and $m_{\tilde{\nu}_e}$.[5] Since the chargino masses and mixing angles, *cf.* eqs. 4.25 and 4.26, depend only on $\cos 2\beta$ and $\sin 2\beta$, they are weakly dependent on $\tan\beta$ if $\tan\beta \gtrsim 5$. The extraction of $\tan\beta$ will then be difficult, and sometimes only a lower limit on it could be set. A fit that is not consistent with the MSSM at 95% C.L. may suggest the NMSSM and allow a model distinction. In order to confirm this, one should elaborate dedicated studies looking for heavier neutralino resonances and singlet Higgs states. If the fit is instead consistent with the MSSM, more information is needed to establish a determination of the NMSSM, especially from the Higgs sector. The limiting (95% C.L.) value of χ^2 varies for different scenarios under consideration depending on the number of observables used in the fit. Further information for parameter reconstruction can be extracted from the $\tilde{\tau}$ sector, if kinematically reachable [170].

[5] For the fit, we shall assume that the mass $m_{\tilde{\nu}_e}$ is related to the $m_{\tilde{e}_L}$ by applying the $SU(2)_L$ relation $m^2_{\tilde{\nu}_e} = m^2_{\tilde{e}_L} + \cos(2\beta)\cos^2\theta_W m^2_Z$. In turn, we use the simplifying assumption $m_{\tilde{e}_L} = m_{\tilde{e}_R}$.

Possible integration of additional information from the Higgs sector.

Detecting a singlet Higgs state automatically excludes the MSSM, however, in the scenarios we study a direct detection is more difficult due the (high) mass of the singlet states and the very low mixing with the Higgs doublets. We consider direct singlet detection just in the scenario described in subsection 4.3.2.

Alternatively, one should consider that a relatively light singlet with substantial mixing with the SM-like Higgs could bring to observable deviations from the SM couplings predictions, that cannot be accommodated within the MSSM as well.

In the selected scenarios we expect small departure from the SM values, so we limit ourselves to compare the NMSSM predictions to the SM model by doing a χ^2-fit of the reduced couplings of the SM-like Higgs to $g, \gamma, W, Z, b, c, \tau$ obtained with `NMSSMTools`. This is useful for us, since an MSSM scenario in the decoupling limit (as the ones we look at) can easily accommodate couplings that are close the SM expectations, while larger deviations are more difficult to explain.

4.3 Classes of scenarios and model distinction

Since we assume to detect the lightest neutralino states $\tilde{\chi}_1^0$ and $\tilde{\chi}_2^0$, it is useful for the purposes of our analysis to categorise different cases on the basis of the phenomenology of these states. In particular, the singlino admixtures of $\tilde{\chi}_1^0$ and $\tilde{\chi}_2^0$ suggest the classification of NMSSM scenarios with the following limiting cases:

1. Light singlino (LS) scenarios: high $\tilde{S}$ admixture in the lightest states $\tilde{\chi}_1^0$ or $\tilde{\chi}_2^0$.
2. Light higgsino (LH) scenarios: higgsino-like $\tilde{\chi}_1^0$, with $\mu_{\text{eff}} < M_1, M_2$ and high $\tilde{S}$ admixture mainly in $\tilde{\chi}_3^0, \tilde{\chi}_4^0, \tilde{\chi}_5^0$.
3. Light gaugino (LG) scenarios: gaugino-like $\tilde{\chi}_1^0$, with $\mu_{\text{eff}} > M_1, M_2$ and high $\tilde{S}$ admixture mainly in $\tilde{\chi}_3^0, \tilde{\chi}_4^0, \tilde{\chi}_5^0$.

Studying these limiting classes of scenarios is also useful to embed intermediate cases, in which the lightest neutralinos nature is more mixed.

In LS scenarios, a high singlino admixture in $\tilde{\chi}_1^0$ and/or $\tilde{\chi}_2^0$ is easily determined and points to supersymmetry beyond the MSSM. In fact, a fit that, reconstructing the higgsino and gaugino components of neutralinos, hypothesizes the MSSM as underlying model, would give in this case a very different result with respect to the original NMSSM scenario. Here, the previously outlined strategy for model distinction seems promising, see [155] and section 4.3.1. The reconstructed MSSM gaugino and neutralino admixtures, indeed, lead to sensibly different cross sections, production channels, and decays.

In LH and LG scenarios, instead, the phenomenology of detected states $\tilde{\chi}_1^0$ and $\tilde{\chi}_2^0$ could be interpreted as MSSM-like, being a fit more likely to be compatible with the MSSM, see subsections 4.3.2 and 4.3.3. In LH and LG scenarios it may be needed then to elaborate a

	M_1 [GeV]	M_2 [GeV]	$\mu, \mu_{\text{eff}} = \lambda \cdot x$ [GeV]	$\tan\beta$	λ	κ
MSSM$_{\text{LS}}$	406	115.8	354	8	-	-
LS	365	111	484	9.5	0.16	0.0585

Table 4.1: Neutralino and chargino parameters for the NMSSM scenario LS and for the corresponding MSSM scenario MSSM$_{\text{LS}}$, at the electroweak scale.

strategy integrating informations from the heavier neutralino states, and/or from the Higgs sector.

For a fixed $\mu_{\text{eff}} = \lambda s$, in the NMSSM neutralino sector the key parameters are λ and κ, since they regulate the singlino admixture in the mass eigenstates, *cf.* the NMSSM neutralino mass matrix eq. (4.18).

In subsections 4.3.2 and 4.3.3 we consider two scenarios with heavy singlino, and we study how the model discrimination method works at the ILC along the (λ, κ)-plane, where the singlino admixtures vary. In order to do so, we scan a grid of ten thousand points in the (λ, κ)-plane for values $\lambda \in [0, 0.7]$ and $\kappa \in [0, 0.7]$. For each point passing our phenomenological and experimental constraints, we perform the χ^2-fit described above. We see how the singlino "mass" vary along the (λ, κ)-plane, and determine the regions with different phenomenology: areas corresponding to very heavy and decoupled singlino, areas in which the singlino is placed among the lightest neutralino states, as well as regions with mixed behaviour.

Note that in the following scenarios the value of $\tan\beta$ is moderately large or large. This is in contrast with the usually relatively small values, $\tan\beta \lesssim 3$–4, required to trigger a large tree-level mass value for the SM-like Higgs in the NMSSM. This may be inconvenient for naturalness but it is of interest for us, since we study challenging and limit NMSSM scenarios that may mimic the MSSM.

4.3.1 Light singlino scenario

We analyse here an NMSSM scenario with wino-like $\tilde{\chi}_1^0$ and large singlino components in $\tilde{\chi}_2^0$, $\tilde{\chi}_3^0$. We refer to it as the light singlino scenario (LS), see table 4.1 for the values of M_1, M_2, μ, $\tan\beta$ at the electroweak scale. We have also selected an MSSM scenario (MSSM$_{\text{LS}}$), *cf.* table 4.1. MSSM$_{\text{LS}}$ that features sensibly different M_1, M_2, μ, $\tan\beta$ but allows to reproduce the NMSSM lower neutralino/chargino spectrum, *cf.* tab. 4.2. Both for LS and MSSM$_{\text{LS}}$ we have $M_1 > M_2$, which is a common feature in AMSB models.

Masses, in [GeV]	$m_{\tilde{\chi}_1^0}$	$m_{\tilde{\chi}_2^0}$	$m_{\tilde{\chi}_3^0}$	$m_{\tilde{\chi}_4^0}$	$m_{\tilde{\chi}_5^0}$	$m_{\tilde{\chi}_1^\pm}$	$m_{\tilde{\chi}_2^\pm}$
MSSM$_{\rm LS}$	104.8	350.4	360.1	426.7	-	105.1	375.0
LS	104.9	350.1	360.5	489.7	504.1	105.1	498.5

Table 4.2: Neutralino and chargino masses in the LS scenario and in the corresponding reference MSSM scenario, in GeV.

Masses, in [GeV]	m_{h_1}	m_{h_2}	m_{h_3}	m_{a_1}	m_{a_2}	$m_{H^\pm}$
LS	124.9	303.0	4467.3	324.0	4467.3	4468.1

Table 4.3: LS scenario: Higgs spectrum calculated at the 1-loop level with full 2-loops contributions from bottom/top Yukawa couplings with `NMSSMTools` [158–160].

We set the other soft parameters of the NMSSM scenario to be

$$A_\lambda = 4200 \text{ GeV}, \quad A_\kappa = -200 \text{ GeV}, \tag{4.34}$$

$$M_3 = 2000 \text{ GeV}, \tag{4.35}$$

$$M_{Q_{1,2}} = M_{u_{1,2}} = M_{d_{1,2}} = 2000 \text{ GeV}, \tag{4.36}$$

$$M_{Q_3} = 1500 \text{ GeV}, \quad M_{u_3} = 1000 \text{ GeV}, \quad M_{d_3} = 800 \text{ GeV}, \tag{4.37}$$

$$M_\ell = M_e = 300 \text{ GeV}, \tag{4.38}$$

$$A_{u_3} = 2750 \text{ GeV}, \quad A_{d_3} = A_{e_3} = 2000 \text{ GeV}. \tag{4.39}$$

The Higgs spectrum is given in table 4.3, where we can see that a SM-like Higgs with $m_h \simeq 125$ GeV is reproduced.[6] With a suitable choice of the stop soft parameters, the mass m_{h_1} can be easily obtained in the MSSM$_{\rm LS}$ scenario as well. The states h_2 and a_1, being both $\sim 100\%$ singlets, are not expected to be visible both at the LHC and ILC because they are not directly coupling to other particles and are relatively heavy.

Table 4.2 shows that the light part of tree-level neutralino and chargino spectrum is nearly indistinguishable between the two scenarios.[7] However, while in both LS and MSSM$_{\rm LS}$ the lightest neutralino is a wino, $\tilde{\chi}_1^0 \sim \tilde{W}$, the other lighter states $\tilde{\chi}_2^0$, $\tilde{\chi}_3^0$ have very different admixtures in the two scenarios, see table 4.4. This leads to distinct production cross sections, due to the particular relative importance of the production channels, depending on the admixtures. The production cross sections are listed in tables 4.5 and 4.6, calculated taking

$$m_{\tilde{e}_L} = 303.5 \text{ GeV}, \quad m_{\tilde{e}_R} = 303.0 \text{ GeV}, \quad m_{\tilde{\nu}_e} = 293.4 \text{ GeV}. \tag{4.40}$$

[6] The code `NMSSMTools` takes the above parameters as inputs at the 2 TeV scale.

[7] One should note that the mass difference $m_{\tilde{\chi}_1^\pm} - m_{\tilde{\chi}_1^0}$ receives significant positive NLO corrections. For such quasi-degenerate states the mass measurement usually has a larger uncertainty than the mass difference itself. While in these analysis we only use tree-level masses, we should have in mind that in a more realistic setting one should use the mass difference as an input rather than the actual masses, see e.g. ref. [171].

	MSSM_{LS}	LS
$\tilde{\chi}_1^0$	$\sim 93\%\,\tilde{W}$	$\sim 97\%\,\tilde{W}$
$\tilde{\chi}_2^0$	$\sim 26\%\,\tilde{B} + 69\%\,\tilde{H}_{u,\,d}$	$\sim 22\%\,\tilde{B} + 73\%\,\tilde{S}$
$\tilde{\chi}_3^0$	$\sim \tilde{H}_{u,\,d}$	$\sim 72\%\,\tilde{B} + 25\%\,\tilde{S}$

Table 4.4: The dominant admixtures of the three lightest neutralinos in the LS scenario and in the corresponding MSSM scenario.

For the fit to the MSSM we only include NMSSM cross sections larger than 1 fb. Since in the NMSSM scenario $\tilde{\chi}_3^0$ is relatively light and can be produced with a sizeable cross section at 500 GeV, we also include in the fit the cross section $\sigma(e^+e^- \to \tilde{\chi}_1^0\tilde{\chi}_3^0)$ for $\mathcal{P} = (-0.9, 0.55)$.

LS		
$\sqrt{s} = 500$ GeV	$\sigma(e^+e^- \to \tilde{\chi}_1^0\tilde{\chi}_2^0)$ [fb]	$\sigma(e^+e^- \to \tilde{\chi}_1^0\tilde{\chi}_3^0)$ [fb]
$\mathcal{P} = (-0.9, 0.55)$	8.6	15.0
$\mathcal{P} = (0.9, -0.55)$	0.1	0.2

$\sigma(e^+e^- \to \tilde{\chi}_1^+\tilde{\chi}_1^-)$ [fb]	$\sqrt{s} = 350$ GeV	$\sqrt{s} = 500$ GeV
$\mathcal{P} = (-0.9, 0.55)$	2575.3	1213.0
$\mathcal{P} = (0.9, -0.55)$	42.4	18.8

Table 4.5: *LS* scenario: production cross sections for $\sigma(e^+e^- \to \tilde{\chi}_1^0\tilde{\chi}_2^0)$, $\sigma(e^+e^- \to \tilde{\chi}_1^0\tilde{\chi}_3^0)$, and $\sigma(e^+e^- \to \tilde{\chi}_1^+\tilde{\chi}_1^-)$ [fb].

The fitted MSSM parameters are

$$\begin{aligned} M_1 &= 430.0 \pm 1.6 \text{ GeV}, \quad M_2 = 111.8 \pm 0.8 \text{ GeV}, \\ \mu_{\text{eff}} &= 370.4 \pm 0.7 \text{ GeV}, \quad m_{\nu_e} = 310.6 \pm 2.8 \text{ GeV}\,, \end{aligned} \tag{4.41}$$

and $\tan\beta$ remains unconstrained (the fit gives indeed $\tan\beta = 100 \pm 98$). Using these parameters we calculate the MSSM neutralino and chargino masses listed in table 4.7 (with $\tan\beta = 100$, being the spectrum dependence on $\tan\beta$ very mild for large $\tan\beta$). The given uncertainties are based on our assumption of having fixed 1% uncertainties on the cross sections and 0.5% on the masses. Therefore, here and in the following cases, the uncertainties on the fit do not depend explicitly on the luminosity, and we assume that for each observable a suitable amount of statistics is collected, coherently with the assumed accuracy.

The χ^2-fit has $10 - 5 = 5$ degrees of freedom (d.o.f.s) and gives a value $\chi^2 = 62.6$, clearly stating that the hypothesized model, the MSSM, is not compatible with the experimental data. In fact, the 95% confidence level (C.L.) is equal to 11.1, *i.e.* it should be $\chi^2 < 11.1$ to be compatible.

MSSM$_{LS}$		
$\sqrt{s} = 500$ GeV	$\sigma(e^+e^- \to \tilde{\chi}_1^0\tilde{\chi}_2^0)$ [fb]	$\sigma(e^+e^- \to \tilde{\chi}_1^0\tilde{\chi}_3^0)$ [fb]
$\mathcal{P} = (-0.9, 0.55)$	24.1	25.1
$\mathcal{P} = (0.9, -0.55)$	0.4	5.7

$\sigma(e^+e^- \to \tilde{\chi}_1^+\tilde{\chi}_1^-)$ [fb]	$\sqrt{s} = 350$ GeV	$\sqrt{s} = 500$ GeV
$\mathcal{P} = (-0.9, 0.55)$	2491.0	1165.4
$\mathcal{P} = (0.9, -0.55)$	39.5	18.3

Table 4.6: MSSM$_{LS}$ scenario: production cross sections for $\sigma(e^+e^- \to \tilde{\chi}_1^0\tilde{\chi}_2^0)$, $\sigma(e^+e^- \to \tilde{\chi}_1^0\tilde{\chi}_3^0)$, and $\sigma(e^+e^- \to \tilde{\chi}_1^+\tilde{\chi}_1^-)$ [fb].

MSSM$_{\text{fit}}$					
$m_{\tilde{\chi}_1^0}$ [GeV]	$m_{\tilde{\chi}_2^0}$ [GeV]	$m_{\tilde{\chi}_3^0}$ [GeV]	$m_{\tilde{\chi}_4^0}$ [GeV]	$m_{\tilde{\chi}_1^\pm}$ [GeV]	$m_{\tilde{\chi}_2^\pm}$ [GeV]
106.0	368.0	378.0	445.9	106.1	389.1

Table 4.7: MSSM neutralino and chargino masses based on the resulting parameters from the fit, see eq. (4.41).

The conclusion from this fit, *i.e.* that the LS scenario can be experimentally distinguished from the MSSM, can be further corroborated by looking for heavier resonances. For example, if the measurement of the mass of the heavy neutralino $\tilde{\chi}_4^0$ is possible at the higher center-of-mass energy at ILC. Additionally, we note that the fitted mass of the heavy chargino, $m_{\tilde{\chi}_2^\pm} = 389.1$ GeV, is relatively low and the production of the mixed chargino pair, $\tilde{\chi}_1^\pm\tilde{\chi}_2^\mp$ would be possible. The expected cross section, ~ 3 fb, could in principle allow for its measurement at $\sqrt{s} = 500$ GeV. The non-observation would provide another hint on the non-minimal nature of chargino/neutralino sector, whose first candidate is the NMSSM. We have then seen that the outlined procedure for model distinction is effective effective in the case of high singlino admixture in the lightest neutralino.

4.3.2 Light higgsino scenario, $\mu_{\text{eff}} < M_1 < M_2$

We study here an NMSSM scenario with a light higgsino (LH), whose chargino/neutralino parameters at the electroweak scale are:

$$M_1 = 450 \text{ GeV}, \quad M_2 = 1600 \text{ GeV}, \quad \mu_{\text{eff}} = \lambda\, s = 120 \text{ GeV}, \quad \tan\beta = 27\,. \tag{4.42}$$

As mentioned before we scan over $\lambda \in [0, 0.7]$ and $\kappa \in [0, 0.7]$; μ_{eff} is kept fixed by varying the singlet vev s. We set the other soft parameters to be

$$A_\lambda = 3000 \text{ GeV}, \quad A_\kappa = -30 \text{ GeV}, \tag{4.43}$$

$$M_3 = 2000 \text{ GeV}, \tag{4.44}$$

$$M_{Q_{1,2}} = M_{u_{1,2}} = M_{d_{1,2}} = 2000 \text{ GeV}, \tag{4.45}$$

$$M_{Q_3} = M_{u_3} = M_{d_3} = 1500 \text{ GeV}, \tag{4.46}$$

$$M_\ell = M_e = 300 \text{ GeV}, \tag{4.47}$$

$$A_{u_3} = 3300 \text{ GeV}, \quad A_{d_3} = A_{e_3} = 2000 \text{ GeV}. \tag{4.48}$$

The slepton masses therefore read

$$m_{\tilde{e}_L} = 303.5 \text{ GeV}, \ \ m_{\tilde{e}_R} = 303.1 \text{ GeV}, \ \ m_{\tilde{\nu}_e} = 293.3 \text{ GeV}. \tag{4.49}$$

In figure 4.3 it is displayed the region scanned in the NMSSM (λ, κ)-plane, after the phenomenological tests. Points in the light-blue-shaded area pass the DM constraints;[8] the purple-shaded boundary area corresponds to points that pass the Higgs sector constraints from `HiggsBounds` and `HiggsSignals`. The solid red area is the region allowed by all the constraints, phenomenological and experimental ones, that are implemented in the codes `NMSSMTools`, `HiggsBounds` and `HiggsSignals`.

We select a reference MSSM scenario, MSSM$_{LH}$, with M_1, M_2, $\mu = \mu_{\text{eff}}$, $\tan\beta$ and the slepton masses given in eqs. (4.42) and (4.49). MSSM$_{LH}$ has the light neutralino spectrum and production cross sections reported in table 4.8. They are very close to the analogue quantities in the NMSSM scenario LH in a vast part of the (λ, κ)-plane, *cf.* figure 4.4(a) for $m_{\tilde{\chi}_1^0}$ and figure 4.5(a) for the corresponding cross sections.

Regarding the Higgs sector, it is possible to get a MSSM counterpart with experimentally the same SM-Higgs mass and a similar spectrum for the other Higgs states, with the exception of the new singlet states, for each point in the (λ, κ)-plane of the LH scenario.

In figure 4.4, the NMSSM $\tilde{\chi}_1^0$ mass and its singlino component are shown. A negligible singlino component corresponds to a region in which the NMSSM $m_{\tilde{\chi}_1^0}$ is very close to the MSSM value $m_{\tilde{\chi}_1^0} = 114.8$ GeV. Vice versa the NMSSM mass of the LSP $m_{\tilde{\chi}_1^0}$ significantly decreases with a higher singlino admixture.

Likewise, the polarised production cross sections $\sigma(e^+e^- \to \tilde{\chi}_1^0\tilde{\chi}_2^0)$ decrease with respect to predictions in the MSSM due to the larger singlino component in $\tilde{\chi}_1^0$, see figure 4.5(a). This is expected since the singlino does not couple directly to the gauge fields. We have that the tree-level NMSSM chargino masses and production cross-sections, $\sigma(e^+e^- \to \tilde{\chi}_1^+\tilde{\chi}_1^-)$, depend only on M_2, μ_{eff}, $\tan\beta$. For this reason, along all the (λ, κ)-plane the chargino production cross sections are identical to the MSSM values, displayed in table 4.8.

[8] We recall that here and in the following, we allow DM density to be below the measured value by Planck [60].

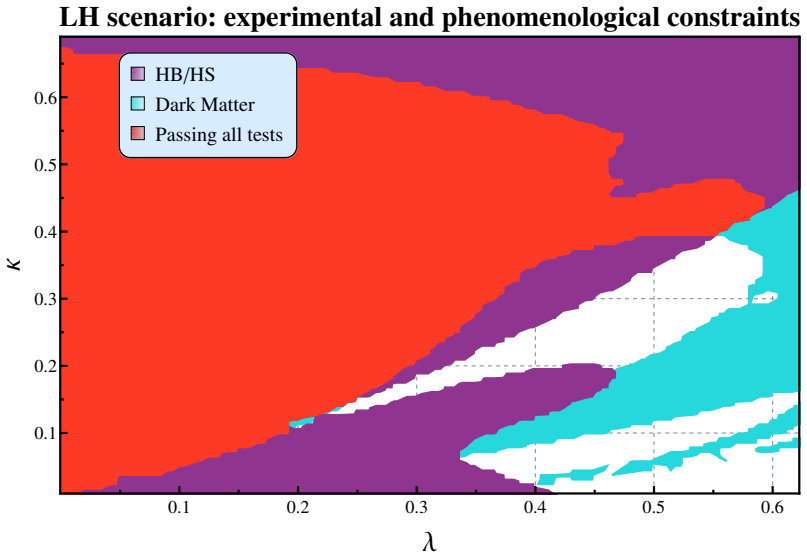

Figure 4.3: Light higgsino scenario: regions in the (λ, κ)-plane allowed by experimental and phenomenological constraints. The light-blue-shaded regions delimited by the light blue boundary pass dark matter constraints. The coloured regions delimited by the purple boundary pass checks within `HiggsBounds` and `HiggsSignals`. The red area is allowed by all the constraints.

For each point in the (λ, κ)-plane of the LH scenario, we assume the experimental measurement of:

- $m_{\tilde{\chi}_1^0}$, $m_{\tilde{\chi}_2^0}$ and $m_{\tilde{\chi}_1^\pm}$ with an uncertainty of 0.5%.
- $\sigma(e^+e^- \to \tilde{\chi}_1^0\tilde{\chi}_2^0)$ for $\mathcal{P} = (\mp 0.9, \pm 0.55)$ at $\sqrt{s} = 350$ and 500 GeV with 1% uncertainty.
- $\sigma(e^+e^- \to \tilde{\chi}_1^+\tilde{\chi}_1^-)$, for $\mathcal{P} = (\mp 0.9, \pm 0.55)$ at $\sqrt{s} = 350$ and 500 GeV with 1% uncertainty.

$\tilde{\chi}_3^0$ is lighter in the areas of the (λ, κ)-plane in which its singlino component is higher, and $e^+e^- \to \tilde{\chi}_2^0\tilde{\chi}_3^0$ may be kinematically accessible, *cf.* fig. 4.5(b). In these cases, we consider in the fit also $m_{\tilde{\chi}_3^0}$ and $\sigma(e^+e^- \to \tilde{\chi}_2^0\tilde{\chi}_3^0)$, if the latter is larger than 1 fb. The production $e^+e^- \to \tilde{\chi}_1^0\tilde{\chi}_3^0$ is negligible almost everywhere. With these assumptions, a χ^2-fit to the MSSM gives the result displayed in figure 4.6. The regions in the (λ, κ)-plane that are at 95% C.L. compatible with the MSSM are coloured in yellow, while in the black area the MSSM is excluded. We find that a significant region of the parameter space, passing the implemented phenomenological and experimental constraints, is distinguishable from the MSSM using neutralino/chargino collider observables only. This is explainable by the higher singlino component in $\tilde{\chi}_3^0$, and partially in $\tilde{\chi}_1^0$ as well, *cf.* figure 4.4(b).

We reconstruct here the MSSM parameters M_1, M_2, μ, $\tan\beta$ and $m_{\tilde{\nu}_e}$ for two sample points in the (λ, κ)-plane of the LH scenario. We choose them to be relatively close to the boundary between the regions of compatibility and incompatibility with MSSM, *cf.* fig. 4.6.

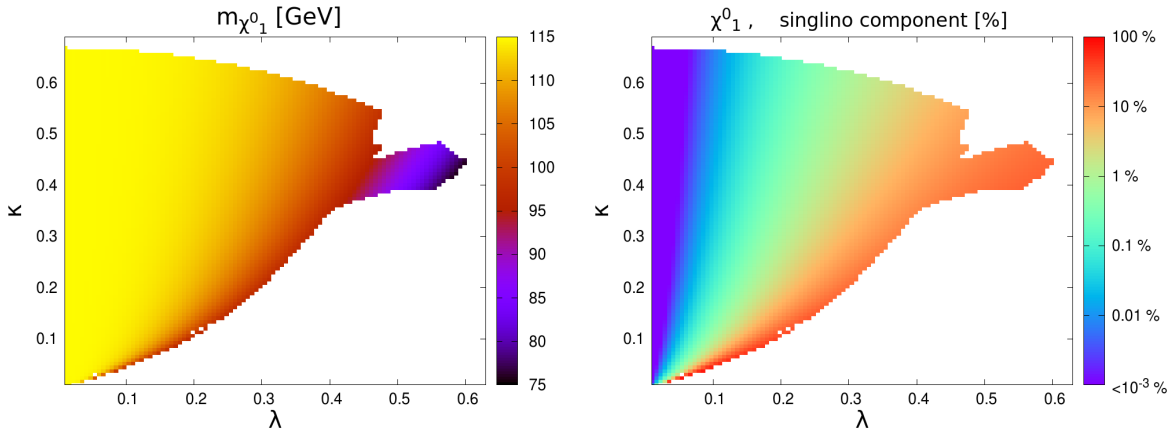

(a) (b)

Figure 4.4: LH scenario: (a) the mass $m_{\tilde{\chi}^0_1}$, in GeV; (b) the $\tilde{S}$ component of $\tilde{\chi}^0_1$, in %.

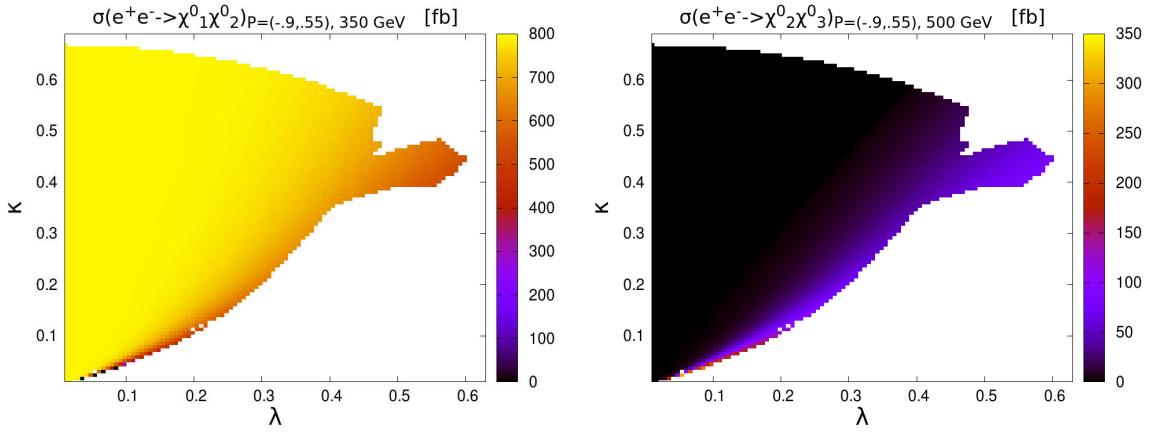

(a) (b)

Figure 4.5: Neutralino production cross sections in the LH scenario: (a) $\sigma(e^+e^- \to \tilde{\chi}^0_1\tilde{\chi}^0_2)$ for $\mathcal{P} = (-0.9, 0.55)$ at $\sqrt{s} = 350$ GeV, in fb; (b) $\sigma(e^+e^- \to \tilde{\chi}^0_2\tilde{\chi}^0_3)$ for $\mathcal{P} = (-0.9, +0.55)$ at $\sqrt{s} = 500$ GeV, in fb.

MSSM$_{LH}$					
$m_{\tilde{\chi}_1^0}$ [GeV]	$m_{\tilde{\chi}_2^0}$ [GeV]	$m_{\tilde{\chi}_3^0}$ [GeV]	$m_{\tilde{\chi}_4^0}$ [GeV]	$m_{\tilde{\chi}_1^\pm}$ [GeV]	$m_{\tilde{\chi}_2^\pm}$ [GeV]
114.8	123.3	454.4	1604.1	119.4	1604.1

$\sigma(e^+e^- \to \tilde{\chi}_1^0\tilde{\chi}_2^0)$ [fb]	$\sqrt{s} = 350$ GeV	$\sqrt{s} = 500$ GeV
$\mathcal{P} = (-0.9, 0.55)$	791.7	391.4
$\mathcal{P} = (0.9, -0.55)$	526.7	261.7

$\sigma(e^+e^- \to \tilde{\chi}_1^+\tilde{\chi}_1^-)$ [fb]	$\sqrt{s} = 350$ GeV	$\sqrt{s} = 500$ GeV
$\mathcal{P} = (-0.9, 0.55)$	2348.8	1218.9
$\mathcal{P} = (0.9, -0.55)$	445.1	246.2

Table 4.8: MSSM$_{LH}$ scenario: neutralino and chargino masses [GeV] and production cross sections $\sigma(e^+e^- \to \tilde{\chi}_1^0\tilde{\chi}_2^0)$, $\sigma(e^+e^- \to \tilde{\chi}_1^+\tilde{\chi}_1^-)$ [fb].

LH1						
$m_{\tilde{\chi}_1^0}$ [GeV]	$m_{\tilde{\chi}_2^0}$ [GeV]	$m_{\tilde{\chi}_3^0}$ [GeV]	$m_{\tilde{\chi}_4^0}$ [GeV]	$m_{\tilde{\chi}_5^0}$ [GeV]	$m_{\tilde{\chi}_1^\pm}$ [GeV]	$m_{\tilde{\chi}_2^\pm}$ [GeV]
111.6	125.2	389.0	454.4	1604	119.4	1604

$\sigma(e^+e^- \to \tilde{\chi}_1^0\tilde{\chi}_2^0)$ [fb]	$\sqrt{s} = 350$ GeV	$\sqrt{s} = 500$ GeV
$\mathcal{P} = (-0.9, 0.55)$	781.5	385.8
$\mathcal{P} = (0.9, -0.55)$	519.9	257.9

Table 4.9: Neutralino masses [GeV] and production cross sections [fb] in the light higgsino scenario, reference point LH1 with (λ, κ) =(0.25, 0.4).

- The point LH1, in $(\lambda, \kappa) = (0.25, 0.4)$, with the masses and cross sections given in tables 4.9. The fit from LH1, with 6 d.o.f.s, turns out to be compatible with the MSSM, since $\chi^2 = 1.1$, while the confidence level is equal to 12.6. The fit yields

$$\begin{aligned} &M_1 = 360 \pm 40 \text{ GeV}, \quad M_2 = 1300 \pm 300 \text{ GeV}, \\ &\mu_{\text{eff}} = 124 \pm 2 \text{ GeV}, \quad \tan\beta \leq 4, \\ &m_{\tilde{\nu}_e} \leq 470 \text{ GeV}\,. \end{aligned} \tag{4.50}$$

- For our second example, the point LH2 in $(\lambda, \kappa) = (0.36, 0.4)$ is taken and the corresponding masses and cross sections are given in tables 4.10. The point LH2 is not compatible with the MSSM, since the fit, with 7 d.o.f.s and confidence level equal to

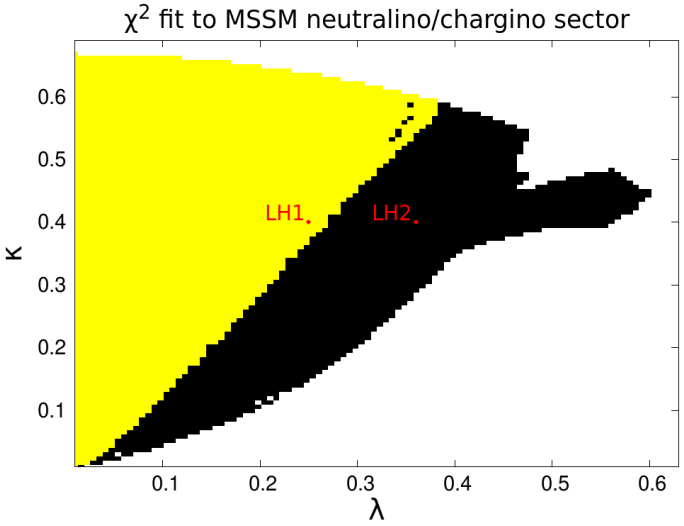

Figure 4.6: LH scenario: fit to the MSSM. Yellow areas are compatible with the MSSM at 95% C.L., while black ones are excluded by the collider observables. The points LH1 $(\lambda, \kappa) = (0.25, 0.4)$ and LH2 $(\lambda, \kappa) = (0.36, 0.4)$ are also shown.

LH2						
$m_{\tilde{\chi}_1^0}$ [GeV]	$m_{\tilde{\chi}_2^0}$ [GeV]	$m_{\tilde{\chi}_3^0}$ [GeV]	$m_{\tilde{\chi}_4^0}$ [GeV]	$m_{\tilde{\chi}_5^0}$ [GeV]	$m_{\tilde{\chi}_1^\pm}$ [GeV]	$m_{\tilde{\chi}_2^\pm}$ [GeV]
104.2	128.4	282.4	454.4	1604	119.4	1604

$\sigma(e^+e^- \to \tilde{\chi}_1^0\tilde{\chi}_2^0)$ [fb]	$\sqrt{s} = 350$ GeV	$\sqrt{s} = 500$ GeV
$\mathcal{P} = (-0.9, 0.55)$	739.0	363.3
$\mathcal{P} = (0.9, -0.55)$	491.5	242.8

$\sigma(e^+e^- \to \tilde{\chi}_2^0\tilde{\chi}_3^0)$ [fb]	$\sqrt{s} = 350$ GeV	$\sqrt{s} = 500$ GeV
$\mathcal{P} = (-0.9, 0.55)$	not accessible	15.4
$\mathcal{P} = (0.9, -0.55)$	not accessible	10.4

Table 4.10: Neutralino and chargino masses [GeV] and neutralino production cross sections [fb] in the light higgsino scenario for the reference point LH2 with (λ, κ) =(0.36, 0.4).

14.1, gives $\chi^2 = 1700$. The fitted parameters are:

$$\begin{aligned} &M_1 \text{ unconstrained}, && M_2 = 317.0 \pm 0.5 \text{ GeV}, \\ &\mu_{\text{eff}} = 129.3 \pm 0.6 \text{ GeV}, && \tan\beta < 1.1, \\ &m_{\tilde{\nu}_e} = 297 \pm 15 \text{ GeV}. \end{aligned} \tag{4.51}$$

The region compatible with the MSSM may be further reduced by using additional information from the heavier neutralino states, such as $\tilde{\chi}_3^0$ (if not already used in the fit as for the

point LH2) or $\tilde{\chi}_4^0$. For example, given a (λ, κ)-coordinate and the corresponding M_1, M_2, μ, $\tan\beta$ reconstructed from the fit, one can derive the masses of the heavier states. These can then be searched at higher energy stages of the ILC or at the LHC, with the possibility of either confirming the fit to the MSSM or pinpointing the NMSSM.

As suggested in section 4.2, our study may be extended by including information from the Higgs sector. We do a naïve 7 d.o.f.s χ^2-fit to the SM using the Higgs reduced couplings to $g, \gamma, W, Z, b, c, \tau$, and we plot it in figure 4.7(a).[9] These are defined as the ratio $g_{h_{\mathrm{SM-like}}}/g_{h_{\mathrm{SM}}}$ between the SM-like Higgs coupling in an NMSSM point to the corresponding SM Higgs coupling, and are calculated through `NMSSMTools`. In large part of the (λ, κ)-plane, the SM-like Higgs of the LH scenario is compatible with the SM ($\chi^2 \lesssim 14$), corresponding to the MSSM-like area from the fit in figure 4.6. Those areas with a higher singlet component in the SM-like Higgs correspond to a worse fit, *cf.* figure 4.7. Two regions are not compatible with the SM and have a different behaviour with respect of MSSM-like areas. We can conclude that the result of this fit on the Higgs reduced couplings is consistent with results of the fit from the neutralino/chargino sector, *cf.* fig. 4.6, without clearly improving our analysis.

If the new Higgs-singlet states are directly visible, they may provide additional information in favour of the NMSSM. This possibility opens up in a region with a higher singlino component in $\tilde{\chi}_3^0$, where the decays $\tilde{\chi}_3^0 \to \tilde{\chi}_{1,2}^0 a_1$ channels open. If the production cross section for $\tilde{\chi}_3^0$ is non-negligible one could observe the pseudoscalar a_1 via its decays $a_1 \to b\bar{b}$. In figure 4.8(a) we show an inclusive cross section for the production of a_1. Both $\tilde{\chi}_3^0$-production modes, $e^+e^- \to \tilde{\chi}_1^0\tilde{\chi}_3^0$ and $e^+e^- \to \tilde{\chi}_2^0\tilde{\chi}_3^0$, have been added up, summing over both polarisation configurations and considering the decays $\tilde{\chi}_3^0 \to \tilde{\chi}_1^0 a_1$ and $\tilde{\chi}_3^0 \to \tilde{\chi}_2^0 a_1$. The new singlet state should be clearly visible in areas of parameter space with cross sections of order 8-10 fb which, not surprisingly, are included in the area not compatible with the MSSM in fig 4.6. The detection of this state could serve as confirmation of the NMSSM, while the MSSM would be definitely excluded. As a reference, in figure 4.8(b) we also show the mass of the pseudoscalar a_1.

[9] In this fit we use, as uncertainty for each reduced coupling, the expected accuracies for the SM-like Higgs boson branching ratios $\Delta\mathrm{Br}/\mathrm{Br}$, from [42].

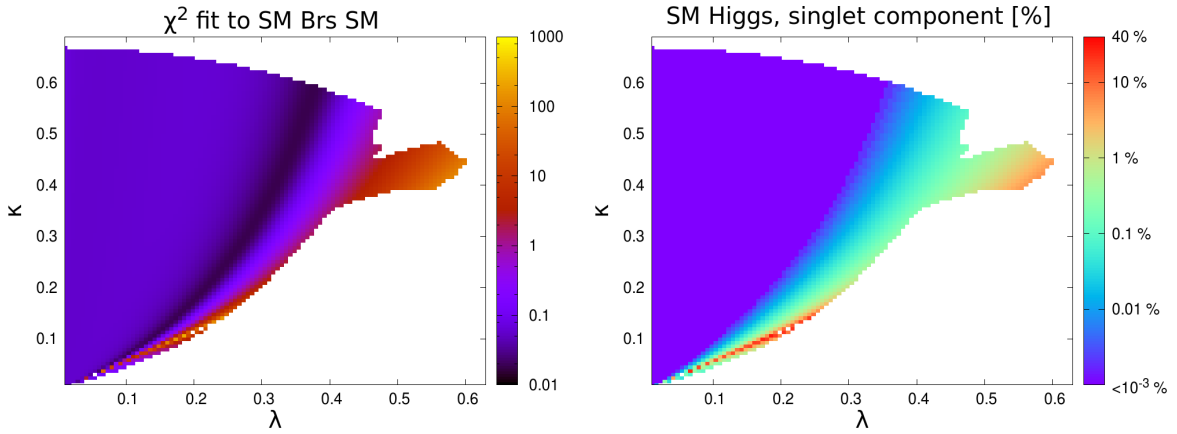

(a) (b)

Figure 4.7: LH scenario: (a) 7-d.o.f. χ^2-fit to the SM of the reduced couplings to $g, \gamma, W, Z, b, c, \tau$; (b) Singlet component in the SM-like Higgs, in %.

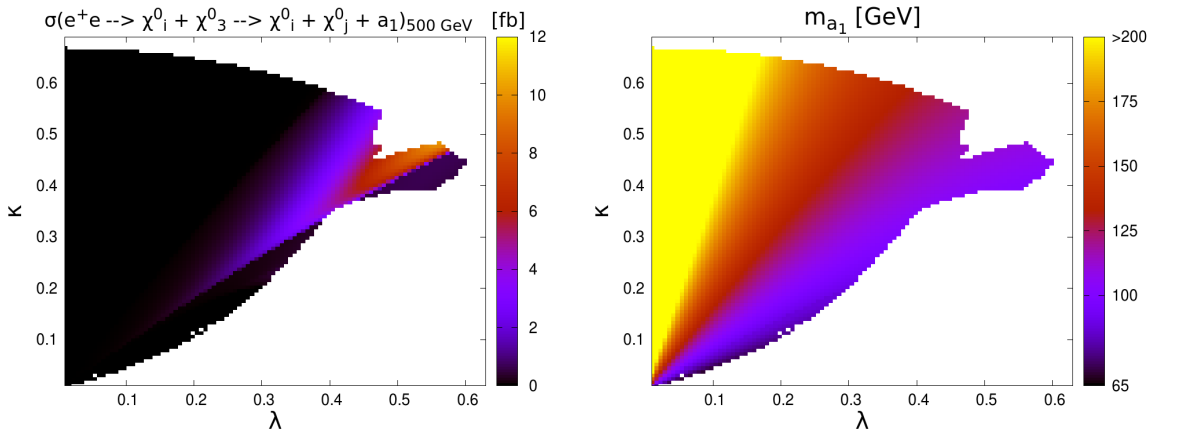

(a) (b)

Figure 4.8: LH scenario: (a) inclusive cross section $e^+e^- \to \tilde{\chi}^0_i\tilde{\chi}^0_3 \to \tilde{\chi}^0_i\tilde{\chi}^0_j a_1$ [fb], with $i, j = 1, 2$; (b) lightest $\mathcal{CP}$-odd Higgs mass m_{a_1} [GeV].

4.3.3 Light gaugino scenario, $\mu_{\rm eff} > M_1 > M_2$

As last example, we study here an NMSSM scenario with light gauginos (LG), whose neutralino/chargino parameters at the electroweak scale are:

$$M_1 = 240 \text{ GeV}, \quad M_2 = 105 \text{ GeV}, \quad \mu = \mu_{\rm eff} = 505 \text{ GeV}, \quad \tan\beta = 9.2\,, \tag{4.52}$$

with $\lambda \in [0, 0.7]$ and $\kappa \in [0, 0.7]$. The other soft parameters are set to

$$A_\lambda = 3700 \text{ GeV}, \quad A_\kappa = -40 \text{ GeV}\,, \tag{4.53}$$
$$M_3 = 2000 \text{ GeV}\,, \tag{4.54}$$
$$M_{Q_{1,2}} = M_{u_{1,2}} = M_{d_{1,2}} = 2000 \text{ GeV}\,, \tag{4.55}$$
$$M_{Q_3} = 1800 \text{ GeV}, \quad M_{u_3} = M_{d_3} = 1500 \text{ GeV}\,, \tag{4.56}$$
$$M_{\ell_{1,2}} = M_{e_{1,2}} = 300 \text{ GeV}, \quad M_{\ell_3} = M_{e_3} = 500 \text{ GeV}\,, \tag{4.57}$$
$$A_{u_3} = 3700 \text{ GeV}, \quad A_{d_3} = 2500 \text{ GeV}, \quad A_{e_3} = 1500 \text{ GeV}\,. \tag{4.58}$$

The first generation slepton masses then are

$$m_{\tilde{e}_L} = 303.4 \text{ GeV}, \quad m_{\tilde{e}_R} = 303 \text{ GeV}, \quad m_{\tilde{\nu}_e} = 293.5 \text{ GeV}\,. \tag{4.59}$$

The result of the scan in the NMSSM (λ, κ)-plane with respect to all tests implemented in `NMSSMTools`, `HiggsBounds` and `HiggsSignals` is displayed in figure 4.9. The colour conventions in figure 4.9 are the same as in fig. 4.3. For the LG scenario the regions allowed by the Higgs sector constraints from `HiggsBounds` and `HiggsSignals` overlap entirely those passing dark matter constraints.

We define the MSSM scenario MSSM$_{LG}$ to have M_1, M_2, μ, $\tan\beta$ and the first generation slepton masses as in eq. (4.52). Its lighter neutralino and chargino mass spectrum and production cross sections are almost indistinguishable (at the tree-level) with the value for the LG scenario along (λ, κ)-plane, see table 4.11.

In particular, in the LG scenario $m_{\tilde{\chi}_1^0}$ is very close to the MSSM$_{LG}$ value of 99.5 GeV, *cf.* figure 4.10. Its value varies very mildly in the (λ, κ)-plane since the singlino component in $\tilde{\chi}_1^0$ is approximately zero. The same pattern applies to the production cross section $\sigma(e^+e^- \to \tilde{\chi}_1^0\tilde{\chi}_2^0)$. Finally, the production cross sections for the process $e^+e^- \to \tilde{\chi}_1^+\tilde{\chi}_1^-$, are exactly identical between the two scenarios at the tree-level, as explained in section 4.3.2.

For our χ^2-fit to the MSSM we only use cross sections larger than 1 fb. Figure 4.11 shows that this fit alone is not sufficient to distinguish between the two models in this case. In fact, basically every point in the allowed region is compatible with the MSSM.

As operative example we select the point LG1 with $(\lambda, \kappa) = (0.2, 0.35)$. The corresponding masses and cross sections are listed in table 4.12. For $\mathcal{P} = (0.9, -0.55)$ the cross section $\sigma(e^+e^- \to \tilde{\chi}_1^0\tilde{\chi}_2^0)$ at $\sqrt{s} = 350$ GeV is below 1 fb and the process $e^+e^- \to \tilde{\chi}_1^0\tilde{\chi}_3^0$ is kinematically not allowed for both at 350 and 500 GeV. The remaining observables lead to a 5 d.o.f.s fit

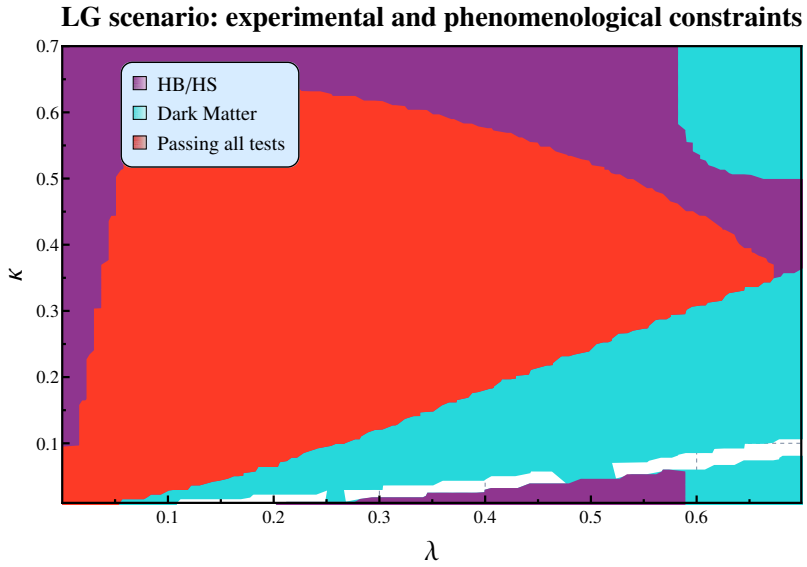

Figure 4.9: The light gaugino scenario: regions in the (λ, κ)-plane allowed by experimental and phenomenological constraints. The light-blue region passes the dark matter constraints. The purple-coloured region passes checks from `HiggsBounds` and `HiggsSignals`. The areas allowed by all the constraints are shown in red.

that is compatible with the MSSM, giving χ^2=0.07. The fitted parameters are

$$\begin{aligned} M_1 &= 239.9 \pm 0.9 \text{ GeV}, \quad M_2 = 104.4 \pm 0.8 \text{ GeV}, \\ \mu_{\text{eff}} &= 504.7 \pm 47.6 \text{ GeV}, \quad \tan\beta = 11.4 \pm 2.8, \\ m_{\tilde{\nu}_e} &= 292.8 \pm 3.9 \text{ GeV}\,. \end{aligned} \tag{4.60}$$

These values are remarkably close to the 'true' input parameters given by eqs. (4.52) and (4.59). Fitting the SM-like Higgs reduced couplings reveals, as well, to be not effective for model distinction, see figure 4.12. Unlike in the LH scenario, all the allowed regions in the (λ, κ)-plane are compatible with the SM.

These conclusions can be explained by analysing the mixing within the neutralino sector. In the NMSSM, the singlino does not mix directly with gauginos but only indirectly via higgsino states, see eq. (4.18). In the case $\mu_{\text{eff}} \gg M_1, M_2$ as in the LG scenario, the mixing remains small even for a relatively light singlino. Therefore the properties of the light chargino and neutralino states, including masses and cross sections, remain very similar throughout the (λ, κ)-plane and cannot be distinguished from the MSSM case. This is in contrast with the LS scenario from section 4.3.1. There, $M_1 = 365$ GeV and $\mu_{\text{eff}} = 484$ GeV are of the similar size, resulting then in a significant mixing: $\tilde{\chi}_2^0 \simeq 22\%\,\tilde{B} + 73\%\,\tilde{S}$ and $\tilde{\chi}_3^0 \simeq 72\%\,\tilde{B} + 25\%\,\tilde{S}$. Since in the LS case the singlino component makes up a significant part of the light neutralinos, the modification of the couplings allows there a clear discrimination from the MSSM.

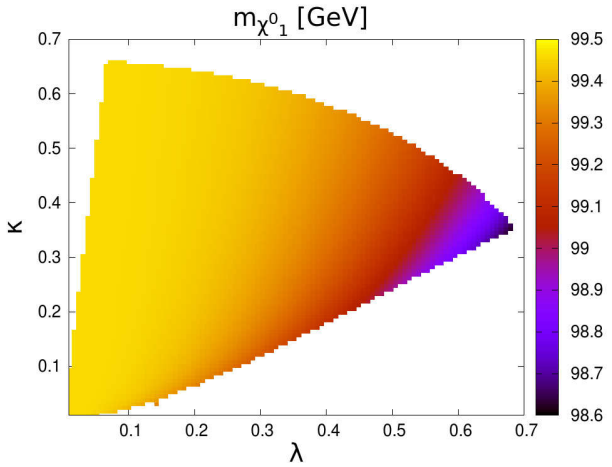

Figure 4.10: The LG scenario: the mass $m_{\tilde{\chi}_1^0}$ [GeV].

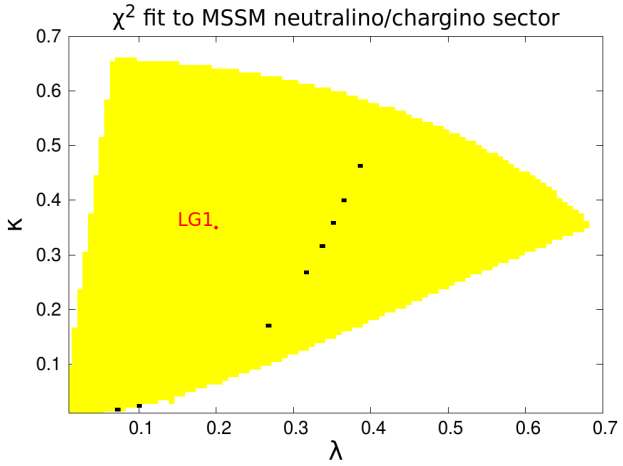

Figure 4.11: LG scenario: fit to the MSSM. Yellow areas are compatible with the MSSM at 95% C.L., while black ones are excluded by the collider observables. The point LG1 (λ, κ) =(0.2, 0.35) is displayed.

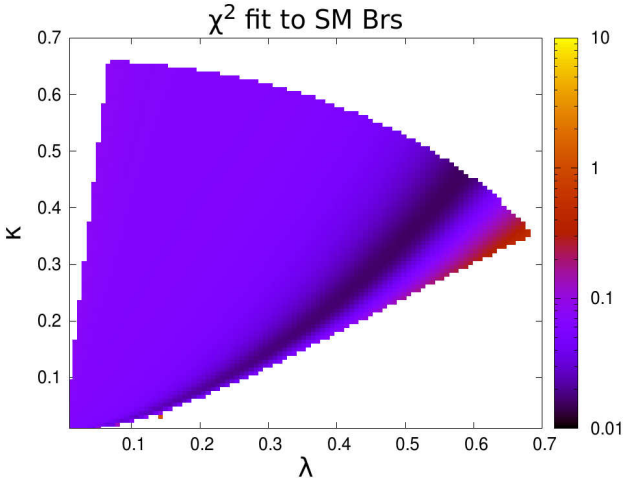

Figure 4.12: LG scenario: χ^2-fit to the SM of the reduced Higgs boson couplings to $g, \gamma, W, Z, b, c, \tau$.

MSSM$_{LG}$					
$m_{\tilde{\chi}_1^0}$ [GeV]	$m_{\tilde{\chi}_2^0}$ [GeV]	$m_{\tilde{\chi}_3^0}$ [GeV]	$m_{\tilde{\chi}_4^0}$ [GeV]	$m_{\tilde{\chi}_1^\pm}$ [GeV]	$m_{\tilde{\chi}_2^\pm}$ [GeV]
99.5	237.0	510.1	518.7	99.6	518.7

$\sigma(e^+e^- \to \tilde{\chi}_1^0\tilde{\chi}_2^0)$ [fb]	$\sqrt{s} = 350$ GeV	$\sqrt{s} = 500$ GeV
$\mathcal{P} = (-0.9, 0.55)$	7.3	113.4
$\mathcal{P} = (0.9, -0.55)$	0.1	1.8

$\sigma(e^+e^- \to \tilde{\chi}_1^+\tilde{\chi}_1^-)$ [fb]	$\sqrt{s} = 350$ GeV	$\sqrt{s} = 500$ GeV
$\mathcal{P} = (-0.9, 0.55)$	2692.1	1252.6
$\mathcal{P} = (0.9, -0.55)$	44.5	19.4

Table 4.11: The reference light gaugino MSSM scenario: neutralino and chargino masses [GeV] and production cross sections $\sigma(e^+e^- \to \tilde{\chi}_1^0\tilde{\chi}_2^0)$, $\sigma(e^+e^- \to \tilde{\chi}_1^+\tilde{\chi}_1^-)$ [fb].

LG1						
$m_{\tilde{\chi}_1^0}$	$m_{\tilde{\chi}_2^0}$	$m_{\tilde{\chi}_3^0}$	$m_{\tilde{\chi}_4^0}$	$m_{\tilde{\chi}_5^0}$	$m_{\tilde{\chi}_1^\pm}$	$m_{\tilde{\chi}_2^\pm}$
99.4 GeV	237.0 GeV	510.4 GeV	518.3 GeV	1768.2 GeV	99.5 GeV	518.7 GeV

$\sigma(e^+e^- \to \tilde{\chi}_1^0\tilde{\chi}_2^0)$	$\sqrt{s} = 350$ GeV	$\sqrt{s} = 500$ GeV
$\mathcal{P} = (-0.9, 0.55)$	7.3 fb	113.5 fb
$\mathcal{P} = (0.9, -0.55)$	0.1 fb	1.8 fb

Table 4.12: Neutralino and chargino masses [GeV] and neutralino production cross sections [fb] in the light gaugino scenario for the reference point LG1 with (λ, κ) =(0.2, 0.35).

4.4 Summary and conclusions

The next-to-minimal supersymmetric SM (NMSSM) minimally extends the MSSM by an additional chiral superfield $\hat{S}$ which is a singlet of the gauge symmetry $SU(3)_C \otimes SU(2)_L \otimes U(1)_Y$. After electroweak symmetry breaking, this translates into an additional $\mathcal{CP}$-even Higgs, an additional $\mathcal{CP}$-odd Higgs, as well as a fifth neutralino with respect to the MSSM. One of the most appealing features of the NMSSM is the fact that it explains the μ-problem dynamically, relating μ to the supersymmetry breaking scale M_{SUSY} via the vev of the singlet, that has been generated at M_{SUSY}. Furthermore, the tree-level Higgs mass receives an additional positive term due to the mixing with the scalar singlet component. In particular, in the NMSSM the SM-like Higgs mass needs smaller radiative corrections to reach the measured value of ~ 125.5 GeV, with the direct consequence of a relaxation of naturalness in the stop sector.

The phenomenology of the NMSSM may be distinguished at the LHC and at the ILC looking at the extended Higgs and neutralino sectors. However, there are classes of NMSSM scenarios that are more difficult to distinguish from the MSSM due to relatively heavy and/or decoupled singlet states, that may not be precisely resolved at the LHC or kinematically reached at the ILC.

In particular, we have studied how much information can be derived from the neutralino and chargino sector at a linear collider for the model distinction. More specifically, we have analysed a series of more intriguing NMSSM scenarios with heavy singlet Higgs. Furthermore the lower Higgs spectrum (including the SM-like Higgs) and the lower neutralino/chargino spectrum of these scenarios are very close in masses and production cross section to some MSSM scenarios. Since we assume to observe the lightest neutralino states, we have categorised these scenarios in several classes, depending on the admixtures of these states, either with high singlino-, or higgsino-, or gaugino component. Given an NMSSM scenario, we have assumed to operate a LC at $\sqrt{s} = 350$ and 500 GeV with polarisations $(\mathcal{P}_{e^-}, \mathcal{P}_{e^+}) = (\pm 0.9, \mp 0.55)$, and to have measured the masses and polarised production cross-sections of $\tilde{\chi}_1^\pm$, $\tilde{\chi}_1^0$, $\tilde{\chi}_2^0$, and $\tilde{\chi}_3^0$, if viable. From the obtained masses and cross sections, and with plausible experimental uncertainties, we have reconstructed through a χ^2-fit the neutralino sector parameters M_1, M_2, μ, $\tan\beta$, as well as $m_{\tilde{\nu}_e}$, assuming the MSSM as the underlying model. A non-compatible fit with the MSSM may suggest the NMSSM as the right model. This could be confirmed by looking for heavier neutralino and chargino resonances at the LC and the LHC or by integrating the information from the Higgs sector, such as deviations in the Higgs couplings or the production of singlet-like states.

We have first analysed a light singlino NMSSM scenario which, having $\tilde{\chi}_2^0$ a dominant singlino component, could allow us to clearly exclude the MSSM, as expectable. We have then studied in the (λ, κ)-plane an NMSSM scenarios with higgsinos as lightest neutralinos, and we could define regions where model distinction was possible, in correspondence of an increase of the singlino component in $\tilde{\chi}_1^0$. This results are also corroborated by the possibility to observe the production of the $\mathcal{CP}$-odd singlet a_1 in some parameter regions. Finally, we could observe how scenarios with light gauginos are very difficult to be distinguished from the MSSM, because of a low mixing with the higgsinos, due to hierarchy between M_1 and M_2 with μ_{eff}.

Chapter 5

Non-decoupling D-terms and the Higgs boson

This chapter is based on the publication [3], done in collaboration with Moritz McGarrie and Gudrid Moortgat-Pick. It describes my research work on non-decoupling D-terms extensions of the MSSM. The study has focussed on the naturalness implications of these models and the experimental reach of the LHC and the ILC to detect correlated deviations in the Higgs couplings. Section 5.1 introduces gauge extensions of the MSSM that at lower energies result in non-decoupling D-terms extensions of the MSSM. In section 5.2 I derive the Higgs masses in two models extending the MSSM with non-decoupling D-terms and discuss the size of the non-decoupling D-terms in view of naturalness. Section 5.3 describes the results on the estimates of the reach of colliders, of which I am the main author. In section 5.4 I summarise and conclude. Part of the text is derived from what I wrote in [3]. The plots have been produced by me, excluding figs. 5.6, 5.7, 5.12. The main resources of this chapter are refs. [91,96,97,172].

5.1 Introduction

5.1.1 Concept

We have seen that relatively heavy stop masses or a high stop mixing are needed in the MSSM to reach the observed Higgs mass value of 125.5 GeV, through large radiative corrections. The tree level Higgs mass, indeed, is bounded from above by $m_Z = 91.2$ GeV. The related naturalness may be relaxed by raising the tree level Higgs mass with additional contributions to the tree-level Higgs quartic potential. This can be done through additional non-decoupling D-terms, as it was originally proposed in [96,97] and in the unpublished talk [173]. The basic concept is to have an extended gauge group that breaks to the MSSM gauge group above the electroweak scale. This gives raise to additional D-terms for the scalars of the model with respect to the MSSM. This additional D-terms would decouple in the supersymmetric limit, giving a negligible contribution to the Higgs mass. Therefore, a supersymmetry-breaking mass term for the field that causes the gauge-symmetry breaking is introduced at or above the

gauge-symmetry breaking.[1] There are several UV completions to models with non-decoupling D-terms, especially quiver models [96,97], where here with *quiver* or *moose* we mean a gauge factor copy. Other examples may be found in the context of extra dimensions [174]. The low energy phenomenology of these models may be seen as that of the MSSM with some deviations in the couplings, of the Higgs particularly.

We show in this section how non-decoupling D-terms may arise in the simplest case of a two-site quiver model [3,91,96,97], *i.e.* in which the gauge group has two copies of the same factor. This logic may be applied also to the case of three or more quiver factors. Other descriptions of quiver models as UV completions of the MSSM may be found in [98,172,175–183].

5.1.2 Basic example: $SU(2) \otimes SU(2)$

We consider a supersymmetric quiver model whose gauge group $\mathcal{G}$ is given by the product of two copies of the $SU(2)$ gauge group, $\mathcal{G}_A = SU(2)_A$ on site A and $\mathcal{G}_B = SU(2)_B$ on site B, such that $\mathcal{G} = \mathcal{G}_A \otimes \mathcal{G}_B$. The two sites may be connected by one or more linking fields that, acquiring vevs, are responsible for diagonal symmetry breaking $\mathcal{G} \to SU(2)_D$.

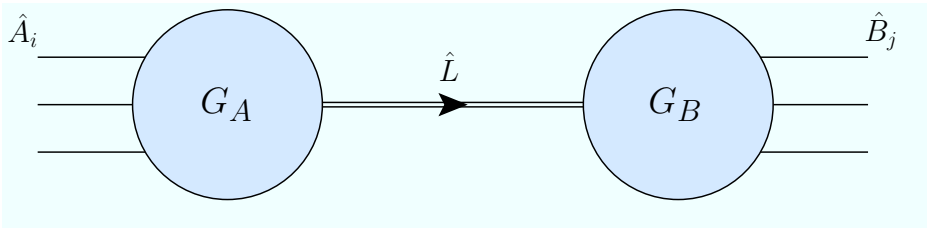

Figure 5.1: The quiver module of the toy model with $\mathcal{G} = SU(2)_A \otimes SU(2)_B$ with $\hat{L}$ connecting the sites and the chiral superfields $\hat{A}_i, \hat{B}_j$ respectively on site A and B. The singlet superfield S is not shown.

Two sites, one linking field As first example we consider the case, *cf.* fig. 5.1, in which a chiral linking superfield $\hat{L}$ connects sites A and B transforming as $(\mathbf{2}, \bar{\mathbf{2}})$ under $\mathcal{G} = \mathcal{G}_A \otimes \mathcal{G}_B = SU(2)_A \otimes SU(2)_B$, as in [172,177–179]. The bidoublet $\hat{L}$ gets vev through the superpotential

$$\mathcal{W}_L = \lambda \hat{S} \left(\frac{1}{2} \hat{L} \cdot \hat{L} - w^2 \right) , \tag{5.1}$$

where an auxiliary singlet chiral superfield $\hat{S}$ has been introduced. With "$\cdot$" here we mean a contraction with two $\epsilon_{\alpha\beta}$ tensors with $SU(2)_A$ and $SU(2)_B$ indices respectively, *i.e.* $\hat{L} \cdot \hat{L} = \hat{L}^{\alpha\dot{\alpha}} \epsilon_{\alpha\beta} \epsilon_{\dot{\alpha}\dot{\beta}} \hat{L}^{\beta\dot{\beta}}$. The gauge interactions for $\hat{L}$ are described by the Kähler potential

$$\mathcal{K}_L = \mathrm{Tr}\, [e^{g_a \hat{V}_a} \hat{L}\, e^{-g_b \hat{V}_b}\, \hat{L}^\dagger] , \tag{5.2}$$

[1] The upper bound on the Higgs mass is perceivably increased if the additional gauge group is asymptotically free [96].

where g_a, g_b are the gauge couplings of $\mathcal{G}_A$, $\mathcal{G}_B$ and $\hat{V}_A$, $\hat{V}_B$ are the corresponding gauge vector supermultiplets (the gauge generators are implicitly inserted in the notation). The rest of the matter content of the model is given by the chiral superfields $\hat{A}_i$ on site A, gauged under $\mathcal{G}_A$, and by the chiral superfields $\hat{B}_j$ on site B, gauged under $\mathcal{G}_B$. Correspondingly, we have

$$\mathcal{K}_{A_i,\,B_j} = \sum_i \hat{A}_i^\dagger e^{g_a \hat{V}_a} \hat{A}_i + \sum_j \hat{B}_j^\dagger e^{g_b \hat{V}_b} \hat{B}_j \,. \tag{5.3}$$

From the Kähler terms (5.2) and (5.3), we can derive the Lagrangian D-terms for the scalar components of the chiral superfields:

$$\mathcal{L}_{D\text{-terms}} = \frac{g_a^2}{2}\left(\mathrm{Tr}\left[L^\dagger T^c L\right] + A_i^\dagger T^c A_i\right)^2 + \frac{g_b^2}{2}\left(\mathrm{Tr}\left[L\, T^c L^\dagger\right] + B_j^\dagger T^c B_j\right)^2 , \tag{5.4}$$

where we recall that to denote the scalars, we remove the hat "$\hat{}$" from the symbol of the corresponding chiral superfield; T^c is the $SU(2)$ generator in the fundamental representation.

We can derive the scalar potential for L from the eqs. (5.1) and (5.4):

$$\mathcal{V}_L(L,\, L^\dagger) = -\frac{\lambda w^2}{2} L\cdot L + \text{h.c.} + \frac{\lambda^2}{4}|L\cdot L|^2 + D\text{-terms} \,. \tag{5.5}$$

Taking $\lambda w^2 > 0$, $\mathcal{V}_L$ has the D-flat minima (meaning that the D-terms in eq. (5.5) vanish),

$$\langle L\rangle = 0 \qquad , \qquad \langle L\rangle = \frac{w}{\sqrt{\lambda}}\,\mathbb{1}_{2\times 2} = u\,\mathbb{1}_{2\times 2} \,. \tag{5.6}$$

The second solution is responsible for the diagonal gauge symmetry breaking $\mathcal{G}_A \otimes \mathcal{G}_B \to \mathcal{G}_D$.[2] After the diagonal symmetry breaking, the bidoublet $\hat{L}$ splits into a complex $SU(2)$-singlet scalar $\hat{L}_S$ and a complex $SU(2)$-triplet scalar $\hat{L}_T$, since $\mathbf{2}\otimes\bar{\mathbf{2}} \to \mathbf{1}+\mathbf{3}$. It can be written as

$$\hat{L} = \left(u + \hat{L}_S\right)\,\mathbb{1}_{2\times 2} + \hat{L}_T^c\,\sigma^c \,, \tag{5.7}$$

where σ^c $(c = 1, 2, 3)$ denote the Pauli matrices.

After the diagonal breaking $\mathcal{G}_A \otimes \mathcal{G}_B \to \mathcal{G}_D$, the gauge vectors V_a and V_b recombine into a massless and a heavy vector bosons that can respectively be written as

$$V_D = \frac{g_a V_b + g_b V_a}{\sqrt{g_a^2 + g_b^2}} \quad , \quad V_H = \frac{-g_a V_a + g_b V_b}{\sqrt{g_a^2 + g_b^2}} \,, \tag{5.8}$$

with the coupling constant g_D for $\mathcal{G}_D$, defined as $g_D^{-2} = g_a^{-2} + g_b^{-2}$. Eqs. (5.8) are equivalent to

$$g_a V_A = g_D V_D - g_D \frac{g_a}{g_b} V_H \quad , \quad g_b V_b = g_D V_D + g_D \frac{g_b}{g_a} V_H \,. \tag{5.9}$$

According to the Super Higgs mechanism [184], when a vev breaks a gauge symmetry (but not necessarily supersymmetry), a massless vector supermultiplet eats a chiral supermultiplet

[2] One may also add in eq. 5.5 a soft term, $+m_L^2\,|L|^2$, giving then $u = \sqrt{\frac{\lambda w^2 - m_L^2}{\lambda^2}}$, provided that $\lambda w^2 > m_L^2$.

to get the additional degrees of freedom to form a massive vector supermultiplet. The latter is made up of a real scalar field, a vector boson and a Dirac fermion, see [49, 185] for details. In our case, correspondingly to the breaking $\mathcal{G}_A \otimes \mathcal{G}_B \to \mathcal{G}_D$, a massive vector superfield $\hat{V}_H$ has formed. It contains the real part of the scalar L_T, the massive vector boson $V_{H\,\mu}$, and a Dirac fermion given by the fermionic component of $\hat{L}_T$ and by λ_H, the gaugino corresponding to the broken generators of the gauge symmetry.

We want now to pass to the low energy phenomenology, at the electroweak scale, and to do this we need to integrate out the heavy vector superfield $\hat{V}_H$. In its Kähler potential, obtained by dropping the vev $\langle L \rangle$ in (5.2), it appears the mass term

$$\mathcal{K}_{V_H} = m_V^2\, \hat{V}_H^2 + \dots\,, \tag{5.10}$$

with the mass $m_V^2 = u^2(g_a^2 + g_b^2)$. We can use equations (5.9) to rewrite the Kähler potential for $\hat{A}_i$, $\hat{B}_j$:

$$\begin{aligned}
\mathcal{K}_{A_i,\,B_j} &= \sum_i \hat{A}_i^\dagger e^{g_a \hat{V}_a} \hat{A}_i + \sum_j \hat{B}_j^\dagger e^{g_b \hat{V}_b} \hat{B}_j \\
&= \sum_i \hat{A}_i^\dagger e^{g_D \hat{V}_D - g_D \frac{g_a}{g_b} \hat{V}_H} \hat{A}_i + \sum_j \hat{B}_j^\dagger e^{g_D \hat{V}_D + g_D \frac{g_b}{g_a} \hat{V}_H} \hat{B}_j \\
&= \sum_i \left(\hat{A}_i^\dagger e^{g_D \hat{V}_D} \hat{A}_i - g_D \frac{g_a}{g_b} \hat{A}_i^\dagger \hat{V}_H \hat{A}_i + \dots \right) \\
&\quad + \sum_j \left(\hat{B}_j^\dagger e^{g_D \hat{V}_D} \hat{B}_j + g_D \frac{g_b}{g_a} \hat{B}_j^\dagger \hat{V}_H \hat{B}_j + \dots \right) .
\end{aligned} \tag{5.11}$$

Finally, integrating out $\hat{V}_H$ using the equations of motion, we get for the chiral superfields the effective Kähler potential:[3]

$$\begin{aligned}
\mathcal{K}^{\text{eff}}_{A_i,\,B_j} &= \sum_i \hat{A}_i^\dagger e^{g_D \hat{V}_D} \hat{A}_i + \sum_j \hat{B}_j^\dagger e^{g_D \hat{V}_D} \hat{B}_j \\
&\quad + \sum_c \frac{g_D^2}{m_V^2} \left(\frac{g_a}{g_b} \sum_i \hat{A}_i^\dagger T_D^c \hat{A}_i - \frac{g_b}{g_a} \sum_j \hat{B}_j^\dagger T_D^c \hat{B}_j \right)^2 ,
\end{aligned} \tag{5.12}$$

having written T_D^c as generators of $SU(2)_D$ in the fundamental representation. The last term in eq. (5.12) gives rise to D-terms of the form

$$\mathcal{L}_{D\text{-terms}} \supset - \sum_c \frac{g_D^2}{2m_V^2} \left(\frac{g_a}{g_b} \sum_i A_i^\dagger T_D^c A_i - \frac{g_b}{g_a} \sum_j B_j^\dagger T_D^c B_j \right)^2 , \tag{5.13}$$

which are decoupled, considering the suppression due to the $\hat{V}_H$-propagator $1/m_V^2$ (with null external momentum). Since we are looking for a mechanism that could enhance quartic scalar

[3] This is equivalent to integrate out the lowest component of $\hat{V}_H$ [97], corresponding to the scalar field eaten by $\hat{V}_H$ with the Super Higgs mechanism, *i.e.* the previously mentioned real part of the scalar L_T.

couplings together with their masses, we need to avoid these D-terms to decouple. This can be done with the introduction of the soft mass m_{soft} for the linking field, at least at the scale of the $\mathcal{G}$ gauge breaking. Therefore, starting again from the Kähler potential eq. (5.2), this is modified to

$$\mathcal{K}_{L,\tilde{L}} = (1+\theta^4 m_{\text{soft}}^2)\left(\text{Tr}\,[e^{g_a\hat{V}_a}\hat{L}\,e^{-g_b\hat{V}_b}\,\hat{L}^\dagger] + \text{Tr}\,[e^{g_b\hat{V}_b}\hat{\tilde{L}}\,e^{-g_a\hat{V}_a}\,\hat{\tilde{L}}^\dagger]\right). \tag{5.14}$$

This leads to the mass term for $\hat{V}_H$:

$$\mathcal{K}_{V_H} = m_V^2\,(1+\theta^4 m_{\text{soft}}^2)\,\hat{V}_H^2 + \dots\,. \tag{5.15}$$

We may now integrate out $\hat{V}_H$, taking into account the equations of motion and the vector superfield propagator

$$\Delta_{V_H}(k,\theta,\bar{\theta}) = -\frac{1}{k^2-m_V^2} + \frac{\theta^4\,m_{\text{soft}}^2}{k^2-(m_V^2+m_{\text{soft}}^2)} + \dots\,, \tag{5.16}$$

where k is the external momentum. We then get the effective Kähler potential,

$$\begin{aligned}\mathcal{K}^{\text{eff}}_{A_i,\,B_j} =& \sum_i \hat{A}_i^\dagger e^{g_D\hat{V}_D}\hat{A}_i + \sum_j \hat{B}_j^\dagger e^{g_D\hat{V}_D}\hat{B}_j \\ &+ \sum_c g_D^2\left(\frac{1}{m_V^2} - \frac{\theta^4 m_{\text{soft}}^2}{m_V^2+m_{\text{soft}}^2}\right)\left(\frac{g_a}{g_b}\sum_i \hat{A}_i^\dagger T_D^c \hat{A}_i - \frac{g_b}{g_a}\sum_j \hat{B}_j^\dagger T_D^c \hat{B}_j\right)^2 .\end{aligned} \tag{5.17}$$

Therefore the D-terms read

$$\mathcal{L}_{D\text{-terms}} \supset -\sum_c \frac{g_D^2}{2}\frac{m_{\text{soft}}^2}{m_V^2+m_{\text{soft}}^2}\left(\frac{g_a}{g_b}\sum_i A_i^\dagger T_D^c A_i - \frac{g_b}{g_a}\sum_j B_j^\dagger T_D^c B_j\right)^2 , \tag{5.18}$$

meaning that they are not decoupled, as desired.

We may now pass to a more concrete case involving two copies of $SU(2)$ that break to the electroweak $SU(2)_L$, *i.e.* $\mathcal{G}_A\otimes\mathcal{G}_B\otimes U(1)_Y \to SU(2)_L\otimes U(1)_Y$, that is the MSSM electroweak group. We take the Higgs superfields to be $\hat{A}_i, = \hat{H}_u,\,\hat{H}_d$, the only chiral superfields apart of $\hat{L}$. The vector bosons V_D corresponds then to W and V_H to a W' boson.

In this specific case, the effective Kähler potential for the Higgs bosons reads

$$\mathcal{K}^{\text{eff}}_{H_i} = \sum_{i=u,d}\hat{H}_i^\dagger e^{g_2 W}\hat{H}_i + \sum_c g_D^2\left(\frac{1}{m_V^2} - \frac{\theta^4 m_{\text{soft}}^2}{m_V^2+m_{\text{soft}}^2}\right)\left(\frac{g_a}{g_b}\sum_{i=u,d}\hat{H}_i^\dagger T^c \hat{H}_i\right)^2 + \dots\,. \tag{5.19}$$

where we set g_D to be the SM coupling g_2, and the ellipsis stands for the terms relative to $U(1)_Y$. From the first term in eq. (5.19) one derives the D-terms corresponding to the MSSM gauge group, from the second term one derives the additional non-decoupling D-terms.

As mentioned above, in the absence of (soft) supersymmetry breaking, the additional supersymmetric D-terms are suppresses via $\sim\mathcal{O}(\mu^2/m_V^2)$ [91,97]. In fact, μ is usually required

to be < 300 GeV while m_V is constrained to be larger than 3 TeV from electroweak analysis of gauge extended models [186]. On the other hand, the additional SUSY breaking D-terms instead are not decoupled and can give an important contribution to Higgs quartics. Therefore the D-terms for the Higgs doublets are

$$\begin{aligned}\mathcal{L}_{D\text{-terms}} = &-\frac{g_1^2}{8}\left(H_u^\dagger H_u - H_d^\dagger H_d\right)^2 \\ &-\sum_c \frac{g_2^2}{2}\left(1+\frac{g_a^2}{g_b^2}\frac{m_s^2}{m_V^2+m_s^2}\right)\left(H_u^\dagger T^c H_u + H_d^\dagger T^c H_d\right)^2 .\end{aligned} \tag{5.20}$$

Therefore, the tree-level Higgs mass looks like

$$m_{h,\text{tree}}^2 \leq \left[m_Z^2 + g_2^2\,\frac{g_a^2}{4g_b^2}\,\frac{m_s^2}{m_V^2+m_s^2}\,v^2\right]\cos^2 2\beta\,, \tag{5.21}$$

where we set g_D to be the SM coupling g_2. The inequality is saturated in the decoupling limit $m_{A^0} \gg m_Z$. From (5.21) it is clear that the MSSM tree-level upper bound on the Higgs mass squared, m_Z^2, may be surpassed with a suitable choice of parameters. The enhancement will be discussed more accurately in the two cases analysed in section 5.2.

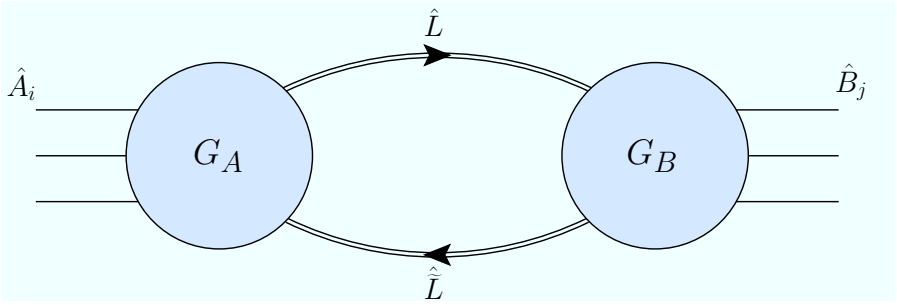

Figure 5.2: The quiver module of the toy model with $\mathcal{G} = SU(2) \otimes SU(2)$ with $\hat{L}, \hat{\tilde{L}}$ connecting the sites and the chiral superfields $\hat{A}_i, \hat{B}_j$ respectively on site A and B.

Two sites, two linking fields Another possibility to obtain similar D-terms corrections with a gauge group $\mathcal{G}_A \otimes \mathcal{G}_B$, is to consider the case in which there are *two* chiral linking superfields $\hat{L}, \hat{\tilde{L}}$ transforming as $(\mathbf{2}, \bar{\mathbf{2}})$ and $(\bar{\mathbf{2}}, \mathbf{2})$ under $\mathcal{G} = \mathcal{G}_A \otimes \mathcal{G}_B = SU(2)_A \otimes SU(2)_B$ [91, 97, 175, 176, 180–183]. The Kähler potential for $\hat{L}, \hat{\tilde{L}}$ is

$$\mathcal{K}_{L,\tilde{L}} = \text{Tr}\,[e^{g_a \hat{V}_a}\,\hat{L}\,e^{-g_b \hat{V}_b}\,\hat{L}^\dagger] + \text{Tr}\,[e^{g_b \hat{V}_b}\,\hat{\tilde{L}}\,e^{-g_a \hat{V}_a}\,\hat{\tilde{L}}^\dagger]\,, \tag{5.22}$$

where g_a, g_b are the gauge couplings of $\mathcal{G}_A$, $\mathcal{G}_B$ and $\hat{V}_A$, $\hat{V}_B$ are the gauge supermultiplets.

We take the rest of the matter content of the model to be coupled as in the previous example, eq. (5.3). We may then write the D-terms:

$$\begin{aligned}\mathcal{L}_{D\text{-terms}} = &\frac{g_a^2}{2}\left(\text{Tr}\left[L^\dagger T^c L\right] + \text{Tr}\left[\tilde{L}\,T^c \tilde{L}^\dagger\right] + A_i^\dagger T^c A_i\right)^2 \\ &+\frac{g_b^2}{2}\left(\text{Tr}\left[L\,T^c L^\dagger\right] + \text{Tr}\left[\tilde{L}^\dagger T^c \tilde{L}\right] + B_j^\dagger T^c B_j\right)^2 .\end{aligned} \tag{5.23}$$

The superpotential for the bidoublets $\hat{L}$, $\hat{\tilde{L}}$ is given by

$$\mathcal{W}_{L,\tilde{L}} = \lambda \left(\det \hat{L} + \det \hat{\tilde{L}} \right) + \rho \, \mathrm{Tr} \hat{L} \hat{\tilde{L}} \, . \tag{5.24}$$

The two possible D-flat minima are:

$$\langle L \rangle = \langle \tilde{L} \rangle = 0 \qquad , \qquad \langle L \rangle = \langle \tilde{L} \rangle = -\frac{\rho}{\lambda} \mathbb{1}_{2\times 2} \, . \tag{5.25}$$

The second solution is responsible for the diagonal gauge symmetry breaking $\mathcal{G}_A \otimes \mathcal{G}_B \to \mathcal{G}_D$.

We may then follow the same steps of the previous example. First, we introduce soft masses for $\hat{L}$ and $\hat{\tilde{L}}$, then we integrate out $\hat{V}_H$, whose scalar component is a combination of the corresponding scalar L, $\tilde{L}$. The additional non-decoupling D-terms then arise as before, *cf.* eq. (5.18).

5.1.3 EW-scale effects

We resume here some of the most important effects at the electroweak scale of non-decoupling D-terms.

- First, we have seen that the non-decoupling D-terms triggered by an extended gauge group raise the tree-level Higgs mass. This allows, as we will see in sec. 5.2, to have lighter stops and/or lower stop mixing to reach the 125.5 GeV observed Higgs mass [3]. This relaxes naturalness. In the more recent reference [187] it has been shown, with a detailed analysis of the fine tuning in the model, that as as long as $\tan\beta$ is not small ($\lesssim 4$), the observed Higgs mass at $\sim$ 125.5 GeV can be accommodated without large D-terms.

- We can see from eq. (5.17) that actually *all* the scalars that are charged under the breaking gauge symmetries like, for instance, Higgs bosons, squarks, and sleptons, receive mass corrections from the additional D-terms. The modified masses for the non-SM-like Higgs bosons, sleptons, and squarks give contributions ΔT to the T parameter. They may compensate the negative contributions coming from a heavy SM-like Higgs boson [179].

  One should also notice that a vev v_T of the triplet linking fields L_T and $\tilde{L}_T$ can arise as a deviation from the diagonal vevs in eqs. (5.6) and (5.25). This vev can also participate to the electroweak symmetry breaking, even though it is constrained by electroweak precision measurements to be $v_T < 3$ GeV [103]. This triplet vev brings a small positive ΔT contribution too. The analysis of the ΔT contributions in these models has been studied in detail in [179], in which a scenario with a light third slepton sector is presented in order to fulfil the electroweak constraints.

- After electroweak symmetry breaking, the gauge bosons in the example described above with gauge group $SU(2)_A \otimes SU(2)_B \otimes U(1)_Y$ have masses [187]:

$$m_W^2 \simeq \frac{g_D^2 v^2}{4}\left(1 - \frac{g_a^4}{g_b^4}\frac{v^2}{2u^2} + 8\frac{v_T^2}{v^2}\right) \tag{5.26}$$

$$m_Z^2 \simeq \frac{\left(g_D^2 + g_1^2\right) v^2}{4}\left(1 - \frac{g_a^4}{g_b^4}\frac{v^2}{2u^2}\right) \tag{5.27}$$

$$m_{W'}^2 \simeq \frac{\left(g_a^2 + g_b^2\right) u^2}{2}\left(1 + \frac{g_a^4}{g_b^4}\frac{v^2}{2u^2} + \frac{\left(g_a^2 - g_b^2\right)^2}{\left(g_a^2 + g_b^2\right)^2}\frac{v_T^2}{u^2}\right) \tag{5.28}$$

$$m_{Z'}^2 \simeq \frac{\left(g_a^2 + g_b^2\right) u^2}{2}\left(1 + \frac{g_a^4}{g_b^4}\frac{v^2}{2u^2} + \frac{v_T^2}{u^2}\right) \tag{5.29}$$

  in the limit $u \gg v \gg v_T$.

- Extended gauge symmetries lead also to an extended neutralino and chargino sector. We define $\psi_L^\pm$ and ψ_T^0 as respectively the charged and neutral fermionic components of $\hat{L}_T$, and ψ_S as the fermionic component of $\hat{L}_S$. In the model with gauge group $\mathcal{G} = SU(2)_A \otimes SU(2)_B \otimes U(1)_Y$ and one linking field, there are four charginos. They are mixing states of $\tilde{W}_1^\pm$, $\tilde{W}_1^\pm$, $\tilde{H}_{u/d}^\pm$, and of $\psi_L^\pm$, coming from the fermionic component of $\hat{L}_T$. There are eight neutralinos, mixing states of $\tilde{B}^0$, $\tilde{W}_1^0$, $\tilde{W}_2^0$, $\tilde{H}_u^0$, $\tilde{H}_d^0$, $\tilde{L}_T^0$, then also the decoupled $\tilde{L}_S$, and the weakly coupled $\tilde{S}$. In some regions of the parameter space with low values of $\tan\beta$ and with relatively third-generations squarks, the modified chargino sector is responsible to an increased $h \to \gamma\gamma$ decay branching ratio through the chargino loop [172].

- Finally, the enhanced Higgs quartic couplings lead, at lower energies, to modified Higgs couplings to fermions and W, Z [91, 146], that will be discussed in section 5.3.

5.2 Non-decoupling D-terms and the tree-level Higgs mass

In the rest of the chapter, we consider two classes of gauge extensions of the MSSM, both with two quiver sites [3]. We adopt a bottom-up approach in that we focus in the low energy effective field theory of these models, resulting in a deformation of the MSSM by a set of non-decoupling D-terms. This effective theory has been obtained after integrating out the heavy gauge bosons related to the symmetry breaking, as previously explained. Therefore we do not take into account of the effects from RGE, as was done in the top-down approach in [174].

The classes of two-sites supersymmetric models consider here, feature a gauge group $\mathcal{G}$ that consists in $SU(3)_c$ and two copies of $SU(2) \otimes U(1)$, located in sites A and B:[4]

$$\mathcal{G} = SU(3)_c \otimes \left(SU(2) \otimes U(1)\right)_A \otimes \left(SU(2) \otimes U(1)\right)_B \ . \tag{5.30}$$

[4] One could introduce a quiver structure also for $SU(3)_c$, *cf.* [97], however, we do not consider this possibility since not directly related to the effects of non-decoupling D-terms on the Higgs mass.

Superfields	Spin 0	Spin $\frac{1}{2}$	$SU(3)_c \otimes G_A \otimes G_B$
$\hat{Q}_i$	$\tilde{Q}_i$	Q_i	$(\mathbf{3}, \mathbf{2}_{1/6}, \mathbf{1}_0)$
$\hat{\bar{d}}_i$	$\tilde{d}^*_{R\,i}$	$d^*_{R\,i}$	$(\overline{\mathbf{3}}, \mathbf{1}_{1/3}, \mathbf{1}_0)$
$\hat{\bar{u}}_i$	$\tilde{u}^*_{R\,i}$	$u^*_{R\,i}$	$(\overline{\mathbf{3}}, \mathbf{1}_{-2/3}, \mathbf{1}_0)$
$\hat{\ell}_i$	$\tilde{\ell}_i$	ℓ_i	$(\mathbf{1}, \mathbf{2}_{-1/2}, \mathbf{1}_0)$
$\hat{\bar{e}}_i$	$\tilde{e}^*_{R\,i}$	$e^*_{R\,i}$	$(\mathbf{1}, \mathbf{1}_1, \mathbf{1}_0)$
$\hat{H}_d$	H_d	$\tilde{H}_d$	$(\mathbf{1}, \mathbf{2}_{-1/2}, \mathbf{1}_0)$
$\hat{H}_u$	H_u	$\tilde{H}_u$	$(\mathbf{1}, \mathbf{2}_{1/2}, \mathbf{1}_0)$
$\hat{L}$	L	ψ_L	$(\mathbf{1}, \mathbf{2}_{-1/2}, \overline{\mathbf{2}}_{1/2},)$
$\hat{\bar{L}}$	$\tilde{L}$	$\psi_{\tilde{L}}$	$(\mathbf{1}, \overline{\mathbf{2}}_{1/2}, \mathbf{2}_{-1/2})$
$\hat{K}$	K	ψ_K	$(\mathbf{1}, \mathbf{1}_0, \mathbf{1}_0)$

Table 5.1: The matter content of the theory that may lead to a vector-Higgs non decoupled D-term for both $SU(2)_L$ and $U(1)_Y$, with the Higgs doublets on site A. $i = 1, 2, 3$ labels the generations. The singlet $\hat{K}$ couples to the linking fields in the superpotential and it is introduced to generate a suitable scalar potential for the linking fields, see also [174]. This model is represented in figure 5.3.

The two sites are connected by two linking fields $\hat{L}$ and $\hat{\bar{L}}$, charged under $\mathcal{G}$ as $\left(\mathbf{1}, \mathbf{2}_{1/2}, \overline{\mathbf{2}}_{1/2}\right)$ and $\left(\mathbf{1}, \overline{\mathbf{2}}_{1/2}, \mathbf{2}_{-1/2}\right)$, respectively. $\hat{L}$ and $\hat{\bar{L}}$ acquire vevs and are responsible for the gauge symmetry breaking to the MSSM group $SU(3)_c \otimes SU(2)_L \otimes U(1)_Y$. The breaking has the diagonal pattern:

$$SU(2)_A \otimes SU(2)_B \to SU(2)_L\,, \qquad U(1)_A \otimes U(1)_B \to U(1)_Y\,. \tag{5.31}$$

5.2.1 Vector Higgs quiver model

We present here the class of models in which both MSSM Higgs doublets are on the same site [96, 97], such that they transform under $\mathcal{G}$ in a vector representation (H_u, H_d). We refer to this class as the "Vector Higgs case". The three quark and lepton generations may be distributed on different sites, with effects that we will mention later. In the present analysis we assume that all the matter, Higgs doublets included, are on site A, according to the charge table 5.1 and the sketch in figure 5.3. This particular case has been implemented within the program `SARAH` [188, 189], where the scalar potentials has been calculated, in correspondence of the gauge breaking $\mathcal{G} \to \mathcal{G}_{\rm SM}$ and the electroweak symmetry breaking.

The superpotential consists in

$$\mathcal{W} = \mathcal{W}_{\rm MSSM} + \frac{Y_K}{2}\hat{K}\left(\hat{L}\hat{\bar{L}} - \varrho^2\right)\,, \tag{5.32}$$

where the gauge singlet superfield $\hat{K}$ has been introduced.

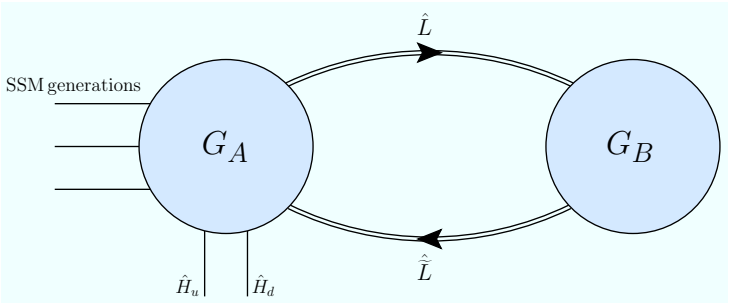

Figure 5.3: The quiver diagram of the electroweak sector of the vector Higgs quiver model, *cf.* table 5.1. The supersymmetric standard model is on site A, the linking fields $\hat{L}$ and $\hat{\tilde{L}}$ connect the two sites. The singlet field $\hat{K}$ is not shown. The resulting non-decoupling vector-Higgs D-terms are displayed in (5.34).

Following the same logic of the case described in section 5.1, the linking fields get vevs

$$\langle L \rangle = \langle \tilde{L} \rangle = v_L \mathbb{1}_{2\times 2}\,, \tag{5.33}$$

that diagonally break the gauge symmetry at a scale $\gtrsim 1$ TeV. Similarly, the heavy gauge superfield $\hat{B}_H$, $\hat{W}^i_H$ are integrated out. We then obtain an effective theory in which the following relevant terms are added to the MSSM Higgs potential:

$$\delta\mathcal{L} = -\frac{g_1^2\Delta_1}{8}(H_u^\dagger H_u - H_d^\dagger H_d)^2 - \frac{g_2^2\Delta_2}{8}\sum_a (H_u^\dagger \sigma^a H_u + H_d^\dagger \sigma^a H_d)^2 + \dots\,. \tag{5.34}$$

The ellipsis denotes D-terms involving the other scalars of the model that are charged under the gauge symmetry, *i.e.* squarks and sleptons. The parameters Δ_1 and Δ_2 are defined as

$$\Delta_1 = \left(\frac{g_{A1}^2}{g_{B1}^2}\right)\frac{m_L^2}{m_{v1}^2 + m_L^2} \quad , \quad \Delta_2 = \left(\frac{g_{A2}^2}{g_{B2}^2}\right)\frac{m_L^2}{m_{v2}^2 + m_L^2}\,, \tag{5.35}$$

where g_{A1}, g_{B1} are the $U(1)$ couplings on site A and B, while g_{A2}, g_{B2} are the $SU(2)$ couplings; m_L is the soft mass, that we assume equal for both the linking fields L and $\tilde{L}$; m_{v_1}, m_{v_2} are the masses of B_H, W^i_H after the symmetry breaking to $SU(2)_L \otimes U(1)_Y$.

The enhancement of the D-terms requires $R_i = g_{A\,i}^2/g_{B\,i}^2$ to be as large as possible. However, this condition may spoil gauge couplings perturbative unification depending on how the matter is distributed between the sites. If most of the matter is charged under G_A as in the case considered, indeed, then a Landau pole may be reached below the GUT scale [3, 97]. In the following we will not require gauge coupling unification, therefore Δ_1 and Δ_2 may arise independently.

Adding the D-terms quartic terms in eq. (5.34) to the MSSM Higgs scalar potential in eq. (2.40) leads to modified minimisation conditions and tree-level Higgs mass matrices, that we report here. Setting for brevity:

$$g_{12}^2 = g_1^2(1+\Delta_1^2) + g_2^2(1+\Delta_2^2)\,, \qquad \hat{g}_{12}^2 = -g_1^2(1+\Delta_1^2) + g_2^2(1+\Delta_2^2)\,, \tag{5.36}$$

the tadpole equations read

$$\frac{\partial V}{\partial H_d^0} = \frac{1}{8}\Big(- 8v_u \mathrm{Re}[B_\mu] + g_{12}^2 v_d^3 + v_d[8m_{H_d}^2 + 8|\mu|^2 - g_{12}^2 v_u^2]\Big)\,, \tag{5.37}$$

$$\frac{\partial V}{\partial H_u^0} = \frac{1}{8}\Big(- 8v_d \mathrm{Re}[B_\mu] + 8v_u|\mu|^2 + v_u[8m_{H_u}^2 - g_{12}^2(-v_u^2 + v_d^2)]\Big)\,. \tag{5.38}$$

We can derive the mass matrix for the CP-even Higgs bosons, which in the basis ($\mathrm{Re}H_d^0$, $\mathrm{Re}H_u^0$) is given by

$$m_h^2 = \begin{pmatrix} m_{h,11} & -\frac{1}{4}g_{12}^2 v_d v_u - \mathrm{Re}[B_\mu] \\ -\frac{1}{4}g_{12}^2 v_d v_u - \mathrm{Re}[B_\mu] & m_{h,22} \end{pmatrix}\,, \tag{5.39}$$

where

$$m_{h,11} = \frac{1}{8}\Big(8m_{H_d}^2 + 8|\mu|^2 + g_{12}^2\Big(3v_d^2 - v_u^2\Big)\Big)\,, \tag{5.40}$$

$$m_{h,22} = \frac{1}{8}\Big(8m_{H_u}^2 + 8|\mu|^2 - g_{12}^2\Big(- 3v_u^2 + v_d^2\Big)\Big)\,. \tag{5.41}$$

The mass matrix for the pseudo-scalar Higgs bosons in the basis ($\mathrm{Im}H_d^0$, $\mathrm{Im}H_u^0$) reads

$$m_{A^0}^2 = \begin{pmatrix} m_{A^0,11} & \mathrm{Re}[B_\mu] \\ \mathrm{Re}[B_\mu] & m_{A^0,22} \end{pmatrix}\,, \tag{5.42}$$

where

$$m_{A^0,11} = \frac{1}{8}\Big(8m_{H_d}^2 + 8|\mu|^2 + g_{12}^2\Big(- v_u^2 + v_d^2\Big)\Big)\,, \tag{5.43}$$

$$m_{A^0,22} = \frac{1}{8}\Big(8m_{H_u}^2 + 8|\mu|^2 - g_{12}^2\Big(- v_u^2 + v_d^2\Big)\Big)\,. \tag{5.44}$$

Finally, the mass matrix for the charged Higgs bosons in the basis $\left(H_d^-, H_u^{+,*}\right)$, $\left(H_d^{-,*}, H_u^+\right)$ reads

$$m_{H^-}^2 = \begin{pmatrix} m_{H^-,11} & \frac{1}{4}\Big(4B_\mu^* + \Big(g_2^2 + g_2^2\Delta_2^2\Big)v_d v_u\Big) \\ \frac{1}{4}\Big(4B_\mu + \Big(g_2^2 + g_2^2\Delta_2^2\Big)v_d v_u\Big) & m_{H^-,22} \end{pmatrix}\,, \tag{5.45}$$

with

$$m_{H^-,11} = \frac{1}{8}\Big(8m_{H_d}^2 + 8|\mu|^2 + g_{12}^2 v_d^2 + \hat{g}_{12}^2 v_u^2\Big)\,, \tag{5.46}$$

$$m_{H^-,22} = \frac{1}{8}\Big(8m_{H_u}^2 + 8|\mu|^2 + g_{12}^2 v_u^2 + \hat{g}_{12}^2 v_d^2\Big)\,. \tag{5.47}$$

After diagonalising the Higgs mass matrices we get the tree-level Higgs masses

$$m_{h,H}^{2,\mathrm{V}} = \frac{m_{A^0}^2 + m_Z^2 + m_\Delta^2}{2} \mp \sqrt{\frac{(m_{A^0}^2 - m_Z^2 - m_\Delta^2)^2}{4} + \left(m_Z^2 + m_\Delta^2\right)\left(m_{A^0}^2 \sin^2(2\beta)\right.}\,, \tag{5.48}$$

$$m_{A^0}^{2,\mathrm{V}} \equiv \frac{2B_\mu}{\sin 2\beta} = 2|\mu|^2 + m_{H_u}^2 + m_{H_d}^2\,, \tag{5.49}$$

$$m_{H^\pm}^{2,\mathrm{V}} = m_{A^0}^2 + m_W^2(1 + \Delta_2)\,, \tag{5.50}$$

where we defined $4m_\Delta^2 = (g_1^2\Delta_1 + g_2^2\Delta_2)v^2$, and "V" denote the vector Higgs case, and we took B_μ to be real. Equations (5.48)–(5.50) can equivalently be obtained by the MSSM relations (2.46)-(2.48) with the substitutions

$$m_Z^2 \to m_Z^2 + m_\Delta^2\,, \qquad m_W^2 \to m_W^2(1+\Delta_2)\,. \tag{5.51}$$

The non-decoupling D-terms contribution causes a shift in the tree level Higgs mass squared $m_{h,\,\text{tree}}^2$ which results in the upper bound

$$m_{h,\,\text{tree}}^{2,\,\text{V}} \leq \left[m_Z^2 + \left(\frac{g_1^2\Delta_1 + g_2^2\Delta_2}{4}\right)v^2\right]\cos^2 2\beta\,. \tag{5.52}$$

that is saturated in the decoupling limit $m_{A^0} \gg m_Z$, that we will consider.

The tree-level shift in equation (5.52) can significantly reduce the fine-tuning in the top-stop sector, *cf.* eq. (2.50). In fact, much smaller radiative corrections to the Higgs mass would be needed to reach the observed 125.5 GeV, therefore allowing for lighter stops and smaller stop mixing. In the following, we will consider the case of decoupling limit with moderately large $\tan\beta$, such that we approximate the 1-loop Higgs mass considering the most relevant two-loop corrections as

$$\begin{aligned} m_h^{2,\,\text{V}} \simeq{}& \left[m_Z^2 + \left(\frac{g_1^2\Delta_1 + g_2^2\Delta_2}{4}\right)v^2\right]\cos^2 2\beta \\ &+ \frac{3}{2\pi^2 v^2}\left[m_{t,\,r}^4\left(\sqrt{m_t M_{\tilde{t}}}\right)\ln\frac{M_{\tilde{t}}^2}{m_t^2} + m_{t,\,r}^4(M_{\tilde{t}})\frac{X_t^2}{M_{\tilde{t}}^2}\left(1 - \frac{X_t^2}{12M_{\tilde{t}}^2}\right)\right]. \end{aligned} \tag{5.53}$$

An accurate estimate of the SM-like Higgs mass for the $SU(2)_A \otimes SU(2)_B \otimes U(1)_Y$ has more recently been derived using the Coleman-Weinberg potential approach [187]. The loop contributions to the physical Higgs mass due to the D-terms, *cf.* eq. (5.34), are subleading with respect to the stop loops in eq. (5.53). However, the explicit breaking of supersymmetry in eq. (5.34) introduces a new source of fine-tuning due to the quadratically divergent contribution to the Higgs mass squared parameter [97]:

$$\left(\frac{\alpha g_1^2\Delta_1 + \beta g_2^2\Delta_2}{4}\right)\frac{m_L^2}{16\pi^2}\,. \tag{5.54}$$

The coefficients α, β are determined by the precise matter content that appears in the non-decoupling D-term. The fine tuning may be naïvely defined by the ratio of m_h^2 over the term in eq. (5.54). To control this fine tuning to be better than 10%, one may require $m_L < 10$ TeV. If one requires $\Delta_i \gtrsim 0.5$, the electroweak constraints then set $m_L > m_V > 3$ TeV [91].

Vector case non-decoupling D-terms and Higgs mass enhancement

We use equation (5.53) to give a qualitative understanding and a predictive guide for the size of the D-terms required to allow for substantially lighter stops or stop mixings. We do not implement here experimental or other phenomenological constraints.

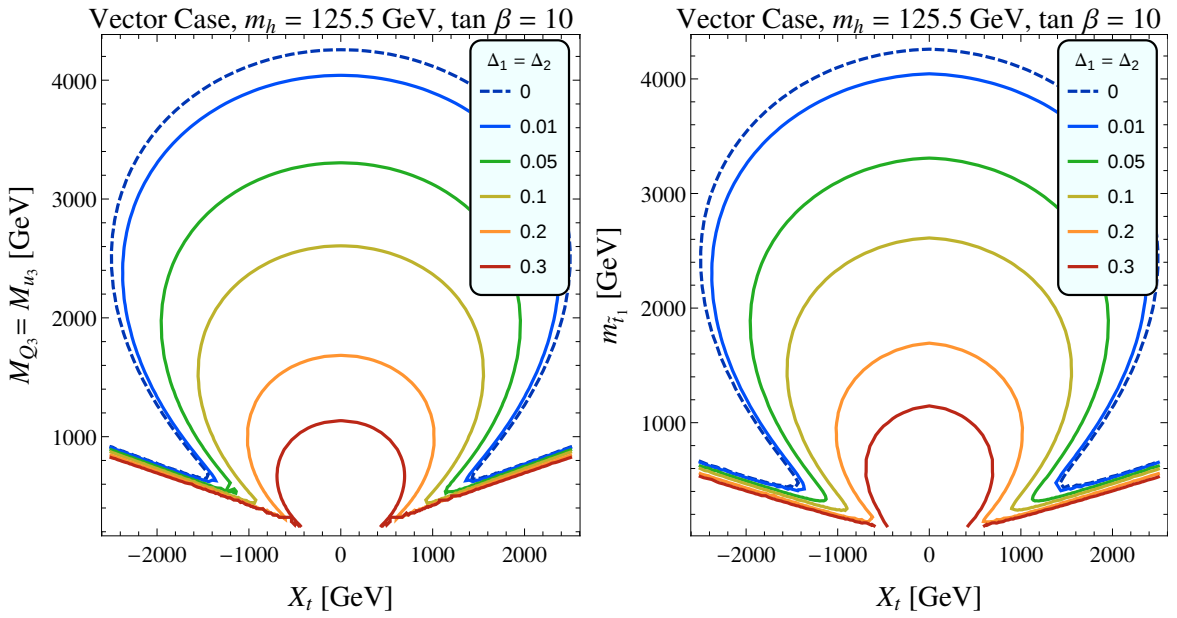

Figure 5.4: Contours of the Higgs mass $m_h = 125.5$ GeV in the (M_{Q_3}, X_t) plane [left panel] and in the $(m_{\tilde{t}_1}, X_t)$ plane [right panel] for different values of $\Delta_1 = \Delta_2$. We set $M_{Q_3} = M_{u_3}$, $\tan\beta = 10$.

We first show how the Higgs mass is raised by the D-terms in fig. 5.4. Here, for a moderately large value $\tan\beta = 10$ and $M_{Q_3} = M_{u_3}$, we plot the Higgs mass from eq. (5.53), for different values of $\Delta \equiv \Delta_1 = \Delta_2$, in the (M_{Q_3}, X_t)-plane (similarly to [91]) and in the $(m_{\tilde{t}_1}, X_t)$-plane.[5] The MSSM limit, defined as $\Delta = 0$, is plotted in dashed line. In this limit, considering null mixing $X_t = 0$ GeV, a lightest stop mass $m_{\tilde{t}_1} \simeq 4$ TeV is required to reproduce the observed Higgs mass, $m_h = 125.5$ GeV. Considering $\Delta = 0.3$, instead, for $X_t = 0$ GeV a mass $m_{\tilde{t}_1} \simeq 1$ TeV is sufficient. We can draw similar conclusions for the maximal mixing scenario, corresponding to the condition $|A_t| \simeq \sqrt{6} M_{\tilde{t}}$ and visible in fig. 5.4 as the sharply acute concave kink in the contours. For increasing Δ, a significantly smaller X_t is requested with respect to the MSSM limit.

One should then discuss the expected order of the size of these D-terms and its meaning. At the tree level, one can observe in figure 5.5 that in principle with Δ of order $\sim \mathcal{O}(1)$ the tree-level Higgs mass would already be sufficiently large to account for the observed 125.5 GeV Higgs mass. In [91], under the request of fine tuning no worse than 10%, it was found that one would expect $\Delta \gtrsim 0.5$, while keeping the stops light. However, as discussed in [3], one may find that Δ of order $\mathcal{O}(0.1\text{–}0.6)$ is more easily obtainable and preferable if to accommodate gauge coupling unification, *cf.* discussion in section C. This depends also on how the matter, *i.e.* quark and lepton supermultiplets, is distributed between sites A and B, since this affect the running of the couplings from higher energies. Since Δ of order $\mathcal{O}(0.1\text{–}0.6)$ still gives a

[5] Even though Δ_1 and Δ_2 may arise independently as we are not requiring coupling unification, for the sake of simplicity we will consider in the following Δ_1 equal to Δ_2, and we will simply refer to them as Δ.

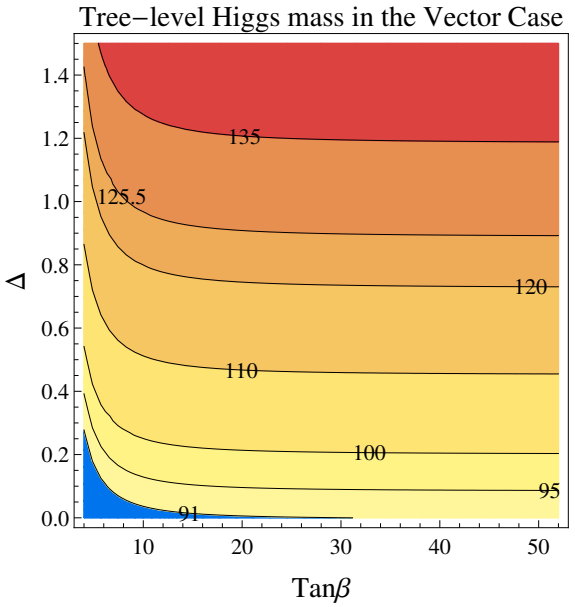

Figure 5.5: Contours of the tree-level Higgs mass in the $(\tan\beta,\, \Delta)$ plane.

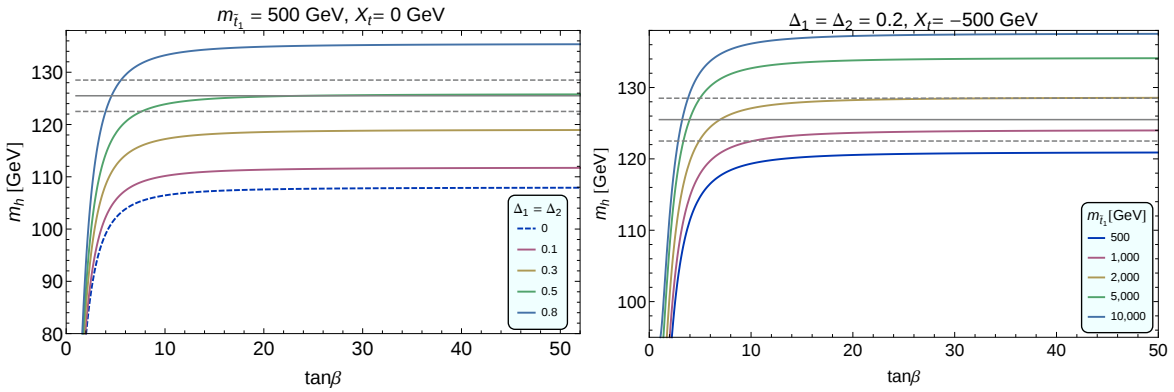

Figure 5.6: Higgs mass m_h with tree-level D-terms corrections vs $\tan\beta$. On the left panel, for different values of $\Delta_1 = \Delta_2$ with $X_t = 0$ and with $m_{\tilde{t}_1} = 500$ GeV. On the right panel, for different values of $m_{\tilde{t}_1}$ with $\Delta_1 = \Delta_2 = 0.2$ and $X_t = -500$ GeV. For comparison, 125.5 ± 3 GeV grid lines are plotted.

noticeable effect on the Higgs mass, we will study the degree to which these slighter deviations from the MSSM can be determined at the LHC and ILC.

Enhancements due to the non-decoupling D-terms arise significantly for $\tan\beta \in [1, 10]$ and stabilise for $\tan\beta \gtrsim 10$, *cf.* figs. 5.5 and 5.6. The same pattern could be observed also with the RG-evolution approach in [174].

Also, in the left panel of fig. 5.7 we can see that with null mixing $X_t = 0$ GeV and $\tan\beta = 10$, $m_{\tilde{t}_1}$ has to be in the 1-4 TeV range for $\Delta \in [0.01, 0.3]$. Finally, we see in the right panel of fig. 5.7 that with the relatively low stop mass $m_{\tilde{t}_1} \sim 500$ GeV, a $|X_t| \sim 1$

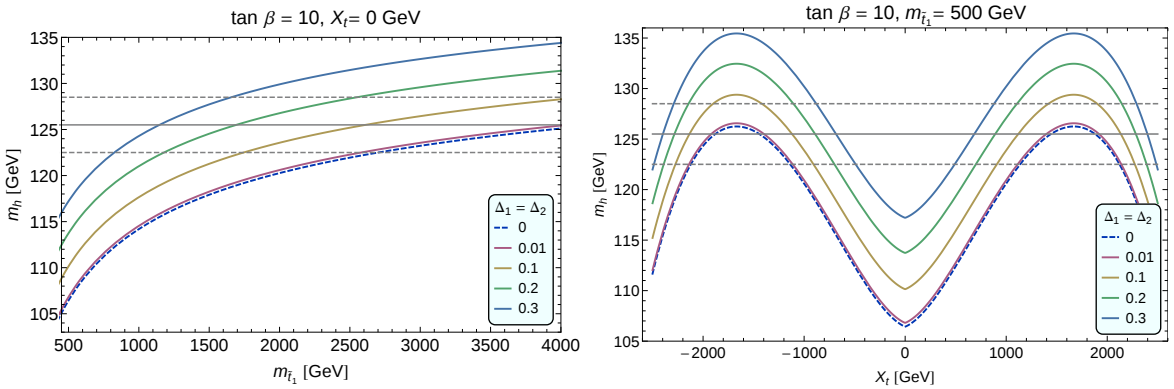

Figure 5.7: Higgs mass m_h with tree-level D-terms corrections for different values of $\Delta_1 = \Delta_2$, with $\tan\beta = 10$ and 125.5 ± 3 GeV grid lines plotted for comparison. On the left panel, m_h vs $m_{\tilde{t}_1}$ with $X_t = 0$ GeV; on the right panel, m_h vs X_t with $m_{\tilde{t}_1} = 500$ GeV.

TeV is required. Concluding, due to the D-term additional contributions to Higgs quartics naturalness relaxes, as we have pointed out for the maximal mixing scenario and for the null mixing scenario.

Sfermion masses

The masses of sfermions, charged under $(SU(2) \otimes U(1))_A \otimes (SU(2) \otimes U(1))_B$, receive tree level contributions from non-decoupling D-terms too. Referring to table 5.1, the mixing matrix $M^2_{\tilde{f}}$ of a generic charged sfermion $\tilde{f}$ is given by

$$M^2_{\tilde{f}} = \begin{pmatrix} M^2_{Q_f} + m_f^2 + \hat{M}_Z^2 \, (I_f^3 - Q_f \, s_W^2) & m_f X_f^* \\ m_f X_f & M^2_{u_f} + m_f^2 + \hat{M}_Z^2 \, Q_f \, s_W^2 \end{pmatrix}, \tag{5.55}$$

denoting $s_w = \sin\theta_W$, and $\hat{M}_Z^2 \equiv (m_Z^2 + m_\Delta^2)\cos 2\beta$. The off-diagonal element X_f is defined in terms of the soft SUSY-breaking trilinear coupling A_f via

$$X_f = A_f - \mu^* \times \{\cot\beta, \tan\beta\}, \tag{5.56}$$

where $\cot\beta$ applies for the up-type quarks, u, c, and t, while $\tan\beta$ applies for the down-type fermions, d, s, b, e, μ, and τ. Note that m_f, Q_f and I_f^3 are the mass, charge and isospin projection of the fermion f, respectively. Once diagonalised, $M^2_{\tilde{f}}$ leads to the sfermion masses $m_{\tilde{f}_1}$ and $m_{\tilde{f}_2}$, with $m_{\tilde{f}_1} \leq m_{\tilde{f}_2}$. In particular the stop masses are given by

$$\begin{aligned} m^2_{\tilde{t}_{1,2}} = & m_t^2 + \frac{1}{2}\left[M^2_{Q_3} + M^2_{u_3} + \frac{1}{2}\hat{M}_Z^2 \cos 2\beta \right. \\ & \left. \mp \sqrt{\left[M^2_{Q_3} - M^2_{u_3} + \hat{M}_Z^2 \cos 2\beta \left(\frac{1}{2} - \frac{4}{3}\sin^2\theta_W \right) \right]^2 + 4 m_t^2 X_t^2} \right], \end{aligned} \tag{5.57}$$

To obtain the MSSM mass expression one has just to set $m_\Delta = 0$. For a light stop scenario, non-decoupling D-terms may have an appreciable effect. Similarly, they may give an interesting contribution for scenarios with light $\tilde{\tau}_1$, which may be the NLSP as in GMSB scenarios [48]. If $g_A > g_B$, eq. (5.55) applies to the third generation scalars on Site A even for the case split sfermion generations in which the first two generations are on site B.
The sneutrinos mass matrix, instead, is given by

$$m_{\tilde{\nu}}^2 = M_L^2 + \frac{1}{2}(m_Z^2 + m_\Delta^2)\cos(2\beta). \tag{5.58}$$

Changing the matter distribution between sites

Vector Higgs D-term extensions of the MSSM may have, as anticipated, generations of matter located on sites A and B in various ways, for example with the first two sfermions generation on site B. This possibility has been exploited to explain flavour hierarchies [98, 174]. Typically, the third generation is taken to be on the same site as H_u, in order the stop mixing parameter X_t to trigger EWSB [177, 178]. Note also that having split generations helps to have asymptotically free $SU(2)_A$, which in turn translates in the possibility to increase at the electroweak scale Δ [177]. Also, if more matter is on site B than site A, this configuration may more easily allow for easier gauge coupling unification [174].

Alternatively, both Higgs doublets can be are on site B. The corresponding D-terms are now given by (5.34) with Δ_1 and Δ_2 respectively equal to

$$\Delta_1^B = \left(\frac{g_{B1}^2}{g_{A1}^2}\right)\frac{m_L^2}{m_{v1}^2 + m_L^2} \quad , \quad \Delta_2^B = \left(\frac{g_{B2}^2}{g_{A2}^2}\right)\frac{m_L^2}{m_{v2}^2 + m_L^2}. \tag{5.59}$$

Notice that the role of the gauge couplings, here $g_{B1}^2 > g_{A1}^2$, is reversed with respect to the scenario discussed above.

5.2.2 Chiral Higgs quiver model

A two-sites quiver extension of the MSSM may have the two Higgs doublets distributed on two different sites. This class of scenarios is called the "Chiral Higgs case" [190], since the Higgs doublets cannot be grouped under the same representation of the gauge group $\mathcal{G}$. Therefore the Higgs doublets will transform, for example, like $H_u \sim (\mathbf{1}, \mathbf{2}_{1/2}, \mathbf{1}_0)$ and $H_d \sim (\mathbf{1}, \mathbf{1}_0, \mathbf{2}_{1/2})$. A couple of linking fields $\hat{L}$ and $\hat{\bar{L}}$ charged under $\mathcal{G}$ as $(\mathbf{1}, \mathbf{2}_{-1/2}, \overline{\mathbf{2}}_{1/2})$ and $(\mathbf{1}, \overline{\mathbf{2}}_{1/2}, \mathbf{2}_{-1/2})$ connects the two sites.

The fact that H_u and H_d are on different sites has the phenomenological consequence that a μ-term like the one in the MSSM superpotential is forbidden by gauge invariance. However, the μ-term can be recovered introducing, for example, a term in the superpotential in which the Higgs doublets couple to the linking field $\hat{L}$. Then, $\hat{L}$ acquires a vev, and in analogy to the NMSSM we have:

$$\mu_L \hat{L}\hat{H}_u\hat{H}_d \xrightarrow{\mu_L\langle\hat{L}\rangle = \mu} \mu\hat{H}_u\hat{H}_d\,. \tag{5.60}$$

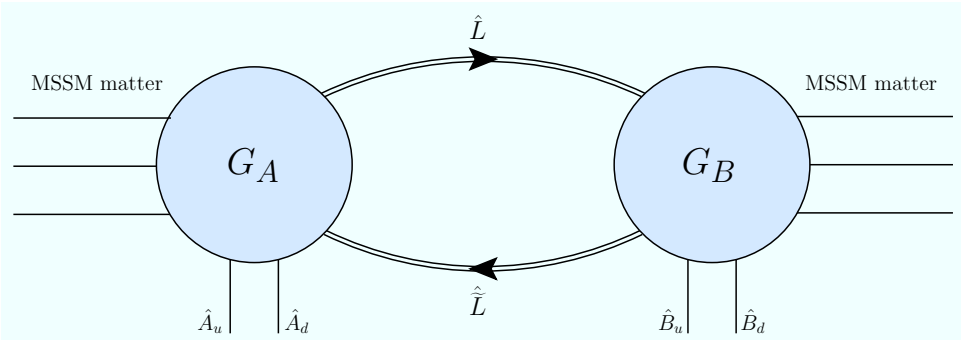

Figure 5.8: A possible 4 Higgs doublets UV completion of the chiral Higgs model. The quark and lepton superfields can be distributed in multiple possibilities between sites A and B.

A possible UV completion that can led us to the superpotential term in eq. (5.60) is given by the model sketched in fig. 5.8. In the example, an up- and a down-type Higgs doublets, $\hat{A}_u$ and $\hat{A}_d$, are charged under $\mathcal{G}_\mathcal{A}$, while the up-type $\hat{B}_u$ and the down-type $\hat{B}_d$ are charged under $\mathcal{G}_\mathcal{B}$. The following terms can then be added to the superpotential [190]:

$$\mathcal{W}_{UV} \supset \mu_A \hat{A}_u \hat{A}_d + \mu_B \hat{B}_u \hat{B}_d + \mu_{\tilde{L}} \hat{\bar{L}} \hat{A}_u \hat{B}_d + \mu_L \hat{L} \hat{A}_d \hat{B}_u \,. \tag{5.61}$$

Taking $\mu_L \langle \hat{L} \rangle \gg \mu_{\tilde{L}} \langle \hat{\bar{L}} \rangle$, we can integrate out $\hat{A}_d$ and $\hat{B}_u$ (at the tree level), such that in a lower energy spectrum we can identify $\hat{A}_u$ with $\hat{H}_u$ and $\hat{B}_d$ with $\hat{H}_d$. Then, at lower energies, but still above the TeV scale, this provides the μ-term for the superpotential of our chiral Higgs model:

$$\mu \hat{H}_u \hat{H}_d = \left(\mu_{\tilde{L}} \langle \hat{\bar{L}} \rangle - \frac{\mu_A \mu_B}{\mu_L \langle \hat{L} \rangle} \right) \hat{H}_u \hat{H}_d \,. \tag{5.62}$$

We can then write the superpotential of the chiral Higgs model just as in eq. (5.32),

$$\mathcal{W} = \mathcal{W}_{\text{MSSM}} + \frac{Y_K}{2} \hat{K} \left(\hat{L} \hat{\bar{L}} - \varrho^2 \right) \,. \tag{5.63}$$

As usual, the squark and slepton generations may be distributed in several ways between sites A and B. This distribution affects the anomaly cancellation considerations and gauge couplings unification but it is not relevant (at least at leading order) for our observations of tree-level mass enhancement and deviations in the SM-like Higgs couplings, *cf.* sec. 5.3. Therefore we stick, more concretely, to the case described in figure 5.9 and in table 5.2, in which the up-type Higgs double H_u and the three generations of matter are on site A, while the down-type Higgs double H_d is on site B.[6]

The superpotential eq. (5.63) and the Kähler potential for the Higgs superfields

$$\mathcal{K}_H = \hat{H}_u^\dagger e^{g_a V_a} \hat{H}_u + \hat{H}_d^\dagger e^{g_b V_b} \hat{H}_d \,, \tag{5.64}$$

[6]The model, in order to get anomaly cancellation, requires a UV completion with additional fields carrying Higgs-like charges, such as in the model described above and sketched in figure 5.8, or alternatively lepton supermultiplets moved on site B [190].

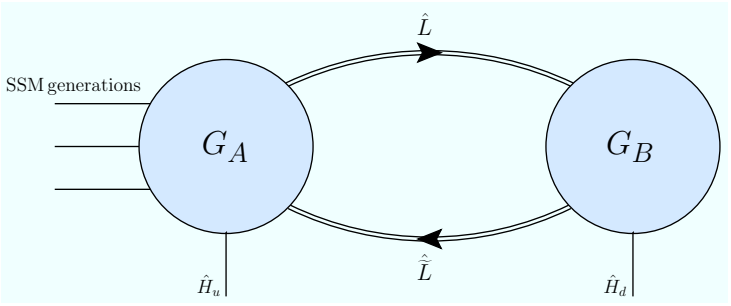

Figure 5.9: The quiver module of the electroweak sector for the chiral Higgs case, as reported in table 5.2. The corresponding non-decoupling D-terms are given in (5.65).

lead, after the gauge symmetry breaking $\mathcal{G} \to \mathcal{G}_{\rm SM}$, and after integrating out the linking fields at low energies, to the following non-decoupling D-terms:

$$\delta\mathcal{L} = -\frac{g_1^2\Omega_1}{8}(\xi_1 H_u^\dagger H_u + \frac{1}{\xi_1} H_d^\dagger H_d)^2 - \frac{g_2^2\Omega_2}{8}\sum_a (\xi_2 H_u^\dagger \sigma^a H_u - \frac{1}{\xi_2} H_d^\dagger \sigma^a H_d)^2 + \dots \,. \tag{5.65}$$

The ellipsis denotes again D-terms involving sleptons and squarks that are charged under the gauge symmetry, see section 5.1, while

$$\xi_i = \frac{g_{Ai}}{g_{Bi}}\,, \qquad \Omega_i = \frac{m_L^2}{m_{vi}^2 + m_L^2} \qquad (i = 1, 2)\,. \tag{5.66}$$

Note that $\Delta_i = \xi_i^2 \cdot \Omega_i$, however, we separately defined ξ_i and Ω_i for later convenience, for the analysis of Higgs couplings. We find the tadpole equations from the Higgs scalar potential to be given by

$$\frac{\partial V}{\partial H_d^0} = -v_u \,\mathrm{Re}\,[B_\mu] + v_d\Big(m_{H_d}^2 + |\mu|^2\Big) + v_d\frac{m_Z^2}{2}\cos(2\beta) + \frac{v_d}{8}\sum_i g_i^2\Omega_i\left(\frac{v_d^2}{\xi_i^2} + v_u^2\right)\,, \tag{5.67}$$

$$\frac{\partial V}{\partial H_u^0} = -v_d \,\mathrm{Re}\,[B_\mu] + v_u\Big(m_{H_u}^2 + |\mu|^2\Big) - v_u\frac{m_Z^2}{2}\cos(2\beta) + \frac{v_u}{8}\sum_i g_i^2\Omega_i\left(v_d^2 + v_u^2\xi_i^2\right)\,. \tag{5.68}$$

The mass matrix for the $\mathcal{CP}$-even Higgs bosons, in the basis $(\mathrm{Re}H_d^0,\, \mathrm{Re}H_u^0)$ is given by

$$m_h^2 = \begin{pmatrix} m_{h,11} & \frac{v_d v_u}{4}\sum_i g_i^2(\Omega_i - 1) - \mathrm{Re}[B_\mu] \\ \frac{v_d v_u}{4}\sum_i g_i^2(\Omega_i - 1) - \mathrm{Re}[B_\mu] & m_{h,22} \end{pmatrix}\,, \tag{5.69}$$

with

$$m_{h,11} = B_\mu \tan\beta + m_Z^2\cos^2\beta + \frac{v^2}{4}\cos^2\beta\sum_i g_i^2\frac{\Omega_i}{\xi_i^2} \tag{5.70}$$

$$m_{h,22} = B_\mu \cot\beta + m_Z^2\sin^2\beta + \frac{v^2}{4}\sin^2\beta\sum_i g_i^2\,\Omega_i\xi_i^2\,. \tag{5.71}$$

Superfields	Spin 0	Spin $\frac{1}{2}$	$SU(3)_c \otimes G_A \otimes G_B$
$\hat{Q}_i$	$\tilde{Q}_i$	Q_i	$(\mathbf{3}, \mathbf{2}_{1/6}, \mathbf{1}_0)$
$\hat{\bar{d}}_i$	$\tilde{d}^*_{R\,i}$	$d^*_{R\,i}$	$(\overline{\mathbf{3}}, \mathbf{1}_{1/3}, \mathbf{1}_0)$
$\hat{\bar{u}}_i$	$\tilde{u}^*_{R\,i}$	$u^*_{R\,i}$	$(\overline{\mathbf{3}}, \mathbf{1}_{-2/3}, \mathbf{1}_0)$
$\hat{\ell}_i$	$\tilde{\ell}_i$	ℓ_i	$(\mathbf{1}, \mathbf{2}_{-1/2}, \mathbf{1}_0)$
$\hat{\bar{e}}_i$	$\tilde{e}^*_{R\,i}$	$e^*_{R\,i}$	$(\mathbf{1}, \mathbf{1}_1, \mathbf{1}_0)$
$\hat{H}_u$	H_u	$\tilde{H}_u$	$(\mathbf{1}, \mathbf{2}_{1/2}, \mathbf{1}_0)$
$\hat{H}_d$	H_d	$\tilde{H}_d$	$(\mathbf{1}, \mathbf{1}_0, \mathbf{2}_{-1/2})$
$\hat{L}$	L	ψ_L	$(\mathbf{1}, \mathbf{2}_{-1/2}, \overline{\mathbf{2}}_{1/2},)$
$\hat{\bar{L}}$	$\tilde{L}$	$\psi_{\tilde{L}}$	$(\mathbf{1}, \overline{\mathbf{2}}_{1/2}, \mathbf{2}_{-1/2})$
$\hat{K}$	K	ψ_K	$(\mathbf{1}, \mathbf{1}_0, \mathbf{1}_0)$

Table 5.2: The matter content of a quiver model that may lead to the Chiral Higgs case and the D-term enhancement of (5.65). This is pictured in figure 5.9. The model requires a UV completion with additional fields carrying Higgs-like charges, such as in figure 5.8, or leptons multiplets on site B instead of A, for anomaly cancellation.

The mass matrix for the pseudo-scalar Higgs bosons, in the basis $(\mathrm{Im}H_d^0, \mathrm{Im}H_u^0)$, reads

$$m^2_{A^0} = \begin{pmatrix} m_{A^0,11} & \mathrm{Re}\,[B_\mu] \\ \mathrm{Re}\,[B_\mu] & m_{A^0,22} \end{pmatrix}, \tag{5.72}$$

with

$$m_{A^0,11} = B_\mu \cot\beta\,, \tag{5.73}$$
$$m_{A^0,22} = B_\mu \tan\beta\,. \tag{5.74}$$

The mass matrix for the charged Higgs bosons in the basis $\left(H_d^-, H_u^{+,*}\right), \left(H_d^{-,*}, H_u^+\right)$ is

$$m^2_{H^-} = \begin{pmatrix} m_{H^-,11} & \frac{1}{4}g_2^2(1-\Omega_2)v_d v_u + B_\mu^* \\ \frac{1}{4}g_2^2(1-\Omega_2)v_d v_u + B_\mu & m_{H^-,22} \end{pmatrix}, \tag{5.75}$$

with

$$m_{H^-,11} = B_\mu \tan\beta + m_W^2 \sin^2\beta(1-\Omega_2)\,, \tag{5.76}$$
$$m_{H^-,22} = B_\mu \cot\beta + m_W^2 \cos^2\beta(1-\Omega_2)\,. \tag{5.77}$$

We derive the corresponding tree-level Higgs masses to be (we consider B_μ real),

$$m^{2,\mathrm{C}}_{h^0,H^0} = \frac{1}{2}\left(m_A^2 + m_Z^2\right) + (C+D) \mp \frac{1}{2}\sqrt{\left(m_A^2 - m_Z^2 + \frac{2\,(C-D)}{\cos(2\beta)}\right)^2 c^2(2\beta) + \left(m_A^2 + m_Z^2 - 2m_\Omega^2\right)^2 s^2(2\beta)}\,, \tag{5.78}$$

$$m^{2,\mathrm{C}}_A \equiv \frac{2B_\mu}{\sin 2\beta} = m_{H_u}^2 + m_{H_d}^2 + 2|\mu|^2 + C + D + m_\Omega^2\,, \tag{5.79}$$

$$m^{2,\mathrm{C}}_{H^\pm} = m_A^2 + m_W^2(1-\Omega_2)\,, \tag{5.80}$$

where $c^2(2\beta) = \cos^2(2\beta)$, $s^2(2\beta) = \sin^2(2\beta)$. We defined

$$C = \frac{v^2}{8}\sum_{i=1,2} g_i^2\Omega_i\xi_i^2\sin^2\beta \quad , \quad D = \frac{v^2}{8}\sum_{i=1,2} g_i^2\Omega_i\frac{\cos^2\beta}{\xi_i^2}\,. \tag{5.81}$$

In the leading order in the $1/\tan\beta$ expansion we can then write the tree-level mass for the lightest $\mathcal{CP}$-even Higgs as

$$m^{,\mathrm{C}}_{h,0} \lesssim \left[m_Z^2 + \left(\frac{g_1^2\xi_1^2\Omega_1 + g_2^2\xi_2^2\Omega_2}{4}\right)v^2\right] + \mathcal{O}(\frac{1}{\tan^2\beta}, \xi_i)\,, \tag{5.82}$$

saturated in the decoupling limit $m_{A^0} \gg m_Z$. In the following, we take for simplicity $\Omega \equiv \Omega_1 = \Omega_2$ and $\xi \equiv \xi_1 = \xi_2$. We consider the decoupling limit, such that we approximate the 1-loop Higgs mass with the most relevant two-loop corrections as

$$m_h^{2,\mathrm{C}} \simeq \left[m_Z^2 + \left(\frac{g_1^2\xi_1^2\Omega_1 + g_2^2\xi_2^2\Omega_2}{4}\right)v^2\right] + \frac{3}{2\pi^2 v^2}\left[m_{t,r}^4\left(\sqrt{m_t M_{\tilde{t}}}\right)\ln\frac{M_{\tilde{t}}^2}{m_t^2} + m_{t,r}^4(M_{\tilde{t}})\frac{X_t^2}{M_{\tilde{t}}^2}\left(1 - \frac{X_t^2}{12M_{\tilde{t}}^2}\right)\right]. \tag{5.83}$$

Chiral case D-terms and Higgs mass enhancement

In fig. 5.10 the Higgs mass from eq. (5.83) is plotted in the $(m_{\tilde{t}_1},\, X_t)$ plane for different values of ξ on the left panel and Ω, on the right panel. ξ corresponds to the ratio between the gauge couplings of the two sites, while Ω parametrises the relative importance between the linking fields vevs and soft masses. Similarly to the vector Higgs case, the 125.5 GeV contour lines show that the D-terms contribution lowers the minimal stop masses required for a given value of X_t. In fig. 5.11, we show the m_h contour lines in the $(\xi,\, \Omega)$-plane for $m_{\tilde{t}_1} = 500$ GeV and 1 TeV, similarly to [190] (note the different notation.).

In the chiral Higgs case too, the explicit supersymmetry breaking in the low energy effective theory leads to a source of fine tuning that can be controlled if $m_L < 10$ TeV.

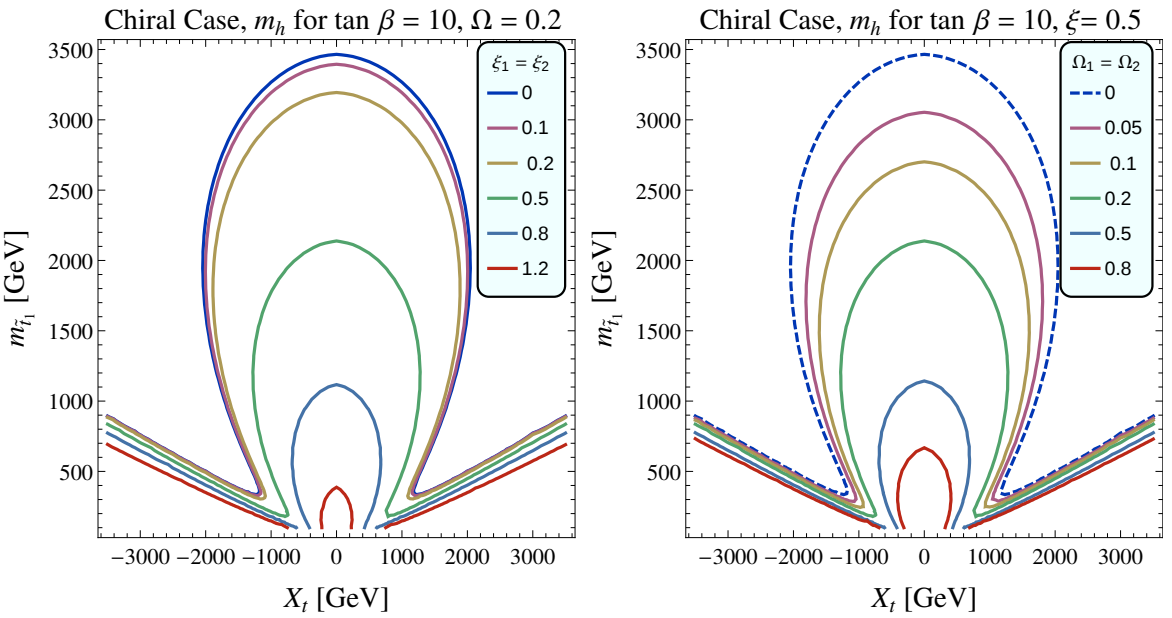

Figure 5.10: Contours of the Higgs mass $m_h = 125.5$ GeV in the $(m_{\tilde{t}_1}, X_t)$ plane for different values of ξ [left panel] and Ω [right panel], with $M_{Q_3} = M_{u_3}$, $\tan\beta = 10$.

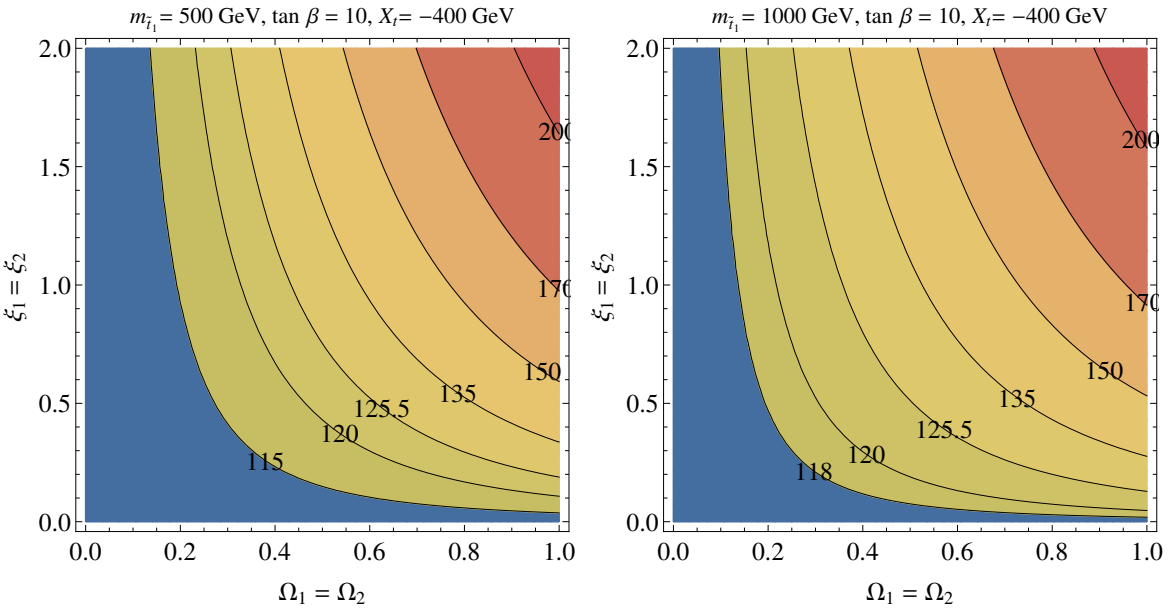

Figure 5.11: The Higgs mass in the (ξ, Ω)-plane, for the chiral Higgs case, with $m_{\tilde{t}_1} = 500$ GeV [left panel] and $m_{\tilde{t}_1}$=1 TeV [right panel], while $\tan\beta = 10$, $A_t = -400$ GeV.

5.3 Higgs couplings and detection at the LHC and ILC

Non-decoupling D-terms induced by the quiver extensions of the MSSM affect also the Higgs boson couplings to fermions and gauge bosons with respect to the SM and the MSSM [91, 190–192]. We are interested to estimate these deviations and to evaluate the potential of current and future colliders to detect them, in the light of the precision programs on Higgs boson couplings measurements. We follow, in fact, a bottom-up approach in order to infer on parameters of the model, i.e. Δ, Ω or m_H, establishing which parameter regions may be explored.

5.3.1 Non-decoupling D-terms effects on the Higgs couplings

A measure of the deviation of the couplings of the Higgs lightest eigenstate h from the couplings of the SM is defined by the ratio of the Higgs coupling over the Higgs coupling in the SM:

$$\kappa_U = g_U/g_U^{SM}\,, \quad \kappa_D = g_D/g_D^{SM}\,, \quad \kappa_V = g_V/g_V^{SM}\,, \tag{5.84}$$

for any up-type fermion $U = u, c, t$, down-type fermion $D = d, s, b, e, \mu, \tau$, or gauge boson $V = W^{\pm}, Z$.

We are restricting to the previously discussed effective field theories of gauge extensions of the MSSM, that give at low energies are given by the MSSM plus additional non-decoupling D-terms. These EFTs can be seen then as two-Higgs-doublets models (2HDMs) of type-II, like the MSSM. Let us consider the general 2HDM Higgs scalar potential

$$\begin{aligned}\mathcal{V}_{\text{2HDM}} =& m_1^2|H_u|^2 + m_2^2|H_d|^2 + m_{12}^2(H_u H_d + H_u^\dagger H_d^\dagger) \\ &+ \frac{\lambda_1}{2}|H_d|^4 + \frac{\lambda_2}{2}|H_u|^4 + \lambda_3|H_u|^2|H_d|^2 + \lambda_4|H_d^\dagger H_u|^2 + \frac{\lambda_5}{2}[(H_u\cdot H_d)^2 + \text{c.c.}] \\ &+ \lambda_6|H_d|^2[(H_u\cdot H_d) + \text{c.c.}] + \lambda_7|H_u|^2[(H_u\cdot H_d) + \text{c.c.}]\,,\end{aligned} \tag{5.85}$$

with all parameters real and CP-conserving. For the MSSM we have, *cf.* eq. (2.40),

$$\begin{aligned}&m_1^2 = (|\mu|^2 + m_{H_u}^2)\,, \quad m_2^2 = (|\mu|^2 + m_{H_d}^2)\,, \quad m_{12}^2 = B_\mu\,, \\ &\lambda_1 = \lambda_2 = \frac{g_1^2+g_2^2}{4}\,, \quad -\lambda_3 = \frac{g_1^2+g_2^2}{4}\,, \quad \lambda_4 = \frac{1}{2}g_2^2\,, \quad \lambda_5 = \lambda_6 = \lambda_7 = 0\,.\end{aligned} \tag{5.86}$$

For 2HDMs we can express exactly the ratios (5.84), also called scaling factors, in terms of the angles β and α [193–196],

$$\kappa_D \equiv -\frac{\sin\alpha}{\cos\beta}\,, \quad \kappa_U \equiv \frac{\cos\alpha}{\sin\beta}\,, \quad \kappa_V \equiv \sin(\beta-\alpha)\,, \tag{5.87}$$

where α is defined as the mixing angle of the CP-even Higgs mass eigenstates,

$$\begin{pmatrix} h_0 \\ H_0 \end{pmatrix} = \sqrt{2}\begin{pmatrix} -\sin\alpha & \cos\alpha \\ \cos\alpha & \sin\alpha \end{pmatrix}\begin{pmatrix} \text{Re}\ H_d^0 \\ \text{Re}\ H_u^0 \end{pmatrix}. \tag{5.88}$$

The SM limit is recovered for $\sin\alpha = -\cos\beta$, $\cos\alpha = +\sin\beta$. In the following, we neglect "wrong couplings", *i.e.* couplings between H_u^0 (H_d^0) and down-type (up-type) quarks, that could come from integrating out squarks, higgsinos and charginos at 1-loop, for which we refer to [91]. Given this, we express as in [91] κ_t, κ_V in terms of $\tan\beta$ and κ_b:

$$\kappa_t = \sqrt{1 - \frac{\kappa_b^2 - 1}{\tan^2\beta}}\,, \quad \kappa_V = \frac{\tan\beta}{1+\tan^2\beta}\left(\frac{\kappa_b}{\tan\beta} + \sqrt{1+\tan^2\beta-\kappa_b^2}\right)\,. \tag{5.89}$$

The Higgs particle that has been observed at the LHC seems SM-like, at least within the experimental accuracy, as said in chapter 3. Since we study the possibility that this SM-like Higgs is the lightest $\mathcal{CP}$-even Higgs of a model like the MSSM, we concentrate here in the case of 2HDMs for moderately large and large $\tan\beta$ ($\tan\beta \gtrsim 4$) and we assume to be in the decoupling limit $m_{A^0} \gtrsim 200$ GeV. In this regime, the lightest Higgs decays predominantly to bs, while the heavier $\mathcal{CP}$-even Higgs is relatively heavy, and can be identified with H_d, see also [197].

Relations (5.87) are exact, however, a more transparent general expression for the scaling factors κ_i can be obtained looking at the specific model considered, *i.e.* writing κ_i in terms of the coefficients in the potential $\mathcal{V}_{\rm 2HDM}$, eq. (5.85). We therefore follow the procedure below, treated more in detail in appendix C, and similar to the ones in [91, 190, 192]
We start from the Higgs Lagrangian

$$\mathcal{L} \supset -\mathcal{V}_{\rm 2HDM} - \left(\bar{u}\,\mathbf{y_u} Q\cdot H_u + \bar{d}\,\mathbf{y_d} Q\cdot H_d + \text{ h.c.}\right)\,, \tag{5.90}$$

neglecting leptons and, we stress again, the wrong couplings. We identify the heavy Higgs states with the Higgs doublet H_d and we integrate them out, obtaining the effective Lagrangian

$$\begin{aligned}\mathcal{L}^{\rm eff} \supset & -\frac{h_2}{2}D^2 h_2 - m_2^2\frac{h_2}{2} - \frac{\lambda_2}{8}h_2^4 + \frac{1}{2}\Theta h_2 \frac{1}{D^2+\Pi^2}\Theta h_2 \\ & - y_t t\,\bar{t}\,h_2 + \frac{y_d}{\sqrt{2}}\frac{\Theta}{D^2+\Pi^2}\,b\bar{b}\,h_2\,,\end{aligned} \tag{5.91}$$

where $h_2 = \mathrm{Re}H_u^0$, $\Theta = m_{12}^2 + \frac{\lambda_7 h_2^2}{2}$ and $\Pi^2 = m_1^2 + \frac{(\lambda_3+\lambda_5)h_2^2}{2}$.

The Higgs couplings can be derived from the effective Lagrangian eq. (5.91) after defining the SM-like Higgs h as

$$h_2 = \left(1 - \frac{1}{2}\left(\frac{\partial\langle\Theta h_2/\Pi^2\rangle}{\partial v_2}\right)^2\right)h\,, \tag{5.92}$$

by normalising it at the order $(\Theta/\Pi^2)^2 \sim 1/\tan^2\beta$. Defining then the ratio between the Higgs couplings to the SM-Higgs couplings as

$$\kappa_b = \kappa_\tau \equiv \frac{v g_{hb\bar{b}}}{m_b} = v\frac{(\frac{\partial\mathcal{V}_b}{\partial h})|_{h=v}}{\mathcal{V}_b|_{h=v}}\,, \tag{5.93}$$

we get, *cf.* appendix C,

$$\kappa_b \simeq \left(1 - \frac{m_h^2}{m_H^2}\right)^{-1}\left(1 - \frac{[\lambda_3+\lambda_5]\,v^2}{m_H^2 - m_h^2}\right) + \dots\,. \tag{5.94}$$

The ellipsis corresponds to non holomorphic couplings that are not present in the models we consider, and to terms proportional to λ_7, equal to zero in these models [190]. Finding the right κ_b expressions for our quiver models is then straightforward, substituting into (5.94) the corresponding λ_3, λ_5. The latter, in the vector Higgs case, may be obtained from the MSSM relations (5.86) plus the additional non-decoupling D-terms (5.34), getting

$$(\lambda_3+\lambda_5)_{\text{vector}} = -\frac{\left[g_2^2(1+\Delta_2)+g_1^2(1+\Delta_1)\right]}{4}\,, \tag{5.95}$$

therefore we have

$$\kappa_b^{\text{vector}} \simeq \left(1-\frac{m_h^2}{m_H^2}\right)^{-1}\left(1+\frac{[g_2^2(1+\Delta_2)+g_1^2(1+\Delta_1)]v^2}{4\left(m_H^2-m_h^2\right)}\right)\,. \tag{5.96}$$

In the chiral Higgs case, from eqs. (5.86) and (5.65), we obtain

$$(\lambda_3+\lambda_5)_{\text{chiral}} = -\frac{\left[g_2^2(1-\Omega_2)+g_1^2(1-\Omega_1)\right]}{4}\,, \tag{5.97}$$

so the scaling factor is

$$\kappa_b^{\text{chiral}} \simeq \left(1-\frac{m_h^2}{m_H^2}\right)^{-1}\left(1+\frac{[g_2^2(1-\Omega_2)+g_1^2(1-\Omega_1)]v^2}{4\left(m_H^2-m_h^2\right)}\right)\,. \tag{5.98}$$

It is important to note that in both the vector and chiral cases κ_b depends only on the D-term parameter (either Δ_i or Ω_i) and on the mass of the heavy $\mathcal{CP}$-even Higgs, m_H. One should note also that in the chiral case κ_b does not depend on $\xi_i^2\cdot\Omega$, as in the vector case. It depends only on Ω_i, *i.e.* it is independent from the ratio between the couplings in the two quiver sites. In both models, the MSSM limit is obtained by setting the non-decoupling D-term contributions to zero, respectively $\Delta_i=0$ and $\Omega_i=0$, while the SM limit is set for $m_H\to\infty$.

5.3.2 Higgs couplings determination at the LHC and ILC

The precise measurement of the Higgs boson couplings is crucial for establishing Higgs properties and the underlying physical model. It is therefore the object of much effort by the ATLAS and CMS collaborations and one of the main goals for the ILC project.

At the LHC, the absolute value of Higgs couplings cannot be directly determined, since only ratios between different Higgs couplings can be derived from the measurements of $\sigma\cdot$Brs. Coupling determination is therefore possible only in the framework of a specific model, under certain, at least minimal, assumptions. For example, one can obtain the scaling factors κ_i from a constrained 7-parameter fit with the assumptions of the absence of non-SM Higgs production and decay modes, together with generation universality ($\kappa_u\equiv\kappa_t=\kappa_c$, $\kappa_d\equiv\kappa_b=\kappa_s$ and $\kappa_l\equiv\kappa_\tau=\kappa_\mu$), see [106]. With these assumptions, we have listed in table 5.3 the coupling determination uncertainties at the LHC at 14 TeV, with integrated luminosity $\int\mathscr{L}dt = 300$ fb^{-1}, and the High Luminosity LHC (HL-LHC), with integrated luminosity equal to 3000 fb^{-1} [106]. They are compared with the expected coupling uncertainties at

the ILC, under the same model assumptions. The ILC stage at 500 GeV has integrated luminosity equal to 750 fb^{-1}, summing also the luminosity collected at 250 GeV. Similarly, the stage at 1000 GeV adds another 1000 fb^{-1}, while for the ILC$_{1000-\mathrm{LumUp}}$ it is assumed a total $\int \mathscr{L} dt = 5250$ fb^{-1}.

	LHC 14	**HL-LHC**	**ILC$_{500}$**	**ILC$_{1000}$**	**ILC$_{1000-\mathrm{LumUp}}$**
κ_W	4–6 %	2–5 %	0.39 %	0.21 %	0.2 %
κ_Z	4–6 %	2–4 %	0.49 %	0.5 %	0.3 %
$\kappa_l = \kappa_\tau$	6–8 %	2–5 %	1.9 %	1.3 %	0.72 %
$\kappa_d = \kappa_b$	10–13 %	4–7 %	0.93 %	0.51 %	0.4 %
$\kappa_u = \kappa_t$	14–15 %	7–10 %	2.5 %	1.3 %	0.9 %

Table 5.3: Expected precisions on κ_b at 1σ, in %, from a constrained 7-parameter fit assuming no non-SM production and decay modes and assuming universality ($\kappa_u \equiv \kappa_t = \kappa_c$, $\kappa_d \equiv \kappa_b = \kappa_s$ and $\kappa_l \equiv \kappa_\tau = \kappa_\mu$), as reported in [106].

The coupling ratios κ_i have currently been determined at the LHC with an accuracy still far from the expected values in table 5.3. For example, we display in figure 5.12 some results on the coupling scale factors by ATLAS and CMS with the assumptions reported in the caption. In figure 5.12 we can see that all the best fits in the couplings are still consistent with the SM value 1, even with 1σ-error bars, apart of the ATLAS slight deviation in $h\gamma\gamma$.

In contrast with the LHC, at the future e^+e^- linear colliders the Higgs *total* width and the Higgs couplings can be determined in a model-independent way.[7] This model independence is possible by exploiting the recoil methods that allow for a decay independent determination of the Higgsstrahlung process production $e^+e^- \to HZ$, a quantity that enters many observables and therefore allow to disentangle the coupling scale factors [110]. As it can be expected, with respect to the estimates with minimal model assumption, there are slightly higher 1σ uncertainties. This is reported in table 5.4, where the estimated ILC accuracies on the Higgs couplings are shown, assuming the theoretical uncertainties to be equal to 0.5% for the ILC stages at $\sqrt{s}$ =250, 500, 1000 GeV and for the luminosity upgrade ILC$_{\mathrm{LumUp}}$ at 250, 500, 1000 GeV, from [110]. It has been estimated that the accuracy may be further increased [199]. While the Higgs determinations in the High-Luminosity LHC are dominated by systematic errors, at the ILC, by contrast, measurements are dominated by statistical errors and are improved with increasing statistics.

5.3.3 Spotting non-decoupling D-terms at colliders

So far, deviations of κ_b, κ_t from the SM-value 1, due an MSSM extension with non-decoupling D-terms, have only been compared with 2012 ATLAS global fits in the specific case of a gauge

[7] Up to some assumptions on detector effects.

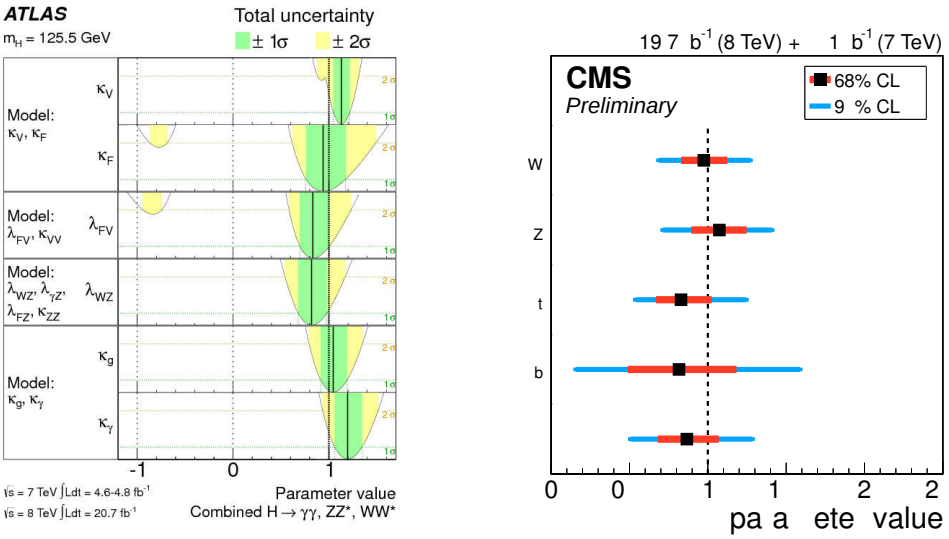

(a) (b)

Figure 5.12: (a) Summary of the measurements of the coupling scale factors for a Higgs boson with mass $m_h = 125.5$ GeV by ATLAS taken from [198]. The solid vertical lines represent the best-fit values, with the $\pm 1\sigma$ and $\pm 2\sigma$ uncertainties respectively given by the green and yellow band. There is strong correlation between the measurements in the various benchmark models, introduced in [198], that are separated by double horizontal lines. (b) Summary of the fits for deviations in the coupling by the CMS collaboration for a generic five-parameter model, in which the loop-induced couplings are assumed to follow the Standard Model structure as in [102], taken from the additional plots of [16]. The best fit values of the parameters are shown, with the corresponding 1σ and 2σ CL intervals.

	$\mathbf{ILC}_{250}$	$\mathbf{ILC}_{500}$	$\mathbf{ILC}_{1000}$	$\mathbf{ILC}_{\mathrm{LumUp}}$
κ_W	4.9 %	1.2 %	1.1 %	0.6 %
κ_Z	1.3 %	1.0 %	1.0 %	0.5 %
κ_τ	5.8 %	2.4 %	1.8 %	1.0 %
κ_b	5.3 %	1.7 %	1.3 %	0.8 %
κ_t	–	14 %	3.2 %	2.0 %

Table 5.4: Expected accuracies on the coupling scaling factors κ_i at 1σ, in %, for a completely model-independent fit assuming theory errors $\Delta F_i/F_i = 0.5\%$, from the ILC Higgs White Paper [110].

group with an additional $U(1)$ factor [146]. Values of m_H below 300 GeV could be excluded in that model.

We compare here the deviations from the SM couplings in the vector and chiral Higgs models, *cf.* eqs. (5.96) and (5.98), with the expected accuracies at the various stages of the LHC and the ILC, *cf.* tables 5.3 and 5.4. The idea is to understand which regions in the (Δ, m_H)- and (Ω, m_H)-planes can be explored by these experiments in the vector and the

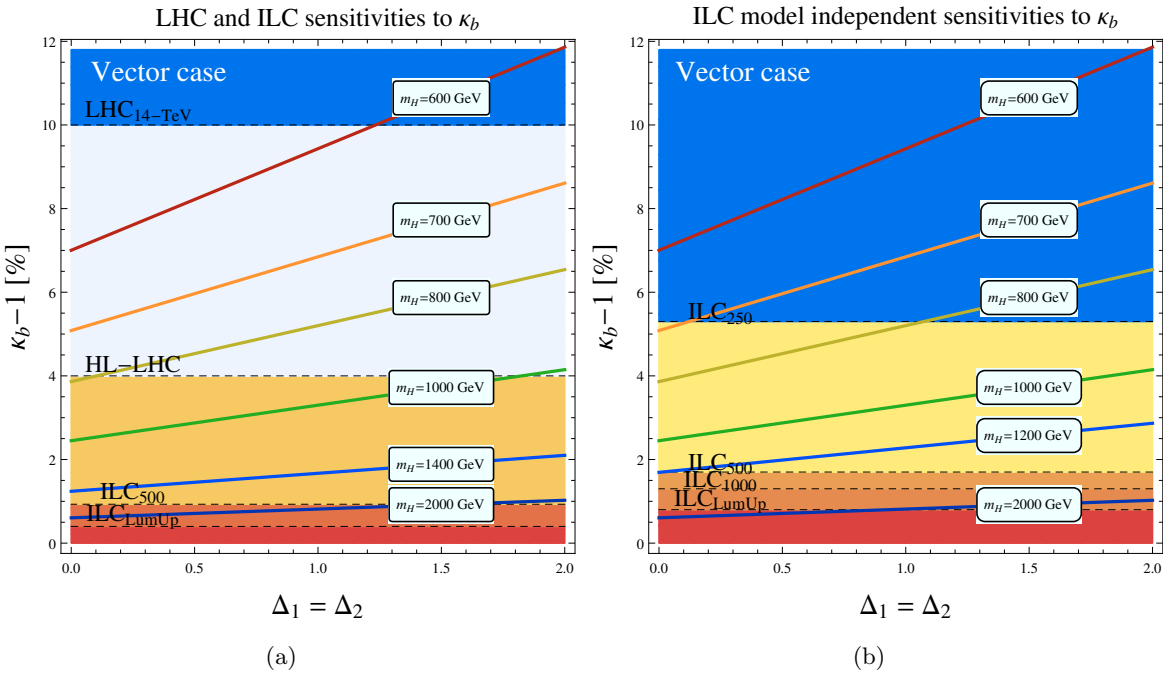

Figure 5.13: Vector case: relative enhancements $\kappa_b - 1$ of the Higgs bottom couplings with respect to the SM are displayed in solid lines, in [%] as function of $\Delta_1 = \Delta_2$, for different values of m_H [GeV]. (a) In dashed lines, the contours of the expected accuracies on the scaling factors κ_b at at the LHC, HL-LHC and ILC, from [106] and table 5.3, centred on the SM value $\kappa_b - 1 = 0$. The accuracies assume no non-SM production and decay modes and assumes universality ($\kappa_u \equiv \kappa_t = \kappa_c$, $\kappa_d \equiv \kappa_b = \kappa_s$ and $\kappa_l \equiv \kappa_\tau = \kappa_\mu$). (b) In dashed lines, the contours of the model-independent ILC sensitivities for each run from [110], see table 5.4, centred on the SM value $\kappa_b - 1 = 0$.

chiral case, respectively. This is possible understanding for which values of (Δ, m_H) and (Ω, m_H) the corresponding κ_i are outside the range of the uncertainties centred in the SM values $\kappa_i = 1$.

In figure 5.13 we plot the deviations from the SM-Higgs bottom coupling due to non-decoupling D-terms in a vector Higgs quiver extension of the MSSM, in comparison with the LHC and ILC sensitivities. The relative enhancement with respect to the SM-Higgs bottom coupling, $\kappa_b - 1$, is plotted as a function of Δ for different values of m_H, *cf.* eq. (5.96). The non-decoupling D-terms in the vector Higgs case enhance the deviation from the SM with respect to the MSSM limit $\Delta = 0$. Larger values of m_H, instead, clearly suppress these effects. In fig. 5.13, the horizontal dashed contour lines correspond to the 1σ-confidence level sensitivities for κ_b determination at the LHC and the ILC, centred in the SM value $\kappa_b - 1 = 0$. A value of $\kappa_b - 1$ that lies above one of these lines corresponds to a deviation from the SM that could be detected at the corresponding run of the machine. In figure 5.13(a), we display the LHC and ILC 1σ-confidence level sensitivities on κ_b from the minimal model assumptions in table 5.3, while in fig. 5.13(b) we refer to the ILC model-independent κ_b determination, *cf.* tab. 5.4. At the LHC at 14 TeV, deviations triggered by Δ of order $\sim \mathcal{O}(1\text{-}2)$ may be detected

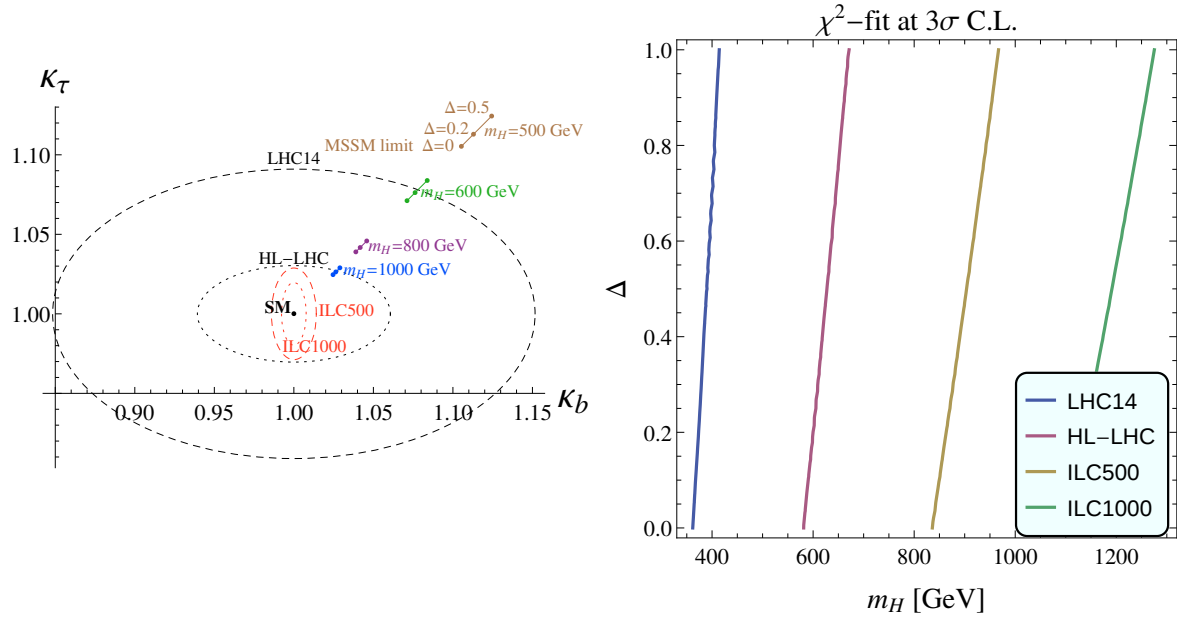

(a) (b)

Figure 5.14: Vector-Higgs case: experimental sensitivity to coupling deviations from the Standard Model, assuming no correlation between κ_i measures. (a) (κ_b, κ_τ) for Δ=0 (SM-limit), 0.1, 0.2, 0.5, at different values of m_H = 500, 600, 800, 1000, 1200 GeV. The experimental sensitivity, centred in the SM value (κ_b, κ_τ)=1, is represented by 1σ-confidence ellipses: black dashed for LHC at 14 TeV and 300 fb^{-1}, black dotted for HL-LHC at 3000 fb^{-1} at 14 TeV, red dashed ILC at 500 GeV and red dotted for ILC at 1000 GeV. (b) χ^2-test of κ_W, κ_Z, κ_τ, κ_b, κ_t in the (m_H, Δ)-plane at the different experiments: areas on the left of the solid lines are not consistent with the SM at 3σ-confidence level.

for a $m_H \lesssim 600$ GeV, while at the HL-LHC the sensitivity is shifted to even more decoupled values, up to $m_H \leq 1$ TeV. Passing to Δ of order $\sim \mathcal{O}(0.1\text{-}0.6)$, more suitable if to consider gauge coupling unification, *cf.* app. C, deviations from the SM are (just) discernible at the HL-LHC for m_H up to 800 GeV. At the ILC instead, we may explore Δ of order $\sim \mathcal{O}(0.1\text{-}0.5)$ for very decoupled values of m_H, up to 1 TeV at 500 GeV, while with the High-luminosity configuration at 1000 GeV, up to $m_H \sim 2$ TeV.

A deviation from the SM of κ_b in figure 5.13 is not sufficient alone to claim to have observed BSM physics, since it could be explained by statistical effects. In figure 5.14 we look at the deviations due the non-decoupling D-terms in κ_b in combination to those in the other scaling factors κ_i. In figure 5.14(a) we plot the 1σ-confidence ellipses for each experiment in the (κ_b, κ_τ)-plane. We show deviations for several values of Δ and m_H: each the point lying outside an ellipsis shows a perceivable deviation from the SM.[8] To be more concrete, in figure 5.14(b) we perform a χ^2-fit to the SM values of κ_W, κ_Z, κ_τ, κ_b, κ_t in the (m_H, Δ)-plane. The 1σ uncertainties are used as errors in the χ^2 calculation. The areas in the (m_H, Δ)-plane

[8] Similar kind of plots, applied to general 2HDM models, may be found in [200].

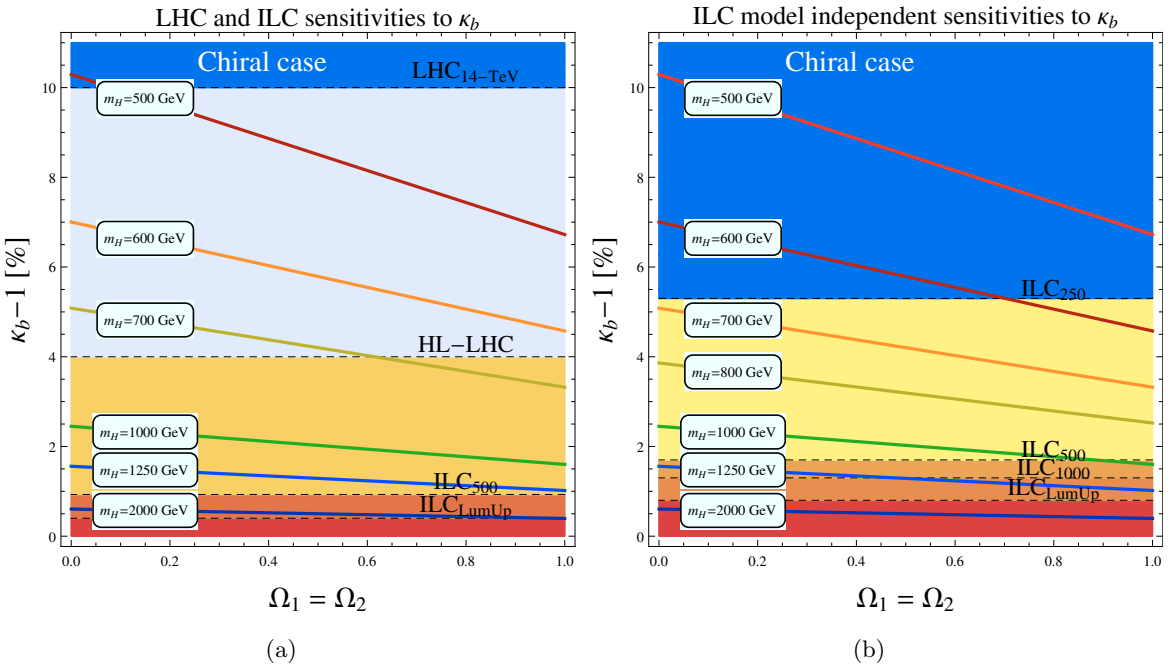

Figure 5.15: Chiral-Higgs case: relative enhancements $\kappa_b - 1$ of the Higgs bottom couplings with respect to the SM are displayed in solid lines, in [%] as a function of $\Omega_1 = \Omega_2$ for different values of m_H [GeV]. (a) In dashed lines, the contours of the expected accuracies on the scaling factors κ_b at the LHC, HL-LHC and ILC, from [106] and table 5.3, centred on the SM value $\kappa_b - 1 = 0$. The accuracies assume no non-SM production and decay modes and assumes universality ($\kappa_u \equiv \kappa_t = \kappa_c$, $\kappa_d \equiv \kappa_b = \kappa_s$ and $\kappa_l \equiv \kappa_\tau = \kappa_\mu$). Correlations are neglected. (b) In dashed lines, the contours of the model-independent ILC sensitivities for each run from [110], see table 5.4, centred on the SM value $\kappa_b - 1 = 0$.

that lye on the left of the solid lines are not consistent with the SM at 3σ-confidence level. Deviations from the SM value 1 for κ_W, κ_Z, κ_t are relatively mild in the vector and chiral Higgs models, see eq. (5.89). Therefore, taking into account the assumed accuracies on κ_i, we can see that most of the contribution to the χ^2 result comes from κ_b and κ_τ. Indeed, κ_b and κ_τ present large deviations from 1 while their determination rely on a relatively good resolution.

We can see that at the first run of the LHC, deviations from the Standard Model are detectable only for a relatively light H, with mass up to $m_H \simeq$ 350-400 GeV. The LHC luminosity upgrade is needed to explore the parameter space up to decoupling masses $m_H \lesssim$ 500 GeV for values of Δ up to 1. The situation would be much improved at the ILC, where deviations in the Higgs couplings could tested, possibly to exclude a decoupled H up to 700 (900) GeV at $\sqrt{s}$ =500 (1000) GeV. In both plots in fig. 5.14 we do not take into account any experimental correlations between the determinations of κ_i.

Passing to the chiral Higgs case, the D-terms trigger deviations of κ_i from 1 in opposite way with respect to the vector case. Here, the D-term contributions are negative, see eq.

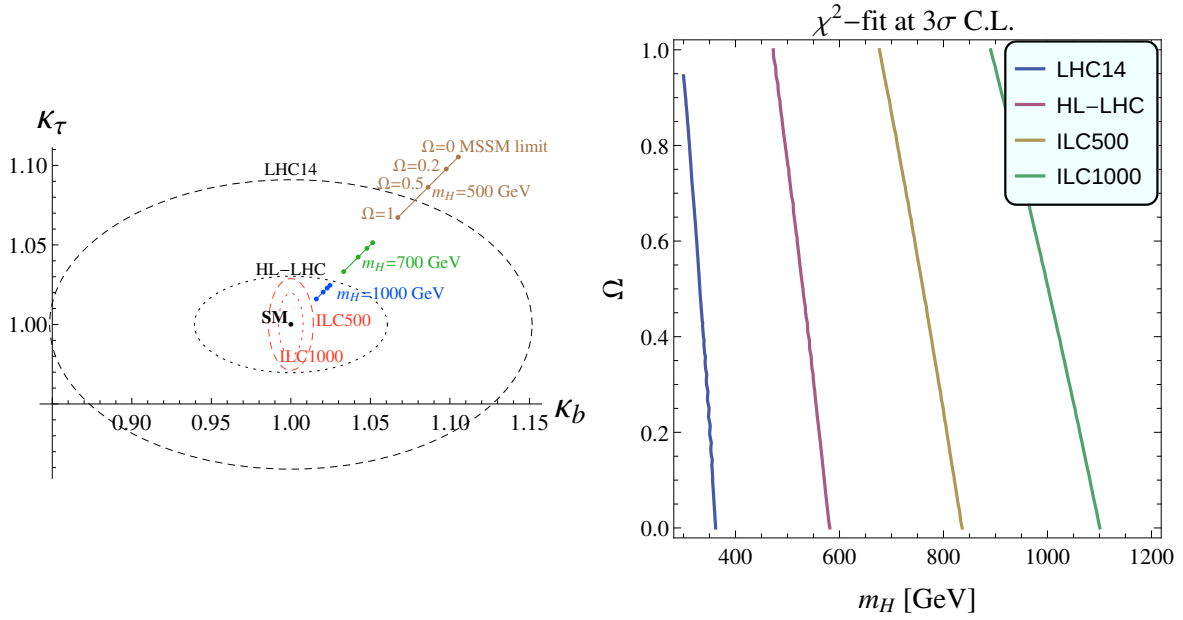

(a) (b)

Figure 5.16: Chiral-Higgs case: experimental sensitivity to coupling deviations from the Standard Model, assuming no correlation between κ_i measures. (a) (κ_b, κ_τ) for Ω=0 (SM-limit), 0.2, 0.5, 1 at different values of m_H = 500, 600, 800, 1000, 1200 GeV. The experimental sensitivity, centred in the SM value (κ_b, κ_τ)=1, is represented by 1σ-confidence ellipses: black dashed for LHC at 14 TeV and 300 fb^{-1}, black dotted for HL-LHC at 3000 fb^{-1} at 14 TeV, red dashed ILC at 500 GeV and red dotted for ILC at 1000 GeV. (b) χ^2-test of κ_W, κ_Z, κ_τ, κ_b, κ_t in the (m_H, Δ)-plane at the different experiments: areas on the left of the solid lines are not consistent with the SM at 3σ-confidence level.

(5.98), pushing the Higgs couplings closer to the SM value. Therefore for increasing Ω, the deviations of the couplings from the SM are more difficult to be seen with respect to the MSSM limit, *i.e.* for Ω = 0, see figures 5.15 and 5.16(a). In figure 5.16(b) we show the 3σ-χ^2 fit on κ_W, κ_Z, κ_τ, κ_b, κ_t in the (m_H, Δ)-plane. For values of Ω of order $\mathcal{O}(1)$, the sensitivity to the deviation of couplings is reduced at the LHC by ∼ 50 GeV and by ∼ 100 GeV at the ILC, with respect to the MSSM limit Ω = 0.

Once deviations in the Higgs couplings with respect to the SM are detected, additional information is required to understand which is the (BSM) supersymmetric model that has been observed. For the non-decoupling D-term extensions of the MSSM we have seen that, in order to do this, the detection of H and the measurement of its mass m_H are fundamental. Only knowing m_H, the Δ or Ω measurement could be decoupled, see equation (5.96). It is also interesting to stress that the non-observation of coupling deviations up to a certain size allow also to exclude H up to a corresponding scale.

5.4 Summary and conclusions

Supersymmetric models with an extended gauge symmetry with respect to the MSSM gauge group offer an interesting alternative to enhance the tree-level Higgs mass through novel contributions to the Higgs quartic terms in the scalar potential.

In this context, we have studied two quiver extensions of the MSSM, *i.e.* supersymmetric models with one or more copies of the factors of the gauge group $\mathcal{G}_{\rm MSSM} = SU(3)_c \otimes SU(2)_L \otimes U(1)_Y$. We concentrated in particular to models with two copies $\mathcal{G}_A$ and $\mathcal{G}_B$ of the electroweak group $SU(2)_L \otimes U(1)_Y$. Each standard MSSM chiral superfield may be on site A or site B, *i.e.* being charged either under $\mathcal{G}_A$ or $\mathcal{G}_B$. Linking chiral superfields $\hat{L}$ and $\hat{\bar{L}}$ are charged under both $\mathcal{G}_A$ and $\mathcal{G}_B$, connecting sites A and B. $\hat{L}$ and $\hat{\bar{L}}$ acquire vevs at a scale $\Lambda_{\mathcal{G}} > 1$ TeV, and are responsible for a diagonal gauge symmetry breaking of $\mathcal{G} = SU(3)_c \otimes \mathcal{G}_A \otimes \mathcal{G}_B \to \mathcal{G}_{\rm MSSM}$. The heavy gauge supermultiplets corresponding to the broken generators of $\mathcal{G}$ may be integrated out, leaving at lower energies an effective theory given by the MSSM plus additional D-terms for the MSSM scalars. In particular, these D-terms are non-decoupled, provided that a soft mass m_L for the linking fields has been introduced at a scale higher than $\Lambda_{\mathcal{G}}$. Therefore the Higgs mass receives sizeable contributions, allowing for a relaxation of naturalness.

We have studied the "vector Higgs" case, in which H_u and H_d are on the same site A, and the "chiral Higgs" case, with H_u on site A and H_d on site B. We analysed how the size of these additional D-terms affects the mass and the couplings of the light $\mathcal{CP}$-even Higgs, that we identify with the Higgs observed at the LHC. The LHC suggests, indeed, that the observed Higgs boson is SM-like within the experimental accuracy, therefore we have focussed to the decoupling limit $m_{A^0} \gg m_Z$ with moderately large or large $\tan\beta$, which could reproduce a similar coupling behaviour.

In both cases, the non-decoupling D-terms contributions to the tree-level Higgs mass are proportional to $\Delta_i = \xi_i^2 \cdot \Omega_i$. The parameter $\xi_i = g_{a\,i}/g_{b\,i}$ is the ratio between the gauge couplings in the two sites. $\Omega_i = m_L^2/(m_V^2 + m_L^2)$ parametrises, instead, the relative magnitude of the soft masses of the linking fields and of the masses of the heavy vector bosons. The latter are directly related to the vevs of the linking fields and the scale of gauge symmetry breaking. We could find that a D-term size parameter Δ of order $\sim \mathcal{O}(1)$ allows to reach a Higgs mass of 125.5 GeV already at the tree-level. A Δ of order $\sim \mathcal{O}(0.1\text{–}0.6)$, that may be preferred if to achieve perturbative unification, may provide a suitable enhancement to the Higgs mass as well.

Non-decoupling D-terms do affect also the SM-like Higgs couplings to fermions and gauge bosons. The Higgs couplings to b and τ are especially sensitive to deviations from the SM and the MSSM values due to D-terms effects, and can be studied at the LHC and ILC. These deviations are however suppressed by m_H. Therefore, for a more decoupled heavy Higgs H, deviations from the SM couplings are smaller and more difficult to spot. In the context of these models, then, the non-observation of these deviations up to a certain size may be used to exclude H below a corresponding scale.

In the vector Higgs case the deviations from the SM couplings increase for larger D-terms, *i.e.* larger Δ. At the high luminosity stage of the LHC, these deviations may be detected for any value of Δ with m_H up to ~ 600 GeV. At the ILC with $\sqrt{s} = 500$ GeV the sensitivity to deviations is much improved, and deviations from the SM for $0 \leq \Delta \leq 0.5$ can be seen with $m_H \leq 800 - 900$ GeV. Further improvement is possible with the ILC 1-TeV upgrade.

In the chiral Higgs case, instead, contributions from the non-decoupling D-terms are negative. They reduce the deviations in the couplings from the SM values with respect to the MSSM limit $\Omega = 0$, and result in a more challenging experimental determination. For example, in correspondence of a maximal D-term contribution to the Higgs mass, *i.e.* for $\Omega = 1$, the sensitivity is reduced and the deviations from the SM are detectable at the ILC with $\sqrt{s} = 500$ TeV only for $m_H \leq 650$ GeV.

We may conclude that once deviations from SM couplings are established, in order to distinguish the model from the MSSM, a precise measurement of m_H is required to obtain the D-terms parameters. We have shown that the precise and largely model-independent measurements of the Higgs couplings at the linear collider are needed, in order to be sensitive to a vast class of gauge extended supersymmetric models.

Chapter 6

Towards precision measurements in an intense field environment

This chapter is based on publications [4–6], written in collaboration with Anthony Hartin and Gudrid Moortgat-Pick. In section 6.1 the physics at the interaction point (IP) of a linear collider is introduced. In section 6.2, quantum electrodynamics (QED) in intense electromagnetic fields and the concept of critical field strength are presented. The magnitude of the fields at the IP of future linear colliders is evaluated. It is argued that, at linear colliders operating at several TeVs, the effect of these fields should be taken into account in all physics processes, including supersymmetry processes. In section 6.3 the Furry picture formalism, that allows to account for external fields exactly, is introduced. Finally, in section 6.4, it is studied the possibility to collide an intense laser beam on the electron/positron beams of the future linear collider, in order to test nonlinear QED, improving and extending the success of the SLAC-E144 experiment. In section 6.5 I summarise and conclude. Part of the text is derived from what I wrote in [4, 5]. All the figures have been made by me. Other external sources of this chapter are refs. [46, 201–203].

6.1 The interaction point of a linear collider

In the previous chapters we have seen that e^+e^--linear colliders may play a paramount rôle in electroweak precision physics and Higgs phenomenology. In particular, linear colliders could become fundamental for the search and study of physics beyond the SM. The key feature of a linear collider (LC) is the clean environment available in the interaction point (IP) of its lepton beams, in contrast with hadron colliders [41, 204].

The LHC, in fact, having proven itself as an extraordinary discovery machine, suffers nevertheless from a large background, mostly due to QCD processes. The LHC, indeed, collides protons that are composite objects made up by partons, *i.e.* gluons and quarks. Protons have an internal structure that is not known exactly but is empirically parametrised by *parton-distribution functions* (PDFs).

Despite the lower background rates, the high precision program of the future LC requires nevertheless a detailed knowledge of all processes occurring at the IP and a consequent optimal performance of the LC detectors. The backgrounds, indeed, limit the effective luminosity. The BSM physics program is particularly sensitive to this.

At a LC one of the main background processes is beamstrahlung. It consists in the radiation of an electron or positron in the electromagnetic field of the oncoming particle bunch. The high energy photons generated by beamstrahlung may interact with the external electromagnetic field too. In this way, they generate coherent electron-positron pairs, in a second background process called coherent pair production. As we said, these background processes are due to interactions between a particle and a macroscopic external field. In addition to them, also incoherent pairs are present, produced by particle-particle interaction processes. These are the Breit-Wheeler process $\gamma + \gamma \to e^+ + e^-$, the Bethe-Heitler process $\gamma + e^\pm \to e^\pm + e^+ + e^-$, the Landau-Lifshitz process $e + e \to e + e + e^+ + e^-$, and bremsstrahlung $e + e \to e + e + \gamma$. Important sources of background are given by synchrotron radiation, muons, and neutrons.

The designs for planned ILC are set to reach energies up to $\sqrt{s}$ = 1-1.5 TeV for the its highest energy stages [41], at CLIC up to $\sqrt{s}$ = 3 TeV are planned to be reached [204]. In order to perform the high precision physics program planned for future linear colliders, also a very high luminosity is needed. The reachable instantaneous luminosity is expected to be very high, in the range of 10^{-34}-10^{-35} cm^{-2}s^{-1}, comparable to the LHC.

To achieve this luminosity, extremely squeezed e^+ and e^- bunches are required. The densities of electrons and positrons in the colliding bunches are directly related to the nominal luminosity $\mathscr{L}$ for a head-on collision of two bunches. Assuming the bunches to be Gaussian, this relation is given by [205],

$$\mathscr{L} = f_r \, N_b \, H_D \, \frac{N_{e^+} N_{e^-}}{4\pi \, \sigma_x \, \sigma_y} \, , \tag{6.1}$$

where N_{e^-}, N_{e^+} are the number of electrons and positrons per bunch, respectively. The bunch propagates along the z direction and has transversal dimensions σ_x, σ_y. Finally, f_r is the bunch collision rate, N_b is number of bunches in each beam train, and H_D is an enhancement factor which depends on the disruption of the bunches. With disruption we mean the bending of the trajectories of the particles, that is due to the electromagnetic field associated to the oncoming beam, pinching the crossing bunches.

A typical bunch at future linear colliders will have order $\sim \mathcal{O}(10^{10})$ electrons or positrons per bunch and σ_x, $\sigma_y \sim$ 1-1000 nm. See table 6.1 for a comparison of ILC and CLIC parameters with LEP II and SLC. At a future LC, a bunch of electrons or positrons can be seen as a (relativistic) electromagnetic current that generates a collective electromagnetic field.

Each colliding particle at the IP, *i.e.* the beam electrons and positrons, will correspondingly see a potentially intense *external* electromagnetic field A_μ, given by the superposition of the collective fields originating from the two beams. In particular, being boosted, each colliding particle will mainly see the field originated by the oncoming bunch. This field can

Machine	LEP II	SLC	ILC-500GeV	ILC-1TeV	CLIC-500GeV	CLIC-3TeV
E [GeV]	94.5	46.6	250	500	250	1500
N (10^{10})	334	4	2	2	0.68	0.37
σ_x [µm]	190	2.1	0.474	0.429	0.202	0.045
σ_y [nm]	3000	900	5.9	2	2.3	1
σ_z [mm]	20	1.1	0.3	0.15	0.072	0.044

Table 6.1: Lepton colliders parameters. N is the number of leptons per bunch, σ_x, σ_y are the transversal dimensions of the bunches, σ_z is its longitudinal dimension. E is the energy of the particles in the bunches. The parameters for ILC-1TeV are taken from a 2011 dataset [206].

be well approximated by a constant field. In fact, the radiation coherence length is usually much shorter than the bunch length [205, 207]. The radiation coherence length is defined as the length that the charge travels in order a photon to be emitted within an angle $1/\gamma$. Given that the colliding particle is ultrarelativistic ($p_0 \gg m_e$), the oncoming external field would also appear as crossed, *i.e.* with the electric and magnetic components that are mutually orthogonal ($\mathbf{E}\perp\mathbf{B}$) and equal in magnitude ($|\mathbf{E}| = |\mathbf{B}|$) [208], *cf.* figure 6.1.

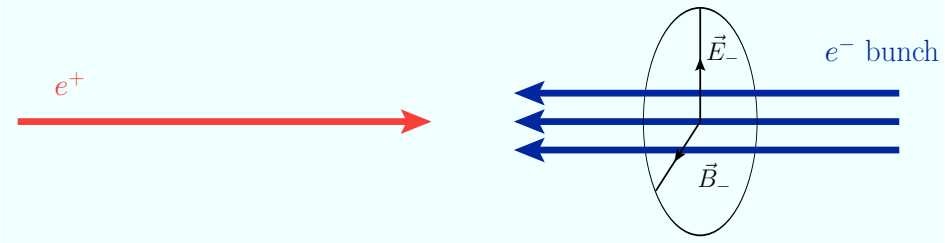

Figure 6.1: Sketch of the electromagnetic current associated to electron beam at the IP of a LC, as seen by a colliding positron.

A constant crossed field (CCF) with momentum k_μ is defined by having a trivial spatial dependence on x^μ,

$$A^\mu(x) = a^\mu\, k\cdot x\,, \tag{6.2}$$

and by the conditions

$$\mathcal{F} = \frac{1}{4}F_{\mu\nu}F^{\mu\nu} = \mathbf{B}^2 - \mathbf{E}^2 = 0\,, \qquad \mathcal{G} = \frac{1}{4}F_{\mu\nu}\tilde{F}^{\mu\nu} = -\mathbf{E}\cdot\mathbf{B} = 0\,. \tag{6.3}$$

$F^{\mu\nu}$ the field strength tensor and $\tilde{F}^{\mu\nu} = \frac{1}{2}\epsilon^{\mu\nu\rho\sigma}F_{\rho\sigma}$. A CCF can be seen as the limit of infinite period of a plane wave field with momentum k.

Approximating A_μ as an *external* field means that it is not affected by the charges of the single colliding particle. In fact, the intense field A_μ, due to its high photon density and corresponding wave function overlap, can be treated as a classical field, rather than a field

composed by independently interacting photons. This is also the case for macroscopic fields and coherent electromagnetic radiation.

At the IP of future LCs, the external field A_μ interacts with the oncoming particles and transfers momentum to them, in a quantity depending on its strength. Because of this, processes otherwise kinematically not allowed in absence of an external electromagnetic field can happen, for example beamstrahlung $e^\pm \to e^\pm + \gamma$ and coherent pair production $\gamma \to e^+ + e^-$. For the same reason, the rate of all the processes allowed in absence of the external field may be modified due to contributions from the external field. This involves the processes that are the object of LC physics program, for example Higgs or BSM particle production.

It is clear then that a comprehension of electromagnetic processes in an intense electromagnetic external field is required, as well as an estimate of the external electromagnetic field that may occur at the planned linear colliders.

6.2 *Horror vacui*: Physics in intense fields

Since the early hours of quantum electrodynamics (QED), the processes in external electromagnetic fields have drawn the attention of physicists. Klein, in 1929, pointed out [209] the paradox that a relativistic electron can transmit via quantum tunnelling through an arbitrary high potential barrier. Shortly afterwards, in 1931, Sauter [210] showed that the transmission coefficient depends exponentially on the intensity of the electric field in the barrier, and that the paradox takes place only in electric fields exceeding the critical value for the field strength

$$F_{\text{cr}} = \frac{m_e^2 c^3}{\hbar |e|} = 1.32 \cdot 10^{18} \text{ V/m} = 4.41 \cdot 10^9 \text{ T}\,. \tag{6.4}$$

Heisenberg and Euler in 1935 then studied the effective action of a free electromagnetic field [211], finding that at F_{cr} electron-positron pairs are spontaneously created. Eventually Schwinger in 1951 [212] found that the base of the Klein paradox is intimately related to the structure of the vacuum in the presence of an external electromagnetic field, as we explain here.

In QED, in the absence of external fields the vacuum, *i.e.* the state of lowest energy, is empty of *real* particles but populated by *virtual* electron positron pairs consisting in vacuum fluctuations. These virtual pairs can be seen as electric dipoles oriented in a random way. However, once an external electric field is switched on ($\vec{E} \neq 0$), the virtual dipoles align along the direction of $\vec{E}$, *cf.* fig. 6.2. The realignment of dipoles affects the vacuum polarisation, which becomes anisotropic.

In this regard, the Sauter-Schwinger critical field strength F_{cr} plays a crucial role. It corresponds to the magnitude of the field required by an electron to get an energy $m_e c^2$ over a Compton wavelength $\lambda\!\!\!^{-}_C = \frac{\hbar}{m_e c}$, which is the length scale of quantum fluctuations in QED. This means that with an external field $\vec{E}$ with field strength F_{cr}, the virtual electron and positron of a pair are accelerated apart and spontaneously separate, being promoted

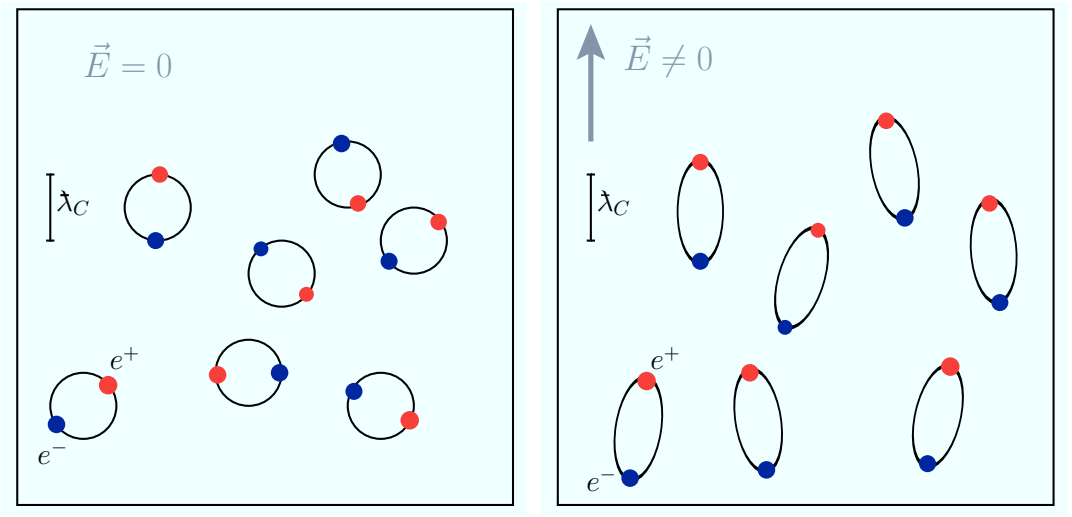

(a) (b)

Figure 6.2: (a) Vacuum state in absence of external electric field $\vec{E} = 0$. (b) Vacuum state for $\vec{E} \neq 0$.

to real particles through the so called *Schwinger effect*. Therefore the vacuum state full of *virtual* particles only becomes unstable and transforms into a more stable polarised vacuum by producing *real* particles [213], in a phase transition. The spontaneous production of real pairs in a constant electric field with strength E has the probability [212]:

$$W_{e^+e^-} = \frac{\alpha_{\text{em}} E^2}{\pi^2} \sum_{n=1}^{\infty} n^{-2} \exp\left[-\pi \frac{n\, F_{\text{cr}}}{E}\right], \tag{6.5}$$

with n the number of pairs and $\alpha_{\text{em}} = g_{\text{em}}^2/(4\pi\hbar c)$ the fine structure constant.[1]

It is important to note that the critical field strength F_{cr} defined in eq. (6.4) is relative to the spontaneous *electron-positron* pair production. In general, in order to have a charged particle-antiparticle pair creation from the vacuum, a corresponding critical field strength $F_{\text{cr, particle}}$ is required. This critical field strength is defined by substituting the mass of the considered particle m_{particle} in place of m_e in eq. (6.4). This means that already for muons spontaneous pair production requires an extremely high field strength $F_{\text{cr, }\mu^\pm} \sim 4 \times 10^4\, F_{\text{cr}}$. Extended reviews about QED in intense fields and unstable vacuum may be found in [201–203, 213, 214].

Very intense fields, sometimes with strength close to or stronger than F_{cr}, may be reached:

- Close to superheavy nuclei, with high atomic number $Z_a \gtrsim 137$, since $|\vec{E}| \approx \frac{Z_a|e|}{\lambda\!\!\!^{-2}_C} = Z_a\, \alpha_{\text{em}} F_{\text{cr}}$ on the surface of a nucleus [202]. $Z_a \gtrsim 137$ can be reached during the collision

[1] Note that pair creation is a purely electric quantum effect. In a magnetic field with strength equal to F_{cr}, Landau levels of electrons are separated by an energy gap equal to $m_e c^2$.

of two heavy ions A and B, such that $Z_a(A) + Z_{at}(B) > 1/\alpha_{\rm em}$. This is possible at RHIC or during LHC Pb-Pb collisions, see [215].

- On the surface of pulsars, where a magnetic field of order $\mathcal{O}(10^8)$ T can be reached. In a special class of these objects, the magnetars, extreme conditions bring the magnetic field well above $F_{\rm cr}$, at the order $\mathcal{O}(10^{11})$ T. For a review on the processes happening in these contexts, see [214].

- In intense lasers, even though the intensity of the critical field, of order 10^{29} W/cm^2, is believed to be hardly accessible. The reason is that QED cascades generated by one charge may consume the energy of the field. So far, optical lasers could reach $I = 2 \times 10^{22}$ W/cm^2, *i.e.* $E \sim 10^{-4} F_{\rm cr}$, with the HERCULES laser [216]. However, planned ultra-intense, petawatt lasers as HiPER [217], ELI [218], are expected to reach intensities between 10^{24}-10^{26} W/cm^2. Another kind of lasers, the X-ray free electron lasers (XFELs), produce strong electromagnetic fields through coherent light sources in the X-ray range. With a lower power but higher focus, the planned European XFEL in DESY is expected to feature very high peak intensities, possibly reaching a field of the order of 10^{19} V/cm^2 [219]. Values of field amplitude close to $F_{\rm cr}$ are reachable in the rest frame of a boosted ultrarelativistic particle colliding with the laser ($E^* \sim F_{\rm cr}$). This principle was followed by the E-144 experiment at SLAC [46], which operated 46.6 GeV electrons, shot through an intense laser, reaching $E^* \sim 0.3 F_{\rm cr}$, see section 6.4.

- At a future linear collider. The field strength generated by an oncoming bunch, indeed, approaches $F_{\rm cr}$ in the rest frame of the colliding ultrarelativistic lepton, due to the large Lorentz factor γ_L [5,6]. See subsection 6.2.1.

Relevant quantities for the description of the physics in an external field with momentum k and pulse ω are the gauge and Lorentz invariants:

$$\eta = \frac{e\sqrt{(A_\mu)^2}}{m} = \frac{eE}{m\omega}\,, \qquad \Upsilon = \frac{e}{m^3}\sqrt{(F_{\mu\nu}p^\mu)^2} = \eta\,\frac{p\cdot k}{m^2}\,, \tag{6.6}$$

where m, e, p denote the mass, the charge, and the momentum of the probe particle, *i.e.* electron, positron or photon.[2] The parameter η can be interpreted as the work done by the external field on the propagating particle over a Compton length $\lambda\!\!\!^{-}_C$, in units of the energy $\hbar\omega$ of the quanta, *i.e.* the photons, of the external field [201,203]. If $\eta \ll 1$, the probe particle is expected to *absorb* a low number of photons, if any at all, from the external field. If $\eta \gtrsim 1$ instead, processes with multiple absorption of photons from the external field are favoured, featuring a nonlinear dependence on the external field strength. In this context we speak about *nonlinear QED*. The quantity η is called the *classical nonlinearity parameter*, since it does not depend on the quantum constant $\hbar$. In processes occurring in a intense laser beam,

[2] In QED processes, when the initial particle is a photon, the mass and charge of the electron are used in the definitions (6.6), see below.

η is the control parameter, and it indicates the intensity of the field for a fixed laser frequency ω. To get a high η for a fixed value of the field intensity one should reduce the frequency ω, such that in the limit of a constant field $\eta \to \infty$.

The Υ parameter represents, in units of mc^2, the work performed by the field over a Compton length in the rest system of the propagating particle. Υ is called the *quantum nonlinearity parameter* and parametrises the magnitude of the quantum nonlinear effects on a probe particle. These are, for example, the photon recoil on an electron or the electron-positron pair production happening in the collisions of a photon with a laser. When considering ultrarelativistic massive particles, Υ describes the intensity of the external field in the particle frame in units of the Sauter-Schwinger critical field:

$$\Upsilon = \frac{\gamma_L E}{E_{\text{cr}}} = \frac{\gamma_L B}{B_{\text{cr}}}\,, \tag{6.7}$$

where E, B are the electric and magnetic components in the laboratory frame. In particular, in the case of highly energetic initial particles, as for linear colliders, the boosted particles may see a field strength close to the critical regime, *i.e.* $\Upsilon \sim O(1)$, even if the field in the laboratory frame is much less intense. When considering a colliding photon, Υ describes the intensity of the external field in the rest frame of a pair generated from this initial photon.

In general, the probabilities W of processes in an external field depend on η, Υ and a set of other gauge and Lorentz invariants f_i, built out of the field strength tensor $F^{\mu\nu}$ and the momenta of the probing particles. In the case of processes with a *single* initial particle in a constant or slowly varying field, the probabilities depend on η, Υ and also on $\mathcal{F}$ and $|\mathcal{G}|$ ($\mathcal{G}$ being a pseudoscalar) [201]. The parameters $\mathcal{F}$ and $|\mathcal{G}|$ describe the external field structure: they are respectively the relative magnitude and orientation between $\mathbf{E}$ and $\mathbf{B}$, *cf.* eqs. (6.3).

If $\eta \gg 1$, it is common to consider a field as being constant during the process, and the dependence of the probabilities on η can be dropped [201]. When considering an ultrarelativistic particle ($p^0 \gg m_e$) in a relatively weak constant field, one has $|\mathcal{F}|, |\mathcal{G}| \ll \min(1, \Upsilon^2)$. The probability of the processes in this regime can then be approximated as the corresponding one in a constant crossed field,

$$W(\Upsilon, \mathcal{F}, |\mathcal{G}|) \simeq W(\Upsilon, 0, 0) + \mathcal{O}(\mathcal{F}, |\mathcal{G}|)\,, \tag{6.8}$$

depending effectively only on the intensity of the external field. This is valid for the processes at the linear collider IP, as well. This confirms that a crossed field is a good approximation for the field seen by the colliding particles at the IP of LCs, since for a constant crossed fields $\mathcal{F} = \mathcal{G} = 0$, *cf.* eqs. (6.3).

6.2.1 Intense fields at the interaction point of a linear collider

We have seen that Υ is the paramount parameter for the processes in the external field at the IP of a linear collider. While for $\Upsilon \ll 1$ we have the classical regime, for $\Upsilon \gg 1$ beamstrahlung photons carry away a consistent fraction of the energy from the radiating

particle. For $0.1 \lesssim \Upsilon \lesssim 100$ we have a transition regime [205]. It is therefore important now to estimate the value of Υ at linear colliders.

Machine	**LEP II**	**SLC**	**ILC-500GeV**	**ILC-1TeV**	**CLIC-500GeV**	**CLIC-3TeV**
$\Upsilon_{average}$	0.00015	0.001	0.06	0.27	0.21	4.9
Υ_{max}	0.00034	0.0019	0.15	0.66	0.48	11.4

Table 6.2: Average and peak values of the Υ parameter of the particle at LEP II, SLC, ILC, and CLIC, with reference to the parameter sets in table 6.1.

Machine	**ILC-1TeV**$_{\texttt{CAIN}}$	**CLIC-3TeV**$_{\texttt{CAIN}}$
$\Upsilon_{\texttt{CAIN}\ average}$	0.27	3.34

Table 6.3: Average values of the Υ parameter of the particle at ILC-1TeV, and CLIC-3TeV, evaluated after simulations with `CAIN` [220], with reference to the parameter sets in table 6.1.

Υ varies during the collision of bunches since the latter are distorted by the pinch and the disruption effects. The average and the peak values for Υ in a Gaussian bunch can be empirically approximated by [207, 221]:

$$\Upsilon_{average} \approx \frac{5}{6}\frac{N r_e^2 \gamma_L}{\alpha_{\rm em}\sigma_z(\sigma_x+\sigma_y)}\,, \qquad \Upsilon_{max} \approx \frac{2N r_e^2 \gamma_L}{\alpha_{\rm em}\sigma_z(\sigma_x+1.85\sigma_y)}\,, \tag{6.9}$$

where N is the number of leptons of the oncoming bunch, $\alpha_{\rm em}$ the fine structure constant, r_e the Compton radius, σ_x, σ_y are the transversal dimensions of the bunches, σ_z the longitudinal dimension. In table 6.2, we report the values of $\Upsilon_{average}$ and Υ_{max} for LEP II, SLC ILC-1 TeV, and CLIC-3 TeV, calculated using eq. (6.9) and the parameter sets in table 6.1 [5, 6]. The estimates for $\Upsilon_{average}$ were reported also in the more recent reference [222], where for ILC-1 TeV the values $N = 1.74 \times 10^{10}$, $\sigma_x = 335$ nm, $\sigma_z = 0.3$ mm are used, from [41], getting $\Upsilon_{average} = 0.20$. We refer here to an older dataset for ILC-1 TeV since utilised as input of a simulation we have done with the IP beam-beam simulation program `CAIN` [220]. The results for $\Upsilon_{average}$ in table 6.2 are consistent with the estimates from this simulation for ILC-1 TeV and slightly less with the ones for CLIC-3 TeV, *cf.* table 6.3. These estimates were obtained after simulations of bunch crossings. The value of Υ obtained in correspondence of each of the $\mathcal{O}(10^6)$ beamstrahlung-photon emission have been averaged over the bunch crossing. For these simulations we used the same parameter sets in table 6.3 as input.

The expected bunch electromagnetic fields in the rest frame of the colliding particle at the IP of the ILC and CLIC-500 GeV are of order $\mathcal{O}(0.1) \cdot F_{\rm cr}$. Only at CLIC-3 TeV the field is expected to surpass the critical value. In both cases field strengths of 3-4 orders of magnitude higher than at SLC, *cf.* eq. (6.7), and 4-5 orders of magnitude higher that at LEP II.

The number of beamstrahlung photons $n_{\gamma,\,\rm bs}$ and the number of coherent pairs $n_{\rm cp}$, is

approximated by (see [222] and references therein),

$$n_{\gamma,\,\mathrm{bs}} = \frac{5}{2}\,\frac{\alpha_{\mathrm{em}}}{\gamma_L\, r_e^2}\,\frac{\sigma_z\,\Upsilon}{\sqrt{1+\Upsilon^{2/3}}}\,, \qquad n_{\mathrm{cp}} = \frac{4\sqrt{3}}{25\pi}\left(\frac{\alpha_{\mathrm{em}}\sigma_z}{\lambda\!\!\!^{-}_C\,\gamma_L}\Upsilon\right)^2 \Xi(\Upsilon)\,, \tag{6.10}$$

where $\Xi(\Upsilon)$ can be approximated for $\Upsilon \ll 1$ as $\Xi(\Upsilon) = 0.5\exp[-16/(3\Upsilon)]$, and for $\Upsilon \gg 1$ as $\Xi(\Upsilon) = 2.6\Upsilon^{-2/3}\ln[\Upsilon]$.

We can understand from equation (6.10) one of the reasons to have extremely short bunches at the CLIC, with σ_z much lower then at SLC and LEP II. It is the need to minimise beamstrahlung and coherent pair production, compensating the very high Υ. For a detailed analysis on the backgrounds from strong field beam-beam processes CLIC, where also a non-negligible rate of the *trident processes* $e \to e + e^+ + e^-$ is expected, see [222].

We may conclude that, if to work with a machine with $\Upsilon \sim \mathcal{O}(1)$ and higher such as CLIC-3 TeV, we should take into account the effects of the intense fields at the IP not only to evaluate the backgrounds. Fields with field strength F_{cr} in rest frame of a colliding particle necessarily affect its momentum and consequently, the rate of the process. In this case, we need to take entirely into account the impact the external fields on the actual physics processes in electroweak and BSM physics, particularly sensitive to these effects. Therefore we argue that strong field effects on ordinary processes at colliders operating in the multi-TeV regime, like CLIC, should be considered as well in event simulator programs, such as `WHIZARD` [223]. For example, in figure 6.3 we show the Feynman diagrams for Higgsstrahlung and for chargino pair production. The effect of the IP external fields is felt by the initial electron and positron, depicted with double lines. The effect on the other (charged) particles of the process should instead be considered negligible due to their mass and lower velocity, even though the process could be fast and entirely occurring within the bunch. In the following section we introduce a method that accounts for the external fields exactly on the propagation of particles.

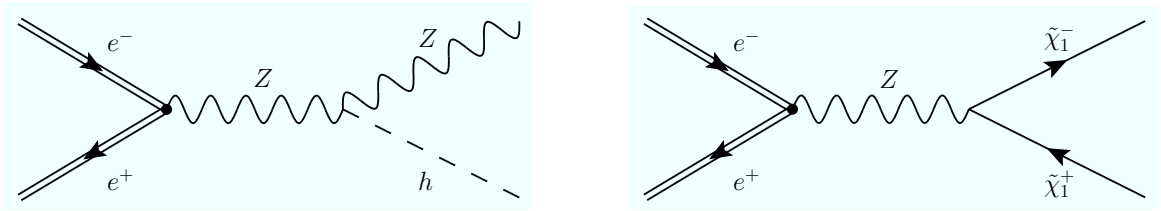

(a) Higgsstrahlung.

(b) Z-mediated chargino pair production.

Figure 6.3: Feynman diagram of (a) the Higgsstrahlung process and of (b) Z-mediated s-channel of chargino pair production at a LC, taking into account the intense external fields seen by the colliding electron and positron at the IP. For the electron and the positron double lines are used, to denote the interaction with the intense external field.

6.3 The Furry Picture

We argued that at future linear colliders, in particular at the high energy stages of CLIC, one should take into account *exactly* the effect of an external field on the colliding particles. This is requested also in laser physics when $\eta \gtrsim 1$, a condition fulfilled by the described constant crossed fields too. The *Furry picture* (FP) of quantum states [224], accounts for the external field exactly with a non perturbative approach, by using the Volkov solutions of the equations of motion in an external field [225]. These solutions are used as the basis for the perturbative expansions of the S-matrix, in order to calculate the probabilities of the physical processes according to the Feynman-Schwinger-Tomonaga theory [208]. The Furry approach can be applied to the classes of external fields whose vacuum is stable under pair production [213]. These are, for example, the (purely) magnetic fields and the plane wave fields, like the constant crossed field we are interested in.[3] In the following, we briefly review the FP method, see also [226].

In the standard Interaction (or Dirac) picture of quantum states, the state vectors and the observables share the time dependence. The corresponding Hamiltonian is given by

$$\mathcal{H} = \mathcal{H}_0 + \mathcal{H}_{\text{int}} \,. \tag{6.11}$$

$\mathcal{H}_0$ is the time-independent unperturbed Hamiltonian, that describes the time evolution of observables. $\mathcal{H}_{\text{int}}$ is the interaction Hamiltonian, regulating the time dependence of the states. In QED, $\mathcal{H}_{\text{int}}$ contains the gauge interactions terms between fermions and photons, corresponding to the Lagrangian term $-e\,\bar{\psi}\gamma_\mu A^\mu \psi$. The eigenstates of $\mathcal{H}_0$ are assumed to be the free states of the particle in the vacuum, in absence of external fields.

The FP Hamiltonian takes into account an external field and is given by

$$\mathcal{H} = \mathcal{H}_0 + \mathcal{H}_{ext} + \mathcal{H}_{\text{int}} = \mathcal{H}_B + \mathcal{H}_{\text{int}} \,, \tag{6.12}$$

where $\mathcal{H}_{ext}$ represents the interaction of the fermions with the external *classical* field. In the FP the basis of the state vectors is made by the bound states of the fermions in the external field, eigenstates of $\mathcal{H}_B$. These bound eigenstates are related to the free particle states of the Interaction picture by a canonical transformation [224]. The FP states obey to commutation relations that in the limit of null external field reduce to the usual Dirac picture commutation relations. The QED Lagrangian for the FP can be written as:[4]

$$\mathcal{L} = \bar{\psi}(i\partial\!\!\!/ - eA\!\!\!/_{ext} - m)\psi - \frac{1}{4}F^{\mu\nu}F_{\mu\nu} - e\bar{\psi}A\!\!\!/\psi \,, \tag{6.13}$$

where A^μ_{ext} is the classical external field and $F^{\mu\nu}$ the electromagnetic field strength tensor. The interaction term of ψ with A^μ_{ext} is explicitly separated by the ψ gauge interaction term.

[3] The class of fields whose vacuum is unstable under pair production (as the purely electric field), needs a generalisation of the FP, see [213].

[4] We denote here with a slash the vectors contracted with the Dirac matrix γ^μ_D, for ex. $\gamma^\mu_D A_\mu = A\!\!\!/$.

Since A^μ_{ext} is a classical external background field, there is no kinetic term $\frac{1}{4}F^{\mu\nu}_{ext}F_{ext\,\mu\nu}$ as for any dynamical field.

From the Lagrangian (6.13) we can write the modified Dirac equation for a fermion ψ in an external field A^μ_{ext}:

$$(i\partial\!\!\!/ - eA\!\!\!/_{ext} - m)\psi = 0\,. \tag{6.14}$$

The solution of this equation for an electromagnetic plane wave $A^\mu(k\cdot x)$ has been found by Volkov in the 1930s [225]:

$$\Psi^V_p(k\cdot x) = \frac{1}{\sqrt{(2\pi)^3 2\epsilon_p}}\, E_p(k\cdot x)\; u(p)\,, \tag{6.15}$$

with

$$E_p(k\cdot x) \equiv \left(1 - \frac{eA\!\!\!/_{ext}k\!\!\!/}{2(k\cdot p)}\right)\exp\left[-ip\cdot x - i\int_0^{(k\cdot x)}\left[\frac{e(A_{ext}(\phi)\cdot p)}{(k\cdot p)} - \frac{e^2 A_{ext}(\phi)^2}{2(k\cdot p)}\right]d\phi\right]\,, \tag{6.16}$$

where k is the momentum of the external field, p and ϵ_p the canonical momentum and energy of the fermion; $u(p)$ is the usual Dirac spinor solution. Solution (6.15) entirely accounts for the effects of the external electromagnetic field on the fermion. The Ψ^V solutions constitute an orthogonal and complete system [227], see also [228].

Analogously to spin-$\frac{1}{2}$ fermionic solutions Ψ^V, one can write FP solutions of equations of motion for charged scalars and charged vector bosons in an external field, see [229]. These solutions are to be used in perturbation theory to write new Feynman rules, listed in appendix D, and draw Feynman diagrams describing electromagnetic and weak processes in an external field.

Using these new Furry-Feynman rules, one can write down every Feynman amplitude that is needed, at each order in perturbation expansion. Typically, doing these probability calculations within the FP, one has to handle integrals over Airy or Bessel functions coming from the E_p factors. These integrals can be simplified using properties of the integral-representation of the special functions, even though they reveal to be involved already at the first order, depending on the structure of A^μ_{ext}.

One of the first processes calculated in this frame was pair production by a photon $\gamma \to e^+e^-$ in an external field by Reiss [230]. The method was further developed by Nikishov, Ritus, and others, who studied pair production and its crossed process, *i.e.* Compton scattering in an intense field $e^- \to e^- + \gamma$, as well as other processes [231–235]. Several external field configurations were considered, as a circularly or linearly polarised plane wave or a constant crossed field.

These studies revealed to have a fruitful application to laser physics, see [203, 236]. For example, interesting developments took place in the context of processes in pulsed laser fields, see the thesis [237] and references therein, or at the E144 experiment [238], see section 6.4. In laser physics there is a natural interpretation of the FP fermion line considering a bare fermion "dressed" by an arbitrary number of photons emitted or absorbed from the laser, *cf.* fig. 6.4 and appendix D.

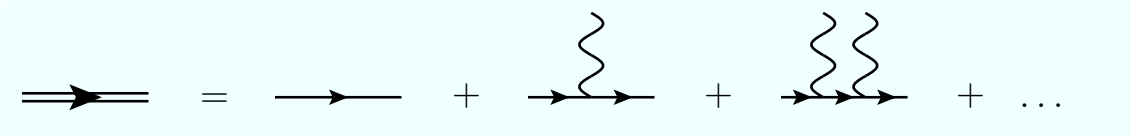

Figure 6.4: Interpretation of the electron propagator derived from the Volkov solution.

Regarding the LC background processes, the FP results obtained by Nikishov and Ritus for Compton scattering and photon annihilation into a pair, can respectively be applied to beamstrahlung and coherent pair production. These processes can be seen as FP processes at the first-order in perturbation theory, see fig. 6.5, and are related by crossing symmetry. Their probabilities can equivalently be calculated by the means of the optical theorem by

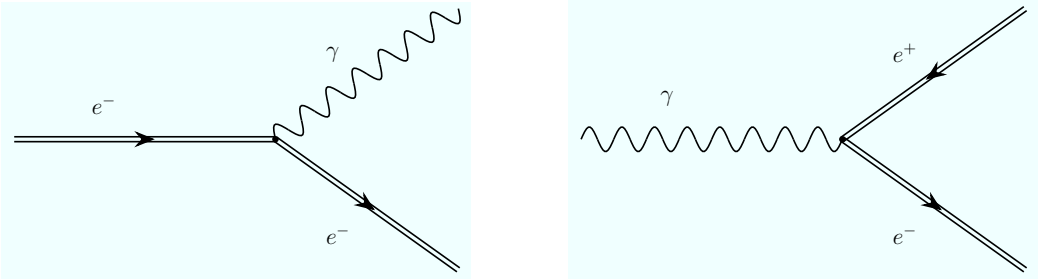

(a) Beamstrahlung. (b) Coherent pair production.

Figure 6.5: Beamstrahlung and coherent pair production as first-order FP processes.

using the Furry-Feynman fermion propagator in the 1-loop electron mass operator or in the photon polarisation operator, respectively, see fig. 6.6. This latter technique has been applied in a series of electroweak processes in [214].

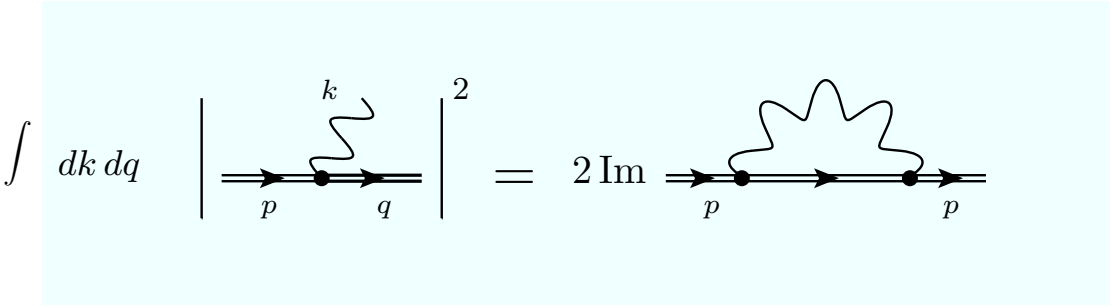

Figure 6.6: Relation between nonlinear Compton scattering probability and the electron mass operator in an intense field, through the optical theorem.

These FP results for beamstrahlung and coherent pair production coincide also with those obtained with the Baĭer-Katkov quasi-classical operator method (QOM) [239–241], even

though this latter method adopts a kinematical approximation. The QOM has been extensively implemented in beam-beam simulation programs and used to evaluate beamstrahlung and coherent pair production at LEP and SLC.

In recent times, efforts have been made to take into account the effect of the fields of both colliding bunches on the propagating particle at the IP of a LC. In order to do this, a Volkov solution for a fermion propagating in *two collinear* constant crossed fields has been proposed [242].

6.4 Testing nonlinear QED at the LC: a proposal

A linear collider offers another opportunity to test strong field QED, in addition to the beam-beam processes at the IP. In particular, vacuum instability and nonlinear effects in QED processes, *i.e.* coming from the absorption of n photons from the external field, can be studied by colliding high energy electron and/or photon beams with an intense laser [238]. This idea was implemented by the previously mentioned SLAC experiment E144 in Stanford [46, 243]. This experiment tested nonlinear QED by impinging a Terawatt laser on the 46.6 GeV electrons of the SLAC Final Focus Test Beam. Processes with multiple laser photon absorption were observed. Nonlinear Compton scattering (NLCS) $e^- + n\omega \to e^- + \gamma$ [244], and multi-photon Breit-Wheeler pair production (BWPP) $\gamma + n\omega \to e^+e^-$ [245],[5] depicted in figure 6.7, were measured to be in agreement with the theoretical predictions [231, 233, 234].

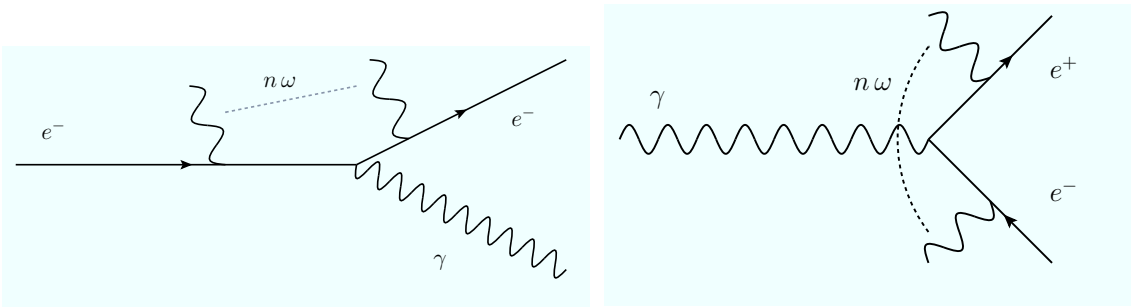

(a) Nonlinear Compton scattering. (b) Breit-Wheeler pair production.

Figure 6.7: Nonlinear processes studied at SLAC-E144.

The key parameters to study nonlinearity effects in electron-laser, photon-laser collisions and vacuum polarisation are just the above defined η and Υ, *cf.* eq. (6.6). These parameters, referring to an experimental set-up similar to SLAC-E144, can be written in natural units $c = \hbar = 1$ as [46, 243],

$$\eta = e\frac{E_{\rm rms}}{\omega\, m_e}\,, \qquad \Upsilon_e = \frac{E^*_{\rm rms}}{E_{\rm cr}}\,, \qquad \Upsilon_\gamma = \frac{2\epsilon_\gamma}{m_e}\frac{E_{\rm rms}}{E_{\rm cr}}\,. \tag{6.17}$$

[5] With ω we denote here the laser photons, with frequency ω.

Υ_e, Υ_γ are respectively the Υ parameters for an electron and for a photon impinging on a laser, $E_{\rm rms}$ is the root-mean-square of the electric field of the laser, ω is its frequency, $E^*_{\rm rms}$ is the root-mean-square of the electric field in the electron rest frame and ϵ_γ is the energy of the incident photon.

As we shall see, η is the control parameter for the absorption of photons from the incident particle. The intensity of the laser is related to $E_{\rm rms}$ by

$$E_{\rm rms} = \sqrt{377[\Omega]\, I[\mathrm{W/cm^2}]}\,, \tag{6.18}$$

therefore η can be regulated by varying the intensity I of the laser through [238]:

$$\eta^2 = 3.7 \cdot 10^{-19}\, I\, \lambda^2\,. \tag{6.19}$$

I is written in $\mathrm{W/cm^2}$ and λ, the wavelength of the laser, in µm. The intensity in turn can be expressed in terms of the energy of the laser beam U, the laser focus area A and the pulse length τ:

$$I = \frac{U}{A\,\tau}\quad . \tag{6.20}$$

On the basis of the success of the SLAC-E144 experiment, we propose to pursue at the future linear collider an extension of this experiment [4]. This can be done by creating in the extraction line of the LC an interaction point between an intense laser and the particle beam. With η, Υ parameters exceeding those at SLAC-E144 by up to one order of magnitude it would be possible to carefully explore nonlinear processes. The reason for this relies on the fact that we could exploit the higher energy of the electron and positron beams at the future linear collider as well as more intense, commercially available, lasers.

	E144 green (measured)	**E144 IR** (measured)	**ILC (E144 las.)**	**ILC ($\mathbf{PL_{9000}}$)**
λ (nm)	527	1053	1053	1064
$\mathcal{E}_{\rm laser}$ (J)	0.016 - 0.5	0.016 - 0.8	0.8	3
Focus	30 μm^2	60 μm^2	60 μm^2	40 μm^2
pulse (ps)	1.5 - 2.5	1.5 - 2.5	1.5	0.5
$I_{\rm peak}$ (W/cm^2)	$\approx 5 \cdot 10^{17}$	$\approx 5 \cdot 10^{17}$	$\sim 9 \cdot 10^{17}$	$\sim 1.5 \cdot 10^{19}$
E_{e^-} (GeV)	46.6	46.6	125 - 500	125 - 500
η	0.32	0.40	~ 0.6	~ 2.5
$\boldsymbol{\Upsilon_e}$	0.27	0.17	~ 0.7 - 2.7	~ 2.7 - 10.9
$\boldsymbol{\Upsilon_\gamma}$	0.16	0.08	~ 0.4 - 2.3	~ 0.6 - 6.0

Table 6.4: Parameter set and peak measured nonlinearity parameters at SLAC-E144 in comparison with proposed tests and estimated peak values at the ILC, keeping the same angle $\alpha = 17°$. For Υ_γ we consider the absorption of one laser photon.

In table 6.4 we compare the values of the key parameters measured at SLAC-E144 with estimates for the ILC we obtained using relations (6.17)-(6.20). At the ILC we expect the field

strength to exceed $F_{\rm cr}$ in the rest frame of the scattering electron, using an IR laser similar to that used at SLAC-E144. Furthermore, as above mentioned, the strong field physics that can be studied at this experiment can be further extended using a more intense currently available laser (for example we use the specifications in [246]). A more modern laser optics for chirped pulse amplification (CPA) and focussing are nowadays also available. We can see then

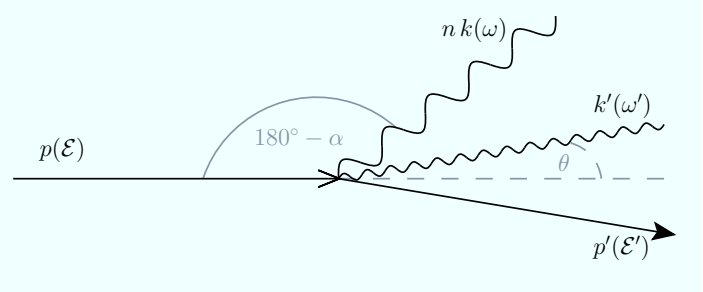

Figure 6.8: Nonlinear Compton scattering dynamics: the momenta (energies) are respectively denoted as $p(\mathcal{E})$ for the beam electron, $k(\omega)$ for the n laser photons, $p'(\mathcal{E}')$ for the scattered electron, and $k'(\omega')$ for the scattered photon.

that in principle an η parameter of one order of magnitude larger than at SLAC-E144 may be achieved. This affects the rates of the Compton scattering and Breit-Wheeler pair production.

With reference to the dynamics in fig. 6.8, the differential rate per unit volume and time for Compton scattering of an unpolarised beam electron of energy $\mathcal{E}$ by n circularly polarized laser photons is given, using the notation in [46], by:[6]

$$\frac{dN_n(\omega')}{d\omega'} = \frac{\pi\, e^4\, \rho_e \rho_\omega}{m_e^2\, \mathcal{E}^2\, \omega} \left[-\frac{4}{\eta^2} J_n^2(z) + \left(2 + \frac{u^2}{1+u}\right) \left[J_{n-1}^2(z) + J_{n+1}^2(z) - 2J_n^2(z)\right] \right] . \tag{6.21}$$

$J_n(z)$ are first-type Bessel functions, ρ_e and ρ_ω are the number density of beam electrons and of laser photons respectively. Then, we define

$$u = \frac{(k\cdot k')}{(k\cdot p')} \simeq \frac{\omega'}{\mathcal{E}'}\,, \qquad z = \frac{2\eta}{u_1}\sqrt{\frac{u(u_n - u)}{1+\eta^2}}\,, \tag{6.22}$$

and

$$u_n = n\, u_1\,, \qquad u_1 = \frac{2(k\cdot p)}{m_e^2(1+\eta^2)} \simeq \frac{2\omega\,\mathcal{E}(1+\beta\cos\alpha)}{m_e^2(1+\eta^2)}\,. \tag{6.23}$$

We can see then that higher η values would allow us to explore higher harmonics in the number n of absorbed laser-photons during NLCS. Their relative importance in the rate, indeed, increase with increasing η. In fig. 6.9(a) we show a typical spectrum of Nonlinear Compton scattering rate that could be observed at the ILC, as a function of the scattered photon

[6] As in [46], we take the number of interactions in a volume dV, time interval dt and energy bin $d\omega$ to be $N = \frac{dN_n}{d\omega} \cdot dV \cdot cdt \cdot d\omega \frac{1}{\hbar c}$.

energy. Electrons scattered with $n > 1$ can be distinguished from the standard Compton scattering by looking to the new kinematic edges in correspondence of increasing n. In fig. 6.9(b) we may see how the relative importance of harmonics varies with increasing η. At SLAC-E144 it has been shown the occurrence of nonlinear Compton scattering, with an acceptable fit with the numerical simulations for up to $n = 3$ absorbed laser photons [46, 247]. The main background process for nonlinear Compton scattering is *multiple* Compton scattering, $e^- + n\omega \to e^- + m\omega$ *prime* which, having an energetically distinct spectrum could be clearly distinguished.

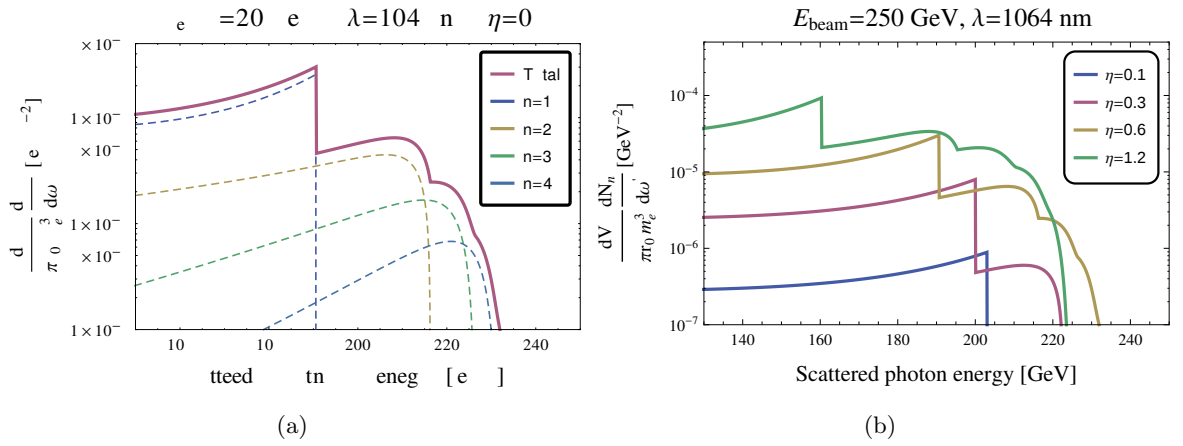

(a) (b)

Figure 6.9: Nonlinear Compton scattering rate for one incident electron on a circularly polarised laser, in units of $\pi r_0 m_e^3$ times GeV^{-2}. The energy of the beam electron is $\mathcal{E} = 250$ GeV, we take $\rho_\omega = \eta^2 \omega \frac{m_e}{r_0}$ as photon density of the laser with $\lambda = 1064$ nm. (a) With $\eta = 0.6$, the contributions from the harmonics $n = 1, \ldots, 4$ and the total sum of the first five are displayed; (b) The sum of the first five harmonics for different values of η.

In fig. 6.9(b) one can also note the energy shift in the Compton edge, that is due to the presence in u_1, *cf.* equation (6.23), of

$$\overline{m}_e^2 = m_e^2 \sqrt{1+\eta^2}\,, \tag{6.24}$$

instead of m_e^2. This fact depends on the oscillations of the colliding electron with the frequency of laser. Since the amplitude of the oscillation is always smaller than the wavelength of the external wave [238], the oscillatory motion cannot be resolved by the light scattered by the quivering electron. Therefore, the electron quiver motion appears as an angular and intensity dependent "quasi-momentum" q, with a corresponding shift in its mass [248, 249],

$$q_\mu = p_\mu + \frac{\eta^2 m_e^2}{2k\cdot p} k_\mu\,, \qquad q^2 = \overline{m}_e^2\,. \tag{6.25}$$

Therefore the electron recoils during scattering for larger η, then the minimum energy of the scattered electron is higher and the kinematic edge accordingly shifts: the maximal energy for

the Compton photon is smaller, as observed in figure 6.9(b). The mass-shift of electrons in SLAC-E144 laser could not be experimentally resolved. Nevertheless, positive hints towards mass shift were given by an experiment at Rochester. This experiment involved the ionization of Neon gas under the impact of an ultra intense laser [250]. It is believed that nowadays current technology may detect this effect [251].

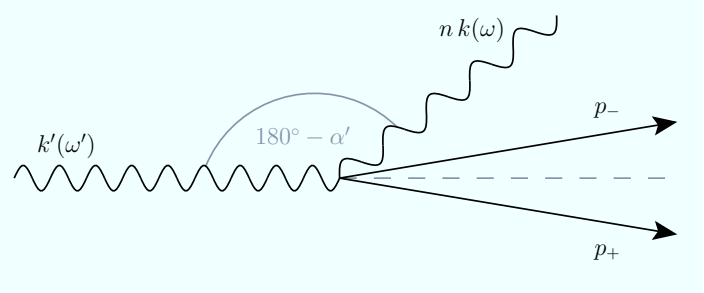

Figure 6.10: Breit-Wheeler pair production dynamics: the momenta (energies) are respectively denoted as $k'(\omega')$ for the high energy photon, $k(\omega)$ for the n laser photons, $p_\pm(\mathcal{E}_\pm)$ for the positron/electron of the pair.

For multi-photon Breit-Wheeler pair production (BWPP), the other key parameter is Υ_γ, *cf.* eq. (6.17), corresponding to the ratio of the field strength in the rest frame of the pair over $F_{\rm cr}$. The higher is the energy of the electron beams, the higher the energy of the scattered photons and the value of Υ_γ can be, enhancing BWPP. Referring to the dynamics in fig. 6.10, the BWPP differential rate per unit volume and time for an unpolarised photon beam colliding with a circularly polarized laser can be written as [46],

$$\frac{dN_{n_p}(\mathcal{E}_\pm)}{d\mathcal{E}_\pm} = \frac{2\pi\, e^4\, \rho_\omega \rho_{\omega'}}{\omega \omega'^2} \left[\frac{2}{\eta^2} J^2_{n_p}(\zeta) + (2w-1)[J^2_{n_p-1}(\zeta) + J^2_{n_p+1}(\zeta) - 2J^2_{n_p}(\zeta)] \right] , \tag{6.26}$$

for the absorption of n_p laser photons. We have

$$w = \frac{(k\cdot k')^2}{4(k\cdot p_-)(k\cdot p_+)} \simeq \frac{\omega'^2}{4\mathcal{E}_\pm(\omega' - \mathcal{E}_\pm)} , \qquad \zeta = \frac{2\eta^2}{\Upsilon_\gamma} \sqrt{w(w_{n_p} - w)(1+\eta^2)} , \tag{6.27}$$

and

$$w_{n_p} = n_p\, w_1 , \qquad w_1 = \frac{(k\cdot k')}{2m^2(1+\eta^2)} . \tag{6.28}$$

In fig. 6.11 we display the BWPP rate of an unpolarised high energy photon impinging a circularly-polarised, as a function of the energy of the positron of the pair. The laser wavelength is $\lambda = 1064$-nm laser and $\eta = 0.6$. We take the energy of the incident photon to be $E_{\omega'} = 190.6$ GeV. This energy is equivalent to the maximal energy for a incident photon that has been produced from $n = 1$ Compton scattering of an 250-GeV electron. The maximal energy occurs when the photon is collinear with the electron ($\theta = 0$). In figure 6.11 we also show the contributions of the first four harmonics in the number of laser photons absorbed

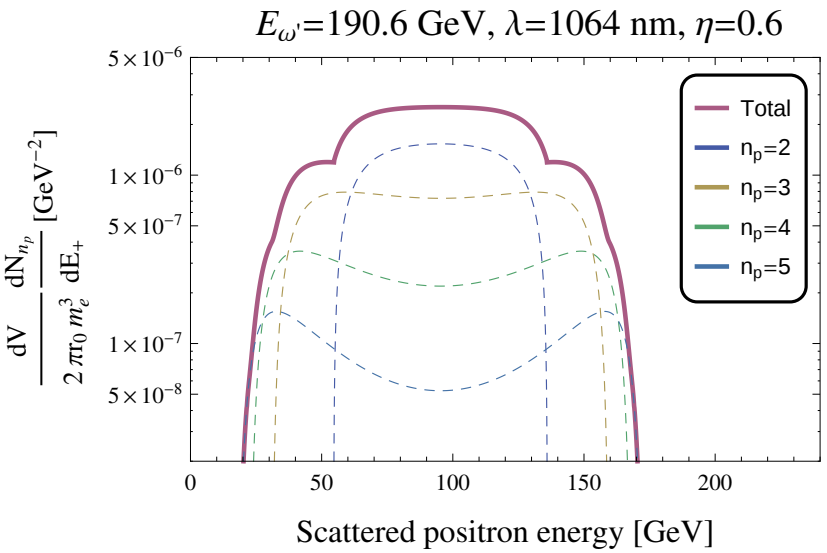

Figure 6.11: Breit-Wheeler pair production rate for an incident unpolarised photon with energy $E_{\omega'} = 190.6$ GeV on a circularly polarised laser, in units of $2\pi r_0 m_e^3$ times GeV^{-2}. The energy of the beam electron is $\mathcal{E} = 250$ GeV, we take $\rho_\omega = \eta^2\omega\frac{m_e}{r_0}$ as photon density of the laser with $\lambda = 1064$ nm with $\eta = 0.6$, the contributions from the harmonics $n_p = 2, \ldots, 5$ and their total sum are displayed.

by the incident photon. These harmonics corresponds to $n_p = 2, \ldots, 5$, in fact, due to energy conservation, the minimal number of photons absorbed to trigger the process is given by:

$$n_{p,0} = \frac{2m^2(1+\eta^2)}{\omega\omega'(1+\beta\cos\alpha)}\,. \tag{6.29}$$

If one considers also incident photons produced from $n > 1$ Compton scattering, which are more energetic is higher, therefore $n_{p,0}$ may lower considering their contribution too.

From observed spectra and yields of the scattered positrons observed at SLAC-E144, it has been unambiguously shown that BWPP occurred, implying that at least four laser photons contributed to the production of e^+e^--pairs [46, 252]. There, a series of backgrounds were considered, in particular the trident process $e^- + n\omega \to e^- + e^+e^-$, which proved to be responsible for $< 1\%$ of detected positrons. Furthermore, positron backgrounds from bremsstrahlung and Bethe-Heitler pair production were taken into account.

6.4.1 Possibility at the future LC

At the future linear collider we could in principle reproduce set-ups for the study of nonlinear Compton scattering and for Breit-Wheeler pair production that are very similar to the ones utilised at SLAC-E144.

The set-up for studying nonlinear Compton scattering at SLAC-E144 is depicted in fig. 6.12. The 46.6 GeV e^- Final Test beam was collided with an incident laser beam at an angle $\alpha = 17°$. The laser was operated at different frequencies (λ_{green}=527 nm, λ_{IR}=1053 nm) and energies (between 10 and 800 mJ). The laser polarisation at the interaction point IP1

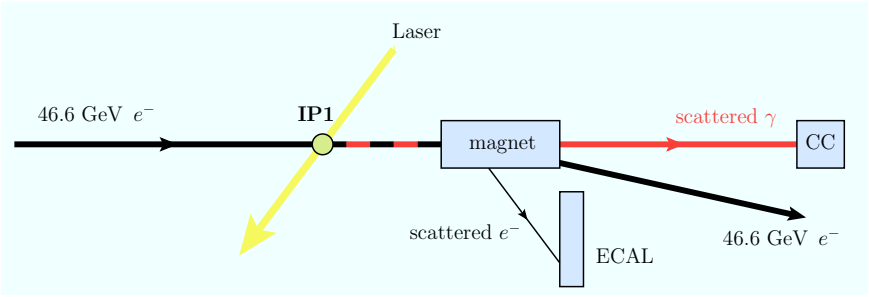

Figure 6.12: Nonlinear Compton scattering set-up at SLAC-E144, repeatable at the ILC.

was also changed, either being circular or linear. The high energy Compton photons were back scattered along the direction of the incoming beam. They were detected by a Čerenkov counter (CC), after the residual 46.6 GeV beam electrons were steered by a magnet into a dump. An electron calorimeter (ECAL) detected the scattered Compton electrons.

A second set-up, see fig. 6.13, was necessary to study Breit-Wheeler pair production. A

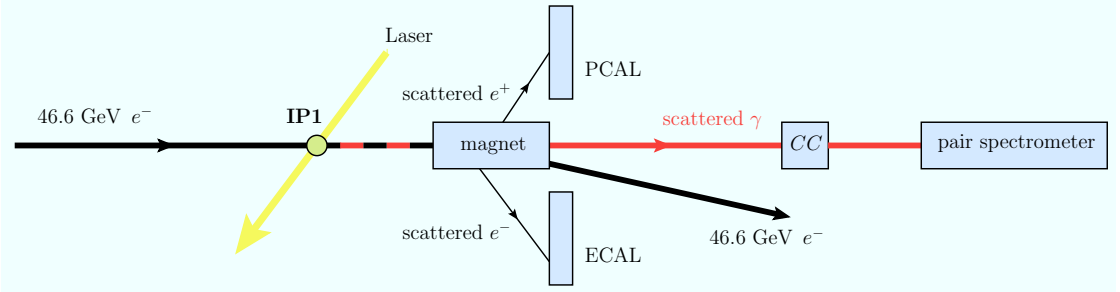

Figure 6.13: Breit-Wheeler pair production set-up at SLAC-E144, repeatable at the ILC.

dump magnet steered the residual 46.6 GeV electrons away from the beam line, while the scattered electrons and positrons were sent respectively to an electron (ECAL) and a positron (PCAL) calorimeter. The scattered photons were detected by a Čerenkov counter (CC) or by a pair spectrometer after being converted into electron-positron pairs.

More concretely, we should consider whether there is the technical possibility to locate the experiments we propose at a future LC. Several options can be considered for their realisation considering the design of the ILC [44, 45], for example:

- One possibility is to locate the experiment in the polarimetry chicane of the extraction line, either making use of the polarimeter laser or a dedicated high intensity laser.
- Another option is to use a high intensity laser in an upstream location, for example in the storage rings, and running it parasitically to the ILC operation.
- Finally, in case there would not be the possibility to perform the experiments at the same time as the main LC program, it would still be viable to work on the LC test-beam, as it was done at SLAC-E144.

We have argued that operating this type of experiment in the extraction line of the future linear collider is particularly appealing, because it is possible to explore higher harmonics of nonlinearity and in more critical conditions. We also find very interesting the possibility to perform such an experiment on the positron beam. The availability of positron bunches such the ones at the ILC would allow, to our knowledge, the first experiment of this type performed on positrons. This would result in a substantial improvement and innovation after the successful results of SLAC-E144. In fact, observing nonlinear effects in processes with a positron in the initial state would be an important test of theoretical predictions in intense fields and nonlinear QED.

It comes by itself that a future specific experimental proposal will have to fully consider the physics of the backgrounds and undergo careful technical feasibility analysis. A series of simulations will be required for example to estimate electromagnetic cascades [253] or radiation interactions, see for example [254]. Recent theory developments have been made on the background processes considered at SLAC-E144, like multiple Compton scattering [255], and the trident process [256–258]. We believe that their effect could be lowered thanks to higher statistics, due to potentially longer running times.

6.5 Summary and conclusions

The wide physics program of the future linear collider requires very high accuracy in the measurements, especially for electroweak precision tests, Higgs physics and BSM studies. In order to do so, a very high luminosity is to be pursued via very dense electron and positron bunches colliding at the interaction point (IP). Correspondingly, intense external electromagnetic fields generated by the bunches may approach, in the rest frame of colliding particles, the Sauter-Schwinger critical field strength $F_{\mathrm{cr}} = 1.32 \cdot 10^{18}$ V/m. F_{cr} corresponds to the field strength at which real electron-positron pairs are spontaneously created in the vacuum, which becomes unstable. We have evaluated the external fields seen by the colliding particles at the IP of several linear collider configurations. These fields, which can be described by constant crossed fields, at the ILC stage with $\sqrt{s} = 1$ TeV could reach an average field strength of order $\mathcal{O}(0.1) \cdot F_{\mathrm{cr}}$, which means respectively 2 and 3 orders of magnitude higher than at SLC and LEP II. These fields are even more intense at CLIC-3 TeV, where they could surpass F_{cr}. Field strengths close to F_{cr} are not only responsible for triggering or enhancing the most important background processes, *i.e.* beamstrahlung, coherent pair production, and incoherent pair processes. They are expected, indeed, to affect all the physics processes that are of interest for the LC physics program. For this reason, at a machine operating at several TeVs, like CLIC-3 TeV, it is required to fully consider these effects. This can be done by the Furry picture of quantum states, which accounts for the external fields *exactly*. The Furry picture, indeed, applies to perturbation theory the Volkov solution of the equation of motion describing a charged particle in an external field. This approach is also being tested

in various contexts like laser physics. At the SLAC experiment 144, for example, a 46.6-GeV electron beam was impinged on an intense laser. Nonlinear processes, *i.e.* occurring through the absorption of laser photons, were studied. We have studied how to repeat and extend this latter experiment at the future linear collider, exploiting the higher energy electron and positron beams, together with the improved available laser systems and techniques. These could allow to reach more extreme conditions, with values of the parameters regulating these effects that are 1 order of magnitude higher than at SLAC-E144. It would be possible then to study nonlinear effects in nonlinear Compton scattering and Breit-Wheeler pair production, in correspondence of higher harmonics of laser photon absorption. A particularly appealing feature is the possibility to perform such tests for the first time also on positrons, which would be a very important test for the validity of the theory.

Chapter 7

Conclusions

In this thesis two classes of non-minimal supersymmetric models have been discussed in the context of their phenomenology at linear colliders, as well as the processes in the strong electromagnetic fields that occur in these machines. In the following, the conclusions of these topics are given separately, before a common summary closes this study.

NMSSM

The first type of non-minimal supersymmetric model that has been discussed in this thesis is the NMSSM, which features an additional gauge singlet supermultiplet with respect to the MSSM. This leads the NMSSM to have in supplement a $\mathcal{CP}$-even Higgs state, a $\mathcal{CP}$-odd Higgs state, and a neutralino. The motivations for this model are its elegant solution to the μ-problem, as well as the additional contribution to the tree-level Higgs mass, that is due to the mixing of Higgs doublets with the singlet state.

We have seen that several classes of NMSSM scenarios, despite the additional Higgs and neutralino states, may feature a low energy spectrum and phenomenology that are remarkably similar to MSSM scenarios. For example, an NMSSM scenario could be experimentally almost indistinguishable from an MSSM in case it has, apart from a SM-like Higgs, a $\mathcal{CP}$-even and a $\mathcal{CP}$-odd Higgs that are mostly singlets, difficult to be clearly seen at the LHC and kinematically not accessible at the ILC. The low energy neutralino sectors of the two scenarios, as well, may present very close masses and production cross sections in such cases.

Therefore it is of primary importance to develop methods to distinguish between the two models in a general. In this thesis we have outlined a model distinction strategy that exploits the mass and polarised cross section measurements of neutralinos and charginos lightest states at a linear collider. We have seen that, from these measurements, a reconstruction of the neutralino and chargino sector parameters M_1, M_2, μ, and $\tan\beta$, assuming the MSSM as underlying model, is possible applying a χ^2-fit as criterion. In case such a fit clearly excludes the MSSM hypothesis this would be a strong indication towards an extended model, with the NMSSM as foremost candidate. The confirmation of this latter hypothesis can be given going for higher energies and looking for heavier neutralino resonances and integrating the analysis

with further information from the Higgs sector, looking for singlet states. In our analysis, we have applied the described distinction method to a series of NMSSM scenarios with low energy neutralino and chargino spectra particularly similar to MSSM scenarios, respectively. We have grouped the phenomenological possibilities in different classes of scenarios, selected by the admixtures of the lightest neutralino states.

Our results show that an NMSSM scenario with a high singlino admixture in the lightest neutralino states, here in particular in $\tilde{\chi}_2^0$, can quite straightforwardly be distinguished from the MSSM. Observing $\tilde{\chi}_3^0$ may confirm the NMSSM. We have also studied a scenario with light higgsinos along the (λ, κ)-plane, being λ and κ the key parameters regulating the singlino admixtures in neutralinos. We could see that a large part of the (λ, κ)-plane features an almost decoupled singlino state and the NMSSM is indistinguishable from the MSSM. However, this changes already in those areas, where the singlino component in $\tilde{\chi}_1^0$ achieves already a few percent, quickly excluding the MSSM. This has also been confirmed by the possibility of detecting the additional singlet-like pseudoscalar Higgs a_1 and measuring precisely the SM-like Higgs couplings. Eventually we have observed that, in general, in NMSSM scenarios with light gaugino states our distinction method is less effective and additional information from the Higgs sector is also needed.

Finally, our studies have shown that the neutralino and chargino sector can provide the crucial information for the model distinction between the MSSM and the NMSSM, that could be complementary added to the standard analyses of the Higgs sector.

Non decoupling D-terms

The second class of non-minimal supersymmetric models that have been discussed is given by extensions of the MSSM with additional non-decoupling D-terms. These extensions may appear, at the TeV scale, as the effective field theories of supersymmetric models with an enlarged gauge group with respect to $SU(3)_c \otimes SU(2)_L \otimes U(1)_Y$ in the MSSM. The extended gauge group breaks, due the vevs of some chiral superfields, to that of the MSSM. These chiral superfields, with soft masses above the scale of gauge symmetry breaking, may be integrated out, leaving the additional non-decoupling D-terms in the Higgs scalar potential.

These terms enhance the tree-level Higgs mass with respect to the MSSM. This is a very interesting feature, since in the MSSM the Higgs mass requires large radiative corrections to accommodate the observed value at 125.5 GeV. These corrections are mainly provided by stop loops and, in order to be large, they require heavy stops or large stop mixing, introducing a certain amount of tuning. Therefore, the enhanced tree-level Higgs mass in non-decoupling D-term extensions of the MSSM relaxes the naturalness in the stop sector, giving the main motivation for these models.

We have focussed on models whose gauge group has two copies of the factor $SU(2) \otimes U(1)$, that diagonally break to the electroweak group $SU(2)_L \otimes U(1)_Y$. In particular, two examples have been discussed: the "vector Higgs" case, with both Higgs doublets charged under the same copy of $SU(2) \otimes U(1)$, and the "chiral Higgs" case, with the Higgs doublets charged

under different copies.

Operatively, the decoupling limit $m_{A^0} \gg m_Z$ with moderately large $\tan\beta$ has been considered, so that we could identify the light $\mathcal{CP}$-even Higgs with SM-like Higgs observed at the LHC. We could see how in both the vector and the chiral Higgs cases the Higgs mass is raised for increasing values of the D-term parameter $\Delta = \xi^2 \cdot \Omega$. The parameter $\xi = g_a/g_b$ is the ratio of the gauge couplings couplings in the two $SU(2) \otimes U(1)$ copies. The parameter $\Omega = m_L^2/(m_V^2 + m_L^2)$, instead, parametrises the relative value of the soft scale of the fields breaking the gauge group (m_L) with respect to the symmetry breaking scale ($\propto m_V$). For values of $\Delta = \xi^2 \cdot \Omega$ in [0.2, 1], the MSSM Higgs mass is raised by several tens of GeV.

Given this, it is important to understand how these supersymmetric models can be distinguished from the SM and the MSSM. The SM-like Higgs couplings to fermions and gauge bosons have, like in the MSSM, an additional contribution with respect to the SM that is suppressed by the mass of the heavy $\mathcal{CP}$-even Higgs, m_H.

With respect to the MSSM, this contribution is enhanced in the vector case by a term proportional to Δ. We could estimate that, at the high-luminosity LHC, the deviations from the SM could be established even for $\Delta \in [0, 0.1]$, with sensitivity to m_H up to ~ 600 GeV. At the ILC operating at 500 GeV the sensitivity is much improved with sensitivity to m_H up to $\sim 800 - 900$ GeV, while high-luminosity stages of the ILC may explore the TeV range. In the context of this the vector Higgs model, a non observation of deviations allows to exclude m_H up to the scale of sensitivity. In the chiral case, instead, the sensitivity is reduced by a term proportional to Ω, such that deviations from the SM are detectable at the ILC operating at 500 GeV with m_H only up to 650 GeV for $\Omega \sim 1$.

In order to distinguish the model, and largely model-independent measurements of the Higgs couplings at a linear collider are required. Given the deviations of the Higgs coupling from the SM, a precise measurement of m_H, possibly exploiting both the ILC and the LHC, becomes fundamental to determine the underlying model in the context of non-decoupling D-terms extensions of the MSSM.

Processes in intense electromagnetic fields

It has been shown that the rôle of a linear collider –due to the possibility of using several energy stages and polarisation configurations, multiplying the number of the available observables– is crucial for studying the precise phenomenology of supersymmetric models. The Higgs sector, as well, can be very precisely studied thanks to a model-independent determination of the Higgs couplings.

In order to fulfil the high precision requirements, also the exact knowledge of the conditions under which the particles interact during beam-beam collisions should be taken into account. At the IP of a linear collider, an ultrarelativistic incident lepton sees in its rest frame an intense electromagnetic fields generated by the oncoming dense bunches. We have estimated that at the ILC at 1 TeV, these fields could be 2 and 3 orders more intense than at SLC and at LEP II. At the CLIC at 3 TeV, these fields could be even one order more intense, potentially

surpassing Sauter-Schwinger critical field strength $F_{\text{cr}} = 1.32 \cdot 10^{18}$ V/m, corresponding to a regime in which electron-positron pairs are spontaneously created in the vacuum, that is unstable.

Therefore, especially if to operate a linear collider like the CLIC at 3 TeV, the effects of these intense external fields at the IP should be included in theoretical calculations. Using the Furry picture of quantum states allows to account for the external fields effects exactly.

Finally, we have studied how to test the theory of processes in external fields and the related nonlinearity effects, via colliding an intense laser beam on the ILC beams. The high energetic beams of the ILC, indeed, offer an optimal opportunity to extend and improve the SLAC experiment 144 to more extreme conditions, increasing the nonlinearity of the generated processes. Last but not least, performing this kind of experiment on the positron beams would offer an unprecedented test for the theory.

Summary and outlook

In this thesis, supersymmetric models extending the MSSM in rather minimal ways have been discussed. It has been shown that they quite naturally solve the main MSSM shortcomings, such as the μ-problem and the naturalness of the stop sector in relation to the Higgs mass. Our results have proven that a linear collider will be an effective tool for the study of these models both looking at the supersymmetric and at the Higgs boson sectors. Precise understanding of the physics processes during beam-beam interaction is required to match the high precision requirements. We conclude that a linear collider like the planned ILC would be a unique machine for revealing the structure and the determination of the underlying model, and that its approval would represent an important leap for particle physics.

Appendix A

Superspace notation

Supersymmetry transformations extend the space-time transformations and mix with the Poincaré group. Therefore it is comfortable and elegant to adopt a notation according to which the supermultiplets are single objects, called *superfields*, that transform in the *superspace*. Superspace is a manifold whose coordinates are given by the usual space-time coordinates x^μ, that are bosonic, and by the fermionic coordinates θ^α and $\overline{\theta}^\dagger_{\dot{\alpha}}$, that are complex anticommuting two-component spinors with indices α, $\dot{\alpha} = 1, 2$. We briefly introduce here the superspace notation, referring to the standard books [50, 51] for more details.
A Chiral superfield $\hat{\Phi}$ corresponds to a chiral supermultiplet. $\hat{\Phi}$ and its conjugate $\hat{\Phi}^*$ are defined by the conditions

$$\mathcal{D}^\dagger_{\dot{\alpha}}\hat{\Phi} = 0\,, \qquad \mathcal{D}_\alpha\hat{\Phi}^* = 0, \tag{A.1}$$

where $\mathcal{D}^\dagger_{\dot{\alpha}} = -\frac{\partial}{\partial\theta^{\dagger\dot{\alpha}}} + i(\theta\sigma^\mu)_{\dot{\alpha}}\partial_\mu$ and $\mathcal{D}_\alpha = \frac{\partial}{\partial\theta^{\dagger\alpha}} - i(\theta\sigma^\mu)_\alpha\partial_\mu$ are chiral covariant derivatives, anticommuting with the supersymmetry generators Q_α and $Q^\dagger_{\dot{\alpha}}$.

The superfields $\hat{\Phi}$ and $\hat{\Phi}^*$ can then be expanded, in terms of their bosonic and fermionic components $\phi(x)$, $\psi(x)$ and F (and conjugates) as [48],

$$\hat{\Phi} = \phi(x) + i\theta^\dagger\overline{\sigma}^\mu\theta\partial_\mu\phi(x) + \frac{1}{4}\theta\theta\theta^\dagger\theta^\dagger\partial_\mu\partial^\mu\phi(x) + \sqrt{2}\theta\psi(x) \tag{A.2}$$

$$- \frac{i}{\sqrt{2}}\theta\theta\theta^\dagger\overline{\sigma}^\mu\partial_\mu\psi(x) + \theta\theta F(x)\,, \tag{A.3}$$

and

$$\hat{\Phi}^* = \phi^*(x) - i\theta^\dagger\overline{\sigma}^\mu\theta\partial_\mu\phi^*(x) + \frac{1}{4}\theta\theta\theta^\dagger\theta^\dagger\partial_\mu\partial^\mu\phi^*(x) + \sqrt{2}\theta^\dagger\psi^\dagger(x) \tag{A.4}$$

$$- \frac{i}{\sqrt{2}}\theta^\dagger\theta^\dagger\theta\sigma^\mu\partial_\mu\psi^\dagger(x) + \theta^\dagger\theta^\dagger F^*(x)\,. \tag{A.5}$$

A vector superfield $\hat{V}$, instead, has to fulfil the condition

$$\hat{V} = \hat{V}^\dagger\,. \tag{A.6}$$

In the Wess-Zumino gauge, $\hat{V}$ can be written in terms of its components A_μ, λ, D as

$$\hat{V} = \theta^\dagger\overline{\sigma}^\mu\theta A_\mu + \theta^\dagger\theta^\dagger\theta\lambda + \theta\theta\theta^\dagger\lambda^\dagger + \theta\theta\theta^\dagger\theta^\dagger D\,. \tag{A.7}$$

Products of superfields are superfields. The components of a superfield that are proportional to $\theta\theta$ and to $\theta\theta\theta^\dagger\theta^\dagger$, are called the F- and the D-components, respectively. The superspace notation allows, then, for a more compact way of writing a supersymmetric Lagrangian density. Let us consider a renormalisable supersymmetric model with i chiral superfields $\hat{\Phi}_i$ and the vector superfield $\hat{V}$ associated to the gauge group $\mathcal{G}$. The corresponding Lagrangian can be written as

$$\mathcal{L}_{\text{general SUSY}} = \frac{1}{16g^2k}\text{Tr}\left[W^\alpha W_\alpha + \overline{W}_{\dot{\alpha}}\overline{W}^{\dot{\alpha}}\right]_F + [\mathcal{K}]_D + \left[\mathcal{W}(\hat{\Phi}_i) + \text{ h.c.}\right]_F . \tag{A.8}$$

In the first term of equation (A.8), g and $k = C_2(\mathcal{G})$ are the gauge coupling and the quadratic Casimir of the gauge group $\mathcal{G}$. Furthermore, W^α and $\overline{W}_{\dot{\alpha}}$ are supersymmetric generalisations of the gauge field strength tensors:

$$W^\alpha = \frac{1}{4}\mathcal{D}^\dagger\mathcal{D}^\dagger\left(e^{-g\hat{V}}\mathcal{D}^\alpha e^{+g\hat{V}}\right) , \qquad \overline{W}_{\dot{\alpha}} = \frac{1}{4}\mathcal{D}\mathcal{D}\left(e^{+g\hat{V}}\mathcal{D}_{\dot{\alpha}}e^{-g\hat{V}}\right) , \tag{A.9}$$

where we denote $\mathcal{D}\mathcal{D} = \mathcal{D}^\beta\mathcal{D}_\beta$ and $\mathcal{D}^\dagger\mathcal{D}^\dagger = \mathcal{D}^{\dagger\,\beta}\mathcal{D}^\dagger_\beta$. The indices α, β are raised (lowered) by the epsilon matrix $\epsilon^{\alpha\beta}$ ($\epsilon_{\alpha\beta}$).

The second term of equation (A.8) is equivalent to the D-component of the so called Kähler potential $\mathcal{K}$, defined by:

$$\mathcal{K} = \hat{\Phi}_i^\dagger\left(e^{g\hat{V}}\right)_{ij}\hat{\Phi}_j , \tag{A.10}$$

which describes the gauge interactions of the chiral superfields. Finally, the last term of equation (A.8) is the F-component of the superpotential:

$$\mathcal{W}(\hat{\Phi}_i) = L^i\hat{\Phi}_i + \frac{1}{2}M^{ij}\hat{\Phi}_i\hat{\Phi}_j + \frac{1}{6}y^{ijk}\hat{\Phi}_i\hat{\Phi}_j\hat{\Phi}_k . \tag{A.11}$$

Appendix B

NMSSM: Higgs sector and conventions

B.1 $\mathbb{Z}_3$-NMSSM Higgs sector

The $\mathbb{Z}_3$-invariant NMSSM superpotential is given by the sum of the terms involving the gauge singlet superfield $\hat{S} = (S, \tilde{S})$,

$$\mathcal{W}_S = \lambda \hat{S} \hat{H}_u \cdot \hat{H}_d + \frac{\kappa}{3} \hat{S}^3 \,, \tag{B.1}$$

and of the Yukawa terms

$$\mathcal{W}_{\text{Yukawa}} = \hat{\bar{u}}\, \mathbf{y_u} \hat{Q} \cdot \hat{H}_u - \hat{\bar{d}} \mathbf{y_d} \hat{Q} \cdot \hat{H}_d - \hat{\bar{e}}\, \mathbf{y_e} \hat{\ell} \cdot \hat{H}_d \,. \tag{B.2}$$

The Higgs soft SUSY breaking lagrangian reads:

$$-\mathcal{L}_{\text{soft}} \supset \mathbf{A_u}\, Q \cdot H_u\, \bar{u} - \mathbf{A_d}\, Q \cdot \bar{d} - \mathbf{A_e}\, \ell \cdot H_d\, \bar{e} \tag{B.3}$$

$$+ \lambda A_\lambda H_u \cdot H_d S + \frac{\kappa}{3} A_\kappa S^3 + \text{h.c.} \tag{B.4}$$

From equations (B.1) and (B.4) one obtains the Higgs scalar potential [127],

$$\begin{aligned} \mathcal{V}_{H,\ \text{NMSSM}} = & \left|\lambda(H_u^+ H_d^- - H_u^0 H_d^0) + \kappa S\right|^2 \\ & + (m_{H_u}^2 + |\mu + \lambda S|^2)\left(|H_u^0|^2 + |H_u^+|^2\right) + (m_{H_d}^2 + |\mu + \lambda S|^2)\left(|H_d^0|^2 + |H_d^-|^2\right) \\ & + \frac{g_1^2 + g_2^2}{8}\left(|H_u^0|^2 + |H_u^+|^2 - |H_d^0|^2 - |H_d^-|^2\right) + \frac{g_2^2}{2}\left|H_u^+ H_d^{0\,*} + H_u^0 H_d^{-\,*}\right|^2 \\ & + m_S^2 |S|^2 + \left(\lambda A_\lambda (H_u^+ H_d^- - H_u^0 H_d^0) S + \frac{k}{3} A_\kappa S^3 + h.c.\right) . \end{aligned} \tag{B.5}$$

Conventionally, taking $v^2 = v_u^2 + v_d^2 = 246\ \text{GeV}^2$ we write

$$H_u^0 = \frac{v_u}{\sqrt{2}} + \frac{1}{\sqrt{2}}\left(\text{Re}H_u^0 + i\text{Im}H_u^0\right) \,, \quad H_d^0 = \frac{v_d}{\sqrt{2}} + \frac{1}{\sqrt{2}}\left(\text{Re}H_d^0 + i\text{Im}H_d^0\right) \,, \tag{B.6}$$

and

$$S = s + \frac{1}{\sqrt{2}}\left(\text{Re}S + i\text{Im}S\right) \,. \tag{B.7}$$

We define $\mu_{\text{eff}} = \lambda\, s$. The CP-even Higgs mass matrix $\mathcal{M}_h^2$ is symmetric with respect to the diagonal, and in the basis (ReH_u^0, ReH_d^0, ReS) its entries are given by [127],

$$\mathcal{M}^2_{h,\,11} = \frac{g_1^2+g_2^2}{4}v_d^2 + \mu_{\text{eff}}\frac{A_\lambda+\kappa s}{\cot\beta}, \tag{B.8}$$

$$\mathcal{M}^2_{h,\,12} = \left(\lambda^2 - \frac{g_1^2+g_2^2}{4}\right) v_u v_d - \mu_{\text{eff}}(A_\lambda+\kappa s), \tag{B.9}$$

$$\mathcal{M}^2_{h,\,13} = \frac{\lambda}{\sqrt{2}}(2\mu_{\text{eff}} v_d - (A_\lambda+2\kappa s)v_u), \tag{B.10}$$

$$\mathcal{M}^2_{h,\,22} = \frac{g_1^2+g_2^2}{4}v_u^2 + \mu_{\text{eff}}(A_\lambda+\kappa s)/\tan\beta, \tag{B.11}$$

$$\mathcal{M}^2_{h,\,23} = \frac{\lambda}{\sqrt{2}}(2\mu_{\text{eff}} v_u - (A_\lambda+2\kappa s)v_d), \tag{B.12}$$

$$\mathcal{M}^2_{h,\,33} = \lambda A_\lambda \frac{v_u v_d}{2s} + \kappa s\,. \tag{B.13}$$

The CP-odd Higgs mass matrix $\mathcal{M}_a^2$, is diagonally symmetric as well, and in the basis (A^0, ImS) reads

$$\mathcal{M}_a^2 = \begin{pmatrix} 2\mu_{\text{eff}}\,(A_\lambda+\kappa s)/\sin 2\beta & \frac{\lambda}{\sqrt{2}}(A_\lambda - 2\kappa s)v \\ & \lambda(A_\lambda+4\kappa s)\frac{v_u v_d}{2s} - 3\kappa A_\kappa s \end{pmatrix}, \tag{B.14}$$

defining $A^0 = \cos\beta\,\text{Im}H_u^0 + \sin\beta\,\text{Im}H_d^0$.
Finally, the NMSSM charged Higgs states $H^\pm$ have the mass:

$$m^2_{H^\pm} = \frac{2\mu_{\text{eff}}(A_\lambda+\kappa s)}{\sin 2\beta} + \frac{v^2}{2}\left(\frac{g_2^2}{2} - \lambda^2\right). \tag{B.15}$$

B.2 Standard Model constants

In the analysis in chapter 4 we use the following definitions:

$$m_t = 173.07\ \text{GeV}, \tag{B.16}$$

$$m_Z = 91.1876\ \text{GeV}, \qquad \Gamma_Z = 2.4952\ \text{GeV}, \tag{B.17}$$

$$m_W = 80.385\ \text{GeV}, \qquad \Gamma_W = 2.085\ \text{GeV}, \tag{B.18}$$

$$\sin^2\theta_W = 1 - m_W^2/m_Z^2, \qquad \alpha_{\text{em}} = 1/127.92, \tag{B.19}$$

$$\alpha_{\text{s}}(m_Z) = 0.1184\,. \tag{B.20}$$

Appendix C

Non-decoupling D-terms

C.1 Perturbative unification and the size of the D-terms

If gauge coupling unification is of interest in the formulation of non-decoupling D-terms extensions of the MSSM, then it may be used as a guide to constrain the size of D-terms [3].[1]

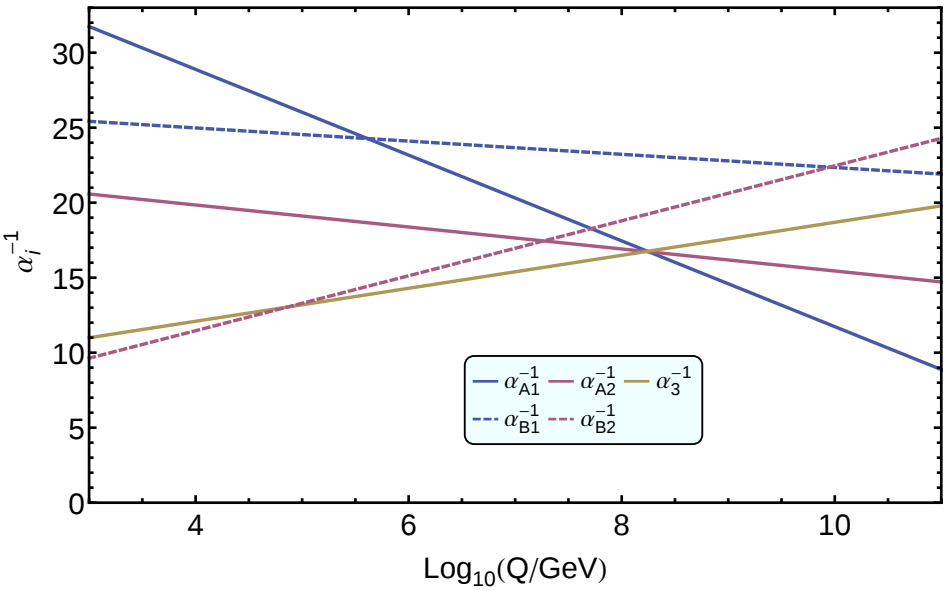

Figure C.1: Perturbative unification of the $G_A \otimes SU(3)_c$ and G_B sites separately, at scales $\sim 10^{8.2}$ and $\sim 10^{10}$ GeV respectively, allowing for the maximal value of the ratios $R_1 = 0.6$, $R_2 = 0.86$. $\tan\beta = 10$.

In the vector Higgs case, for example, one would require that the ratio of gauge couplings, $R_i = g_{Ai}^2/g_{Bi}^2$, to be as large as possible in order to maximise the effect of the D-terms, *cf.*

[1] In this appendix, we take g_1 to be $SU(5)$-GUT normalised. Therefore we switch notation, substituting $g_1 \to \sqrt{5/3}g_1$, such that we have $m_Z^2 = \frac{1}{4}(\frac{3}{5}g_1^2 + g_2^2)(v_u^2 + v_d^2)$.

eq. (5.35). However, one should remember the fact that having large gauge couplings at the electroweak scale, may affect perturbativity of the gauge couplings at higher energies. Even though in the examples we considered in chapter 5 there are not full GUT multiplets of matter, we can nevertheless explore the possibility of unification in these models. The presence of additional matter, indeed, changes the gauge couplings β-functions, and may cause the theory to unify at a scale that is much lower than 10^{15} GeV [97]. This also depends on how the matter is distributed between the gauge sites. For concreteness we refer to the model defined in table 5.1. The beta functions at one loop are then given by

$$\beta_{g_u} = \frac{d}{dt} g_u = \frac{b_u}{16\pi^2} g_u^3 \quad \text{with} \quad b_u = (2, \frac{39}{5}, -5, \frac{6}{5}, -3)\,. \tag{C.1}$$

Defining $\alpha_i = g_i^2/(4\pi\hbar c)$, the parameter space is restricted by the perturbativity requirement $\alpha_i(\Lambda_{GUT}) < 1$. Furthermore we assume $SU(3)_c \otimes SU(2)_A \otimes U(1)_A$ to separately unify on site A and $SU(2)_B \otimes U(1)_B$ on site B. This translates in the following gauge unification conditions:

$$\alpha_{g_{1A}}(\Lambda_{GUT\,A}) = \alpha_{g_{2A}}(\Lambda_{GUT\,A}) = \alpha_{g_3}(\Lambda_{GUT\,A})\,, \tag{C.2}$$

$$\alpha_{g_{1B}}(\Lambda_{GUT\,B}) = \alpha_{g_{2B}}(\Lambda_{GUT\,B})\,. \tag{C.3}$$

We plot in figure C.1 the RGE evolution of couplings, for the largest values of R_i allowing for perturbative unification, taking $\tan\beta = 10$. We find at the electroweak scale $R_1 \sim 0.6$ and $R_2 \sim 0.86$. Unification on site A occurs at the scale $\Lambda_{GUT\,A} \sim 10^{8.2}$ GeV, and on site B at $\Lambda_{GUT\,B} \sim 10^{10}$ GeV. Since we have that

$$\Delta = \left(\frac{g_A^2}{g_B^2}\right) \frac{m_L^2}{m_v^2 + m_L^2} \leq R\,, \tag{C.4}$$

we can conclude that maximal values the D-term parameters are $\Delta_1^{Max} = 0.6$ and $\Delta_2^{Max} = 0.86$, respectively.

C.2 Derivation of κ_b

In chapter 5, we are considering the decoupling regime $m_{A^0} \gg m_Z$ with moderately or large $\tan\beta$, and we may identify H_d with the heavy Higgs states. It is useful then to derive here κ_b following the guidelines sketched in [192]. We start from the Higgs Lagrangian from equation (5.90),

$$\mathcal{L} \supset -\mathcal{V}_{\text{2HDM}} - \left(\bar{u}\,\mathbf{y_u} Q \cdot H_u + \bar{d}\,\mathbf{y_d} Q \cdot H_d + \text{ h.c.}\right)\,, \tag{C.5}$$

where leptons and the wrong couplings have been neglected. Defining $h_2 = \text{Re}H_u^0$, we may write the effective Lagrangian from equation (5.91),

$$\begin{aligned} \mathcal{L}^{\text{eff}} \supset & -\frac{h_2}{2} D^2 h_2 + \frac{1}{2}\Theta h_2 \frac{1}{D^2 + \Pi^2}\Theta h_2 \\ & - m_2^2 \frac{h_2}{2} - \frac{\lambda_2}{8} h_2^4 \\ & - y_t t\bar{t} h_2 + \frac{y_d}{\sqrt{2}} \frac{\Theta}{D^2 + \Pi^2} b\bar{b} h_2\,, \end{aligned} \tag{C.6}$$

where $\Theta = m_{12}^2 + \frac{\lambda_7 h_2^2}{2}$ and $\Pi^2 = m_1^2 + \frac{(\lambda_3+\lambda_5)h_2^2}{2}$. As pointed out in [192], by a comparison with the basis used in the standard reference [196], we have $\Theta/\Pi^2 \sim 1/\tan\beta$.
Looking at the first line in equation (C.6), we canonically normalise the SM-like Higgs h through the relation

$$h_2 = \left(1 - \frac{1}{2}\left(\frac{\partial\langle\Theta h_2/\Pi^2\rangle}{\partial v_2}\right)^2\right) h = \left(1 - \frac{f'^2}{2}\right) h\,. \tag{C.7}$$

where we have done an expansion at the order $\mathcal{O}(\Theta^2/\Pi^4)$. We define the scale factor or ratio between the Higgs bottom couplings to the SM case as

$$\kappa_b = \frac{v g_{hb\bar{b}}}{m_b} = v\frac{(\frac{\partial\mathcal{V}_b}{\partial h})|_{h=v}}{\mathcal{V}_b|_{h=v}}\,, \tag{C.8}$$

where $\mathcal{V}_b$ is derived by the last term in equation (C.6), considering the Higgs bottom coupling,

$$\mathcal{V}_b = \frac{Y_b}{\sqrt{2}}\frac{1}{\Box + \Pi^2}\Theta h_2\,. \tag{C.9}$$

The D'Alambertian operator $\Box$ acting on the field h gives $\Box \to -m_h^2$. Therefore the numerator in equation (C.8) becomes

$$\frac{\partial\mathcal{V}_b}{\partial h} = \frac{Y_b}{\sqrt{2}}\frac{\left(\Theta'(1-\frac{f'^2}{2})h + \Theta\frac{\partial h_2}{\partial h}\right)\left(\Pi^2 - m_h^2\right) - \Theta(1-\frac{f'^2}{2})h\Pi^{2\prime}}{\left(\Pi^2 - m_h^2\right)^2}\,, \tag{C.10}$$

where

$$\Theta' \equiv \frac{\partial\Theta}{\partial h} = \lambda_7\left(1 - \frac{f'^2}{2}\right)^2 h\,, \tag{C.11}$$

$$\Pi^{2\prime} \equiv \frac{\partial\left(\Pi^2 - m_h^2\right)}{\partial h_2} = \lambda_{35}\left(1 - \frac{f'^2}{2}\right)^2 h\,. \tag{C.12}$$

When $\Box$ acts on the vacuum v, instead, we have $\Box \to 0$. Therefore for the denominator of equation (C.8) we have:

$$\mathcal{V}_b|_{h=v} = \frac{Y_b}{\sqrt{2}}\frac{\Theta(1-\frac{f'^2}{2})h}{\Pi^2}|_{h=v}\,, \tag{C.13}$$

Substituting in (C.8):

$$\kappa_b = v\cdot\frac{\left(\Theta'(1-\frac{f'^2}{2})h + \Theta\frac{\partial h_2}{\partial h}\right)\left(\Pi^2 - m_h^2\right) - \Theta(1-\frac{f'^2}{2})h\Pi^{2\prime}}{\left(\Pi^2 - m_h^2\right)^2}\cdot\frac{\Pi^2}{\Theta(1-\frac{f'^2}{2})h}|_{h=v} \tag{C.14}$$

$$= \left(1 - \frac{m_h^2}{\Pi^2}\right)^{-1}\cdot\frac{(\Theta' h + \Theta)\left(\Pi^2 - m_h^2\right) - \Theta h\Pi^{2\prime}}{\left(\Pi^2 - m_h^2\right)}\cdot\frac{v}{\Theta h}|_{h=v} \tag{C.15}$$

$$= \frac{1}{\left(1 - \frac{m_h^2}{\Pi^2}\right)}\cdot\left[1 + \frac{\lambda_7 h_2^2\left(\Pi^2 - m_h^2\right) - \Theta\lambda_{35}h_2^2}{\left(\Pi^2 - m_h^2\right)}\cdot\frac{v}{\Theta h}|_{h=v}\right]\,. \tag{C.16}$$

Finally we obtain,

$$\kappa_b = \frac{1}{1-\frac{m_h^2}{\Pi^2}}\left[1+\frac{(\lambda_7 v_2^2)}{\Theta}-\frac{\lambda_{35}v_2^2}{(\Pi^2-m_h^2)}+O(\Pi^{-4})\right]. \tag{C.17}$$

In the case considered in chapter 5, the MSSM with additional non-decoupling D-terms, we have $\lambda_7 = 0$. Moreover, Π can be substituted by m_H, in an approximation at order $(\Theta/\Pi^2)^2 \sim 1/\tan^2\beta$ that is valid for low Θ (*i.e.* B_μ in the MSSM and its D-terms extensions) [192]. We therefore write for general non-decoupling D-terms extensions of the MSSM as,

$$\kappa_b \simeq \left(1-\frac{m_h^2}{m_H^2}\right)^{-1}\left(1-\frac{[\lambda_3+\lambda_5]\,v^2}{m_H^2-m_h^2}\right)+\dots\,. \tag{C.18}$$

Appendix D

The QED Furry-Feynman rules

We write the QED Lagrangian for the Furry Picture (FP) as,

$$\mathcal{L} = \bar{\psi}(i\partial\!\!\!/ - eA\!\!\!/_{ext} - m)\psi - \frac{1}{4}FF - e\bar{\psi}A\!\!\!/\psi\,, \tag{D.1}$$

where the external field A^{μ}_{ext} is treated classicaly and has no dynamical terms. One can derive then the modified Dirac equation for a fermion ψ in an external field A^{μ}_{ext}:

$$(i\partial\!\!\!/ - eA\!\!\!/_{ext} - m)\psi = 0\,. \tag{D.2}$$

The corresponding Volkov solution for an external plane wave is given by [225]:

$$\Psi^{V}_{p}(k\cdot x) = \frac{1}{\sqrt{(2\pi)^3 2\epsilon_p}}\, E_p(k\cdot x)\; u(p)\,, \tag{D.3}$$

with

$$E_p(k\cdot x) \equiv \left(1 - \frac{eA\!\!\!/_{ext}k\!\!\!/}{2(k\cdot p)}\right)\exp\left[-ip\cdot x - i\int_0^{(k\cdot x)}\left[\frac{e(A_{ext}(\phi)\cdot p)}{(k\cdot p)} - \frac{e^2 A_{ext}(\phi)^2}{2(k\cdot p)}\right]d\phi\right]\,, \tag{D.4}$$

where k is the momentum of the external field, p and ϵ_p the canonical momentum and energy of the fermion; $u(p)$ is the usual Dirac spinor solution.

We list here the QED Furry-Feynman rules, that can straightforwardly be derived from solution (D.3), see also [213, 229].

- The fermion two-point function in the coordinate space is given by, see Fig. D.1(a):

$$G(x,x') = \frac{1}{(2\pi)^4}\int_{-\infty}^{+\infty} d^4p\; E_p(k\cdot x)\frac{p\!\!\!/ + m}{p^2 - m^2}\,\overline{E}_p(k\cdot x')e^{ip\cdot(x'-x)}, \tag{D.5}$$

  where the usual fermion propagator is sandwiched between E_p and $\overline{E}_p = E_p^{\dagger}\gamma_D^0$ factors coming from the Volkov solutions. Noteworthy, there is a non trivial dependence on the coordinates x, x' within which the fermion propagates, instead of their difference $x'-x$ as in the usual QED Green functions [208].

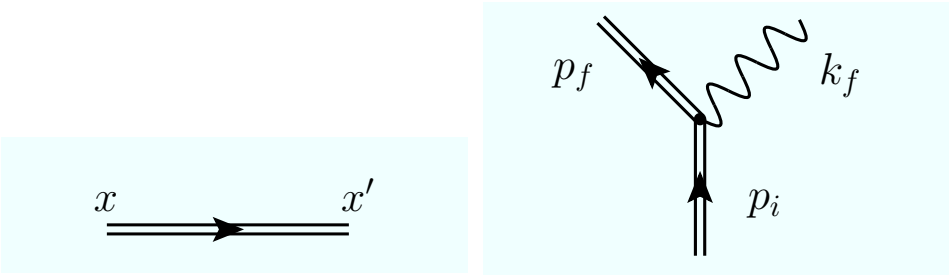

(a) (b)

Figure D.1: (a) The FP fermion propagator, where the double line represents the Volkov solution. (b) The FP vertex of QED.

- The QED vertex in fig. D.1(b) is given by:

$$-ie\,\gamma_e^\mu = -ie\,(2\pi)^4 \sum_{r=-\infty}^{+\infty} \overline{E}_{p_f}(r)\gamma_D^\mu E_{p_i}(r)\;\; \delta^4(p_f + k_f - p_i \;-\; r\,k)\,. \tag{D.6}$$

  Each term of the sum is given by the usual Dirac matrix γ_D^μ, sandwiched between the factors E_p, $\overline{E}_p$. Each term is also multiplied by a δ-function representing the momentum conservation law in the argument, which contains the term $-rk$, *i.e.* the momentum exchanged with the external field.

  For the relevant case of a constant crossed field the sum in the vertex becomes an integral:

$$-ie\,\gamma_e^\mu = -ie\,(2\pi)^4 \int_{-\infty}^{+\infty} dr\;\; \overline{E}_{p_f}(r)\gamma_D^\mu E_{p_i}(r)\;\; \delta^4(p_f + k_f - p_i \;-\; r\,k)\,. \tag{D.7}$$

- Having grouped the E_p, $\overline{E}_p$ factors in the Feynman rules for the QED vertex, *cf.* eqs. (D.6) and (D.7), when writing an amplitude one should use for the initial and final fermions just the usual Dirac spinors $u_p, \bar{u}_p, v_p, \bar{v}_p$.

- Finally, the photon propagator at tree level is unchanged, as the photon is not charged and it does not interact directly at first order to the external field.

With the Furry-Feynman rules, one has all the tools needed to build every Feynman diagram for processes in an external field, at each order in perturbation expansion. One has then to substitute in E_p, $\overline{E}_p$ a suitable form of the external field A^μ_{ext}, depending on the physical case considered.

The sum in equation (D.6) leads to a naïve interpretation for the Feynman diagram in the FP, when an amplitude expression is written down [259]. For beamstrahlung, for example, the diagram in left side of figure D.2 can be seen as sum over all the Feynman graphs each one due to the emission or absorption of r photons from the external field. Within the Furry

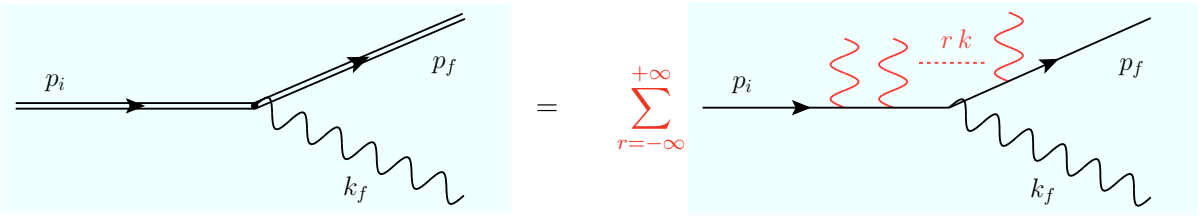

Figure D.2: Naïve interpretation of FP beamstrahlung diagram.

picture the external field is treated classicaly, without considering its quanta. It's interesting to note that these quanta "appear" through the expression of the Furry-Feynman rule for the QED vertex.

Bibliography

[1] G. Moortgat-Pick, S. Porto, and K. Rolbiecki, *Neutralinos betray their singlino nature at the ILC*, *JHEP* **1409** (2014) 002, [arXiv:1406.7701].

[2] S. Porto, G. A. Moortgat-Pick, and K. Rolbiecki, *Towards discrimination of MSSM and NMSSM scenarios at colliders*, arXiv:1404.1053.

[3] M. McGarrie, G. Moortgat-Pick, and S. Porto, *Confronting Higgs couplings from D-term extensions and Natural SUSY at the LHC and ILC*, *Eur.Phys.J.* **C75** (2015), no. 4 150, [arXiv:1411.2040].

[4] A. Hartin, S. Porto, and G. Moortgat-Pick, *Testing nonlinear-QED at the future linear collider with an intense laser*, arXiv:1404.0810.

[5] S. Porto, A. Hartin, and G. Moortgat-Pick, *Methods for evaluating physical processes in strong external fields at e^+e^- colliders: Furry picture and quasi-classical approach*, *PoS* **Corfu2012** (2013) 039, [arXiv:1304.4241].

[6] A. Hartin, G. Moortgat-Pick, and S. Porto, *Strong field effects on physics processes at the Interaction Point of future linear colliders*, *PoS* **ICHEP2012** (2013) 480, [arXiv:1304.2632].

[7] Moortgat-Pick et al., *Physics at the e^+e^- Linear Collider*, arXiv:1504.01726 (2015).

[8] **ATLAS Collaboration**, G. Aad et al., *Observation of a new particle in the search for the Standard Model Higgs boson with the ATLAS detector at the LHC*, *Phys.Lett.* **B716** (2012) 1–29, [arXiv:1207.7214].

[9] **CMS Collaboration**, S. Chatrchyan et al., *Observation of a new boson at a mass of 125 GeV with the CMS experiment at the LHC*, *Phys.Lett.* **B716** (2012) 30–61, [arXiv:1207.7235].

[10] S. Glashow, *Partial Symmetries of Weak Interactions*, *Nucl.Phys.* **22** (1961) 579–588.

[11] S. Weinberg, *A Model of Leptons*, *Phys.Rev.Lett.* **19** (1967) 1264–1266.

[12] A. Salam, *Weak and Electromagnetic Interactions*, *Conf.Proc.* **C680519** (1968) 367–377.

[13] **ATLAS Collaboration**, G. Aad et al., *Evidence for the spin-0 nature of the Higgs boson using ATLAS data*, *Phys.Lett.* **B726** (2013) 120–144, [arXiv:1307.1432].

[14] **CMS Collaboration**, S. Chatrchyan et al., *Study of the Mass and Spin-Parity of the Higgs Boson Candidate Via Its Decays to Z Boson Pairs*, *Phys.Rev.Lett.* **110** (2013) 081803, [arXiv:1212.6639].

[15] **ATLAS Collaboration**, *Updated coupling measurements of the Higgs boson with the ATLAS detector using up to 25 fb^{-1} of proton-proton collision data*, tech. rep., ATLAS-CONF-2014-009, ATLAS-COM-CONF-2014-013, 2014.

[16] **CMS Collaboration**, *Precise determination of the mass of the Higgs boson and studies of the compatibility of its couplings with the standard model*, Tech. Rep. CMS-PAS-HIG-14-009, CERN, Geneva, 2014, `https://twiki.cern.ch/twiki/bin/view/CMSPublic/Hig14009TWiki`.

[17] F. Englert and R. Brout, *Broken Symmetry and the Mass of Gauge Vector Mesons*, *Phys.Rev.Lett.* **13** (1964) 321–323.

[18] P. W. Higgs, *Broken symmetries, massless particles and gauge fields*, *Phys.Lett.* **12** (1964) 132–133.

[19] P. W. Higgs, *Broken Symmetries and the Masses of Gauge Bosons*, *Phys.Rev.Lett.* **13** (1964) 508–509.

[20] G. Guralnik, C. Hagen, and T. Kibble, *Global Conservation Laws and Massless Particles*, *Phys.Rev.Lett.* **13** (1964) 585–587.

[21] S. Weinberg, *Implications of Dynamical Symmetry Breaking*, *Phys.Rev.* **D13** (1976) 974–996.

[22] S. Weinberg, *Implications of Dynamical Symmetry Breaking: An Addendum*, *Phys.Rev.* **D19** (1979) 1277–1280.

[23] E. Gildener, *Gauge Symmetry Hierarchies*, *Phys.Rev.* **D14** (1976) 1667.

[24] H. Miyazawa, *Baryon Number Changing Currents*, *Prog.Theor.Phys.* **36** (1966), no. 6 1266–1276.

[25] P. Ramond, *Dual Theory for Free Fermions*, *Phys.Rev.* **D3** (1971) 2415–2418.

[26] A. Neveu and J. Schwarz, *Factorizable dual model of pions*, *Nucl.Phys.* **B31** (1971) 86–112.

[27] J.-L. Gervais and B. Sakita, *Field Theory Interpretation of Supergauges in Dual Models*, *Nucl.Phys.* **B34** (1971) 632–639.

[28] Y. Gol'fand and E. Likhtman, *Extension of the Algebra of Poincare Group Generators and Violation of p Invariance*, *JETP Lett.* **13** (1971) 323–326.

[29] J. Wess and B. Zumino, *Supergauge Transformations in Four-Dimensions*, *Nucl.Phys.* **B70** (1974) 39–50.

[30] D. B. Kaplan and H. Georgi, $SU(2) \times U(1)$ *Breaking by Vacuum Misalignment*, *Phys.Lett.* **B136** (1984) 183.

[31] D. B. Kaplan, H. Georgi, and S. Dimopoulos, *Composite Higgs Scalars*, *Phys.Lett.* **B136** (1984) 187.

[32] **ATLAS Collaboration,** `https://twiki.cern.ch/twiki/bin/view/AtlasPublic/`.

[33] **CMS Collaboration,** `https://twiki.cern.ch/twiki/bin/view/CMSPublic/PhysicsResults`.

[34] **ATLAS Collaboration,** `https://twiki.cern.ch/twiki/bin/view/AtlasPublic/SupersymmetryPublicResults`.

[35] **CMS Collaboration,** `https://twiki.cern.ch/twiki/bin/view/CMSPublic/PhysicsResultsSUS`.

[36] M. Redi, V. Sanz, M. de Vries, and A. Weiler, *Strong Signatures of Right-Handed Compositeness*, *JHEP* **1308** (2013) 008, [arXiv:1305.3818].

[37] J. Reuter and M. Tonini, *Can the 125 GeV Higgs be the Little Higgs?*, *JHEP* **1302** (2013) 077, [arXiv:1212.5930].

[38] J. Reuter, M. Tonini, and M. de Vries, *Little Higgs Model Limits from LHC - Input for Snowmass 2013*, arXiv:1307.5010.

[39] J. Reuter, M. Tonini, and M. de Vries, *Littlest Higgs with T-parity: Status and Prospects*, *JHEP* **1402** (2014) 053, [arXiv:1310.2918].

[40] G. Ross, *SUSY: Quo Vadis?*, *Eur.Phys.J.* **C74** (2014) 2699.

[41] T. Behnke, J. E. Brau, B. Foster, J. Fuster, M. Harrison, et al., *The International Linear Collider Technical Design Report - Volume 1: Executive Summary*, arXiv:1306.6327.

[42] H. Baer, T. Barklow, K. Fujii, Y. Gao, A. Hoang, et al., *The International Linear Collider Technical Design Report - Volume 2: Physics*, arXiv:1306.6352.

[43] C. Adolphsen, M. Barone, B. Barish, K. Buesser, P. Burrows, et al., *The International Linear Collider Technical Design Report - Volume 3.I: Accelerator & in the Technical Design Phase*, arXiv:1306.6353.

[44] C. Adolphsen, M. Barone, B. Barish, K. Buesser, P. Burrows, et al., *The International Linear Collider Technical Design Report - Volume 3.II: Accelerator Baseline Design*, arXiv:1306.6328.

[45] T. Behnke, J. E. Brau, P. N. Burrows, J. Fuster, M. Peskin, et al., *The International Linear Collider Technical Design Report - Volume 4: Detectors*, arXiv:1306.6329.

[46] C. Bamber, S. Boege, T. Koffas, T. Kotseroglou, A. Melissinos, et al., *Studies of nonlinear QED in collisions of 46.6-GeV electrons with intense laser pulses*, *Phys.Rev.* **D60** (1999) 092004.

[47] C. M. Becchi and G. Ridolfi, *An introduction to relativistic processes and the standard model of electroweak interactions*. Springer, 2014.

[48] S. P. Martin, *A Supersymmetry primer*, hep-ph/9709356.

[49] J. Terning, *Modern supersymmetry: Dynamics and duality*. Oxford University Press, 2006.

[50] J. Wess and J. Bagger, *Supersymmetry and supergravity*. Princeton university press, 1992.

[51] M. Drees, R. Godbole, and P. Roy, *Theory and phenomenology of sparticles: An account of four-dimensional N=1 supersymmetry in high energy physics*. World Scientific, 2004.

[52] R. Ellis, W. Stirling, and B. Webber, *QCD and Collider Physics*. Cambridge Monographs on Particle Physics, Nuclear Physics and Cosmology. Cambridge University Press, 2003.

[53] L. Faddeev and V. Popov, *Feynman diagrams for the yang-mills field*, *Physics Letters B* **25** (1967), no. 1 29 – 30.

[54] M. E. Peskin and D. V. Schroeder, *An introduction to quantum field theory*. Westview, 1995.

[55] **Super-Kamiokande Collaboration**, Y. Fukuda et al., *Evidence for oscillation of atmospheric neutrinos*, *Phys.Rev.Lett.* **81** (1998) 1562–1567, [hep-ex/9807003].

[56] A. Djouadi, *The Anatomy of electro-weak symmetry breaking. I: The Higgs boson in the standard model*, *Phys.Rept.* **457** (2008) 1–216, [hep-ph/0503172].

[57] A. Sakharov, *Violation of CP Invariance, c Asymmetry, and Baryon Asymmetry of the Universe*, *Pisma Zh.Eksp.Teor.Fiz.* **5** (1967) 32–35.

[58] A. Riotto, *Theories of baryogenesis*, hep-ph/9807454.

[59] **WMAP Collaboration**, E. Komatsu et al., *Seven-Year Wilkinson Microwave Anisotropy Probe (WMAP) Observations: Cosmological Interpretation*, *Astrophys.J.Suppl.* **192** (2011) 18, [arXiv:1001.4538].

[60] **Planck Collaboration**, P. Ade et al., *Planck 2013 results. XVI. Cosmological parameters*, *Astron.Astrophys.* **571** (2014) A16, [arXiv:1303.5076].

[61] H. Murayama, *Physics Beyond the Standard Model and Dark Matter*, arXiv:0704.2276.

[62] **GERDA Collaboration**, M. Agostini et al., *Results on Neutrinoless Double-β Decay of ^{76}Ge from Phase I of the GERDA Experiment*, *Phys.Rev.Lett.* **111** (2013), no. 12 122503, [arXiv:1307.4720].

[63] D. Volkov and V. Akulov, *Possible universal neutrino interaction*, *JETP Lett.* **16** (1972) 438–440.

[64] S. R. Coleman and J. Mandula, *All Possible Symmetries of the S Matrix*, *Phys.Rev.* **159** (1967) 1251–1256.

[65] R. Haag, J. T. Łopuszański, and M. Sohnius, *All Possible Generators of Supersymmetries of the s Matrix*, *Nucl.Phys.* **B88** (1975) 257.

[66] S. Dimopoulos and H. Georgi, *Softly Broken Supersymmetry and SU(5)*, *Nucl.Phys.* **B193** (1981) 150.

[67] L. Girardello and M. T. Grisaru, *Soft Breaking of Supersymmetry*, *Nucl.Phys.* **B194** (1982) 65.

[68] **Super-Kamiokande Collaboration**, A. Himmel, *Recent results from Super-Kamiokande*, *AIP Conf.Proc.* **1604** (2014) 345–352, [arXiv:1310.6677].

[69] H. Baer and M. Brhlik, *QCD improved $b \to s$ gamma constraints on the minimal supergravity model*, *Phys.Rev.* **D55** (1997) 3201–3208, [hep-ph/9610224].

[70] G. L. Kane, C. F. Kolda, L. Roszkowski, and J. D. Wells, *Study of constrained minimal supersymmetry*, *Phys.Rev.* **D49** (1994) 6173–6210, [hep-ph/9312272].

[71] A. Djouadi, *The Anatomy of electro-weak symmetry breaking. II. The Higgs bosons in the minimal supersymmetric model*, *Phys.Rept.* **459** (2008) 1–241, [hep-ph/0503173].

[72] J. R. Ellis, G. Ridolfi, and F. Zwirner, *On radiative corrections to supersymmetric Higgs boson masses and their implications for LEP searches*, *Phys.Lett.* **B262** (1991) 477–484.

[73] J. L. Lopez and D. V. Nanopoulos, *New theoretical lower bounds on the Higgs sector of minimal SUSY*, *Phys.Lett.* **B266** (1991) 397–402.

[74] M. S. Carena, J. Espinosa, M. Quiros, and C. Wagner, *Analytical expressions for radiatively corrected Higgs masses and couplings in the MSSM*, *Phys.Lett.* **B355** (1995) 209–221, [hep-ph/9504316].

[75] H. E. Haber, R. Hempfling, and A. H. Hoang, *Approximating the radiatively corrected Higgs mass in the minimal supersymmetric model*, *Z.Phys.* **C75** (1997) 539–554, [hep-ph/9609331].

[76] G. Degrassi, S. Heinemeyer, W. Hollik, P. Slavich, and G. Weiglein, *Towards high precision predictions for the MSSM Higgs sector*, *Eur.Phys.J.* **C28** (2003) 133–143, [hep-ph/0212020].

[77] E. Cremmer, S. Ferrara, L. Girardello, and A. Van Proeyen, *Yang-Mills Theories with Local Supersymmetry: Lagrangian, Transformation Laws and SuperHiggs Effect*, *Nucl.Phys.* **B212** (1983) 413.

[78] M. Dine, A. E. Nelson, Y. Nir, and Y. Shirman, *New tools for low-energy dynamical supersymmetry breaking*, *Phys.Rev.* **D53** (1996) 2658–2669, [hep-ph/9507378].

[79] G. F. Giudice, M. A. Luty, H. Murayama, and R. Rattazzi, *Gaugino mass without singlets*, *JHEP* **9812** (1998) 027, [hep-ph/9810442].

[80] L. Randall and R. Sundrum, *Out of this world supersymmetry breaking*, *Nucl.Phys.* **B557** (1999) 79–118, [hep-th/9810155].

[81] L. Ibanez and G. Ross, *Supersymmetric Higgs and radiative electroweak breaking*, *Comptes Rendus Physique* **8** (2007) 1013–1028, [hep-ph/0702046].

[82] J. R. Ellis, S. Kelley, and D. V. Nanopoulos, *Probing the desert using gauge coupling unification*, *Phys.Lett.* **B260** (1991) 131–137.

[83] U. Amaldi, W. de Boer, and H. Furstenau, *Comparison of grand unified theories with electroweak and strong coupling constants measured at LEP*, *Phys.Lett.* **B260** (1991) 447–455.

[84] C. Giunti, C. Kim, and U. Lee, *Running coupling constants and grand unification models*, *Mod.Phys.Lett.* **A6** (1991) 1745–1755.

[85] H. Goldberg, *Constraint on the Photino Mass from Cosmology*, *Phys.Rev.Lett.* **50** (1983) 1419.

[86] J. R. Ellis, J. Hagelin, D. V. Nanopoulos, K. A. Olive, and M. Srednicki, *Supersymmetric Relics from the Big Bang*, *Nucl.Phys.* **B238** (1984) 453–476.

[87] J. E. Kim and H. P. Nilles, *The μ-Problem and the Strong CP-Problem*, *Phys.Lett.* **B138** (1984) 150.

[88] J. R. Ellis, J. Gunion, H. E. Haber, L. Roszkowski, and F. Zwirner, *Higgs Bosons in a Nonminimal Supersymmetric Model*, *Phys.Rev.* **D39** (1989) 844.

[89] G. Giudice and A. Masiero, *A Natural Solution to the mu Problem in Supergravity Theories*, *Phys.Lett.* **B206** (1988) 480–484.

[90] R. Kitano and Y. Nomura, *A Solution to the supersymmetric fine-tuning problem within the MSSM*, *Phys.Lett.* **B631** (2005) 58–67, [hep-ph/0509039].

[91] K. Blum, R. T. D'Agnolo, and J. Fan, *Natural SUSY Predicts: Higgs Couplings*, *JHEP* **1301** (2013) 057, [arXiv:1206.5303].

[92] A. Azatov, J. Galloway, and M. A. Luty, *Superconformal Technicolor*, *Phys.Rev.Lett.* **108** (2012) 041802, [arXiv:1106.3346].

[93] A. Azatov, J. Galloway, and M. A. Luty, *Superconformal Technicolor: Models and Phenomenology*, *Phys.Rev.* **D85** (2012) 015018, [arXiv:1106.4815].

[94] J. Espinosa and M. Quiros, *Higgs triplets in the supersymmetric standard model*, *Nucl.Phys.* **B384** (1992) 113–146.

[95] J. Espinosa and M. Quiros, *Upper bounds on the lightest Higgs boson mass in general supersymmetric Standard Models*, *Phys.Lett.* **B302** (1993) 51–58, [hep-ph/9212305].

[96] P. Batra, A. Delgado, D. E. Kaplan, and T. M. Tait, *The Higgs mass bound in gauge extensions of the minimal supersymmetric standard model*, *JHEP* **0402** (2004) 043, [hep-ph/0309149].

[97] A. Maloney, A. Pierce, and J. G. Wacker, *D-terms, unification, and the Higgs mass*, *JHEP* **0606** (2006) 034, [hep-ph/0409127].

[98] N. Craig, S. Dimopoulos, and T. Gherghetta, *Split families unified*, *JHEP* **1204** (2012) 116, [arXiv:1203.0572].

[99] Y. Zhang, H. An, X.-d. Ji, and R. N. Mohapatra, *Light Higgs Mass Bound in SUSY Left-Right Models*, *Phys.Rev.* **D78** (2008) 011302, [arXiv:0804.0268].

[100] K. Babu and A. Patra, *Higgs Boson Spectra in Supersymmetric Left-Right Models*, arXiv:1412.8714.

[101] S. King, S. Moretti, and R. Nevzorov, *Theory and phenomenology of an exceptional supersymmetric standard model*, *Phys.Rev.* **D73** (2006) 035009, [hep-ph/0510419].

[102] **LHC Higgs Cross Section Working Group**, S. Heinemeyer et al., *Handbook of LHC Higgs Cross Sections: 3. Higgs Properties*, arXiv:1307.1347.

[103] **Particle Data Group**, K. Olive et al., *Review of Particle Physics*, *Chin.Phys.* **C38** (2014) 090001.

[104] S. Heinemeyer, O. Stal, and G. Weiglein, *Interpreting the LHC Higgs Search Results in the MSSM*, *Phys.Lett.* **B710** (2012) 201–206, [arXiv:1112.3026].

[105] **LHC Higgs Cross Section Working Group,** `https://twiki.cern.ch/twiki/bin/view/LHCPhysics/LHCHXSWG`.

[106] S. Dawson, A. Gritsan, H. Logan, J. Qian, C. Tully, et al., *Higgs Working Group Report*, arXiv:1310.8361.

[107] **ATLAS Collaboration**, *Measurements of the properties of the Higgs-like boson in the two photon decay channel with the ATLAS detector using 25* fb^{-1} *of proton-proton collision data*, Tech. Rep. ATLAS-CONF-2013-012, CERN, Geneva, Mar, 2013.

[108] **ATLAS Collaboration,** `https://twiki.cern.ch/twiki/bin/view/AtlasPublic/HiggsPublicResults`.

[109] **CMS Collaboration,** `https://twiki.cern.ch/twiki/bin/view/CMSPublic/PhysicsResultsHIG`.

[110] D. Asner, T. Barklow, C. Calancha, K. Fujii, N. Graf, et al., *ILC Higgs White Paper*, arXiv:1310.0763.

[111] **ATLAS Collaboration**, G. Aad et al., *Search for neutral Higgs bosons of the minimal supersymmetric standard model in pp collisions at* $\sqrt{s} = 8$ *TeV with the ATLAS detector*, *JHEP* **1411** (2014) 056, [arXiv:1409.6064].

[112] **ATLAS Collaboration**, *Search for charged Higgs bosons in the* τ*+jets final state with pp collision data recorded at* $\sqrt{s} = 8$ *TeV with the ATLAS experiment*, Tech. Rep. ATLAS-CONF-2013-090, CERN, Geneva, Aug, 2013.

[113] **CMS Collaboration**, *Search for charged Higgs bosons with the* $H^+ \to \tau^+\nu_\tau$ *decay channel in the fully hadronic final state at* $\sqrt{s} = 8$ *TeV*, Tech. Rep. CMS-PAS-HIG-14-020, CERN, Geneva, 2014.

[114] **CMS Collaboration**, V. Khachatryan et al., *Searches for supersymmetry using the* M_{T2} *variable in hadronic events produced in pp collisions at 8 TeV*, arXiv:1502.04358.

[115] **ATLAS Collaboration**, *Search for squarks and gluinos with the ATLAS detector using final states with jets and missing transverse momentum and 5.8* fb^{-1} *of* $\sqrt{s}$*=8 TeV proton-proton collision data*, Tech. Rep. ATLAS-CONF-2012-109, CERN, Geneva, Aug, 2012.

[116] M. Tonini, *Beyond the Standard Higgs at the LHC: present constraints on Little Higgs models and future prospects*, *Universität Hamburg* (2014) DESY–THESIS–2014–038.

[117] M. de Vries, *Strongly Coupled Models at the LHC*, *Universität Hamburg* (2014) DESY–THESIS–2014–035.

[118] **MSSM Working Group**, A. Djouadi et al., *The Minimal supersymmetric standard model: Group summary report*, hep-ph/9901246.

[119] H. K. Dreiner, M. Kramer, and J. Tattersall, *How low can SUSY go? Matching, monojets and compressed spectra*, *Europhys.Lett.* **99** (2012) 61001, [arXiv:1207.1613].

[120] L. J. Hall and M. Suzuki, *Explicit R-Parity Breaking in Supersymmetric Models*, *Nucl.Phys.* **B231** (1984) 419.

[121] A. Bharucha, S. Heinemeyer, and F. von der Pahlen, *Does the LHC exclude SUSY Particles at the ILC?*, arXiv:1404.0365.

[122] D. Chung, L. Everett, G. Kane, S. King, J. D. Lykken, et al., *The Soft supersymmetry breaking Lagrangian: Theory and applications*, *Phys.Rept.* **407** (2005) 1–203, [hep-ph/0312378].

[123] **LUX Collaboration**, D. Akerib et al., *First results from the LUX dark matter experiment at the Sanford Underground Research Facility*, *Phys.Rev.Lett.* **112** (2014), no. 9 091303, [arXiv:1310.8214].

[124] **Muon G-2 Collaboration**, G. Bennett et al., *Final Report of the Muon E821 Anomalous Magnetic Moment Measurement at BNL*, *Phys.Rev.* **D73** (2006) 072003, [hep-ex/0602035].

[125] M. Davier, A. Hoecker, B. Malaescu, and Z. Zhang, *Reevaluation of the Hadronic Contributions to the Muon g-2 and to $\alpha(M_Z^2)$*, *Eur.Phys.J.* **C71** (2011) 1515, [arXiv:1010.4180].

[126] K. Hagiwara, R. Liao, A. D. Martin, D. Nomura, and T. Teubner, *$(g-2)_\mu$ and $\alpha(M_Z^2)$ re-evaluated using new precise data*, *J.Phys.* **G38** (2011) 085003, [arXiv:1105.3149].

[127] U. Ellwanger, C. Hugonie, and A. M. Teixeira, *The Next-to-Minimal Supersymmetric Standard Model*, *Phys.Rept.* **496** (2010) 1–77, [arXiv:0910.1785].

[128] S. Choi, A. Djouadi, M. Guchait, J. Kalinowski, H. Song, et al., *Reconstructing the chargino system at e^+e^- linear colliders*, *Eur.Phys.J.* **C14** (2000) 535–546, [hep-ph/0002033].

[129] K. Desch, J. Kalinowski, G. A. Moortgat-Pick, M. Nojiri, and G. Polesello, *SUSY parameter determination in combined analyses at LHC / LC*, *JHEP* **0402** (2004) 035, [hep-ph/0312069].

[130] S. King and P. White, *Nonminimal supersymmetric Higgs bosons at LEP-2*, *Phys.Rev.* **D53** (1996) 4049–4062, [hep-ph/9508346].

[131] U. Ellwanger, M. Rausch de Traubenberg, and C. A. Savoy, *Phenomenology of supersymmetric models with a singlet*, *Nucl.Phys.* **B492** (1997) 21–50, [hep-ph/9611251].

[132] A. Vilenkin, *Cosmic Strings and Domain Walls*, *Phys.Rept.* **121** (1985) 263–315.

[133] D. Suematsu and Y. Yamagishi, *Radiative symmetry breaking in a supersymmetric model with an extra U(1)*, *Int.J.Mod.Phys.* **A10** (1995) 4521–4536, [hep-ph/9411239].

[134] U. Ellwanger, J. F. Gunion, C. Hugonie, and S. Moretti, *Towards a no lose theorem for NMSSM Higgs discovery at the LHC*, hep-ph/0305109.

[135] J.-J. Cao, Z.-X. Heng, J. M. Yang, Y.-M. Zhang, and J.-Y. Zhu, *A SM-like Higgs near 125 GeV in low energy SUSY: a comparative study for MSSM and NMSSM*, *JHEP* **1203** (2012) 086, [arXiv:1202.5821].

[136] J. Cao, Z. Heng, J. M. Yang, and J. Zhu, *Status of low energy SUSY models confronted with the LHC 125 GeV Higgs data*, *JHEP* **1210** (2012) 079, [arXiv:1207.3698].

[137] R. Benbrik, M. Gomez Bock, S. Heinemeyer, O. Stål, G. Weiglein, et al., *Confronting the MSSM and the NMSSM with the Discovery of a Signal in the two Photon Channel at the LHC*, *Eur.Phys.J.* **C72** (2012) 2171, [arXiv:1207.1096].

[138] K. Choi, S. H. Im, K. S. Jeong, and M. Yamaguchi, *Higgs mixing and diphoton rate enhancement in NMSSM models*, *JHEP* **1302** (2013) 090, [arXiv:1211.0875].

[139] S. Munir, L. Roszkowski, and S. Trojanowski, *Simultaneous enhancement in $\gamma\gamma, b\bar{b}$ and $\tau^+\tau^-$ rates in the NMSSM with nearly degenerate scalar and pseudoscalar Higgs bosons*, *Phys.Rev.* **D88** (2013), no. 5 055017, [arXiv:1305.0591].

[140] J. Cao, F. Ding, C. Han, J. M. Yang, and J. Zhu, *A light Higgs scalar in the NMSSM confronted with the latest LHC Higgs data*, *JHEP* **1311** (2013) 018, [arXiv:1309.4939].

[141] C. Beskidt, W. de Boer, and D. Kazakov, *A comparison of the Higgs sectors of the CMSSM and NMSSM for a 126 GeV Higgs boson*, *Phys.Lett.* **B726** (2013) 758–766, [arXiv:1308.1333].

[142] B. Ananthanarayan, J. Lahiri, P. Pandita, and M. Patra, *Invisible decays of the lightest Higgs boson in supersymmetric models*, *Phys.Rev.* **D87** (2013), no. 11 115021, [arXiv:1306.1291].

[143] P. Pandita and M. Patra, *Invisible decays of low mass Higgs bosons in supersymmetric models*, arXiv:1405.7163.

[144] S. Moretti and S. Munir, *Di-photon Higgs signals at the LHC in the next-to-minimal supersymmetric standard model*, *Eur.Phys.J.* **C47** (2006) 791–803, [hep-ph/0603085].

[145] U. Ellwanger and A. M. Teixeira, *Excessive Higgs pair production with little MET from squarks and gluinos in the NMSSM*, arXiv:1412.6394.

[146] R. S. Gupta, M. Montull, and F. Riva, *SUSY Faces its Higgs Couplings*, *JHEP* **1304** (2013) 132, [arXiv:1212.5240].

[147] D. Das, U. Ellwanger, and A. M. Teixeira, *Modified Signals for Supersymmetry in the NMSSM with a Singlino-like LSP*, *JHEP* **1204** (2012) 067, [arXiv:1202.5244].

[148] U. Ellwanger and A. M. Teixeira, *NMSSM with a singlino LSP: possible challenges for searches for supersymmetry at the LHC*, *JHEP* **1410** (2014) 113, [arXiv:1406.7221].

[149] B. Dutta, Y. Gao, and B. Shakya, *Light Higgsino Decays as a Probe of the NMSSM*, arXiv:1412.2774.

[150] **ECFA/DESY LC Physics Working Group**, J. Aguilar-Saavedra et al., *TESLA: The Superconducting electron positron linear collider with an integrated x-ray laser laboratory. Technical design report. Part 3. Physics at an e^+e^- linear collider*, hep-ph/0106315.

[151] S. Choi, J. Kalinowski, G. A. Moortgat-Pick, and P. Zerwas, *Analysis of the neutralino system in supersymmetric theories*, *Eur.Phys.J.* **C22** (2001) 563–579, [hep-ph/0108117].

[152] S. Choi, J. Kalinowski, G. A. Moortgat-Pick, and P. Zerwas, *Analysis of the neutralino system in supersymmetric theories: Addendum*, hep-ph/0202039.

[153] K. Desch, J. Kalinowski, G. Moortgat-Pick, K. Rolbiecki, and W. Stirling, *Combined LHC/ILC analysis of a SUSY scenario with heavy sfermions*, *JHEP* **0612** (2006) 007, [hep-ph/0607104].

[154] A. Bharucha, J. Kalinowski, G. Moortgat-Pick, K. Rolbiecki, and G. Weiglein, *One-loop effects on MSSM parameter determination via chargino production at the LC*, *Eur.Phys.J.* **C73** (2013) 2446, [arXiv:1211.3745].

[155] G. A. Moortgat-Pick, S. Hesselbach, F. Franke, and H. Fraas, *Distinguishing between mssm and nmssm by combined LHC and ILC analyses*, *JHEP* **0506** (2005) 048, [hep-ph/0502036].

[156] P. Z. Skands, B. Allanach, H. Baer, C. Balazs, G. Belanger, et al., *SUSY Les Houches accord: Interfacing SUSY spectrum calculators, decay packages, and event generators*, *JHEP* **0407** (2004) 036, [hep-ph/0311123].

[157] B. Allanach, C. Balazs, G. Belanger, M. Bernhardt, F. Boudjema, et al., *SUSY Les Houches Accord 2*, *Comput.Phys.Commun.* **180** (2009) 8–25, [arXiv:0801.0045].

[158] U. Ellwanger, J. F. Gunion, and C. Hugonie, *NMHDECAY: A Fortran code for the Higgs masses, couplings and decay widths in the NMSSM*, *JHEP* **0502** (2005) 066, [hep-ph/0406215].

[159] U. Ellwanger and C. Hugonie, *NMHDECAY 2.0: An Updated program for sparticle masses, Higgs masses, couplings and decay widths in the NMSSM*, *Comput.Phys.Commun.* **175** (2006) 290–303, [hep-ph/0508022].

[160] G. Belanger, F. Boudjema, C. Hugonie, A. Pukhov, and A. Semenov, *Relic density of dark matter in the NMSSM*, *JCAP* **0509** (2005) 001, [hep-ph/0505142].

[161] D. Das, U. Ellwanger, and A. M. Teixeira, *NMSDECAY: A Fortran Code for Supersymmetric Particle Decays in the Next-to-Minimal Supersymmetric Standard Model*, *Comput.Phys.Commun.* **183** (2012) 774–779, [arXiv:1106.5633].

[162] M. Muhlleitner, A. Djouadi, and Y. Mambrini, *SDECAY: A Fortran code for the decays of the supersymmetric particles in the MSSM*, *Comput.Phys.Commun.* **168** (2005) 46–70, [hep-ph/0311167].

[163] G. Belanger, F. Boudjema, A. Pukhov, and A. Semenov, *micrOMEGAs_3: A program for calculating dark matter observables*, *Comput.Phys.Commun.* **185** (2014) 960–985, [arXiv:1305.0237].

[164] P. Bechtle, O. Brein, S. Heinemeyer, O. Stål, T. Stefaniak, et al., *HiggsBounds-4: Improved Tests of Extended Higgs Sectors against Exclusion Bounds from LEP, the Tevatron and the LHC*, *Eur.Phys.J.* **C74** (2014) 2693, [arXiv:1311.0055].

[165] P. Bechtle, S. Heinemeyer, O. Stål, T. Stefaniak, and G. Weiglein, *HiggsSignals: Confronting arbitrary Higgs sectors with measurements at the Tevatron and the LHC*, *Eur.Phys.J.* **C74** (2014) 2711, [arXiv:1305.1933].

[166] G. Moortgat-Pick, T. Abe, G. Alexander, B. Ananthanarayan, A. Babich, et al., *The Role of polarized positrons and electrons in revealing fundamental interactions at the linear collider*, *Phys.Rept.* **460** (2008) 131–243, [hep-ph/0507011].

[167] S. Choi, A. Djouadi, H. K. Dreiner, J. Kalinowski, and P. Zerwas, *Chargino pair production in e^+e^- collisions*, *Eur.Phys.J.* **C7** (1999) 123–134, [hep-ph/9806279].

[168] G. A. Moortgat-Pick, A. Bartl, H. Fraas, and W. Majerotto, *Beam polarization and spin correlation effects in chargino production and decay*, hep-ph/0004181.

[169] F. James and M. Roos, *Minuit - a system for function minimization and analysis of the parameter errors and correlations*, *Computer Physics Communications* **10** (1975), no. 6 343 – 367.

[170] M. M. Nojiri, K. Fujii, and T. Tsukamoto, *Confronting the minimal supersymmetric standard model with the study of scalar leptons at future linear e^+e^- colliders*, *Phys.Rev.* **D54** (1996) 6756–6776, [hep-ph/9606370].

[171] M. Berggren, F. Brümmer, J. List, G. Moortgat-Pick, T. Robens, et al., *Tackling light higgsinos at the ILC*, *Eur.Phys.J.* **C73** (2013) 2660, [arXiv:1307.3566].

[172] R. Huo, G. Lee, A. M. Thalapillil, and C. E. Wagner, *$SU(2) \otimes SU(2)$ Gauge Extensions of the MSSM Revisited*, *Phys.Rev.* **D87** (2013) 055011, [arXiv:1212.0560].

[173] L. Randall, "Warped geometries and branes." The 10th International Conference on Supersymmetry and Unification of Fundamental Interactions SUSY '02, 17-23 June, Hamburg, Germany.

[174] A. Bharucha, A. Goudelis, and M. McGarrie, *En-gauging Naturalness*, *Eur.Phys.J.* **C74** (2014) 2858, [arXiv:1310.4500].

[175] C. Csaki, J. Erlich, C. Grojean, and G. D. Kribs, *4-D constructions of supersymmetric extra dimensions and gaugino mediation*, *Phys.Rev.* **D65** (2002) 015003, [hep-ph/0106044].

[176] H. Cheng, D. Kaplan, M. Schmaltz, and W. Skiba, *Deconstructing gaugino mediation*, *Phys.Lett.* **B515** (2001) 395–399, [hep-ph/0106098].

[177] P. Batra, A. Delgado, D. E. Kaplan, and T. M. Tait, *Running into new territory in SUSY parameter space*, *JHEP* **0406** (2004) 032, [hep-ph/0404251].

[178] A. Delgado, *Raising the Higgs mass in supersymmetric models*, *"Supersymmetry and unification of fundamental interactions."* *Proceedings, 12th International Conference, SUSY 2004, Tsukuba, Japan, June 17-23, 2004* (2004) 757–760, [hep-ph/0409073].

[179] A. D. Medina, N. R. Shah, and C. E. Wagner, *A Heavy Higgs and a Light Sneutrino NLSP in the MSSM with Enhanced SU(2) D-terms*, *Phys.Rev.* **D80** (2009) 015001, [arXiv:0904.1625].

[180] A. De Simone, J. Fan, M. Schmaltz, and W. Skiba, *Low-scale gaugino mediation, lots of leptons at the LHC*, *Phys.Rev.* **D78** (2008) 095010, [arXiv:0808.2052].

[181] M. McGarrie, *General Gauge Mediation and Deconstruction*, *JHEP* **1011** (2010) 152, [arXiv:1009.0012].

[182] R. Auzzi, A. Giveon, S. B. Gudnason, and T. Shacham, *A Light Stop with Flavor in Natural SUSY*, *JHEP* **1301** (2013) 169, [arXiv:1208.6263].

[183] R. T. D'Agnolo, E. Kuflik, and M. Zanetti, *Fitting the Higgs to Natural SUSY*, *JHEP* **1303** (2013) 043, [arXiv:1212.1165].

[184] P. Fayet, *Supergauge Invariant Extension of the Higgs Mechanism and a Model for the electron and Its Neutrino*, *Nucl.Phys.* **B90** (1975) 104–124.

[185] H. E. Haber and G. L. Kane, *The Search for Supersymmetry: Probing Physics Beyond the Standard Model*, *Phys.Rept.* **117** (1985) 75–263.

[186] R. S. Chivukula, H.-J. He, J. Howard, and E. H. Simmons, *The Structure of electroweak corrections due to extended gauge symmetries*, *Phys.Rev.* **D69** (2004) 015009, [hep-ph/0307209].

[187] E. Bertuzzo and C. Frugiuele, *A natural SM-like 126 GeV Higgs via non-decoupling D-terms*, arXiv:1412.2765.

[188] F. Staub, *SARAH*, *SARAH Hepforge* (2008) [arXiv:0806.0538].

[189] F. Staub, *SARAH 3.2: Dirac Gauginos, UFO output, and more*, *Computer Physics Communications* **184** (2013) pp. 1792–1809, [arXiv:1207.0906].

[190] N. Craig and A. Katz, *A Supersymmetric Higgs Sector with Chiral D-terms*, *JHEP* **1305** (2013) 015, [arXiv:1212.2635].

[191] A. Arvanitaki and G. Villadoro, *A Non Standard Model Higgs at the LHC as a Sign of Naturalness*, *JHEP* **1202** (2012) 144, [arXiv:1112.4835].

[192] K. Blum and R. T. D'Agnolo, *2 Higgs or not 2 Higgs*, *Phys.Lett.* **B714** (2012) 66–69, [arXiv:1202.2364].

[193] H. Huffel and G. Pocsik, *Unitarity Bounds on Higgs Boson Masses in the Weinberg-Salam Model With Two Higgs Doublets*, *Z.Phys.* **C8** (1981) 13.

[194] G. Pocsik and G. Zsigmond, *On the Production of Neutral Higgs Bosons in the Weinberg-Salam Model With Two Higgs Doublets*, *Z.Phys.* **C10** (1981) 367.

[195] J. F. Gunion, H. E. Haber, G. L. Kane, and S. Dawson, *The Higgs Hunter's Guide*, *Front.Phys.* **80** (2000) 1–448.

[196] J. F. Gunion and H. E. Haber, *The CP conserving two Higgs doublet model: The Approach to the decoupling limit*, *Phys.Rev.* **D67** (2003) 075019, [hep-ph/0207010].

[197] L. Randall, *Two Higgs Models for Large Tan Beta and Heavy Second Higgs*, *JHEP* **0802** (2008) 084, [arXiv:0711.4360].

[198] **ATLAS Collaboration**, G. Aad et al., *Measurements of Higgs boson production and couplings in diboson final states with the ATLAS detector at the LHC*, *Phys.Lett.* **B726** (2013) 88–119, [arXiv:1307.1427].

[199] M. E. Peskin, *Estimation of LHC and ILC Capabilities for Precision Higgs Boson Coupling Measurements*, arXiv:1312.4974.

[200] S. Kanemura, K. Tsumura, K. Yagyu, and H. Yokoya, *Fingerprinting non-minimal Higgs sectors*, arXiv:1406.3294.

[201] V. Ritus, *Quantum effects of the interaction of elementary particles with an intense electromagnetic field*, *Journal of Soviet Laser Research* **6** (1985) 497–617.

[202] W. Greiner, B. Müller, and J. Rafelski, *Quantum Electrodynamics of Strong Fields*. Springer-Verlag, Berlin, 1985.

[203] A. Di Piazza, C. Muller, K. Hatsagortsyan, and C. Keitel, *Extremely high-intensity laser interactions with fundamental quantum systems*, *Rev.Mod.Phys.* **84** (2012) 1177, [arXiv:1111.3886].

[204] L. Linssen, A. Miyamoto, M. Stanitzki, and H. Weerts, *Physics and Detectors at CLIC: CLIC Conceptual Design Report*, arXiv:1202.5940.

[205] P. Chen, *An introduction to beamstrahlung and disruption*, in *Frontiers of Particle Beams*, pp. 495–532. Springer, 1988.

[206] **ILC Collaboration**, *internal communication*, 2011.

[207] K. Yokoya and P. Chen, *Beam-beam phenomena in linear colliders*, *Lect.Notes Phys.* **400** (1992) 415–445.

[208] V. B. Berestetskii, E. M. Lifshitz, and L. P. Pitaevskiĭ, *Quantum electrodynamics*, vol. 4. Butterworth-Heinemann, 1982.

[209] O. Klein, *Die Reflexion von Elektronen an einem Potentialsprung nach der relativistischen Dynamik von Dirac*, *Z.Phys.* **53** (1929) 157.

[210] F. Sauter, *Uber das Verhalten eines Elektrons im homogenen elektrischen Feld nach der relativistischen Theorie Diracs*, *Z.Phys.* **69** (1931) 742–764.

[211] W. Heisenberg and H. Euler, *Folgerungen aus der Diracschen Theorie des Positrons*, *Z.Phys.* **98** (1936) 714–732, [physics/0605038].

[212] J. S. Schwinger, *On gauge invariance and vacuum polarization*, *Phys.Rev.* **82** (1951) 664–679.

[213] E. S. Fradkin, D. M. Gitman, and S. M. Shvartsman, *Quantum electrodynamics with unstable vacuum*. Springer, 1991.

[214] A. Kuznetsov and N. Mikheev, *Electroweak processes in external electromagnetic fields*, *Springer Tracts Mod.Phys.* **197** (2004) 1–120.

[215] G. Baur, K. Hencken, and D. Trautmann, *Electron-Positron Pair Production in Relativistic Heavy Ion Collisions*, *Phys.Rept.* **453** (2007) 1–27, [arXiv:0706.0654].

[216] V. Yanovsky, V. Chvykov, G. Kalinchenko, P. Rousseau, T. Planchon, T. Matsuoka, A. Maksimchuk, J. Nees, G. Cheriaux, G. Mourou, and K. Krushelnick, *Ultra-high intensity- 300-TW laser at 0.1 Hz repetition rate*, *Opt. Express* **16** (Feb, 2008) 2109–2114.

[217] M. Dunne, N. Alexander, F. Amiranoff, P. Aguer, S. Atzeni, H. Azechi, V. Bagnoud, P. Balcou, J. Badziak, D. Batani, et al., *HiPER–technical background and conceptual design report*, .

[218] **ELI**, G. Mourou, G. Korn, W. Sandner, and J. Collier, eds., *ELI–Extreme Light Infrastructure Science and Technology with Ultra-Intense Lasers, Whitebook*. Berlin, THOSS Media GmbH, 2011.

[219] A. Ringwald, *Pair production from vacuum at the focus of an x-ray free electron laser*, *Physics Letters B* **510** (2001), no. 1 107–116.

[220] *CAIN Users Manual, Version 2.35*, 2003.

[221] R. J. Noble, *Bremsstrahlung From Colliding Electron - Positron Beams With Negligible Disruption*, *Nucl.Instrum.Meth.* **A256** (1987) 427.

[222] J. Esberg, I. Uggerhøj, U. B. Dalena, and D. Schulte, *Strong field processes in beam-beam interactions at the compact linear collider*, *Phys. Rev. ST Accel. Beams* **17** (May, 2014) 051003.

[223] W. Kilian, T. Ohl, and J. Reuter, *WHIZARD: Simulating Multi-Particle Processes at LHC and ILC*, *Eur.Phys.J.* **C71** (2011) 1742, [arXiv:0708.4233].

[224] W. Furry, *On Bound States and Scattering in Positron Theory*, *Phys.Rev.* **81** (1951) 115–124.

[225] D. Wolkow, *Uber eine Klasse von Losungen der Diracschen Gleichung*, *Z.Phys.* **94** (1935) 250–260.

[226] G. Moortgat-Pick, *The Furry picture*, *J.Phys.Conf.Ser.* **198** (2009) 012002.

[227] V. Ritus, *Radiative corrections in quantum electrodynamics with intense field and their analytical properties*, *Annals Phys.* **69** (1972) 555–582.

[228] M. Boca and V. Florescu, *The completeness of Volkov spinors*, *Rom. J. Phys* **55** (2010) 511–525.

[229] A. V. Kurilin, *Particle physics in intense electromagnetic fields*, *Nuovo Cim.* **A112** (1999) 977–1000, [hep-ph/0210194].

[230] H. R. Reiss, *Absorption of light by light*, *Journal of Mathematical Physics* **3** (1962), no. 1 59–67.

[231] A. Nikishov and V. Ritus, *Quantum Processes in the Field of a Plane Electromagnetic Wave and in a Constant Field 1*, *Sov.Phys.JETP* **19** (1964) 529–541.

[232] I. Goldman, *Intensity effects in Compton scattering*, *Physics Letters* **8** (1964), no. 2 103–106.

[233] N. Narozhnyi, A. I. Nikishov, and V. Ritus, *Quantum processes in the field of a circularly polarized electromagnetic wave*, *Zh. Eksperim. i Teor. Fiz.* **47** (1964).

[234] A. Nikishov and V. Ritus, *Nonlinear effects in Compton scattering and pair production owing to absorption of several photons*, *SOVIET PHYSICS JETP-USSR* **20** (1965), no. 3 757.

[235] A. Nikishov and V. Ritus, *Pair production by a photon and photon emission by an electron in the field of an intense electromagnetic wave and in a constant field*, *Soviet Journal of Experimental and Theoretical Physics* **25** (1967).

[236] T. Heinzl and A. Ilderton, *Extreme field physics and QED*, arXiv:0809.3348.

[237] D. Seipt, *Strong-Field QED Processes in Short Laser Pulses*. PhD thesis.

[238] K. McDonald, *Proposal for experimental studies of nonlinear quantum electrodynamics*, 1986.

[239] V. N. Baĭer and V. M. Katkov, *Processes involved in the motion of high energy particles in a magnetic field*, *Sov. Phys. JETP* **26** (1968) 854.

[240] V. N. Baĭer and V. M. Katkov, *Quasiclassical theory of bremsstrahlung by relativistiv particles*, *Sov. Phys. JETP* **28** (1969) 807.

[241] V. N. Baier, V. M. Katkov, and V. M. Strakhovenko, *Electromagnetic processes at high energies in oriented single crystals*. World Scientific, 1998.

[242] A. Hartin, *Furry picture transition rates in the intense fields at a lepton collider interaction point*, arXiv:1502.04564.

[243] C. Bula et al., *Proposal for a Study of QED at Critical Field Strength in Intense Laser-High-Energy-Electron Collisions at the Stanford Linear Accelerator Center*, *SLAC Proposal E-144* (1991).

[244] **E144 Collaboration**, C. Bula et al., *Observation of nonlinear effects in Compton scattering*, *Phys.Rev.Lett.* **76** (1996) 3116–3119.

[245] D. Burke, R. Field, G. Horton-Smith, T. Kotseroglou, J. Spencer, et al., *Positron production in multi - photon light by light scattering*, *Phys.Rev.Lett.* **79** (1997) 1626–1629.

[246] *Powerlite DLS 9000 Specifications*, `http://www.continuumlasers.com`.

[247] C. Bula, K. T. McDonald, E. J. Prebys, C. Bamber, S. Boege, T. Kotseroglou, A. C. Melissinos, D. D. Meyerhofer, W. Ragg, D. L. Burke, R. C. Field, G. Horton-Smith, A. C. Odian, J. E. Spencer, D. Walz, S. C. Berridge, W. M. Bugg, K. Shmakov, and A. W. Weidemann, *Observation of nonlinear effects in Compton scattering*, *Phys. Rev. Lett.* **76** (Apr, 1996) 3116–3119.

[248] L. S. Brown and T. Kibble, *Interaction of Intense Laser Beams with Electrons*, *Phys.Rev.* **133** (1964) A705–A719.

[249] T. Kibble, *Frequency Shift in High-Intensity Compton Scattering*, *Phys.Rev.* **138** (1965) B740–B753.

[250] D. D. Meyerhofer, J. P. Knauer, S. J. McNaught, and C. I. Moore, *Observation of relativistic mass shift effects during high-intensity laser–electron interactions*, *J. Opt. Soc. Am. B* **13** (Jan, 1996) 113–117.

[251] C. Harvey, T. Heinzl, A. Ilderton, and M. Marklund, *Intensity-dependent electron mass shift in a laser field: Existence, universality, and detection*, *Phys. Rev. Lett.* **109** (Sep, 2012) 100402.

[252] D. L. Burke, R. C. Field, G. Horton-Smith, J. E. Spencer, D. Walz, S. C. Berridge, W. M. Bugg, K. Shmakov, A. W. Weidemann, C. Bula, K. T. McDonald, E. J. Prebys, C. Bamber, S. J. Boege, T. Koffas, T. Kotseroglou, A. C. Melissinos, D. D. Meyerhofer, D. A. Reis, and W. Ragg, *Positron production in multiphoton light-by-light scattering*, *Phys. Rev. Lett.* **79** (Sep, 1997) 1626–1629.

[253] S. Bulanov, C. Schroeder, E. Esarey, and W. Leemans, *Electromagnetic cascade in high energy electron, positron, and photon interactions with intense laser pulses*, *Phys.Rev.* **A87** (2013), no. 6 062110, [arXiv:1306.1260].

[254] N. Neitz and A. Di Piazza, *Electron-beam dynamics in a strong laser field including quantum radiation reaction*, arXiv:1403.2450.

[255] F. Mackenroth and A. Di Piazza, *Nonlinear Double Compton Scattering in the Ultrarelativistic Quantum Regime*, *Phys.Rev.Lett.* **110** (2013), no. 7 070402, [arXiv:1208.3424].

[256] H. Hu, C. Muller, and C. H. Keitel, *Complete QED theory of multiphoton trident pair production in strong laser fields*, *Phys.Rev.Lett.* **105** (2010) 080401, [arXiv:1002.2596].

[257] A. Ilderton, *Trident pair production in strong laser pulses*, *Phys.Rev.Lett.* **106** (2011) 020404, [arXiv:1011.4072].

[258] B. King and H. Ruhl, *Trident pair production in a constant crossed field*, *Phys.Rev.* **D88** (2013), no. 1 013005, [arXiv:1303.1356].

[259] A. Nikishov and V. Ritus, *Quantum Processes in the Field of a Plane Electromagnetic Wave and in a Constant Field 2*, *Sov.Phys.JETP* **19** (1964) 1191–1199.

Acknowledgements

First of all, I am deeply grateful to my supervisor Gudrid Moortgat-Pick for her guidance, her support, and for many inspiring and fruitful discussions. I owe her the great opportunity to work in these years in the very interesting and stimulating environment of DESY. I would like to thank Jürgen Reuter for correcting my dissertation and for his course on supersymmetry that revealed itself to be very useful for my work. I thank also my Masters' supervisor Donal O'Connell, for his kindness and for always being available for suggestions. I am very thankful to my collaborators Krzysztof Rolbiecki, Moritz McGarrie, and Anthony Hartin for all the discussions, face-to-face and Skype-to-Skype. I further want to thank Mikael Berggren, Paolo Bolzoni, Florian Domingo, Peter Drechsel, Jenny List, Germano Nardini, Georg Weiglein, and Lisa Zeune for useful discussions. I acknowledge support by the Deutsche Forschungsgemeinschaft within the Sonderforschungsbereich 676 "Particles, Strings and the Early Universe." I thank Martin Sprenger, Marco Tonini, and Maikel de Vries for proofreading parts of the thesis. Furthermore, I thank Thomas Konstandin, Jan Louis, and Christian Sander for agreeing to be referees of my disputation.

During these years I have met some special friends that were always there, *seguendo le regole*, and deserve particular thanks. Francisco for being the one to remember to pick me up for lunch, for translating in English every my second word, for the *pastéis de nata*, and for the beautiful ride to Kiel. Maikel for his sensitivity (or sensibility?) to me, for the frank opinions, *i.e.* complaints, for the bike, for the unbeatable gaffes, and for eventually learning not to cut spaghetti. Marco for our friendship that, arriving from Padua together, has grown with us into a deep understanding, fundamental for me in some difficult circumstances. Martin for being the best officemate I could have hoped for, always ready to help or to laugh, for the example, and for our semi-formal Fridays. Paolo, *eccolo*, for all the special time spent together, for the comfort, the patience, the kindness, and for always having a smile on his face.

I am also very grateful to *Dottori* Marco and Sara, and, *since there is not two without three*, also Mattia, for opening the dances and for the motivation that they give me in my path, and all the fun together. Thanks to Marco and Lorenzo for all our special dinners with football, Italian, briscola and laughs. Thank you Alessandra, Anne-Julia, Francesco, Francesca, Jennifer, Ivan, Martina, Ninetta, Sonja, Valentina for our friendships. Thanks to Harald, our apartment was home for me. Thanks to Elina and Matthias for all our chats,

switching languages; to Valerie for all our tandem hours; to Marcos, Javier, Andreas and also Rob for the time together in the office, always awesome; to the friends met in schools and conferences, Abhishek, Aniello, Lucia, Matteo, and Simone. I want also to thank all the other guys at DESY that made my days better, at lunch and making Ph.D. hats: Aleksandrina, Alessandro, Alex, c'Andrey, Annika, Bijan, Clemens, Daniel, Emanuele, Florian, Jasone, Julia, Julian, Kazuki, Koji, Lucila, Luigi, Markus, Martin, Matteo, Matthias, Michal, Mikhail, Nezhla, Pavel, Pedro, Peter, Reinke, Samantha, Sebastian, Shireen, Shruti, Simone, So Young, Stefan, Tigran, Tobias, Václav, Yuri, and many others.

Finally, my family. I am deeply thankful to Elena and my parents Teresa and Giandomenico, for always supporting me, whichever choice I made. Thanks also to Giulia, Tommaso, Silvia and Maurizio who welcomed me. I dedicate this thesis to my dear Anna, every day being with me, showing me that Hamburg and Heidelberg are just next-door. Without her I could not put this . (dot)

Ringraziamenti

Sono profondamente grato alla mia relatrice Gudrid Moortgat-Pick per la sua guida, il suo sostegno e per le molte discussioni ispiratrici e costruttive. Le devo la grande opportunità di aver lavorato in questi anni nell'interessantissimo e stimolante clima di DESY. Vorrei ringraziare Jürgen Reuter per la correzione della mia dissertazione e per il suo corso sulla supersimmetria, rivelatosi molto utile per il mio lavoro. Un grazie anche al mio relatore degli studi magistrali, Donal O'Connell, per la sua gentilezza e per essere sempre stato disponibile a dare consigli. Sono molto grato ai miei collaboratori Krzysztof Rolbiecki, Moritz McGarrie e Anthony Hartin per tutte le discussioni, faccia a faccia e via Skype. Vorrei inoltre ringraziare Mikael Berggren, Paolo Bolzoni, Florian Domingo, Peter Drechsel, Jenny List, Germano Nardini, Georg Weiglein e Lisa Zeune per utili discussioni. Riconosco il supporto della Deutsche Forschungsgemeinschaft nell'ambito del Sonderforschungsbereich 676 "Particles, Strings and the Early Universe." Ringrazio Martin Sprenger, Marco Tonini e Maikel de Vries per aver revisionato parti della tesi. Inoltre, ringrazio Thomas Konstandin, Jan Louis e Christian Sander per aver accettato di far parte della commissione della mia discussione.

Durante questi anni ho incontrato alcuni amici speciali, sempre presenti, *seguendo le regole*, e che meritano particolari ringraziamenti. Francisco per essere colui che si ricordava di venirmi a prendere a pranzo, per tradurre in inglese ogni mia parola su due, per i *pastéis de nata* e per la bellissima corsa fino a Kiel. Maikel per la sua sensibilità nei miei confronti, per le franche opinioni, *i.e.* lamenti, per la bici, per le imbattibili gaffe e per aver infine imparato a non tagliare gli spaghetti. Marco per la nostra amistà che, arrivando da Padova assieme, è con noi cresciuta in una profonda comprensione, fondamentale per me in certe circostanze difficili. Martin per essere stato il miglior compagno d'ufficio che potessi sperare, sempre pronto ad aiutare e a ridere, per l'esempio e per i nostri venerdì semi informali. Paolo, *eccolo*, per tutto il tempo speciale passato assieme, per il conforto, la pazienza, la gentilezza e per aver sempre il sorriso sul viso.

Sono molto grato anche ai *Dottori* Marco e Sara e, visto che non c'è due senza tre, anche Mattia, per aver aperto le danze e per la motivazione che mi danno nel mio percorso e per tutto il divertimento assieme. Grazie a Marco e Lorenzo per tutte le nostre cene speciali con il calcio, l'italiano, la briscola e le risate. Grazie ad Alessandra, Anne-Julia, Francesco, Francesca, Jennifer, Ivan, Martina, Ninetta, Sonja, Valentina per le nostre amicizie. Grazie a Harald, il nostro appartamento è stato casa per me. Grazie ad Elina e Matthias per tutte le

chiaccherate, cambiando lingua; a Valerie per tutte le nostre ore di tandem; a Marcos, Javier, Andreas e anche Rob per il tempo passato assieme in ufficio, sempre bello; agli amici conosciuti alle scuole e alle conferenze, Abhishek, Aniello, Lucia, Matteo e Simone. Vorrei ringraziare anche tutti i ragazzi di DESY che hanno migliorato le mie giornate, a pranzo e costruendo cappelli di dottorato: Aleksandrina, Alessandro, Alex, c'Andrey, Annika, Bijan, Clemens, Daniel, Emanuele, Florian, Jasone, Julia, Julian, Kazuki, Koji, Lucila, Luigi, Markus, Martin, Matteo, Matthias, Michal, Mikhail, Nezhla, Pavel, Pedro, Peter, Reinke, Samantha, Sebastian, Shireen, Shruti, Simone, So Young, Stefan, Tigran, Tobias, Václav, Yuri e molti altri.

Infine, la mia famiglia. Sono profondamente grato ad Elena ed ai miei genitori Teresa and Giandomenico, per avermi sempre su/opportato, qualunque scelta abbia fatto. Grazie anche a Giulia, Tommaso, Silvia e Maurizio per avermi accolto. Dedico questa tesi alla mia cara Anna, ogni giorno con me, dimostrandomi che Amburgo e Heidelberg sono accanto. Senza di lei non potrei mettere questo . (punto)